Highly Luminescent Lanthanide Chirality Probes

NEIL, EMILY,ROSE

Durham University
Department of Chemistry

Highly Luminescent Lanthanide Chirality Probes

Emily Rose Neil

A thesis submitted for the degree of Doctor of Philosophy

2015

Declaration

The work described herein was undertaken at the Department of Chemistry, Durham University between October 2012 and December 2015. All of the work is my own, except where specifically stated otherwise. No part has previously been submitted for a degree at this or any other university.

Statement of Copyright

Abstract

The chirality of biological systems can be probed using highly emissive lanthanide complexes with the aid of circularly polarised luminescence and emission spectroscopy. Such chirality probes can be synthesised through the incorporation of a remote chiral centre within the ligand framework, which can preferentially stabilise a particular stereoisomer giving an enantiopure complex of well-defined helicity. Alternatively, lanthanide chirality probes can be derived from achiral or dynamically racemic ligands, where the selective induction of a CPL signal can be monitored as a function of the nature and concentration of a selected chiral analyte.

A series of chiral lanthanide complexes has been synthesised. Each complex is based on an amide substituted 1,4,7-triazacyclononane system derived from either *R*-(+) or *S*-(-)-α-methylbenzyl amine. The stereochemistry of the amide moiety controls the helicity of the complex, and one major diastereoisomer is formed for each lanthanide metal. The absolute stereochemistry of the major diastereoisomer was determined by X-ray crystallography (*S*-Δ-$\lambda\lambda\lambda$ and *R*-Λ-$\delta\delta\delta$). Inclusion of an aryl-alkynyl chromophore generated complexes that exhibited large extinction coefficients (up to 55,000 M^{-1} cm^{-1}) and high quantum yields (up to 37%) in water.

A second set of bright Eu (III) complexes has been prepared based on an achiral heptadentate ligand system, which vary in the nature of the pyridyl donor (phosphinate, carboxylate and amide). The binding of a number of chiral acids including lactate, mandelate and cyclohexylhydroxyacetate was monitored by a change in the emission spectrum and the induction of strong CPL. Empirical analysis of the $\Delta J = 4$ region of each of the Eu (III) complexes allows an assignment of the complex-anion adducts as *R*-Δ and *S*-Λ. Furthermore, variations in the sign and magnitude of CPL allow the enantiomeric purity of samples with unknown enantiomeric composition to be assessed.

Finally, several dynamically racemic lanthanide chirality probes have been synthesised and characterised. Induced CPL has been assessed, which arises as a result of the change in complex constitution upon binding to important chiral biomolecules such as, sialic acid, *O*-phosphono-amino acids and peptides and oleoyl-*L*-lysophosphatidic acid (LPA). This work presents the first example of induced CPL in the detection of cancer biomarkers, sialic acid and LPA, and demonstrates the utility of this class of dynamically racemic Eu (III) complexes as chirality probes.

Acknowledgements

I would like to thank the following people for making this work possible:-

My supervisor Professor David Parker for giving me the opportunity to work on such an interesting and engaging project, for the inspiration and ideas he has provided and his unwavering encouragement and enthusiasm.

My family, particularly Mum, Michael, Alex, Grandad and Nana – who is no longer with us, for their love, support and enthusiastic attempts at 'understanding' the work that I have been doing throughout my academic career so far.

A very special thank you to Mike, for his love, laughter and everlasting belief in me.

Thank you to the members of the fantastic Durham analytical service teams: Dr. Alan Kenwright, Dr. Juan Aguilar Malavia, Catherine Heffernan and Raquel Belda-vidal for their help with NMR spectroscopy, going above and beyond the call of duty and providing copious supplies of chocolate biscuits; Dr. Jackie Mosely and the team for help with MS; and Dr. Aileen Congreve for help with HPLC.

Dr. Lars-Olof Pålsson and Dr. Robert Pal (Robek) for the construction of the CPL spectrometer at Durham University. A big thank you to Robek for all of his help with fixing the CPL spectrometer malfunctions as I know it is his least favourite thing to do.

Dr. Mark Fox for the DFT computations and insightful discussions regarding the binding mechanisms.

Dr. Dmitry Yufit for crystal structure determinations.

Past and present members of CG27 for making it such a great place to come in and work every day. Thanks to Cidalia, Matthieu, Amandine, Andrew and Sergey. Particular thanks goes to Katie for going through this journey with me, being a kind friend and a tidy housemate; Brian, Nick, Rachel and Martina for bestowing a great deal of synthetic and emission-based knowledge on me and providing lots of laughs, inside and outside the lab; to Steve for not only being a mentor but a true friend and for making this experience so much easier and more enjoyable (hakuna matata); Alex and Nicola for their patience and always being at hand to help with paramagnetic NMR spectroscopy and Kanthi for sorting out any problem, be it chemistry or non-chemistry related, over a cup of tea.

For Mum and Dad

Abbreviations

9-N_3	1,4,7-triazacyclononane
12-N_4	1,4,7,10-tetraazacyclododecane
(+)-facam	3-trifluoroacetyl-(+)-camphorate
(+)-hfbc	3-heptafluorobutyryl-(+)-camphorate
α_1-AAT	α_1-antitrypsin
α_1-AAT	α_1-acid glycoprotein
Å	Angstrom
AC	alternating current
aq.	aqueous
$B(\lambda)$	brightness (B = emission quantum yield x extinction coefficient)
bda	2,2'-bipyridine-6,6'-dicarboxylic acid
BINAPO	2,2′-bis(diphenylphosphoryl)-1,1′-binaphthalene
BINOL	1,1'-bi-(2-naphthol)
BIPYO	3,3'-bis(diphenylphosphoryl)-2,2'-bipyridine
BM	Bohr magneton
BOC	*tert*-butoxycarbonyl
BODIPY	boron dipyrromethene
BSA	bovine serum albumin
CD	circular dichroism
conc.	concentrated
COSY	correlation spectroscopy
CPL	circularly polarised luminescence
DC	direct current

DFT	density functional theory
DIPEA	*N*,*N*-diisopropylethylamine
DMF	dimethylformamide
DMSO	dimethyl sulfoxide
DNA	deoxyribonucleic acid
DOTA	1,4,7,10-tetraazacyclododecane-*N*',*N*'',*N*''',*N*''''-tetraacetic acid
dpa	pyridine-2,6-dicarboxylate
DTPA	diethylenetriaminepentaacetic acid
ECD	electronic circular dichroism
EDC	1-ethyl-3-(3-dimethylaminopropyl)carbodiimide
EDTA	ethylenediaminetetraacetic acid
ee	enantiomeric excess
equiv.	equivalents
ESI-MS	electrospray ionisation mass spectrometry
EtOAc	ethyl acetate
EXSY	exchange spectroscopy
FWHM	full width at half maximum
GC	gas chromatography
g_{em}	emission dissymmetry factor
HEPES	4-(2-hydroxyethyl)-1-piperazineethanesulfonic acid
hfa	1,1,1,5,5,5-hexa-fluoropentanedione
HMBC	heteronuclear multi-bond correlation
HOBt	hydroxybenzotriazole
HPLC	high pressure liquid chromatography
HRMS	high resolution mass spectrometry

HSA	human serum albumin
HSQC	heteronuclear single quantum coherence
IAM	2-hydroxyisophthalamide
ICT	internal charge transfer
ida	iminodiacetate
ISC	intersystem crossing
LC-MS	liquid chromatography-mass spectrometry
LED	light-emitting diode
LIA	lock-in amplifier
Ln	lanthanide
LPA	oleoyl-α-lysophosphatidic acid
MRI	magnetic resonance imaging
NAG	*N*-acetylglucosamine
NMR	nuclear magnetic resonance
NOESY	nuclear Overhauser effect spectroscopy
oda	2,2'-oxydiacetic acid
OLED	organic light-emitting diode
pba	phenylboronic acid
PCA	2-pyrrolidine-5-carboxylic acid
pda	1,10-phenanthroline-2,9-dicarboxylic acid
PEM	photoelastic modulator
PMT	photomultiplier tube
ppm	parts per million
PSYCHE	pure-shift yielded by chirp excitation (pure-shift NMR)
pybox	bis(oxazolinyl)pyridine

q	hydration number
R_f	retention factor
rf	radiofrequency
ROESY	rotating frame nuclear Overhauser effect spectroscopy
SAP	square antiprism
SOM	small organic molecule
TBAF	tetra-*n*-butylammonium fluoride
TD-DFT	time-dependent density functional theory
TFA	trifluoroacetic acid
TFEF	2,2,2-trifluoroethylformate
THF	tetrahydrofuran
TL	total luminescence
TLC	thin layer chromatography
TOCSY	total correlation spectroscopy
TSAP	twisted square antiprism
TQD	tandem quadrupole detector
UV	ultra-violet

List of Publications

Synthesis, stereocontrol and structural studies of highly luminescent chiral tris-amidepyridyl-triazacyclononane lanthanide complexes

E. R. Neil, A. M. Funk, D. S. Yufit and D. Parker, *Dalton Trans.*, 2014, **43**, 5490.

EuroTracker® dyes: design, synthesis, structure and photophysical properties of very bright europium complexes and their use in bioassays and cellular optical imaging

S. J. Butler, M. Delbianco, L. Lamarque, B. K. McMahon, **E. R. Neil**, R. Pal, D. Parker, J. W. Walton and J. M. Zwier, *Dalton Trans*., 2015, **44**, 4791.

Critical analysis of the limitations of Bleaney's theory of magnetic anisotropy in paramagnetic lanthanide coordination complexes

A. M. Funk, K. N. A. Finney, P. Harvey, A. Kenwright, **E. R. Neil**, N. J. Rogers, P. K. Senanayake and D. Parker, *Chem. Sci*., 2015, **6**, 1655.

Chiral probe development for circularly polarised luminescence: comparative study of structural factors determining the degree of induced CPL with four heptacoordinate europium(III) complexes

E. R. Neil, M. A. Fox, R. Pal, L. O. Pålsson, B. A. O'Sullivan and D. Parker, *Dalton Trans*., 2015, **44**, 14937.

Table of Contents

CHAPTER ONE
INTRODUCTION

1.1. Overview

Molecular chirality is a description applied to molecules that are non-superimposable on their mirror images through translation and/or rotation. The word chirality is derived from the Greek word for hand (cheir) as it is a mathematical approach to the 'handedness' of a molecule. Although enantiomers (molecules related to each other as mutual mirror images) have identical chemical properties, their three-dimensional structure profoundly alters their interaction with the surroundings. This property is of particular relevance in the pharmaceutical industry, where it is imperative to accurately determine the enantiomeric purity of a drug molecule. The molecular recognition of a guest molecule can also provide an in-depth understanding of a variety of chemical and biological processes, including structure-function relationships. There is a wide range of chiral biomolecules of interest, and development of accurate and informative chiral recognition studies is of considerable importance.

Europium and terbium luminescence occurs on a millisecond timescale and has been used as an analytical tool for many years, with a wide range of applications in material[1] and biological sciences.[2–4] In particular, the signalling and sensing of reversible anion binding to a lanthanide centre has been studied using emission and luminescence lifetime measurements.[5] However, to date, there is relatively little consideration given to the three-dimensional structure, or chirality, of the chosen analyte. Circularly polarised luminescence (CPL) spectroscopy exists as a tool that in conjunction with a highly luminescent probe, allows for detailed investigation of the chiral environment of the molecule or system of interest.

This chapter begins with a comprehensive discussion of CPL spectroscopy, including the key equations that underpin the theory, and the methods and instrumentation that are used to record CPL spectra. A review of the types of system that exhibit this phenomenon is discussed, ranging from small organic molecules through to transition metal and lanthanide complexes. In the context of this thesis, particular emphasis will be placed on the design of chiral lanthanide complexes that exhibit strong CPL. The final section reviews examples of lanthanide complexes as chiral probes that exhibit modulation or induction of their CPL output, following a change in their environment.

1.2. Circularly polarised luminescence

Since the 1940s and Samoilov's first observation of the phenomenon of circularly polarised luminescence (CPL) from a sodium uranyl acetate crystal,[6] the measurement of CPL or CPL spectroscopy has become a well-developed technique and has been applied in the study and structural determination of optically active chiral molecules.[7–9]

1.2.1. CPL spectroscopy: background theory and equations

Before we begin analysing the theoretical principles surrounding the phenomenon of CPL, consider first the classical description of polarised light. Electromagnetic waves (light) are made up of two vectors which are the electric and magnetic fields. The light's polarisation direction is by convention, along the direction of the electric field. The electric field vector itself can be split into two components that are perpendicular to one another and oscillate with identical frequency. In the case of circularly polarised light, these two components have the same amplitude, but are phase shifted by exactly one quarter of the wavelength (Figure 1). This results in one component being at a maximum or minimum value, while the other component is at zero. Therefore, circular polarisation confers helical chirality to a beam of light depending upon the propagation mode. Circularly polarised light can be generated by passing linearly polarised light through a quarter-wave plate at an angle of 45º to the optic axis or by the interaction of light (linear or unpolarised) with a chiral molecule.

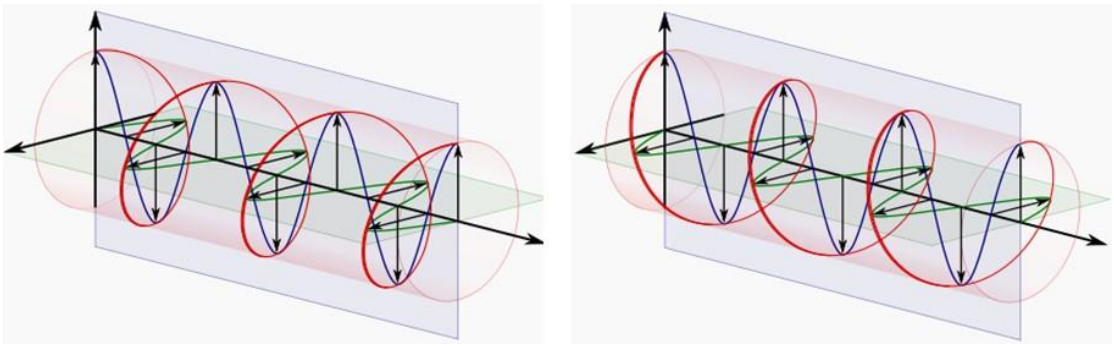

Figure 1 – Left and right circularly polarised light (from the point of source). The two perpendicular components of the electric field vector are depicted in blue and green.

By definition, CPL spectroscopy measures the differential spontaneous emission of left *versus* right circularly polarised light from a luminescent system, ΔI.[2,10,11]

$$\Delta I(\lambda) = I_L(\lambda) - I_R(\lambda) \qquad \textbf{(1.1)}$$

As it is difficult to measure absolute values of emission intensity, the degree of CPL at a particular wavelength is reported in terms of the emission dissymmetry factor, g_{em}, as defined in equation **1.2**.

$$g_{em}(\lambda) = \frac{2\Delta I(\lambda)}{I_L(\lambda) + I_R(\lambda)} \qquad (\mathbf{1.2})$$

In their pioneering studies into the observation of CPL from chiral molecules in solution, Emeis and Oosterhof were able to demonstrate that in the limit when the orientational distribution of emitting molecules is isotropic, an analogy can be drawn between the CPL observables and the molecular properties of the system.[12] Within this limit, the degree of CPL can be linked to a single fundamental molecular property – the rotatory strength parameter, equation **1.3**.

$$R_{ij} = Im(\langle j|\boldsymbol{\mu}|i\rangle\langle i|\boldsymbol{m}|j\rangle) \qquad (\mathbf{1.3})$$

In this equation the rotatory strength of the electronic transition$|j\rangle \rightarrow |i\rangle$, is defined as the scalar product of the electric, **μ**, and magnetic, **m**, transition dipole vectors. Orientational averaging of the system yields a second equation, in which the emission dissymmetry value can be defined in terms of this molecular parameter, equation **1.4**.

$$g_{em} = \frac{4R_{ji}}{D_{ji}} \qquad (\mathbf{1.4}) \qquad\qquad D_{ji} = |m|^2 + |\mu|^2 \qquad (\mathbf{1.5})$$

Here, D_{ji} is the dipole strength of the transition, also defined in terms of the magnetic and electric transition dipole moments, and is influential in determining the intensity of the total emission, equation **1.5**. If we assume that the magnetic transition dipole moment is much smaller than its electric counterpart, as is typically the case, equation **1.4** can be scaled and consequently g_{em} can be expressed by equation **1.6**,

$$g_{em} = \frac{4|m|}{|\mu|} cos\tau \qquad (\mathbf{1.6})$$

where τ is the mutual orientation angle between the magnetic and electric transition dipole moments and is dependent on the geometry of the system. It should be noted that a value of zero for g_{em} corresponds to no circular polarisation in the emission output; the maximum value

is ± 2. An important piece of information to acknowledge from these equations is that, generally speaking, transitions that are magnetic dipole allowed and electric dipole forbidden will exhibit large g_{em} values.

1.2.2. Advantages and limitations of CPL

The chiral character of a beam of light is the basis of chiral photonics or chiroptics. Circular dichroism (CD) is the more widely recognised spectroscopic technique in this area and is based on the differential absorption of left and right circularly polarised light. CPL is the emission equivalent of CD and therefore gives us information about the chiral properties of a molecule in its excited state. The two techniques exist as complementary tools, allowing information about geometry differences in the ground and excited state to be elucidated. There are, however, a few advantages to take into account when employing an emission based chiroptical technique such as CPL.[7] CPL is inherently more sensitive than CD and it is often possible to observe weak CD transitions, i.e. transitions from excited states that are only weakly accessible *via* absorption processes. Also, interpretation of spectra in CPL is often simpler and only selected transitions are observed particularly in systems containing many chromophores, as only select luminophores will respond at a specific excitation wavelength.

The measurement of CPL also has some inherent limitations, the most severe being that the system under investigation must contain a luminescent chromophore with a reasonable quantum yield. This drawback can be addressed by intelligent probe design and will be discussed in greater detail in subsequent sections (Sections 1.3 to 1.5).

1.2.3. Measurement techniques and instrumentation

The technique of measuring CPL from chiral molecules in solution dates back to the 1970s in the laboratories of Professors Oosterhof,[12] Richardson[13] and Dekkers.[14] Yet despite this, the first commercial CPL spectrometer has only recently become available (JASCO CPL-200). As a result, the majority of CPL studies in the literature have been performed using 'in-house' built spectrometers which share many common features in their setup. The technique has been developed to a point where detection of CPL for moderately luminescent chiral systems can be performed with a high degree of reliability and sensitivity (~1 part in 10^4-10^5).

In a typical experiment, the incident light used to excite the sample is linearly polarised or unpolarised. The sample is excited at 90º to the direction of emission detection and the emitted light is collimated and selectively modulated by a photoelastic modulator (PEM). The PEM is made of an isotropic clear optical material, such as quartz, that becomes anisotropic on application of periodic stress. The PEM can be driven by an AC signal at a frequency of ~50 kHz, thereby acting as an oscillating quarter-wave plate. On alternate cycles, the PEM retards or accelerates the wavelength of emitted light, which results in the right and left components of the circularly polarised light being converted to the appropriate linear polarisation. The monochromated light is then selected by a linear polariser orientated at 45º and passed on to a photomultiplier tube (PMT). A typical detection system may comprise of a lock-in amplifier (LIA) which detects the difference signal (AC) and the total intensity (DC) and converts them to the CPL and total luminescence (TL) respectively after background correction (Scheme 1).[15,16,17] An alternative detection method may utilise photon counting. This method has been shown to be more reliable than the analogous lock-in detection and less influenced by electronic problems such as ground loops.[18]

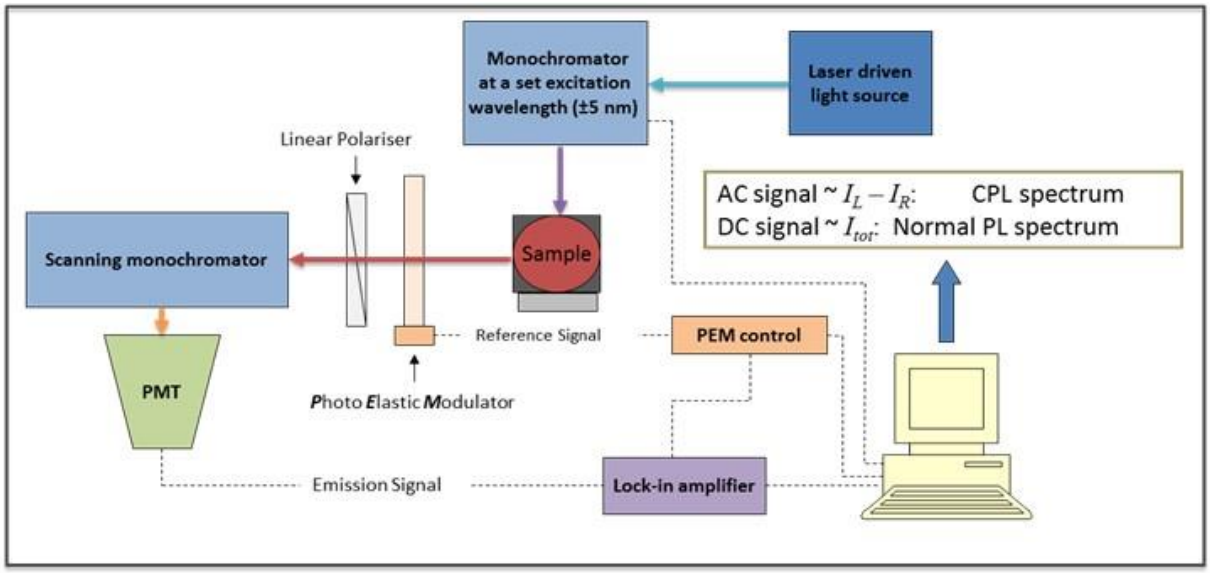

Scheme 1 - Schematic diagram showing a typical instrumentation set-up for the measurement of CPL based on a lock-in detection system.[15]

It is not difficult to imagine that small changes to the conventional spectrometer set-up allows for alternative CPL experiments to be devised. One example of this is the induction of CPL from a racemic mixture of molecules by employing circularly polarised light as the excitation

source. This technique has been used in the determination of optical purity of partially resolved systems by achieving preferential excitation of one enantiomer.[19,20] Another method of inducing and measuring CPL from an achiral, optically inactive system is *via* the application of a static magnetic field along the direction of emission detection. This technique is termed magnetic circularly polarised luminescence (MCPL) and is particularly useful in eliciting electronic structural information.[21] Despite the utility of these techniques, the remainder of this review will focus primarily on zero-field CPL where a linearly polarised or unpolarised excitation source is used to elucidate key stereochemical information from naturally optically active systems.

1.2.4. Calibration standards for CPL

It is important to be able to measure accurately the sign and magnitude of CPL signals and emission dissymmetry values. Therefore, it is imperative to ensure effective spectrometer calibration with the use of a reliable standard to certify that recorded data is transferable and comparable between other 'home-built' and commercial spectrometers.

The commercially available NMR shift reagent *tris*(3-trifluoroacetyl-(+)-camphorato)europium (III) (Eu((+)-facam)$_3$) in DMSO is the most commonly used CPL calibration standard.[22] However, there are some drawbacks associated with this lanthanide complex that limit its use as an effective calibrating agent. Of these, the most notable is the relative sensitivity of Eu((+)-facam)$_3$ to water in DMSO. This drawback severely limits the reliability of this complex as a CPL standard as g_{em} values can vary depending on the water content of the solution.

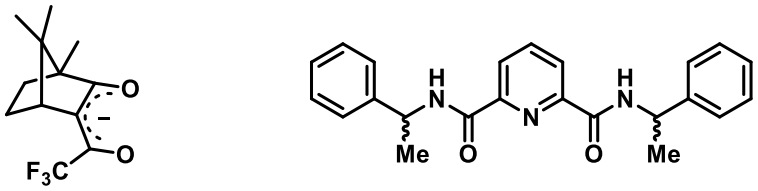

facam

(*R*,*R*)-**L**^{1}
(*S*,*S*)-**L**^{1}
(*R*,*S*)-**L**^{1}

Scheme 2 - Chemical structure of facam (*left*) and *N*,*N*'-bis(1-phenylethyl)-2,6-pyridine carboxamide **L**^{1} (*right*).[22,23]

More recently, an alternative europium complex has been proposed in an attempt to improve accurate routine CPL calibration tests. The CPL standard is based on chiral *N,N'*-bis(1-phenylethyl)-2,6-pyridine carboxamide ligands, $\mathbf{L^1}$, in a 1:3 (Eu: ligand) ratio (Scheme 2).[23] Ligand **1** can be prepared in a simple one-step synthesis in high yield (90%). The most prominent advantage of this standard over the traditional Eu((+)-facam)$_3$ calibration agent is the solution stability. For instance, no change to g_{em} values were found between fresh and several month old solutions of the complex. The standard was also found to be stable to photobleaching under continuous UV irradiation over several days. This complex may present an attractive alternative to the traditionally used (Eu((+)-facam)$_3$ standard. However, the reliability of the speciation of the complex is worth considering. The authors claim that by mixing Eu^{3+} and the ligand in a 1:5 ratio, only the $[Eu.(\mathbf{L^1})_3]^{3+}$ species is formed, yet provide limited evidence that this is in fact the species that is being observed. It may be time for the development of a better defined complex for use in the calibration and routine tests of CPL spectrometers, to allow for more comparable results across the literature.

1.3. Systems that exhibit CPL

There is a wide variety of systems documented in the literature that exhibit the phenomenon of CPL, including simple organic molecules, transition metal complexes and lanthanide-based structures. This section aims to review the literature surrounding the intense development of each class of CPL-active system and discuss potential applications, advantages and draw-backs of each approach.

1.3.1. CPL from simple organic molecules

CPL from simple organic molecules (SOMs) dates back to the emergence of CPL spectroscopy and the study of bicyclic chiral ketones in the laboratories of Emeis and Oosterhof in 1967.[24] There lies a great challenge in the development of small, non-aggregated organic molecules that are able to emit circularly polarised light efficiently due to the lack of magnetic dipole character present in most of the considered transitions (e.g. π-π*). The attractive properties of SOMs, such as their small size and organic solubility, means that they are very amenable for application in display devices,[25] optical storage devices[26] and in asymmetric photochemical

synthesis.[27] This has led to considerable effort focussed on improving the CPL properties of this class of molecules, which will be reviewed in this section.[9]

1.3.1.1. Simple carbonyl compounds and extended π-conjugated systems

Original efforts were focused upon simple organic ketones and the *n*-π^* electronic transition, which is not inherently chiral in itself, but is chirally perturbed within the structure in which it is embedded.[14,28,29] This work was further advanced by Dekkers in the study of the excited state of dynamically coupled chirally-perturbed carbonyl chromophores of polycyclic β,γ-enones.[30] It provided one of the first examples of using CPL as a tool to elucidate chiral structural information of a molecule in the excited state. The study found that the bonding interaction in the excited state differs dramatically from that of the ground state. The authors hypothesised that as the carbonyl bond becomes stretched upon excitation, the geometry around carbon switches from planar to pyramidal resulting in an increased bonding interaction with the β,γ-olefinic bond. The asymmetric distortion causes the molecule to become chiral and exhibit CPL activity.

The very poor fluorescence efficiencies of simple carbonyl compounds has led to the development of extended π-conjugated systems and CPL from π-π^* transitions in polymers and simple organic molecules.[31] One of the most commonly employed chromophores in these systems is the achiral BODIPY moiety.[32]A recent example of this type of CPL-SOM has been developed by de la Moya, SOM-1, in which a set of C^2 symmetric chiral enantiomers is used to chirally perturb an achiral BODIPY chromophore resulting in the emission of CPL (Figure 2).[33] Small g_{em} values were calculated of the order of 10^{-3}, which is typical for an organic chromophore (CPL <0.1%). However, the system did exhibit a high fluorescence quantum yield (46%).

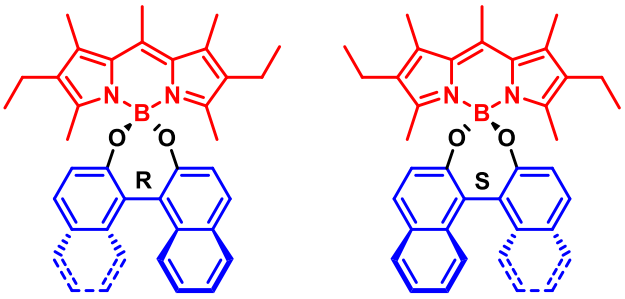

Figure 2 – Chemical structure of spiro-BODIPY enantiomers (SOM-1) exhibiting equal and opposite CPL upon radiation at 529 nm in $CHCl_3$. Axially chiral 1,1-binapthyl unit (*blue*), achiral BODIPY chromophore (*red*).[33]

1.3.1.2. Helicenes

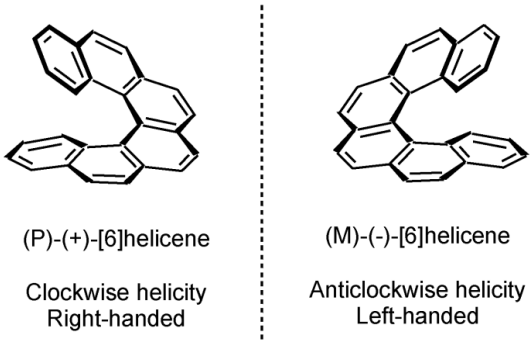

Figure 3 – Stereochemical description and chemical structure of right (*P* or *Δ*) and left (*M* or *Λ*) handed carbohelicenes.[34]

Based upon the attractive emission properties associated with π-conjugated systems (section 1.3.1.1), attention turned to improving the CPL properties of this class of SOMs. This approach led to the development of simple organic molecules consisting of *n-ortho*-fused aromatic rings with inherent helical chirality, governed by a conformational distortion of the π-system imposed by the high steric strain (Figure 3). The molecules are termed 'helicenes' and demonstrate good chiroptical activity; the direction of which depends upon the handedness of the helical twist.

To ensure that good emission and CPL properties are obtained, it is important to avoid aggregation of the molecules and thereby circumvent associated problems such as excited state quenching and linear polarisation complications.[35] A nice example of a non-aggregating helicene was published by Venkataraman and co-workers which included bulky functional groups along the helicene backbone.[36] Each enantiomer of the triarylamine helicene exhibited oppositely signed CPL when irradiated at 434 nm in $CHCl_3$ with a g_{em} value of 0.001 at 442 nm. It should be noted that despite the increased helical overlap provided by the additional aromatic ring in *Δ*-**3** compared with *Λ*-**2**, there is still only a small net circular polarisation in the emission, suggesting that net chirality of the observed transitions is not just a function of molecular geometry (Figure 4).

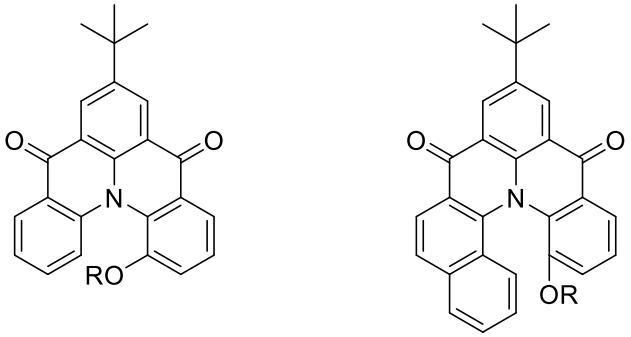

***Λ*-2** ***Δ*-3**

Figure 4 – Structures of triarylamine helicenes.[36]

Often the preparation of enantiopure helicenes poses significant synthetic issues, most notably in the separation of the resulting enantiomers. Separation of enantiomeric helicenes can be achieved by chiral resolution in conjunction with a resolving agent but typically results in a low yield.[37] A more attractive alternative is to employ an enantioselective synthesis strategy.[34] An example of such an approach was adopted by Tanaka in the synthesis of S-shaped double aza-helicenes that showed good CPL activity (g_{em}(492 nm) = 0.0028 in $CHCl_3$).[38] The double-helicenes were synthesised in >99% *ee via* Au-catalysed sequential intramolecular hydroarylation of alkynes.

1.3.1.3. Simple organic molecules as responsive probes

One of the first examples of an anion responsive SOM-CPL probe was based on an extended π-conjugated design, (section 1.3.1.1). Introduction of a BINOL-boron moiety coordinated to a dipyrrolyldiketone ligand results in the formation of a symmetrical environment that is broken upon anion binding.[39] When the probe, **4**, interacts with an anion such as chloride or acetate, a CPL signal was obtained from the previously CPL-silent system. The induced CPL was attributed to a key conformational change of the π-planes, resulting from a flipping of the two pyrrole rings as a result of anion binding (Figure 5). This example demonstrates the first example of a chemical-stimuli responsive CPL probe based on an organic framework.

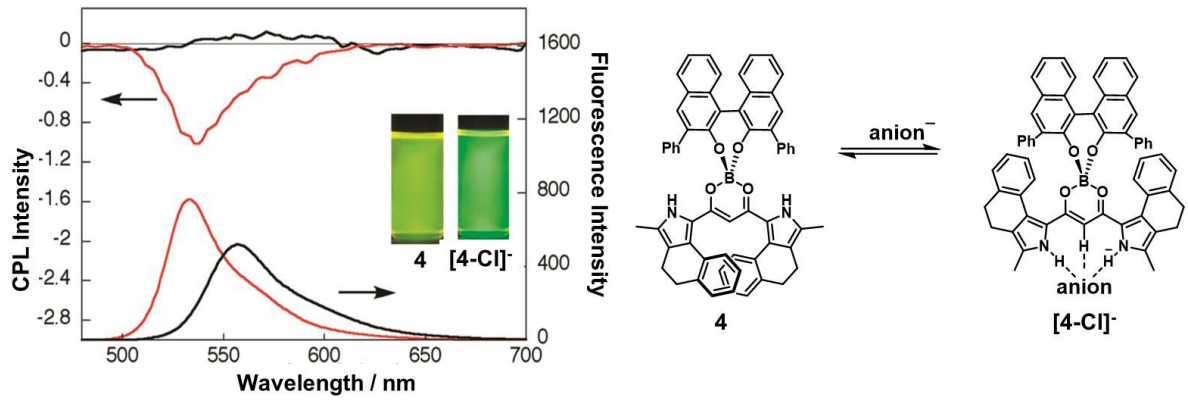

Figure 5 - *Left*: fluorescence (*bottom*) and CPL (*top*) spectral change for **4** in the absence (*black*) and presence of 200 equiv. chloride ion (*red*) – insets show solution change of **4** upon anion binding. *Right*: anion binding mode of **4** showing key conformational change on anion binding.[39]

Maeda later reported a set of probes based on a similar design to **4** that were able to produce CPL signals on forming diastereomeric pairs with chiral cations[40] and also direct binding to chiral analytes, more specifically, amino acids.[41] The second set of responsive probes were based upon dimers of a π-conjugated system, connected by a terphenyl spacer group to ensure a large enough binding cavity for the chiral analyte, **5** (Figure 6). The geometry of the acute angled terphenyl spacer group was either *meta-meta-meta* or *para-ortho-para*. The authors found that the point chirality of the amino acid (*S*-phenylalanine) could induce opposite helical chirality in probe **5,** depending on the geometry of the spacer, resulting in the induction of CPL (Figure 6). This study demonstrates the use of SOMs as CPL probes in an example where a very low concentration (µM) of chiral auxiliary can induce a chiral response. The biggest drawback to systems based on this class of probes is the very low g_{em} values that are measured. Experiments were carried out at -50 ºC, as it was hypothesised that the low temperature would increase the conformational rigidity of the helices and also alter the distribution of Λ and Δ diastereoisomers. However, even within this restraint, the g_{em} values were measured at 10^{-4}. Potentially, the most useful application that could be envisaged would not be in biological recognition but in material applications, such as multifunctional molecular devices.

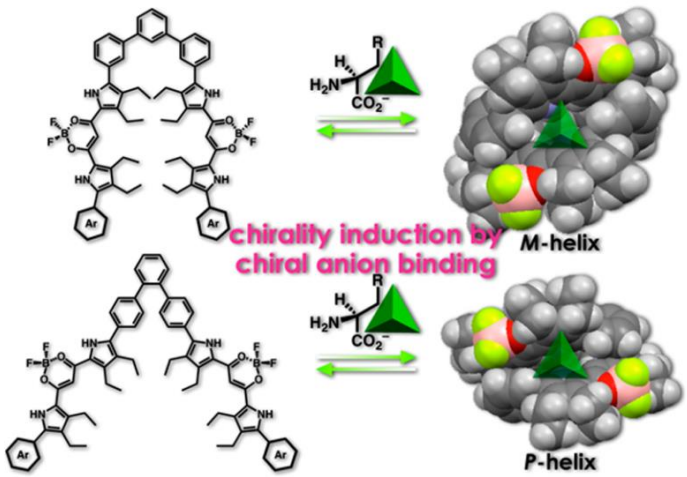

Figure 6 – Probe **5** design based on a π-conjugated dimer linked by a terphenyl spacer unit. Point chirality of the amino acid induces opposite helical conformation (Λ or Δ) depending on the geometry of the spacer group.[41]

1.3.2. CPL from transition metal coordination complexes

1.3.2.1. Metallohelicenes

The impressive chiroptical properties exhibited by inherently chiral helicenes were discussed earlier (Section 1.3.1.2). An important challenge in further expanding the potential of these molecules is in the design of a variety of helical frameworks that allow for tuneable chiroptical properties, with a focus on application as OLEDs and in chiral displays. Recent advances have seen the incorporation of transition metal ions, such as Re,[42] Os,[43] and Pt,[44–46] into the backbone of the helical ligand. The presence of a heavy metal ion improves the π-conjugation of the system, exhibits close electronic interaction with the helicoidal ligand system and as a result, phosphorescent CPL-active systems can be investigated.

Metallohelicenes incorporating platinum ions tend to exhibit the best chiroptical activities. These types of systems exhibit the largest g_{em} values compared to other transition metal helicenes, and are phosphorescent, due to spin-orbit coupling. Although platinum is not a stereogenic centre, the enhanced properties can be attributed to the platinum 5d orbitals being the most conjugated with the π-system of the helical ligand. One of the first examples in the literature describes a mono-(platinahelicene) with interesting photophysical and chiroptical properties that can be fine-tuned by chemical oxidation of the metal centre. However, the measured g_{em} value was no greater than that of the simple organo-helicene.[44] A more recent example has demonstrated an enantiopure mono-(platinahelicene), Pt-[6]helicene, with a g_{em} value of the order of 10^{-2}, an order of magnitude greater than the non-platinated system and the

biggest value recorded for molecular helicenes.[46] The large emission dissymmetry values, and interesting tuneable photophysical properties of Pt-[6]helicene are promising for future development into its use in chiral optical displays.

1.3.2.2. Platinum and iridium chiral complexes

A very good illustration of the potential utility of transition metal CPL-active complexes in chiral displays such as chiral memory, chiral switching devices and also as biosensors has been developed by You et al.[47] The design is based on a Pt (II) complex, probe **6**, that is able to aggregate in aqueous solution *via* π-π and hydrophobic-hydrophobic interactions resulting in a novel helical structure which is CPL active. However, the CPL activity can be reversibly 'switched' by an external stimulus, in this case temperature. Upon heating to 353 K, the CPL activity becomes zero, most likely due to deaggregation or decomposition of the Pt (II) complexes at higher temperatures (Figure 7).

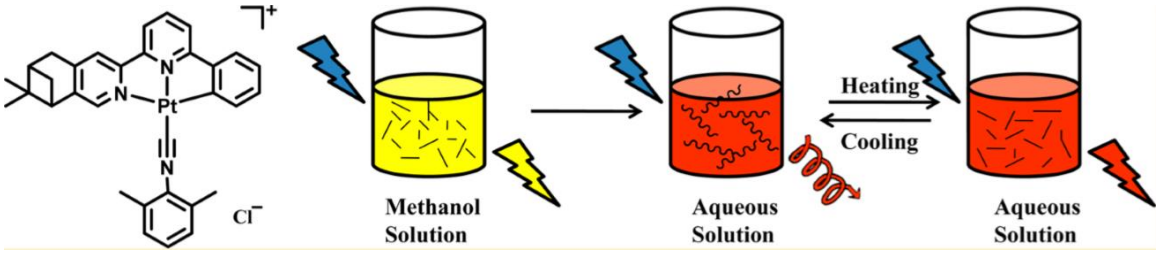

Figure 7 – Structure of chiral cyclometalated platinum (II) complex, probe **6**, and process of reversible 'CPL switching' in aqueous solution upon changing the temperature.[47]

The final example of a CPL active transition metal complex that will be discussed is based upon neutral Δ and Λ bidentate iridium (III) complexes. Iridium complexes are readily colour tuned through systematic modification of the ligand system, possess high phosphorescent quantum yields and are therefore readily employed in optical devices. Enantiomeric resolution of a racemic mixture of Δ and Λ iridium complexes, **7**, was achieved using chiral supercritical fluid chromatography and the resulting enantiomers displayed net circular polarisation in their emission.[48] A g_{em} value of 0.002 at 495 nm was measured for the C_3 symmetric complex (Figure 8) which is significantly larger than the value for related C_2 complexes. This is an important observation, showing the need for high symmetry and strong conformational rigidity in a system in order to obtain large g_{em} values and observe strong CPL activity. The authors were

also able to employ a novel TD-DFT approach to predict the magnitude of the emission dissymmetry value of a number of Ir (III) complexes and also Ru (II) and Zn (II) hemicages; calculated values correlated well with experimental determinations.

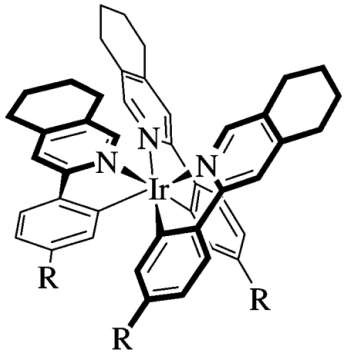

Figure 8 – Structure of homoleptic C_3 symmetric Ir(III) complex, **7**.[48]

1.3.3. CPL from emissive lanthanide complexes

Organic and transition metal based CPL-active systems, including their attractive properties for specific applications, have been considered in detail, most markedly in smart chiral materials and in biosensing (Sections 1.3.1 and 1.3.2). However, it is apparent that there is still a major inherent flaw for use of these systems in conjunction with CPL, and that is the very small degree of circular polarisation in the emission output, resulting from the intrinsic nature of the transitions. The magnitude of the consequential emission dissymmetry values is very small, typically 10^{-3}-10^{-4}, and are thus difficult to measure.

The emission of CPL from lanthanide complexes dominates the literature in this area and this is a result of the attractive spectroscopic features they possess.[8,49,50] From early examples of carboxylic acid based Eu^{3+} and Tb^{3+} complexes studied by Luk and Richardson in the 1970s,[51] to the highest ever recorded g_{em} value of +1.38 from a europium complex of a chiral tetrakis(3-heptafluoro-butyryl-(+)-camphorato) ligand (~85% of emitted photons are left circularly polarised),[52] it is clear why lanthanide complexes make such attractive candidates for CPL applications.

1.3.3.1. Lanthanide luminescence properties

In order to fully understand the importance of chiral luminescent lanthanide-based probes, their unusual photophysics must be considered. Most lanthanide complexes are luminescent but their

emissiveness depends on a variety of factors. The specific requirements to consider when determining which lanthanides are the most suited to luminescence studies are: i) the ease at which the excited state can be populated and ii) the energy gap between the lowest level excited state and the highest energy level of the ground state multiplet.[53] If the energy gap is too small, it can give rise to non-radiative deactivation pathways, such as quenching by high energy vibrations, for example O-H or N-H oscillators. As can be seen from the energy diagram (Figure 9), Eu^{3+}, Gd^{3+} and Tb^{3+} have a sufficiently large energy gap between the emissive state and the highest energy level of the ground state multiplet (ΔE = 12 300, 32 200 and 14 800 cm^{-1} respectively). Gd^{3+} emits in the UV region of the spectrum and so has limited use in biological applications. For the remainder of this review, examples of Eu^{3+} and Tb^{3+} complexes as chiral luminescent probes will be considered.

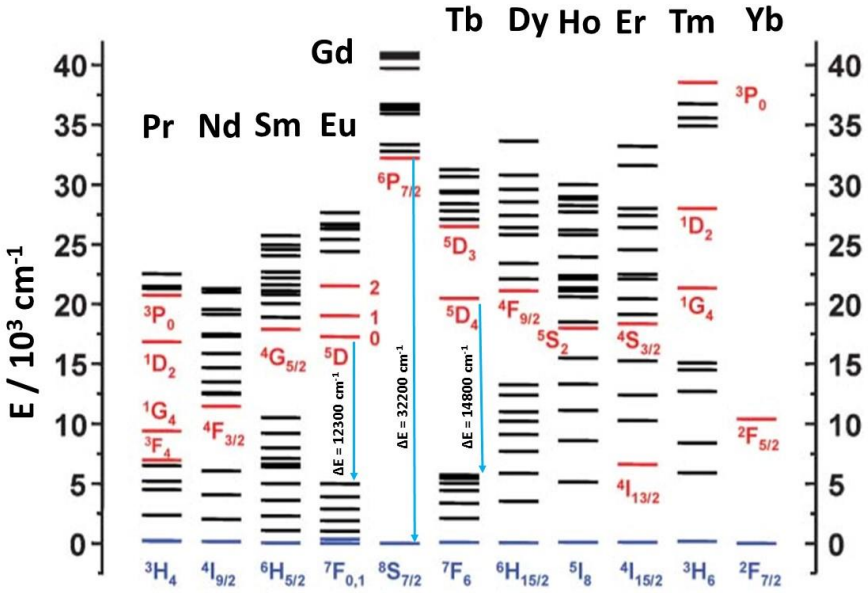

Figure 9 - Partial energy level diagram for lanthanide (III) ions. [53]

The lanthanoids are a unique set of elements, as they resemble each other so closely in their chemical properties. The electronic configuration of their tripositive ions, $[Xe]4f^n$ where n = 0-14, demonstrates that the 4*f* electrons are shielded by the filled $5p^6 6s^2$ subshells giving rise to their interesting spectroscopic features. The sharp, narrow emission bands arise from the Laporte-forbidden *f-f* transitions. They are characteristic of the particular metal in question and are well separated from the broad fluorescence of organic fluorophores. The forbidden nature of these transitions gives rise to long luminescent lifetimes (milliseconds in the case of Eu^{3+}

and Tb^{3+}). However, this feature also leads to low molar extinction coefficients for direct excitation of the lanthanide metal.

The poor absorption and emission efficiency of the lanthanide ion can be overcome through integration of a chromophore ligand into the complex. Such an approach has been termed the 'antenna effect' and was discovered by Weissmann in 1942 in his study of europium complexes.[54] He observed europium luminescence following irradiation of light that selectively excited the organic components of the system. The energy of the ligand triplet excited-state must lie at least 1700 cm^{-1} above the energy of an accepting lanthanide energy level in order to prevent thermally activated back-energy transfer to the sensitiser triplet state.[55] On the other hand, if the energy gap is too great, then the efficiency of the ligand to metal energy transfer step is compromised. Therefore, it is important to optimise the energy gap between the lowest lying triplet energy level of the ligand and the Ln^{3+} emitting state, taking into account these two opposing factors.

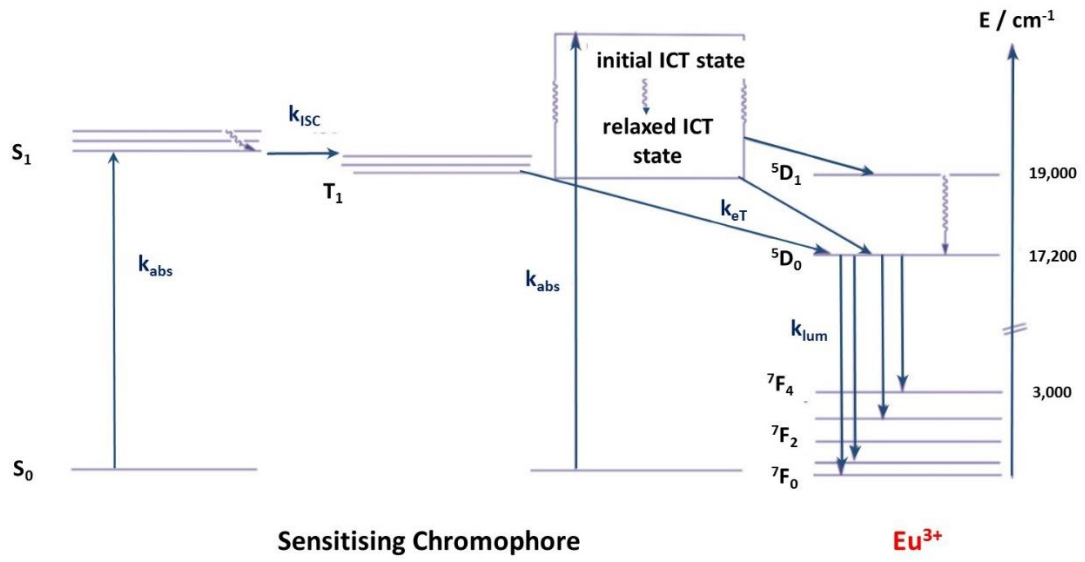

Figure 10 – Simplified Jablonski diagram illustrating sensitised emission of a Eu^{3+} complex, *via* an intermediate ligand triplet or solvent-relaxed internal charge transfer excited state.

The sensitising moiety is initially excited from its ground state to its singlet state (S_1). Vibrational relaxation then occurs to the lowest vibrational level of the S_1 excited state, according to Kasha's rule.[56] Intersystem crossing (ISC) from the sensitiser singlet state (S_1) to the triplet state (T_1) then occurs. This spin-forbidden process is facilitated by spin-orbit coupling from the heavy metal. Energy is finally transferred to the metal centre which relaxes

and emits light from the excited state (Figure 10). There are a number of possible quenching and deactivation processes that occur along this pathway which can affect the luminescence output of the system, as shown in Figure 11.

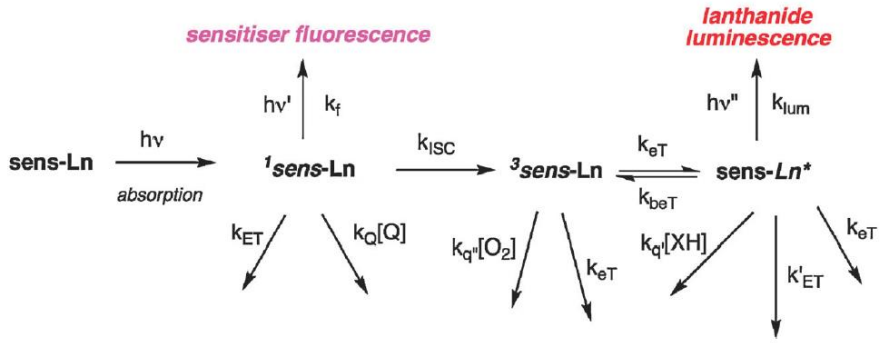

Figure 11 - Photophysical processes occurring during sensitised emission, presenting the different quenching processes that can occur to modulate lanthanide luminescence (eT: energy transfer; ET: electron transfer).[5]

The mechanism of energy transfer between the organic chromophore and the lanthanide centre may proceed *via* the Dexter mechanism, involving electron transfer between the chromophore and the lanthanide centre through-bond interaction and therefore requires good overlap between ligand and metal orbitals.[57] An alternative, more likely pathway is the Förster mechanism, in which energy is transferred through space and is dependent on r^{-6} (r = the distance between the antenna and the metal centre).[58] It relies upon the dipole moment associated with the T_1 state of the ligand coupling with the dipole moment of the Ln 4*f* orbitals.

For a complex to be effectively employed in chiroptical and biological applications, it is necessary that it possesses a high quantum yield. This feature ensures that the probe produces signals that are easy to measure with good accuracy above background noise. For a sensitised lanthanide complex, the overall quantum yield can be defined by equation **1.7**.

$$\Phi = \eta_{ISC}\eta_{ET}\Phi^{Ln} \qquad \textbf{(1.7)}$$

The efficiency of intersystem crossing between the S_1 and T_1 excited states of the sensitiser is denoted by η_{ISC}, the efficiency of energy transfer from the ligand to the lanthanide centre is given by η_{ET} and the intrinsic quantum yield of the lanthanide ion is defined as ϕ^{Ln}.[59] From equation **1.7** it is evident that ligands possessing high efficiency, η, values will produce a lanthanide complex possessing a high quantum yield. This issue has been exemplified in the

work of Delbianco et al. for a series of europium complexes based on aromatic sulfonate derivatives of phosphinate ligands appended to a 9-N_3 macrocyclic core, employing strongly absorbing arylalkynyl chromophores [Eu.$\mathbf{L^2}$]$^{3-}$ (Figure 12).[60] In this study, the authors report a quantum yield of 32% in water; one of the highest ever reported vales for a europium complex in aqueous solution.

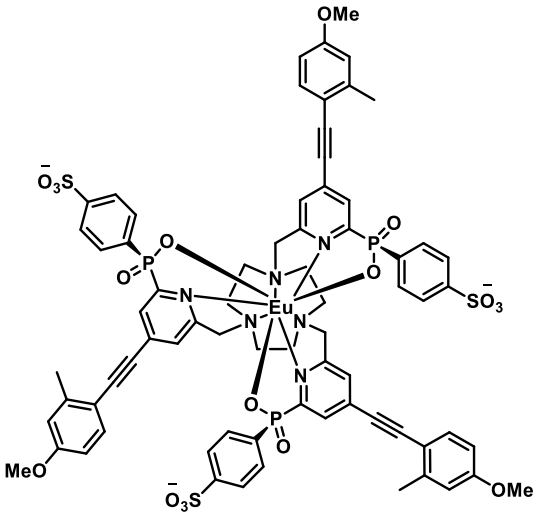

Figure 12 – Structure of the europium complex [Eu.$\mathbf{L^2}$]$^{3-}$ which exhibits a quantum yield of 32% in pure water.[60]

The brightness, $B(\lambda)$, of a complex is a key parameter to consider when selecting a suitable chromophore. It is typically defined as the product of the molar extinction coefficient, $\varepsilon(\lambda)$, and the overall quantum yield, $\phi_{em}(\lambda)$. Therefore, it is important to employ a chromophore that will generate a complex with not only a high quantum yield value, but also a large molar extinction coefficient, to ensure maximum brightness, $B(\lambda)$.

A final consideration when selecting a suitable chromophore is to minimise radiationless deactivation pathways of the lanthanide metal through interaction with external solvent molecules. This can be achieved by maximising the coordination number around the lanthanide centre (7-9) using multidentate chelating ligands. The chelate effect also acts to improve the thermodynamic and kinetic stability of the resulting lanthanide complex. There is a wealth of literature surrounding the selection of appropriate chromophores for Eu^{3+} and Tb^{3+} that satisfies the factors discussed within this section, and the reader is directed to selected reviews for further information.[4,61–64]

1.3.3.2. Chiroptical properties of emissive lanthanide complexes: selection rules

In a number of experimental studies on lanthanide optical activity, a clear trend has been demonstrated concerning the observation that certain electronic transitions exhibit significantly greater emission dissymmetry values than others. Lanthanide 4*f*-4*f* transitions exhibiting particularly large g_{em} values have been termed 'CPL-sensitive' transitions.[10] The selection rules that are operative in determining the CPL-sensitivity of lanthanide 4*f*-4*f* transitions are discussed in detail by Richardson, in a study considering only the free ion electronic quantum numbers and term to term transitions.[65] The study highlights lanthanide transitions that are most strongly optically active and therefore are most useful in the study of diagnostic chiroptical probes. The key selection rules that were presented were based entirely on considerations of angular quantum numbers (*S*, *L* and *J*) and parity (Figure 13).

$$\Delta J = 0 \text{ or } \pm 1 \text{ (excluding } J=J'=0) \qquad \Delta L = 0 \qquad \Delta S = 0$$

Figure 13 – Selection rules governing magnetic dipole allowed transitions between perturbed 4*f*-electron states.

It is evident at this point that the selection rules and thus related transitions for large dissymmetry values are not the same as for large CPL intensities. The largest g_{em} values will be exhibited by transitions that are magnetic dipole allowed and electric dipole forbidden, as noted in equation **1.6** (Section 1.2.1). The largest CPL intensities will be displayed by transitions that are magnetic and electric dipole allowed. The transitions in Eu^{3+} and Tb^{3+} complexes that are predicted to display the greatest optical activity are shown in Table 1. This prediction is in agreement with experimental data in each case.[8,10] The largest recorded g_{em} value (+1.38) for a Eu^{3+} complex is associated with the $^7F_1 \leftarrow {}^5D_0$ ($\Delta J = 1$) transition.[52]

Table 1 – Transitions that exhibit high optical activity (the largest rotatory strengths and g_{em} values).

	Electronic Configuration	Transition	E / cm^{-1}	Wavelength / nm
Eu^{3+}	$[Xe]4f^6$	$^7F_1 \leftarrow {}^5D_0$	16700-17100	595
Tb^{3+}	$[Xe]4f^8$	$^7F_5 \leftarrow {}^5D_4$	18000-18500	545
		$^7F_3 \leftarrow {}^5D_4$		

It is also worth noting that no CPL activity should be observed for the $\Delta J = 0$ transition. This transition is purely electric dipole allowed and magnetic dipole forbidden and can be accounted for by the axial crystal field splitting. The electric dipole moment of the transition is of odd parity and so the $^7F_1$ and $^7F_0$ states cannot mix; such mixing would be required in order to create magnetic dipole intensity in the $^7F_0 \leftarrow\!\!- {}^5D_0$ transition.[66]

1.3.3.3. Chiroptical spectra-structure correlations

There is very little literature concerning generalised correlations of lanthanide complex structure with CPL spectral form. For the most part, any conclusions are empirical in nature. The reason for this is not due to the lack of robust theories relating local symmetry to electronic and chiroptical behaviour associated with lanthanide *f-f* transitions, as demonstrated in the preceding section. It may however, be due to the absence of many structurally rigid chiral lanthanide complexes that possess well-defined solution speciation. The majority of the work in this area dates back to the work of Richardson, surrounding spectra-structure correlation of the $\Delta J = 1$ transition of 9-coordinate Eu^{3+} complexes using magnetic and time resolved CPL methods.[67–69] The complexity of analysis has limited the amount of information that can be obtained. However, a number of key observations can be drawn leading to some useful spectra-structure comparisons.

An unpolarised emission spectrum of a lanthanide complex in itself is very useful for basic structural interpretation, as it shows sensitivity to the ligand environment. Europium has a simpler crystal field splitting parameter than terbium, which allows for better interpretation of its luminescence and CPL spectra. For example, in a europium complex the intensity of the hypersensitive electric dipole allowed $^7F_2 \leftarrow\!\!- {}^5D_0$ transition provides information about the polarisability of the donor ligand.[70,71] The magnetic dipole allowed $^7F_1 \leftarrow\!\!- {}^5D_0$ can reveal information concerning the nature of the ligand field and allows the second order crystal field parameter, B_0^2, to be estimated.[72] CPL spectroscopy can provide another level of resolution when compared to the unpolarised emission spectrum. For example, if two peaks are overlapping and not fully resolved in the total emission spectrum, the transitions may have opposite rotatory strength and can be clearly observed in the CPL spectrum. This behaviour is clearly demonstrated in the case of a triphosphinate Eu^{3+} complex, [Eu.$\mathbf{L^3}$], where the $\Delta J = 1$ (~595 nm) and $\Delta J = 4$ (685-720 nm) bands display enhanced resolution in the CPL spectrum (Figure 14).[73]

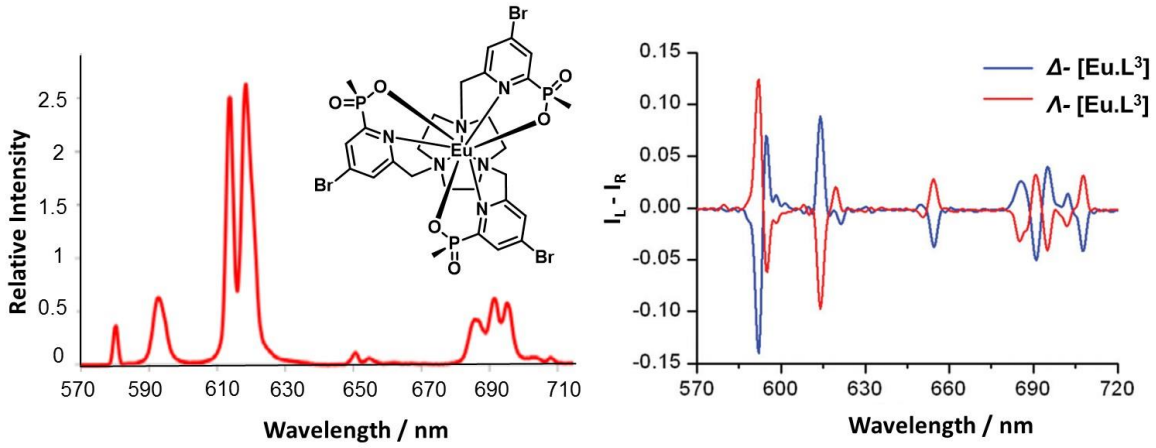

Figure 14 – Total emission (*left*) and CPL spectra (*right*) of *Δ*-[Eu.**L**^{3}] and *Λ*-[Eu.**L**^{3}] (H_2O, 295 K).[73]

The sign of the CPL signal can confirm the relative helicity of the complex, for example, in Figure 14 the CPL spectra of the Δ and *Λ* complexes are mirror images.[73] The calculated dissymmetry factors, g_{em}, can also aid in eliciting structural information. The degree of twist generating the local helicity at a metal centre, determines the angle between the electric and magnetic dipole transition moment vectors and hence the rotatory strength of the transition in a static coupling mechanism. The relative CPL is defined by a sin2θcos2θ function as the CPL associated with the degree of twist at 0º, 45º and 90º must vanish. This effect has been demonstrated for 8 or 9 coordinate antiprismatic complexes based on tri – and tetra-amide DOTA; the angle, θ, that gives the maximum CPL signal (and largest g_{em} value) is 22.5°.[74] The more conformationally rigid tri- and tetra-amide complexes exhibited significantly enhanced CPL activity compared to the bis-substituted equivalent, once again highlighting the importance of conformational rigidity in maximising CPL output.

The structure of CsEu-[(+)-$(hfbc)_4$] reveals a robust coordination cage with eight coordination sites. The square antiprismatic coordination cage is not unlike the lanthanide complexes discussed in the preceding paragraph.[74] However, CsEu-[(+)-$(hfbc)_4$] gives a g_{em} value in the $\Delta J = 1$ transition that is an order of magnitude greater than for the amide complexes. The extraordinary value of g_{em} therefore cannot be due to the geometry of the coordination polyhedron, as had been originally suggested, in terms of a static coupling mechanism (i.e. associated with the value of τ in equation **1.6**, section 1.2.1).[74] Di Bari suggests that the high value may be largely attributed to dynamic coupling involving the diketonate π–π^* transition. The dynamic coupling mechanism describes an electrostatic interaction between an electric multipole, associated with the lanthanide magnetic transition, and the ligand centred electric

dipole, μ. The D_4 symmetry of the complex is broken if μ is skewed. The related dipoles (ligand centred π-π^* transition moment) display a skew angle of $|\psi| = 27°$ (Figure 15), with respect to the main symmetry axis. This value is relatively close to the ideal value of 45° required to induce maximum rotatory strength and maximum polarised luminescence (a $|\psi|$ angle of 0º and 90º describes an achiral situation).[75]

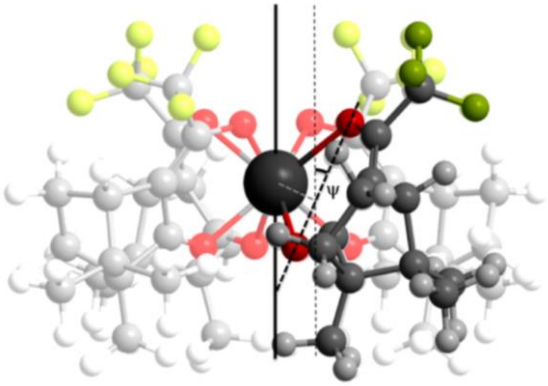

Figure 15 – Calculated solution structure of CsYb derivative, view perpendicular to the D_4 axis showing skew angle, ψ.[75]

The spectra-structure correlations that have been discussed in this section not only allow for determination of the factors that permit enhanced CPL activity and thus aid in probe design, but also allow the resulting CPL spectrum to be related back to the stereochemical structure of the probe in question, in its excited state.

1.4. Lanthanide complexes based on chiral ligands

Lanthanide complexes based on enantiopure ligand systems have been shown to exhibit strong CPL activity and large g_{em} values (section 1.3.3.2). In addition, the lanthanide (III) ions are pure spherical emitters avoiding any associated problems with anisotropy. Considerable progress has been made to develop this class of compounds into optical chirality probes where upon binding of a chiral analyte, there is preferential interaction with one enantiomer or diastereoisomer of the chiral Ln^{3+} complex, resulting in a modulation of the CPL spectrum.

1.4.1. Controlling the chirality of a lanthanide complex: ligand design strategy

There are a number of different approaches that can be adopted in the design of chirally well-defined lanthanide complexes.[8] The chirality of mono- and multi-centre lanthanide complexes may arise from the spatial disposition of multiple, well-defined chiral ligands around the lanthanide centre (Section 1.4.1.1), by the formation of helices (Section 1.4.1.2), or the stereochemical orientation of a multidentate ligand (Section 1.4.1.3). By careful design of an enantiomerically pure ligand, the preferential formation of a particular stereoisomer of the lanthanide complex can be achieved with high levels of stereocontrol.

1.4.1.1. Bidentate β-diketonate ligands

Perhaps the simplest approach is to integrate a chiral ligand into a system, taking advantage of multiple bidentate ligand interactions. Lanthanide β-diketonates, particularly Eu^{3+} complexes, have been exploited for numerous applications as highly luminescent materials displaying excellent emission quantum yields. The ease of preparation and effectiveness of energy transfer to the Ln^{3+} ion contributes to the wide employment of this type of complex in various applications.[76–78] Typically, three bidentate β-diketonate ligands will occupy the inner coordination sphere of the lanthanide ion (coordination number = 6) to generate a neutral complex. This leaves two vacant sites remaining, which can be filled by a Lewis base or an additional bidentate ligand. If the additional ligand is chiral, then stereochemical information can be transferred to the lanthanide ion, generating a chiral complex that exhibits CPL.

An example of this approach was given by Harada and co-workers, in which an axially chiral phosphine oxide ligand, 2,2'-bis(diphenylphosphoryl)-1,1'-binaphthyl (BINAPO), was employed to control the geometry of a europium tris-β-diketonate complex containing 1,1,1,5,5,5-hexa-fluoropentanedione (hfa) ligands (Figure 16).[79] [Eu((*R*)-BINAPO)$(hfa)_3$] displayed an emission quantum yield of 0.53 in CD_3CN solution and strong CPL activity in the $\Delta J = 1$ manifold, which was not present in the corresponding achiral complex. However, the measured g_{em} value was small (0.03).

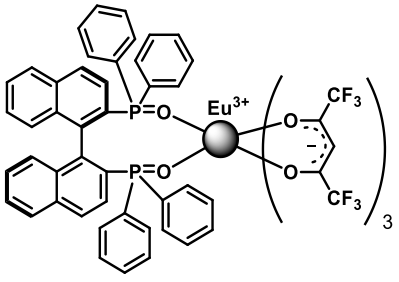

Figure 16 – Chemical structure of [(Eu(*R*)-BINAPO).$(hfa)_3$].[79]

A very similar idea has been documented by Kawai, using an alternative chiral ligand, bis(oxazolinyl)pyridine (pybox), to control the geometry of the resulting europium complex.[80] Three complexes were studied in which slight alterations were made to the chiral ligand structure: [(Eu(*R*)-Ph-pybox).(hfa)$_3$], [(Eu(*R*)-^{i}Pr-pybox).(hfa)$_3$], [(Eu(*R*)-Me-Ph-pybox).(hfa)$_3$] (Figure 17). It was found that the [(Eu(*R*)-Ph-pybox).(hfa)$_3$] complex produced a CPL spectrum with opposite sign in the magnetic dipole allowed transition to the other two complexes studied. The authors used X-ray crystallography to show that the chiral ligand was able to alter the asymmetric arrangement of the hfa ligands around the metal centre, in which the geometry varied depending on the ligand-ligand interactions present. This study successfully highlights the utility of CPL in providing key structural information about the molecule in the excited state. However, no further methods of analysis to assess the structure and speciation of the complex in solution were attempted.

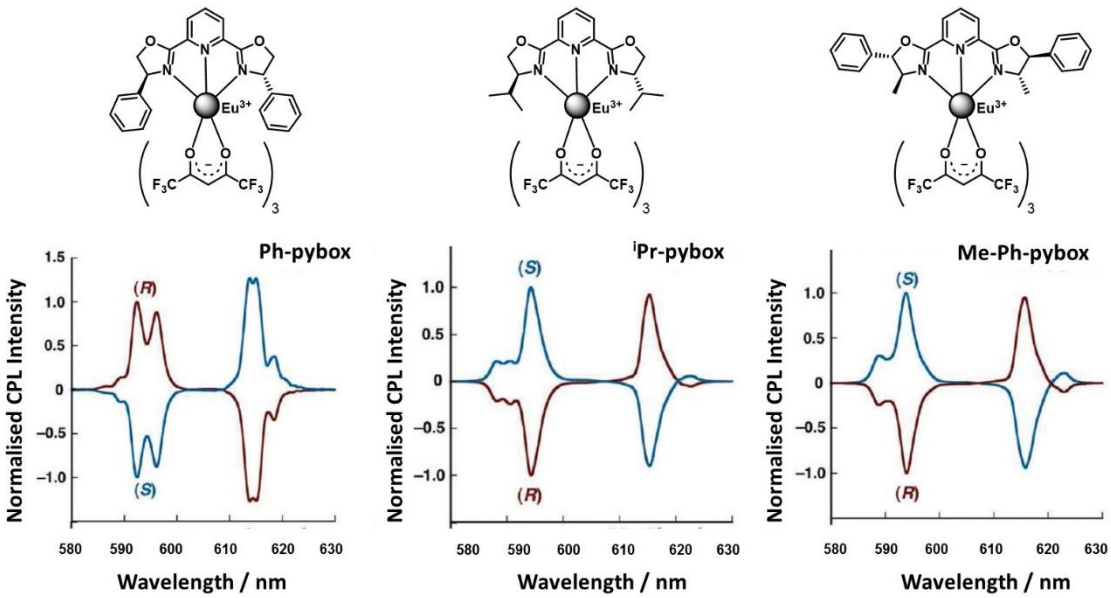

Figure 17 – $\Delta J = 1$ transition of the CPL spectra of *R*- and *S*-[(Eu-Ph-pybox).(hfa)$_3$], [(Eu-^{i}Pr-pybox).(hfa)$_3$] and [(Eu-Me-Ph-pybox).(hfa)$_3$] (*left* to *right*).[80]

The optical chirality of lanthanide complexes with β-diketonate camphor ligands (hfbc) has also been extensively studied, incorporating ligands with axially chiral phosphine oxide ligands,[81] pybox ligands[82] and in the synthesis of $M^I[Ln((+)\text{-hfbc})_4]$.[52] CPL sign reversal has been observed for a Eu^{3+} camphorate complex containing the bidentate ligand, 3,3-bis(diphenylphosphoryl)-2,2-bipyridine (BIPYPO).[83] The sign reversal was attributed to the

hinge-like twisting of the bidentate ligand, resulting in dynamic *cis-trans* isomerism of the chiral Eu^{3+} complex in various solvent systems.

1.4.1.2. Triple stranded helicates

Simple linear oligo-multidentate ligands self-assemble with Ln^{3+} ions to produce stable mono- and di-nuclear triple stranded helicates. The systems are inherently chiral but exist as a rapidly interconverting mixture of *Δ* and *Λ* conformers.[84] One helical enantiomer can be preferentially stabilised by the incorporation of a chiral substituent at some point along the multidentate ligand, resulting in a net diastereomeric excess and a system that exhibits CPL.

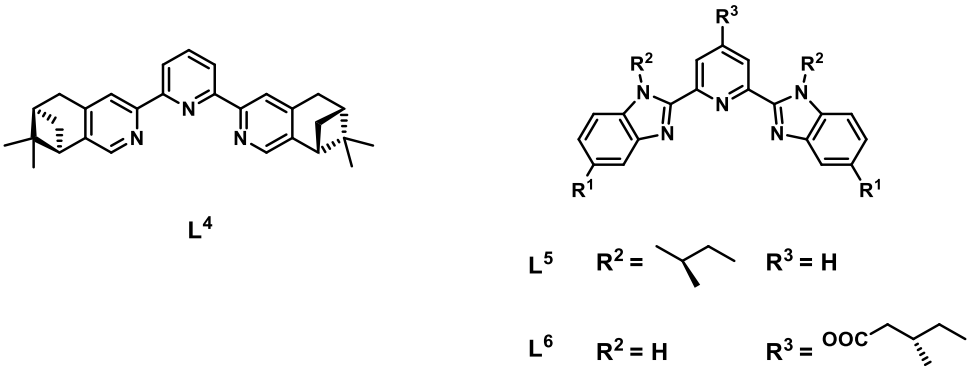

Figure 18 - Structures of C_2 symmetric and chiral neopentyl derived ligands for the preparation of enantiopure triple stranded helicates.[85,86]

Initial work by von Zelewsky and Bünzli defined the first example of diastereoselective formation of a lanthanide triple helical complex, based on an enantiopure *C2* symmetric ligand, **L4**.[85] Bünzli also investigated a series of lanthanide complexes based on chiral tridentate bis(benzimadazole)pyridine ligands with different substituents at the R^2 and R^3 positions, Figure 18.[86–88] Introduction of a chiral neopentyl group at the R^3 position, **L6**, led to the formation of a thermodynamically stable triple helical complex, $[Ln.(\mathbf{L^6})_3]^{3+}$. CPL studies confirmed the helical wrapping of the ligand around the metal centre and a small diastereomeric excess in solution. On the contrary, incorporation of the bulky chiral moiety at the R^2 position, **L5**, precludes helical wrapping around the lanthanide ion. X-ray crystal analysis revealed that only two of the ligands can effectively wrap around the metal centre, with the third ligand lying perpendicular to the other two. The interaction between the ligand and the Ln^{3+} ion can be quantified by UV-Vis and ^1H NMR data. The interactions between **L6** and Eu^{3+} are stronger than those with **L5** and Eu^{3+}, as indicated by the stability constants where $\Delta\log K_3(\mathbf{L^6}\text{-}\mathbf{L^5}) = 3.7$.[88]

The ease of which dipicolinic acid (dpa) ligands can be synthetically modified has led to another set of lanthanide supramolecular structures that have been developed incorporating this useful moiety. Bünzli and co-workers have investigated the influence of a chiral moiety in the 4-position of the pyridine ring of dipicolinic acid upon assembly with Eu^{3+}.[87] The ^1H NMR data suggests that there is one main $M.L_3$ species present in solution on an NMR timescale with overall trigonal symmetry. However, the chiroptical data suggests otherwise and implies fast interconversion of the enantiomeric helices, and only a small diastereomeric excess in solution. The CPL activity of these complexes was very weak with only small g_{em} values calculated (g_{em} = 0.02 at ~ 590 nm). The weak CPL activity can also be attributed to the presence of the $M.L_2$ species (~8%), evident from the calculated stability constants, which is expected to generate a much smaller chiral effect.

A more promising method of inducing diastereomeric resolution of 9 coordinate triple helical lanthanide complexes using chiral dpa ligands has been demonstrated by Muller *via* inclusion of a chiral centre directly on the amide group.[89] The enantiomers of *N,N'*-bis(1-phenylethyl)-2,6-pyridinedicarboxamide ((*R,R*) and (*S,S*)) were shown to effectively self-assemble with Ln^{3+} ions and induce the resulting helicity in the lanthanide complex ((*R,R*) =*Λ* and (*S,S*) =*Δ*). The main drawback of this class of compounds is the relatively small luminescent quantum yields, consistent with poor efficiency of the sensitisation by the ligand (ϕ_{em} = 0.01 for $[Eu.(\mathbf{L^1})_3]^{3+}$). However, the ability of the ligand to induce *Δ* and *Λ* helicity in the complex has led to strong CPL activity and suggested the application of these complexes as CPL calibration standards (section 1.2.4.).[23]

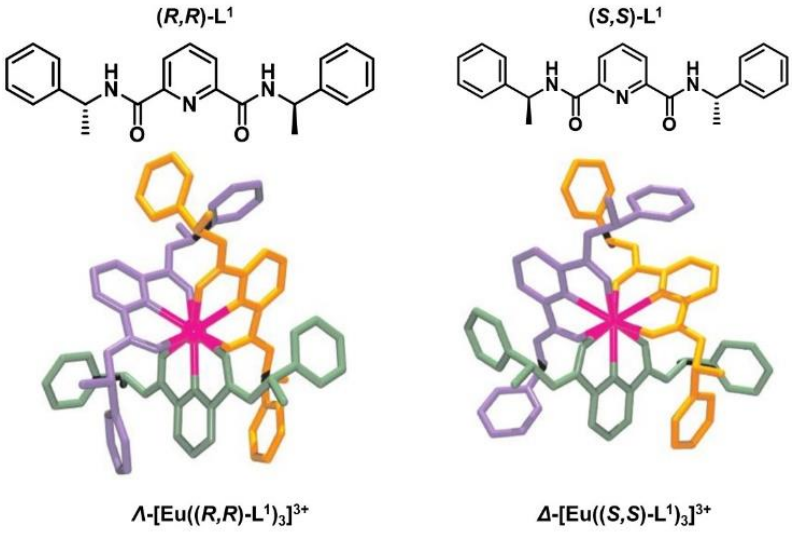

Figure 19 – Structures of (*R,R*)-$\mathbf{L^1}$ and (*S,S*)-$\mathbf{L^1}$ and their *Λ* and *Δ* europium complexes respectively.[89]

The group of Gunnlaugsson has developed a similar range of dpa derivatives.[90,91] Chiral 1-naphthyl, $\mathbf{L^7}$, and 2-naphthyl, $\mathbf{L^8}$, derivatives of dipicolinic acid were shown to self-assemble with Eu^{3+} ions, generating an enantiopure triple stranded helical complexes in a 1:3 metal to ligand ratio. The use of CPL spectroscopy established the chiral nature of the complexes, confirming that it is the chirality of the amide centre that dictates the absolute configuration of the resulting complex, (*R*,*R*) =*Λ* and (*S*,*S*) =*Δ*. X-ray crystallography was used to investigate the solid state structure of the two sets of complexes. The data revealed that the 1-naphthyl complex, [Ln.$(\mathbf{L^7})_3$], is more tightly packed compared to the 2-naphthyl complex, [Ln.$(\mathbf{L^8})_3$], due to enhanced *π*-*π* stacking interactions. The greater conformational rigidity may account for the improved total luminescence and CPL activity of this complex.

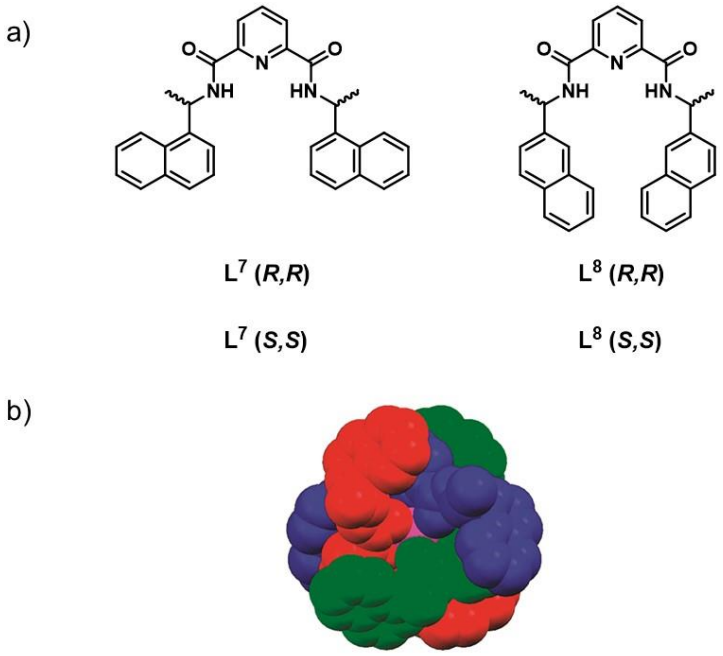

Figure 20 – a) Ligands $\mathbf{L^7}$ and $\mathbf{L^8}$ ((*R*,*R*) and (*S*,*S*)). b) X-ray crystal structure of (*R*,*R*)-[Nd.$\mathbf{L^7}$] down the crystallographic c axis, showing the helical arrangement of the three ligands around the Nd^{3+} centre (*pink*).[91]

Further work investigated a dinuclear system based on a 1-naphthyl antenna, $[Eu_2.(\mathbf{L^9})_3]$ (Figure 21).[92] The stereochemical configuration was investigated by ^{1}H NMR studies and CPL spectroscopy. The results implied that the absolute configuration was once again determined by the chirality at the amide centre, generating complexes of the same helicity as the corresponding monomers, i.e. (*R*,*R*) =*ΛΛ* and (*S*,*S*) =*ΔΔ*.[91]

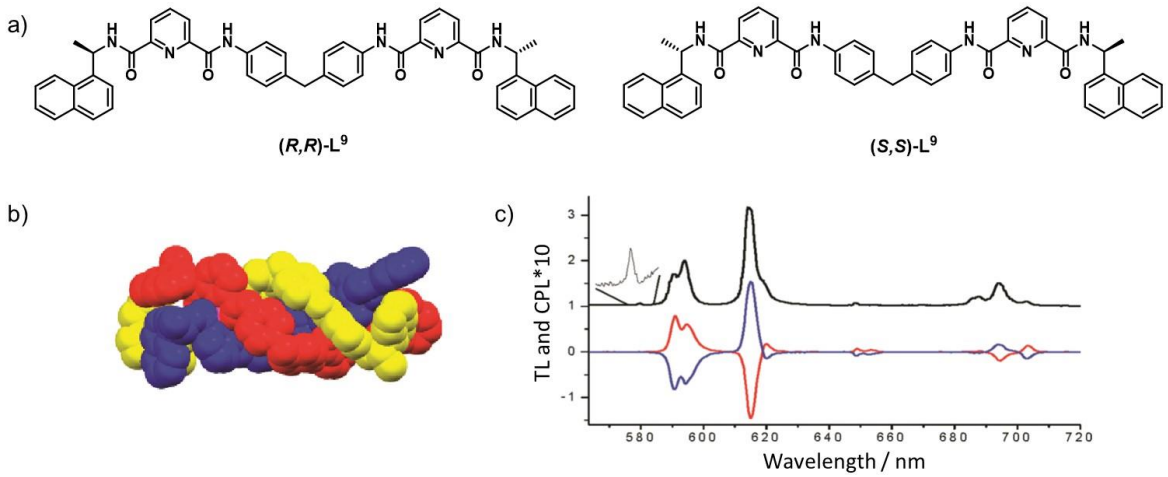

Figure 21 – a) Structures of ligand $\mathbf{L^9}$ (*R*,*R*) and (*S*,*S*). b) Model of triple stranded helicate [Eu_2.($\mathbf{L^9}$)$_3$]. c) Total luminescence of (*S*,*S*)-[Eu_2.($\mathbf{L^9}$)$_3$] (*black*) and CPL spectra for (*R*,*R*)-[Eu_2.($\mathbf{L^9}$)$_3$] (*blue*) and (*S*,*S*)-[Eu_2.($\mathbf{L^9}$)$_3$] (*red*) in MeOH.[92]

The stereoselective self-assembly of chiral luminescent Eu^{3+} tetrahedral cages has recently been reported employing ligands based on dpa.[93] The chirality of the ligand is transferred to the metal generating [Eu_4.($\mathbf{L^{10}}$)$_6$] and [Eu_4.($\mathbf{L^{11}}$)$_4$] species with *Δ* and *Λ* chirality, Figure 22, (*R* =*Λ*, *S* = *Δ)*. Solution CD data was able to confirm the stereochemistry of the complexes in agreement with X-ray crystal data and shows that the complexes derived from *R* and *S* ligands are enantiomeric. No CPL data has been reported for this set of luminescent europium tetrahedral cages, probably because the naphthyl excited state is quenched by the Eu^{3+} ion in an electron transfer process. However, there are a number of other well-defined examples of luminescent lanthanide *f-f* supramolecular structures that give rise to CPL including a heptanuclear europium wheel[94] and lanthanide directed interlocked structures.[95]

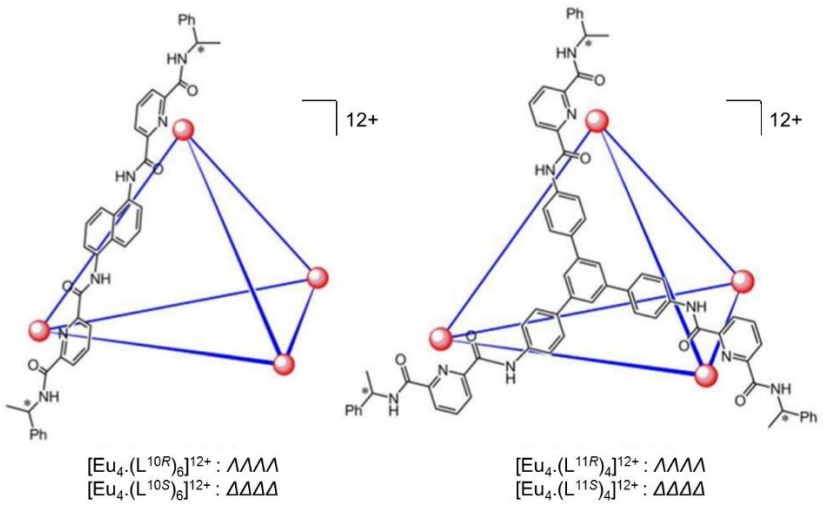

Figure 22 - Europium coordination tetrahedral cages with both [Eu_4.($\mathbf{L^{10}}$)$_6$] and [Eu_4.($\mathbf{L^{11}}$)$_4$] stoichiometries. (Eu^{3+} ions at the four vertices are drawn as red spheres; only one ligand is shown on each tetrahedron).[93]

1.4.1.3. Multidentate macrocycles and podates

The final approach that will be discussed here is the stereochemical orientation of multidentate macrocyclic and podate ligands. When designing a chiral lanthanide probe, it is necessary to examine complexes with well-defined solution speciation so that correlations of structure with spectral form can be confidently made. One of the best ways to achieve this is to design relatively rigid systems, for example, those based on a macrocycle such as cyclen (12-N_4)[96–99] or 1,4,7-triazacyclononane (9-N_3)[100–102], in which the twist of the macrocyclic arms around the lanthanide centre generates a lanthanide complex with well-defined *Δ* and *Λ* helicity. The second element of chirality is associated with the sign of the torsional angle of the ethylene backbone (NCCN) of the macrocyclic ring, resulting in *δ* and *λ* chirality.[49] Thus, four stereoisomers can be obtained in each case. A more detailed description of the chirality of 9-N_3 systems will be discussed in Chapter 2.

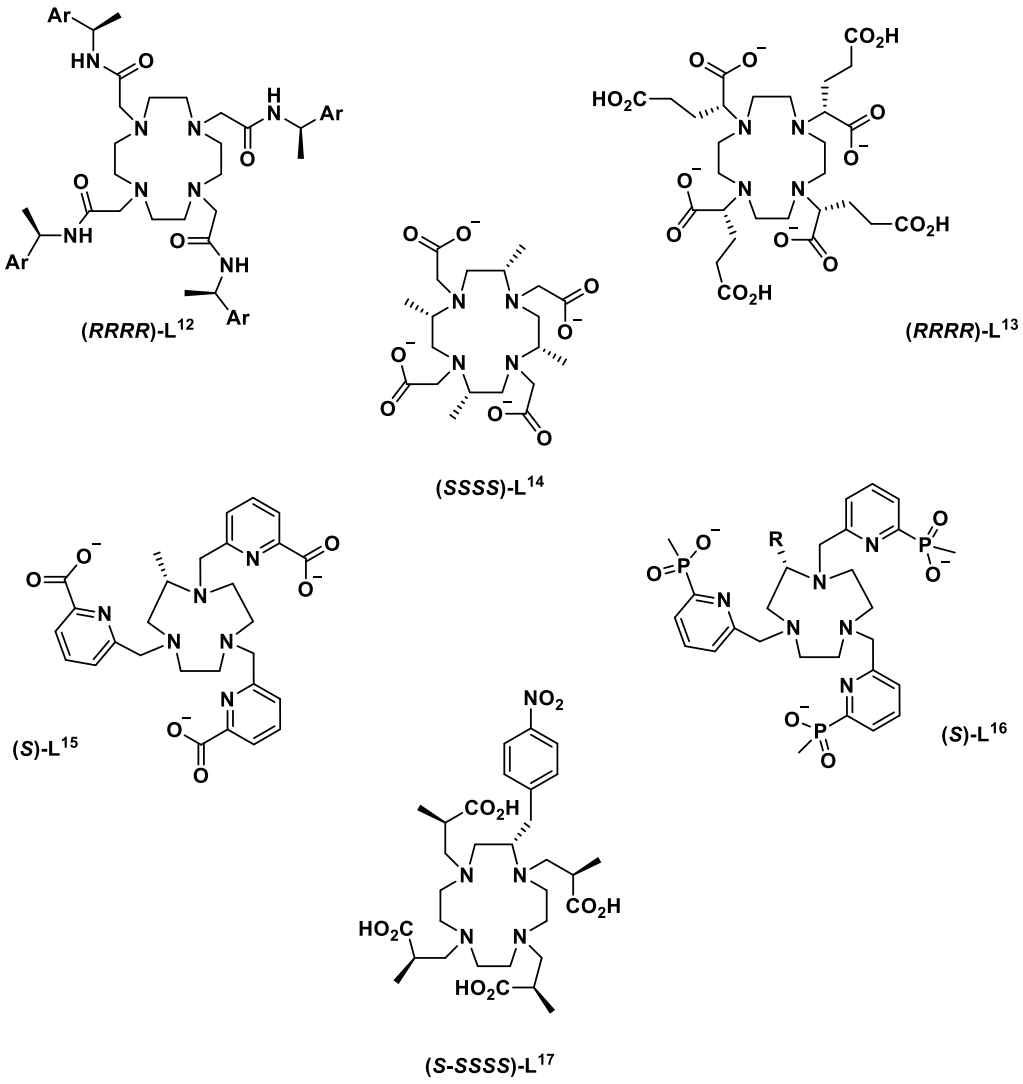

Scheme 3 - Representative macrocyclic ligand structures incorporating a remote stereocentre on the pendant arm and through C-substitution on the macrocyclic ring.[73,103–106]

A remote chiral centre can be incorporated into the pendant arms of the ligand framework in order to restrict arm rotation. For example, in the series of enantiopure tetraamide-cyclen based ligands, **L**[12], investigated by Parker et al., in which the remote chiral centre of the amide dictates the helicity of the complex, resulting in the formation of one predominant stereoisomer of the lanthanide complex in solution, (*RRRR*)-*Λ* and (*SSSS*)-*Δ*.[103] The sense of chiral induction is the same that was seen in the triple helicate complexes of Muller[89] and Gunnlaugsson.[91] It has also been demonstrated that integration of an α-substituent on the acetate arm of 1,4,7,10-tetraazacyclododecane-1,4,7,10-tetraacetic acid **(**DOTA) can 'sterically lock' the conformation of the pendant arms in the lanthanide complex, e.g. **L**[13].[104]

Another way to control the chirality of the resulting complex is to inhibit ring inversion through incorporation of a C-substituent directly on the macrocyclic ring, generating a stereogenic centre. Desreux demonstrated that incorporation of methyl groups onto a DOTA backbone resulted in the prevalence of a major stereoisomer upon complexation, **L**[14].[105,107] ^{1}H NMR studies showed that the methyl groups prefer to adopt an equatorial position, thereby locking the ring conformation. Thus, (*SSSS*)-[Yb.(Me_4DOTA)] exists only as *Δ*-(*λλλλ*) and *Λ*-(*λλλλ*) isomers with the former being favoured in a 1:0.095 ratio. A more recent study by Parker has also shown that C-substitution on the ring induces formation of a single enantiomer of a complex with >96% isomeric purity, this time for mono-substitution of a 9-N_3 ligand, e.g. **L**[15] and **L**[16].[60,73] The absolute configuration of each complex was determined by the stereogenicity of the C-substituent and was assigned by comparative CPL studies, examining the sign and relative magnitude of each transition (*S* at C gives *Λ*, *R* at *C* gives *Δ*).

One may envisage that combining these two approaches, incorporating both a chiral substituent on the pendant arm and a C-substituent on the macrocyclic ring, would provide optimal stereocontrol and formation of only one isomer, **L**[17].[106] The coordination isomer that was obtained was determined by the chirality at each stereogenic centre. For example, HR-NMR spectroscopy revealed that the *S-RRRR* complex had SAP (square antiprism) geometry (*Δ*-(*λλλλ*)), and the *S-SSSS* complex had TSAP (twisted square antiprism) geometry (*Δ*-(*δδδδ*)). However, a number of COSY experiments later revealed the presence of two possible regioisomers for each coordination geometry, as there are two non-equivalent positions where the C-substituent can be located.[108]. The *p*-nitrobenzyl substituent can either be located on the corner or the side of the macrocyclic ring. Therefore, two possible regioisomers can be produced for each SAP/TSAP geometry depending upon the direction of approach of the metal ion and the conformation of the ligand at the time of reaction.

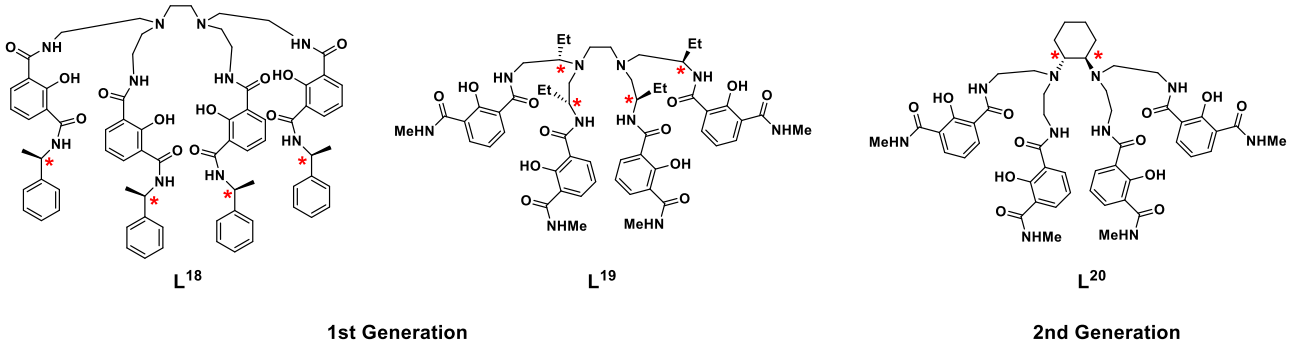

Figure 23 – Ligands based on 2-hydroxyisophthalamides (IAM). * highlights the stereocentres in 1st generation complexes (sensitiser) and second generation complexes (ligand backbone).[109–111]

Another class of multidentate ligands that can be used to effectively sensitise lanthanide ions (Eu^{3+}, Tb^{3+}, Dy^{3+} and Sm^{3+}) and transmit chirality to the resulting complex are based on the octadentate podate structures of Raymond and co-workers (Figure 23).[109,110] The chiral moiety is introduced into the sensitiser, 2-hydroxyisophthalamide (IAM), onto the open face of the tetrapodal ligand framework, **L**^{18} and **L**^{19}. The stereocentre transfers chiral information to the ligand influencing the helical sense that the arms wrap around the metal centre (1st generation complexes). The resulting complexes exhibit good complementarity in the CPL signals between *R*(+) and *S*(-) enantiomeric forms. The measured g_{em} value at 543 nm for the first generation complex [Tb.**L**^{18}] is +0.044. Unfortunately, the coordination and geometry mode of these complexes remains undetermined, and it is clear from the number of observed bands in the magnetically allowed $\Delta J = 1$ transition of the europium complex, that there exists more than one major emissive species in solution. Further work saw the development of a second generation of complexes based on a different strategy where the stereogenic moiety, diaminocyclohexane or diphenylethylenediamine, was incorporated into the ligand backbone to create a complex with increased conformational rigidity (2nd generation complexes).[111] Iterations employing an alternative sensitiser for europium, 1-hydroxy-2-pyridinone (1,2-HOPO), have also been reported with the aim to improve water solubility of the complexes.[112,113] The second generation complex, [Tb.**L**^{20}]$^{3+}$, displays a high quantum yield, ϕ_{em} 0.60, and improved CPL signal strength, g_{em}(542 nm) = +0.20, in aqueous solution. Luminescent lifetime and NMR data suggests that there is one dominant diastereoisomer present for these more conformationally rigid systems.

1.4.2. Chiral lanthanide complexes as responsive probes

Reversible anion binding in aqueous media has become an effective means of signalling and sensing the presence of selected anions.[5] Particular consideration needs to be given to the target anion binding affinity and the manner in which selectivity over competing species is to be achieved. Well-defined lanthanide complexes are particularly suited to this application, as they are relatively stable in aqueous solution and the binding event can be studied using NMR, microscopy, chiroptical and emission based techniques.[114] Anion binding often accompanies the displacement of metal bound water molecules. An increase in the luminescent lifetime, τ, is expected since closely diffusing O-H oscillators are known to quench the lanthanide excited state (section 1.3.3.1). The $\Delta J = 2$ and $\Delta J = 4$ bands are hypersensitive to change in the lanthanide coordination environment. Such behaviour allows for ratiometric analysis as the intensity of the hypersensitive band can be monitored compared to a magnetically dipole allowed transition, that shows little change to the environment allowing internal calibration. Chirality probes based on enantiopure lanthanide complexes are therefore endowed with an intrinsic CPL fingerprint that can be modified in relative intensity, shape and sign on interaction with a target analyte.[49,50]

1.4.2.1. Lanthanide probes to target oxyanions

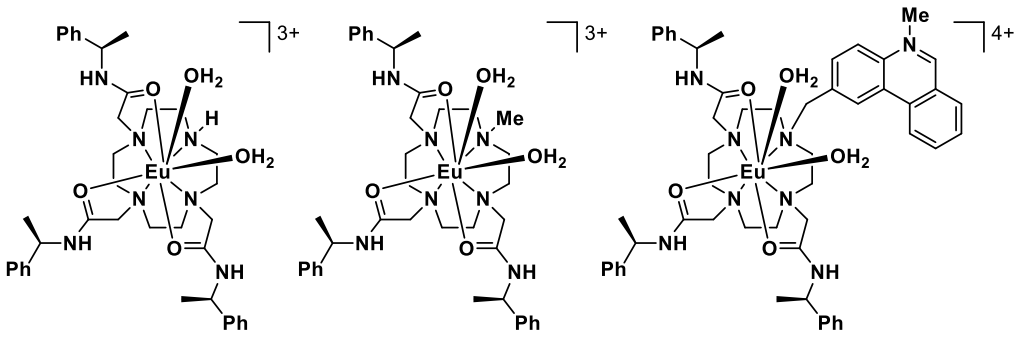

(*RRR*)-Λ-[Eu.**L**^{21}]$^{3+}$ (*RRR*)-Λ-[Eu.**L**^{22}]$^{3+}$ (*RRR*)-Λ-[Eu.**L**^{23}]$^{4+}$

Scheme 4 – Structures of Eu^{3+} complexes used in the signalling of a number of oxyanions.[115]

An early example of a responsive chirality probe saw the employment of the enantiopure triamide complex, [Eu.**L**^{21}]$^{3+}$, in the sensing of a number of oxyanions.[116] In aqueous solution, excited state lifetime measurements in H_2O and D_2O allowed the inner sphere hydration

number to be measured.[117] Two metal bound water molecules were found to be present within the inner coordination sphere. Addition of bicarbonate HCO_3^- (pH 6.5) and carbonate CO_3^{2-} (pH 11) to [Eu.**L**^{21}]$^{3+}$ led to a large increase in the overall emission intensity and an increase in the excited state lifetimes. The luminescence data suggested that both metal bound water molecules were displaced and the anion was bound as a chelate (Scheme 5). A marked change in the CPL spectrum was also observed, particularly in the ΔJ = 1 manifold. The original hypothesis attributed the change to an alteration in the helicity of the complex. However, subsequent studies quickly determined that it was due to the change in polarisability of the axial donor.[118] It is worth noting that phosphate, HPO_4^{2-}, was found to bind to [Eu.**L**^{21}]$^{3+}$ in which a monoaqua species was formed, with phosphate acting as a monodentate ligand.

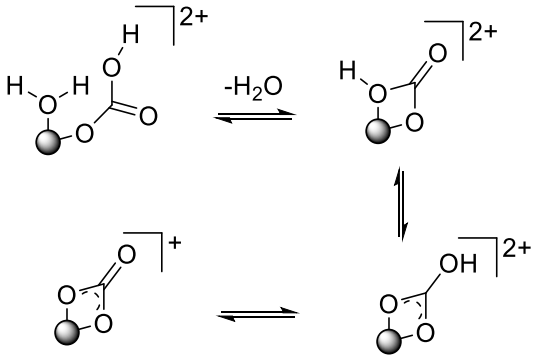

Scheme 5 – Diagrammatic representation of carbonate binding to a lanthanide centre *via* displacement of two metal bound water molecules.[116]

The synthesis of related *N*-alkylated derivatives, [Eu.**L**^{22,23}]$^{3+}$ (*N*-Me, *N*-methylphenanthridinium group), allowed further expansion of the scope of this lanthanide probe.[115] Strong binding affinities, *K*, for CO_3^{2-}/HCO_3^-, lactate, citrate and malonate were calculated for the *N*-alkylated complex, [Eu.**L**^{22}]$^{3+}$. Changes in the intensity of the ΔJ = 2 and ΔJ = 1 bands were followed as a function of added anion concentration. The resulting binding isotherms were fitted to a 1:1 binding model by linear least squares iterative analysis. Citrate and malonate exhibited the largest binding affinities due to the increased negative charge on the analyte. The interaction of carbonate with [Eu.**L**^{23}]$^{4+}$ (*N*-methylphenanthridinium group) in a competitive anionic background was also studied. The reversible anion binding could be signalled by emission spectral changes as discussed previously, and also by changes in the circular polarisation of emission (Figure 24). The emission spectral changes were consistent with carbonate binding, suggesting high selectivity for the chosen analyte.

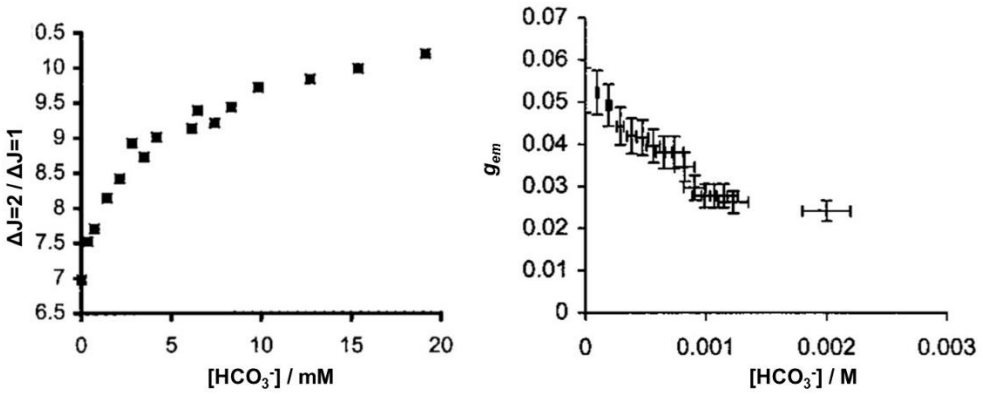

Figure 24 – *left*: variation in the $\Delta J = 2$ / $\Delta J = 1$ bands in the total emission spectrum, *right*: variation in emission dissymmetry value, g_{em} for [Eu.**L**^{23}]$^{4+}$ as a function of added $NaHCO_3$ (1.5 mM complex, 0.1 M collidine/HCl buffer, pH 7.4, 100 mM NaCl, 0.9 mM Na_2HPO_4, 0.13 mM sodium citrate, 2.3 mM sodium lactate).[115]

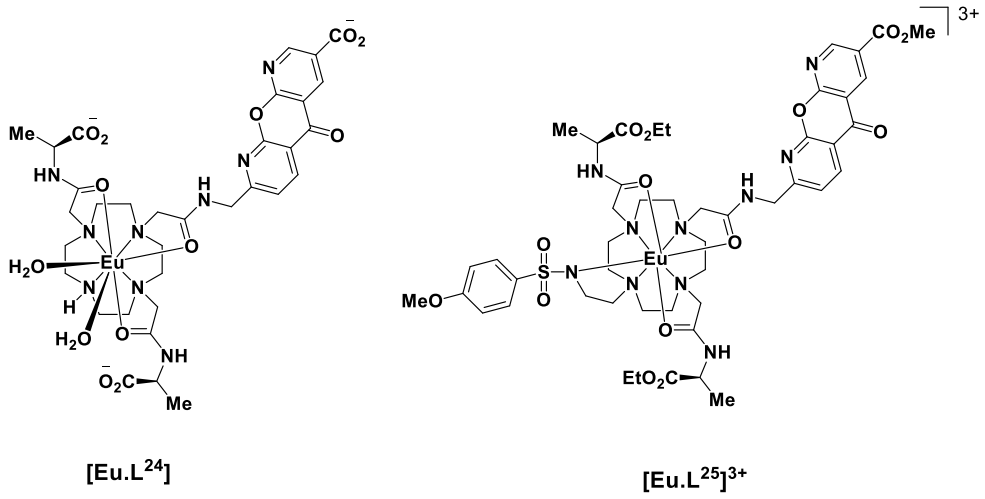

Scheme 6 – Structures of Eu (III) complexes bearing azaxanthone chromophores.[119,120]

A more recent example has used Eu^{3+} and Tb^{3+} complexes bearing an azaxanthone sensitiser, [Eu.**L**^{24}], to estimate equilibrium bicarbonate concentrations inside the mitochondrial region of living cells and in neat human serum, using emission spectroscopy.[119] The enantiopure lanthanide complexes can also signal reversible binding of bicarbonate in the presence of endogenous anions, by distinctive modulation of the CPL spectrum. Addition of a weakly bound sulfonamide arm to the complex, [Eu.**L**^{25}]$^{3+}$, allowed the pH change of the system to be monitored by CPL.[120] At high pH values, the sulfonamide arm is bound to the metal centre generating a conformationally rigid structure with a high g_{em} value. As the pH is decreased, the sulfonamide arm protonates and dissociates, and the g_{em} value decreases accordingly. A plot of pH *versus* g_{em} generates a pH curve from which a pK_a value of 5.65 was calculated (Figure 25).

This value is in agreement with that estimated by emission spectroscopy. This study demonstrates the first example of the use of CPL modulation to signal pH variation.

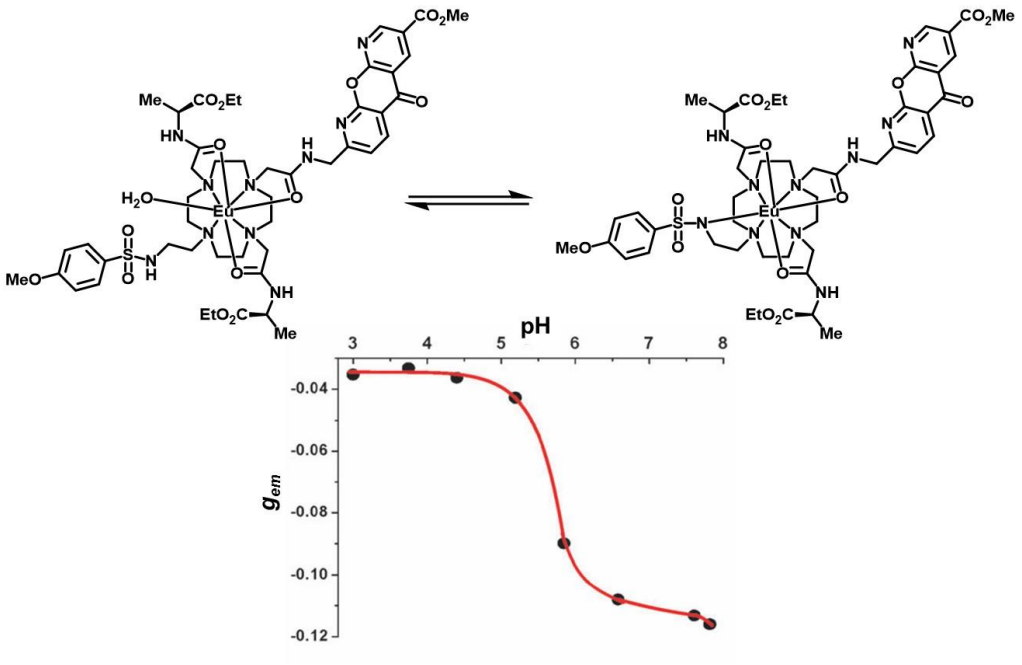

Figure 25 – Variation of g_{em} (632 nm) with pH for [Eu.**L**^{25}]$^{3+}$ showing the fit to the observed data (pK_a = 5.65 ± 0.04, 295 K, 0.1 M NaCl).[120]

The family of anions based on pentavalent phosphorus, notably *O*-phosphorylated amino acids and peptides is of particular interest in biological applications. One such application is the signalling of the behaviour of *O*-phosphono-*L*-tyrosine (*O*-P-Tyr) sites on a protein. The same series of chiral macrocyclic lanthanide complexes based on a heptadentate ligand framework have been employed to probe this class of molecules, [Eu.**L**^{21}]$^{3+}$ and [Eu.**L**^{22}]$^{3+}$.[121] ^{1}H NMR, emission and CPL spectroscopy were employed to assess the binding interactions and a number of conclusions can be drawn from this work. Chemoselective ligation of the phosphate moiety, over the terminal amino acid residue, was observed for Eu^{3+} complexes. Such behaviour was in contrast to that observed for Tm and Yb complexes, where *N*-ligation through the terminal amino acid was shown to occur. A significant preference for *O*-P-Tyr binding compared to other phosphorylated amino acids (30:1) was observed, most likely due to the decreased hydration energy of the amino acid. The emission dissymmetry values did not vary significantly and were typically calculated at ±0.06 for the most polarised transitions in each case. However, the form of the emission and CPL spectra differed significantly between the

non-alkylated, [Eu.**L**^{21}]$^{3+}$, and *N*-alkylated, [Eu.**L**^{22}]$^{3+}$ complexes, on addition of the chiral phosphate anion.

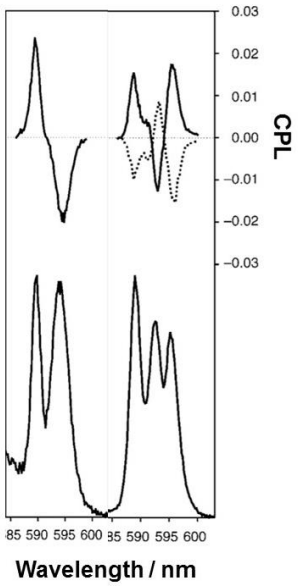

Figure 26 – CPL (*top*) and emission spectra (*bottom*) of: *left* - (*SSS*)-*Δ*-[Eu.**L**^{21}]$^{3+}$, *right* - (*SSS*)-*Δ*-[Eu.**L**^{22}]$^{3+}$ (*dashed*) and (*RRR*)-*Δ*-[Eu.**L**^{22}]$^{3+}$ (*bold*) on the addition of 10 equiv. *O*-P-Tyr (0.1 M MOPS, pH 7.4).[121]

1.4.2.2. Lanthanide probes to target DNA

Focussing on the same 12-N_4 ligand framework, enantiopure Ln^{3+} triamide complexes bearing an *N*-methylphenanthridinium chromophore, [Ln.**L**^{23}]$^{4+}$, have been employed in the sensing of oligonucleotides and calf thymus DNA (CT-DNA).[122–124] The lanthanide coordination environment and helicity remained unchanged upon binding of DNA but distinctive selectivity in affinity was observed between the *Δ* and *Λ* isomers. [Eu.**L**^{23}]$^{4+}$ binds to DNA *via* reversible ligation of the nucleotide phosphate group, as determined by comparison of the emission spectrum to the spectral changes on addition of hydrogen phosphate. In the bound form, the luminescence of the complex was significantly quenched by a rapid charge-transfer mediated deactivation of the chromophore S_1 state by the electron-rich base pairs. This behaviour prohibited any further studies with this particular chromophore.

Later studies investigated a series of lanthanide complexes incorporating an alternative tetraazatriphenylene chromophore.[125,126] Exciton-coupled naphthyl groups and a tetraazatriphenylene sensitiser allowed for efficient intramolecular energy transfer, leading to population of the naphthyl triplet state.[126] Addition of poly(dGdC), poly(dAdT) and CT-DNA to [Eu.**L**^{26}]$^{3+}$ led to a significant increase in the intensity and lifetime of the emission (Figure

27). The increase in emission lifetime upon DNA binding is indicative of the deactivation of a process that quenches the Eu^{3+} excited state. However, the complexity of the photophysical processes occurring, competing with Eu emission, limited the amount of structural information that could be gathered.

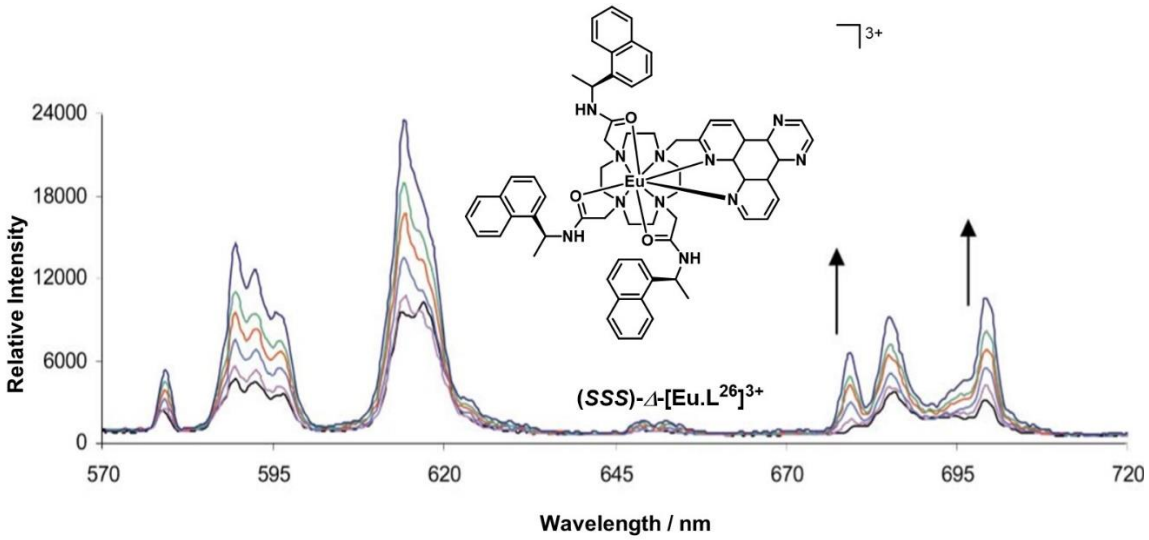

Figure 27 – Changes in europium emission spectrum of [Eu.$\mathbf{L}^{\mathbf{26}}$]$^{3+}$ on addition of poly(dGdC), 0.8 mM, from 0 to 1 base-pair per complex (λ_{exc} = 340 nm, pH 7.4, 10 mM HEPES, 10 mM NaCl).[126]

1.4.2.3. Lanthanide probes to target proteins

An alternative mode by which a lanthanide complex can function as a responsive chirality probe is through concerted arm rotation or rearrangement of the coordination polyhedron as a result of non-covalent interactions. The first report of dynamic helicity inversion following enantioselective analyte binding involved the enantioselective regulation of a lanthanide complex, following reversible binding to serum albumin.[127] Incremental addition of human (or bovine) serum albumin to (*SSS*)-*Δ*-[Tb.$\mathbf{L}^{\mathbf{27}}$]$^{3+}$ led to a reduction in the intensity and lifetime of the terbium luminescence. An apparent 1:1 binding constant was calculated, log*K* = 5.1, in aqueous solution. A very different response was observed for (*RRR*)-*Δ*-[Tb.$\mathbf{L}^{\mathbf{27}}$]$^{3+}$, consistent with a much lower affinity constant. Arguably the most interesting information was derived from the CPL behaviour. With the (*RRR*)-*Δ* isomer, no change in the emission polarisation was observed upon adding excess protein. However, in the case of the (*SSS*)-*Δ* complex, an inversion in the sign of the CPL spectrum was evident (Figure 28). Such behaviour is consistent with the inversion of complex helicity in the protein-bound complex. Taken together, this

information suggests the selective binding of *Δ*-[Ln.**L**^{27}]$^{3+}$ to 'drug site II' of serum albumin *via* concerted arm rotation ((*SSS*)-*Δ* → (*SSS*)-*Λ*).[128]

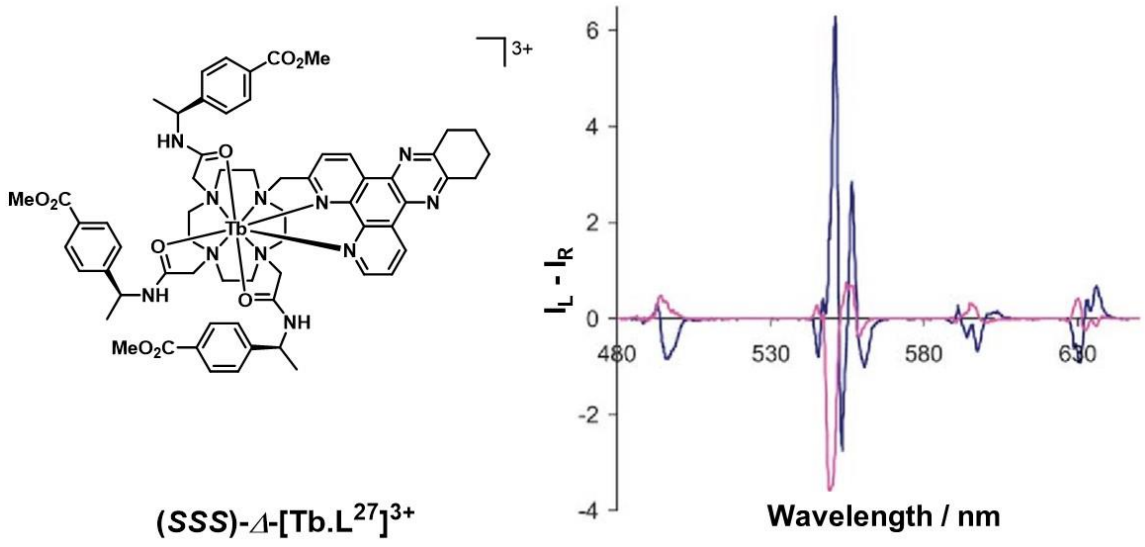

Figure 28 – Structure of and CPL spectra of (*SSS*)-*Δ*-[Tb.**L**^{27}]$^{3+}$ (*blue*) and in the presence of added BSA (*pink*) (295 K, D_2O, λ_{exc} = 348 nm, 15 μM complex, 30 μM protein).[127]

More recently, a completely different approach has been adopted by Yuasa and co-workers.[129] The fingerprint CPL signatures were recorded for a 1-biphenyl-3-perfluoroethyldiketonate Eu^{3+} complex covalently bound to various proteins, including Staphylococcus aureus recombinant nuclease A, BSA and insulin. The protein itself serves to fill the coordination sphere of the β-diketonate Eu^{3+} complex, providing an asymmetric environment within the inner coordination sphere. The authors claim that an optical fingerprint for target proteins can be recorded using this method, as well as the ability to monitor protein conformational change. However, the CPL intensity and g_{em} values are very small (g_{em} ± 0.005 – 0.05) and there is a lack of discussion regarding the nature of the binding interaction. This system is not particularly well-defined and the results are more observational in nature than previous examples that have been discussed.

1.5. Lanthanide complexes based on achiral ligands

Lanthanide complexes based on achiral ligands can also be employed as responsive CPL probes. In contrast to the enantiopure systems that have been discussed where a modulation of

the CPL is monitored, for achiral lanthanide systems an induced CPL response can be recorded following the addition of a chiral species.

1.5.1. Dynamically racemic CPL probes

It is assumed that in the absence of any other effects, the perturbation of the racemic equilibrium of the ground state *via* outer sphere non-covalent interactions, will be reflected in the excited state, leading to induced optical activity. Therefore, it is expected that the effect of adding a chiral biomolecule results in the preferential stabilisation of the more energetically favourable diastereomeric outer-sphere association complex. This phenomenon is termed the Pffeifer effect.[130] Much of the early work by Brittain, Richardson and Riehl focuses on the *Δ* / *Λ* equilibrium of dynamically racemic D_3 lanthanide complexes (Figure 29). The addition of a variety of chiral additives including amino acids,[131,132] sugars[133,134] and chiral carboxylic acids,[135] has been extensively reviewed.[49,50,136,137] The induction of a CD signal from dynamically racemic D_3 lanthanide complexes based on 2,2'oxydiacetic acid (oda) ligands has also been demonstrated, following the addition of the chiral additive *L*-proline.[138] Contrary to early studies that assumed the 'Pfeiffer effect' is a direct consequence of the absolute configuration of the added chiral species, later studies have shown that the explanation is not quite so simple in every case. More recently, the effect of various non-covalent chiral interactions such as hydrogen bonding, Coulombic forces, π-stacking, hydrophobic and steric effects on the CPL sign and magnitude have been investigated.[139] However, the sign and magnitude of CPL has still shown no meaningful correlation to any specific structural characteristics, and the results of these studies tend to be mainly observational in nature.

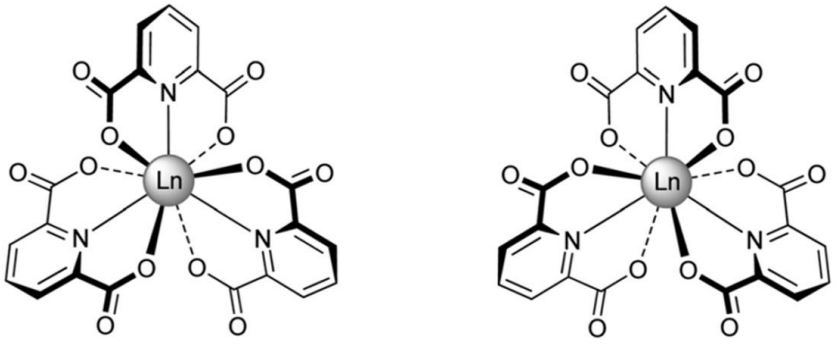

Δ-[Ln.(dpa)$_3$]$^{3-}$ *Λ*-[Ln.(dpa)$_3$]$^{3-}$

Figure 29 - Structures of the enantiomeric Δ-[Ln.(dpa)$_3$]$^{3-}$ and *Λ*-[Ln.(dpa)$_3$]$^{3-}$ viewed down the symmetry axis.

The perturbation of a dynamically racemic mixture can also occur in the excited state *via* an enantioselective excited state quenching process. The interconversion between *Δ* and *Λ* isomers must be fast on the laboratory timescale but slow compared to the excited state lifetime of the complex. Collisions with an enantiopure quencher can result in stereoselective electronic energy transfer to the acceptor, generating an enantiomeric excess in the excited state and an induced CPL signal. This effect has been observed with dynamically racemic D_3 lanthanide complexes, such as $[Ln.(dpa)_3]^{3-}$ ($Ln = Eu^{3+}$, Tb^{3+} and Dy^{3+}), interacting with a number of chiral quenchers including transition metal complexes,[140–143] proteins[144] and corrinoid B_{12}.[145]

A third example of the induction of CPL from a dynamically racemic complex is when there is an alteration in the complex constitution upon binding of an analyte directly to the metal centre, in the same manner that was discussed in the previous section (1.4.2). However, if the chosen analyte is chiral, a particular diastereoisomer may be stabilised and a CPL signal can be 'switched on'.

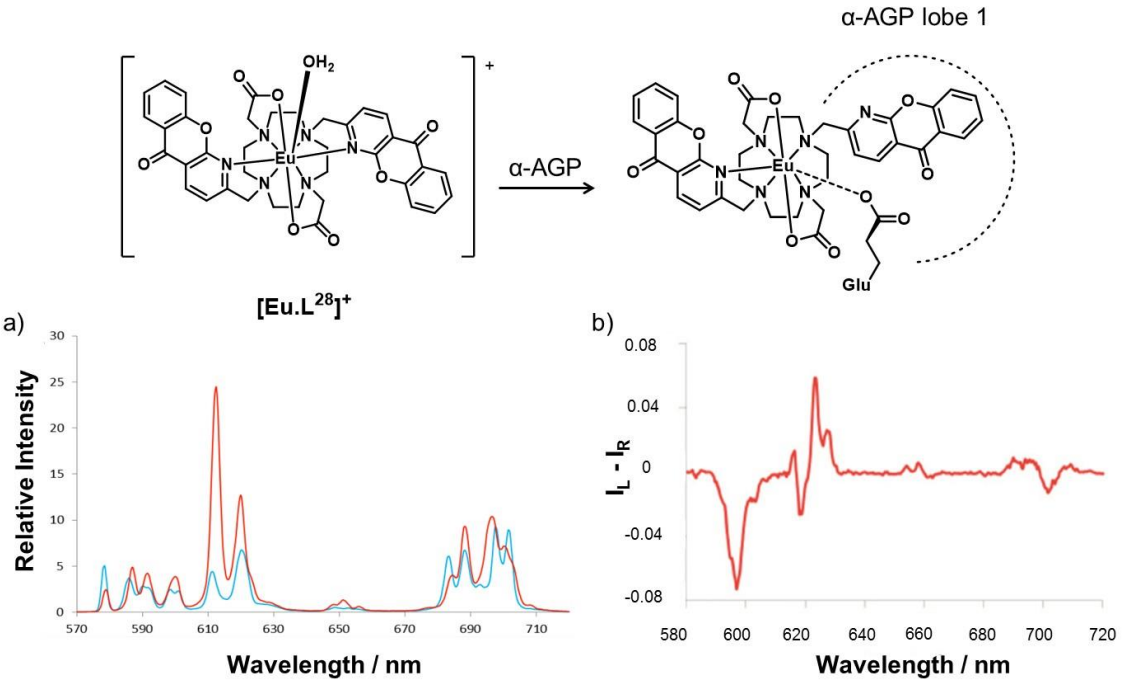

Figure 30 – Structure of [Eu.**L**^{28}]$^+$ and proposed binding mechanism with α_1-AGP. a) Europium emission spectral changes of [Eu.**L**^{28}]$^+$ in the absence (*blue*) and on the addition of 50 μM α_1-AGP (*red*) (20 μM complex, pH 7.4, 0.1 M NaCl). b) CPL spectrum of [Eu.**L**^{28}]$^+$ on the addition of 50 μM α_1-AGP.[146]

A recent example of a well- defined dynamically racemic europium complex in the sensing of acute phase proteins, α_1-AGP and α_1-AAT, demonstrates the utility of this class of probes.[146] The achiral complex, [Eu.**L**^{28}]$^+$, has previously been shown to bind to HSA.[147] The complex

was shown to bind to α_1-AGP (log$K$ = 5.73) by a significant change in the total emission spectrum and through the induction of strong CPL signals, g_{em}(598 nm) = -0.23 (Figure 30). A similar response was observed for α_1-AAT, however the binding affinity was an order of magnitude lower (log$K$ = 4.72). A thorough investigation into the binding mechanism of the lanthanide complex with the protein was conducted. A large increase in the relative intensity of the ΔJ = 2 band was observed, signalling a significant change in the polarisability of the axial donor, perhaps through the displacement of a metal-bound water molecule with a glutamate carboxylate of the protein. ECD studies revealed two distinct negative Cotton transitions, consistent with a relatively rigid coordination environment. The resolved fine structure of each transition showed two bands, suggesting that the two azaxanthone chromophores are in slightly different local environments. The authors hypothesised that while one azaxanthone is bound to the metal centre, the other becomes dissociated and included in the protein binding cavity, providing a secondary binding interaction. This hypothesis was further validated by a competition experiment with chlorpromazine, a drug molecule that is known to bind to α_1-AGP.[148] Incremental addition of chlorpromazine to the Eu-protein adduct led to a progressive diminution of the induced ECD signal suggesting displacement of the complex from the protein binding site. The direct and rapid assessment of the inflammatory response of α_1-AGP was conducted in human serum solution using emission spectroscopy. However, the changes in the induced CPL response were weaker and less well-defined, so this method could not be used for *in situ* analysis.

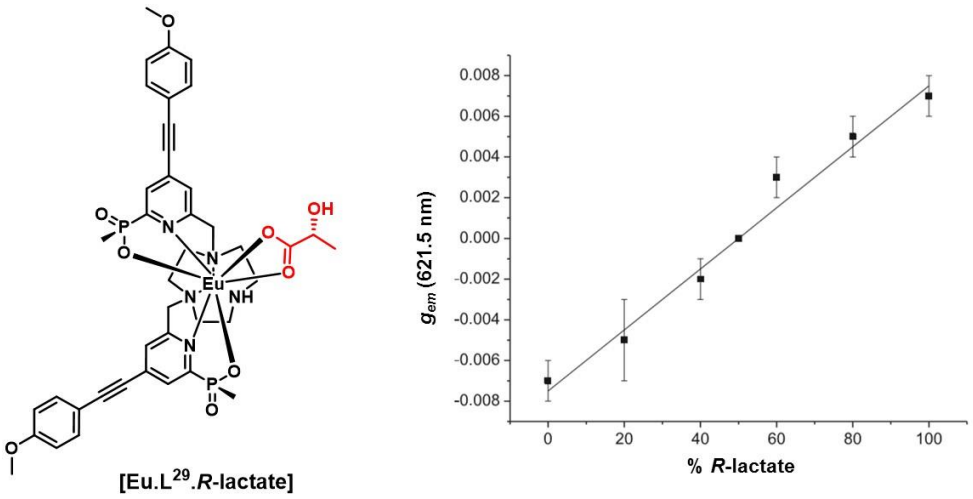

Figure 31 – Structure of [Eu.**L**^{29}.*R*lactate] and variation of g_{em} (621.5 nm) with % *R*-lactate; error bars indicate the standard deviation averaged over 5 runs (R^2 0.98 for shown linear fit).[15]

The direct metal binding of α-hydroxy acids, such as lactate to europium complexes, has also been demonstrated by [Eu.$\mathbf{L}^{28}$]$^+$ and another dynamically racemic complex based on an achiral 9-N_3 bis-phosphinate ligand, [Eu.$\mathbf{L}^{29}$]$^+$.[15] The complex [Eu.$\mathbf{L}^{29}$]$^+$ has been shown to bind to a wealth of different anions, showing selective and signature total emission responses.[149] The binding of each of these europium complexes to lactate was signalled by strong induced CPL. The helicity of the complex, i.e. which enantiomer is preferentially stabilised, is entirely dependent on the chirality of the α-hydroxy acid (*R* or *S*). The g_{em} values vary linearly with enantiomeric composition which allowed a calibration curve to be plotted (Figure 31). Therefore, the enantiomeric purity of a sample with unknown enantiomeric composition can be measured. This study has shown the potential of monitoring changes in the local chiral environment by induced CPL, with particular emphasis on the ability of such complexes to determine the enantiomeric purity of a sample after prior calibration.

1.5.2. Achiral CPL probes

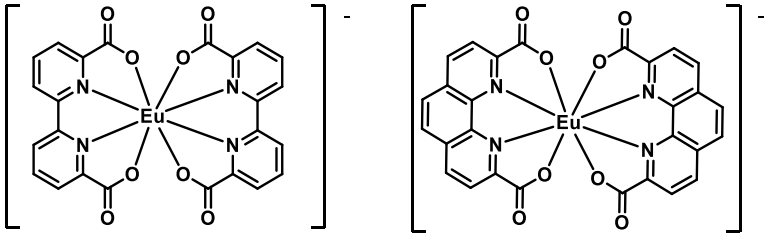

Figure 32 - Structure of europium complexes based on achiral bda and pda ligands.[150,151]

The addition of a chiral analyte can induce a CPL signal by a change in the geometry of the complex, as opposed to the stabilisation or preferential formation of an enantiomer from a racemic mixture. Such an effect has been demonstrated by Iwamura, investigating the effect of added chiral species to the achiral complexes [Eu.$(bda)_2$]$^-$ (bda = 2,2'-bipyridine-6,6'-dicarboxylic acid) and [Eu.$(pda)_2$]$^-$ (pda = 1,10-phenanthroline-2,9-dicarboxylic acid).[150,151] The addition of *R*- and *S*-2-pyrrolidine-5-carboxylic acid (PCA) to [Eu.$(bda)_2$]$^-$ induces CPL signals of equal and opposite sign, from the previously CPL silent system, with a small calculated g_{em} of ±0.03 at λ = 591 nm.[150] The total luminescence spectrum remains relatively unchanged, providing a good example of a system where CPL can be used to monitor changes

that are not apparent in the total emission spectrum. An investigation into the dependence of g_{em} on PCA concentration was conducted revealing the presence of a 1:1 species in the resulting adduct (Figure 33). The pH response of the system was also studied and showed that the largest g_{em} value was observed when the chiral acid was in a deprotonated form. The authors hypothesised that the chiral species interacts with the europium complex by direct coordination of the carboxylate group to the metal centre. The additional coordination of PCA to the metal distorts the structure of the bda ligands, generating a local chiral environment at the europium centre.

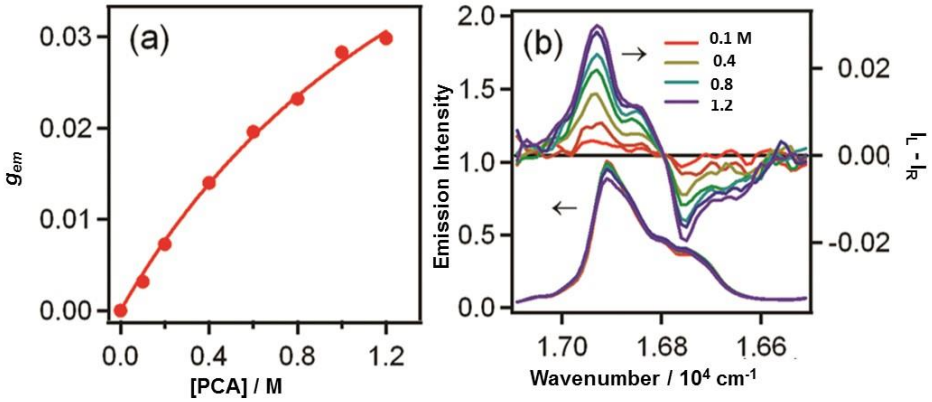

Figure 33 – a) A plot of the variation of g_{em} at 591 nm with concentration of PCA. b) Dependence of CPL (*upper*) and total luminescence (*lower*) spectra of $[Eu.(bda)_2]^-$ on the addition of (*S*)-PCA.[150]

Further work examined the interaction of a number of amino acids, specifically with $[Eu.(pda)_2]^-$.[151] The geometry of the europium complex in solution in the absence of a chiral host was ill-defined. The total emission spectrum revealed that the solution structure is markedly different from the solid-state crystal structure and there is in fact more than one europium species present in solution, indicated by the presence of multiple peaks in the $\Delta J = 0$ manifold, Figure 34. Upon binding to the amino acid, a significant change in the total emission spectrum occurred. The $\Delta J = 2/\Delta J = 1$ ratio was altered, indicative of slightly distorted D_{2d} symmetry,[152] and the presence of one emissive species was suggested by observation of a single transition in the $\Delta J = 0$ band. Large induced CPL was recorded following addition of arginine and histidine ($g_{em} = \pm 0.08$ in the magnetic dipole allowed $\Delta J = 1$ transition). The g_{em} dependence on amino acid concentration revealed that more than one chiral species was present in the adduct that generates CPL. Such behaviour is in contrast to that observed for $[Eu.(bda)_2.(PCA)]^{2-}$. The exact binding interaction remains undetermined and the lack of a well-defined adduct structure means that the constitution of the emissive species that is

contributing to the induced CPL, is not fully understood. The small g_{em} values suggest the presence of other more emissive achiral europium species that may be present in solution. Further experiments addressing the constitution of the emissive species, such as ESI-MS, may aid in eliciting information about the interaction that is taking place in the chiral adduct.

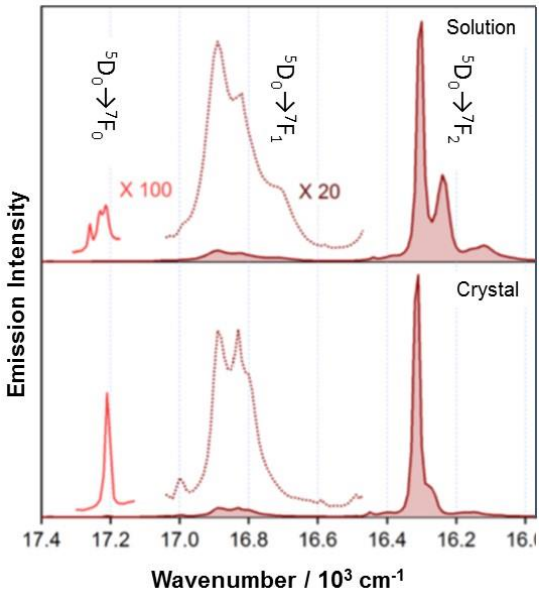

Figure 34 – Total emission spectrum of $[Eu.(pda)_2]^-$ in solution (*upper*) and of a $(C_6H_{16}N)[Eu.(pda)_2]$ crystal (*lower*) showing the splitting in the $\Delta J = 0$ band ($^7F_0 \leftarrow ^5D_0$) of the solution species (λ_{exc} = 310 nm).[151]

It is worth noting that another example of this type of achiral CPL probe has been published, based on a Eu^{3+} complex coordinated to a β-diketonate unit of an achiral polymer chain.[153] Addition of *R*- and *S*-proline induced an intense CPL signal with a high g_{em} value (± 0.41 in $\Delta J = 1$ transition at 590 nm). However, once again, further work must be undertaken to understand the nature of the binding interaction and allow further development for this type of probe.

1.6. Project aims

For many years, the majority of lanthanide based probes have exploited changes in emission spectral form and the excited state luminescent lifetime as a means of a detection technique. The attractive photophysical and chiroptical properties of lanthanide complexes, as discussed in Section 1.3.3, have also allowed CPL modulation upon analyte binding, to report on the stereochemical environment surrounding the lanthanide ion. Many examples of enantiopure

and achiral lanthanide complexes have been reported that have the ability to act as effective CPL probes, Sections 1.4.2 and 1.5.

The aim of the work described in this thesis is to expand the range of lanthanide chirality probes that exploit CPL spectroscopy as a signalling mechanism. Chapter 2 describes the synthesis of a novel set of enantiopure lanthanide complexes incorporating a remote amide chiral centre. The degree of stereocontrol imposed by the chiral ligand is assessed and compared to other examples that have previously been reported. Inclusion of four different extended pyridyl-aryl-alkynyl chromophores into the ligand framework, allows the key photophysical parameters to be optimised.

Chapter 3 investigates a different type of lanthanide chirality probe, based on dynamically racemic ligands. The induction of CPL from a lanthanide complex after the binding of a chiral analyte is an area of growing interest. To date, there are very few examples of well-defined systems that employ this technique for chirality detection and structural determination. This work aims to expand the scope of well-defined, dynamically racemic lanthanide complexes that exhibit a strong induced CPL response to signal the presence of a chiral analyte of interest. The key structural and photophysical properties are identified and incorporated into the ligand design of a series of novel dynamically racemic lanthanide chirality probes.

The work in Chapter 4 embraced the design and syntheses of two novel europium (III) CPL probes that sense important chiral biomolecules, including sialic acid (Neu-5-Ac), *O*-phosphono-amino acids and peptides and oleoyl-*L*-α-lysophosphatidic acid. The design of these chirality probes set out to meet the following criteria:

i) the probe must be bright and highly emissive with a high emission quantum yield, ϕ_{em}, extinction coefficient, ε, and a long excitation wavelength, λ_{exc};
ii) the probe must be able to bind the target analyte reversibly over the appropriate biological concentration;
iii) interconversion between the Δ and Λ isomers of the lanthanide probe must be fast on the emission timescale;
iv) the analyte-bound adduct must be sufficiently conformationally rigid to generate large induced CPL with measurable and accurate g_{em} values;
v) the probe design should be sufficiently flexible to permit substituted analogues to be prepared, allowing enhanced affinity for the chosen analyte with a heightened selectivity over competing species.

CHAPTER TWO

DEVELOPMENT OF NOVEL ENANTIOPURE LANTHANIDE COMPLEXES

2.1. Introduction

There are a number of strategies that have been used to design chiral ligand systems that give complexes with well-defined three-dimensional structure, Section 1.4. Complete stereocontrol has previously been achieved through incorporation of a remote chiral centre in a 12-N_4 tetra-amide complex derived from *R* or *S* α-methylbenzylamine.[103] The contents of this chapter will detail the work outlining the preparation of a novel enantiopure ligand, $\mathbf{L^{30}}$, based on chiral tris-amidepyridyl derivative of triazacyclononane. By employing a similar stereochemical approach, our aim was to assess the degree of stereocontrol in lanthanide complex formation. By analogy with recent work, the related ligands $\mathbf{L^{31a-d}}$ were also prepared, as the introduction of the arylalkynyl moiety greatly enhances the absorption characteristics of the ligand and permits efficient sensitisation of Eu emission.[154]

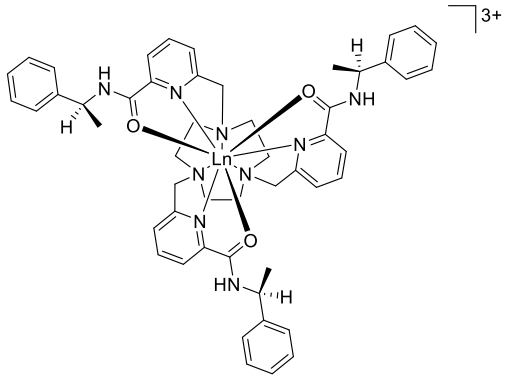

(*S*)-[Ln.$\mathbf{L^{30}}$]$^{3+}$

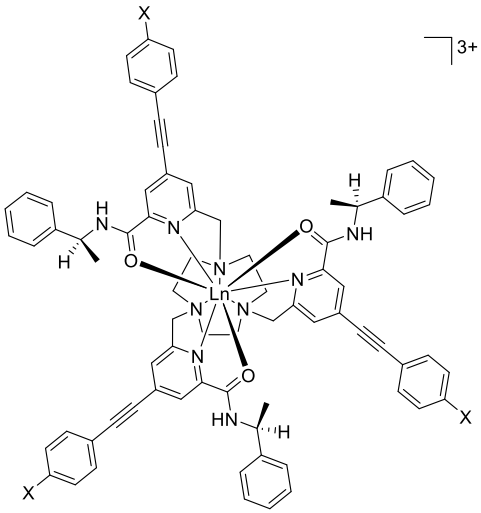

(*S*)-[Ln.$\mathbf{L^{31a}}$]$^{3+}$, X = H
[Ln.$\mathbf{L^{31b}}$]$^{3+}$, X = CO_2Me
[Ln.$\mathbf{L^{31c}}$]$^{3+}$, X = OMe
[Ln.$\mathbf{L^{31d}}$]$^{3+}$, X = NHCOMe

Triazacyclononane, 9-N_3, is a small macrocycle that is easily functionalised to generate thermodynamically and kinetically stable lanthanide complexes. There are two elements of chirality that can arise in a nonadentate C_3 symmetric lanthanide complex based on 9-N_3. One element of chirality is associated with the torsional angle of the NCH_2CH_2N backbone of the macrocyclic ring which can be ± 60º. A positive angle results in δ chirality and a negative dihedral angle gives a λ configuration. The second element of chirality arises from the twist of the pendant arms around the lanthanide centre. If the sign of the $NCCN_{py}$ angle is positive, then

Δ helicity results, and if it is negative then *Λ* helicity is defined. If we now consider the possible combinations of these two elements of chirality, then four stereoisomers, existing as two enantiomeric pairs, can be formed (Scheme 7). Interconversion between the stereoisomers may occur through cooperative arm rotation, *Δ*↔*Λ*. Ring inversion is slow and has not been observed by NMR spectroscopy in solution at room temperature, *δ*↔*λ*.[49]

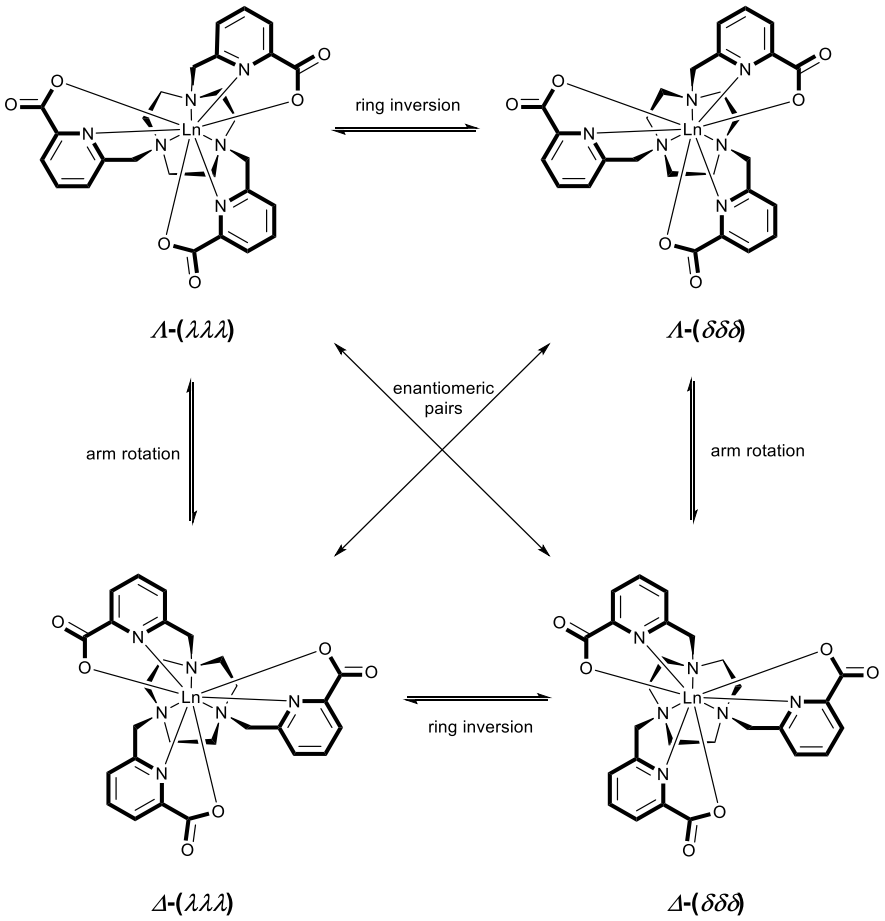

Scheme 7 – The four stereoisomers arising from a C_3 symmetric 9-N_3 system.[49]

Nine coordinate tris-pyridyl-carboxylate and amide 9-N_3 complexes of Ln^{3+} ions have been reported by Latva, Mazzanti and co-workers, [Ln.**L**^{33}] and [Ln.**L**^{34}]$^{3+}$.[101,155,156] More recent variants include a series of tri-pyridylphosphinate systems, [Ln.**L**^{32}], that were shown to exist in the solid state in a tri-capped trigonal prism coordination geometry, and define an isostructural series across the lanthanide block.[100] The prepared lanthanide complexes [Ln.**L**^{30}]$^{3+}$, were directly compared to the related tri-phosphinate and tri-carboxylate analogues, allowing us to deepen our understanding of ligand field effects in lanthanide complexes of high symmetry.

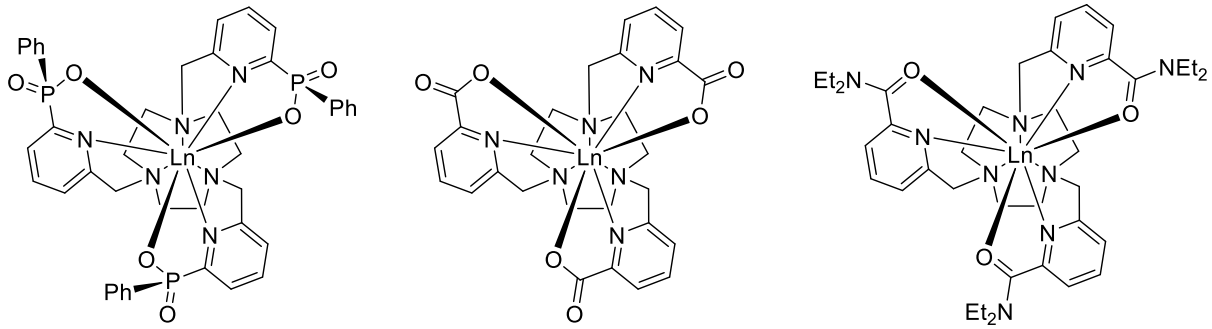

[Ln.**L**^{32}] [Ln.**L**^{33}] [Ln.**L**^{34}]$^{3+}$

Scheme 8 – Structures of related tris-pyridyl 9-N_3 complexes based on phosphinate, carboxylate and amide ligands.[100,101,155,156]

2.2. Synthetic aspects

2.2.1. Synthesis of the parent complex, [Ln.L^{30}](CF$_3$SO$_3$)$_3$

The parent ligand, **L**^{30}, was prepared in six steps from commercially available precursors. The enantiomeric purity of the primary amine, α-methylbenzylamine, was first established using the NMR chiral solvating agent, *R*-*O*-acetylmandelic acid.[157] The -CHC<u>H</u>$_3$ doublets were well resolved in the diastereomeric adducts, and the limit of detection was assessed by analysing the relative intensity of the ^{13}C satellite signals (doublet, J = 140 Hz, 1.08% total for the ^{12}C signal). The enantiomeric purity of the starting material was calculated as >99% *ee* and was considered sufficiently pure for use in the subsequent amide coupling reaction.

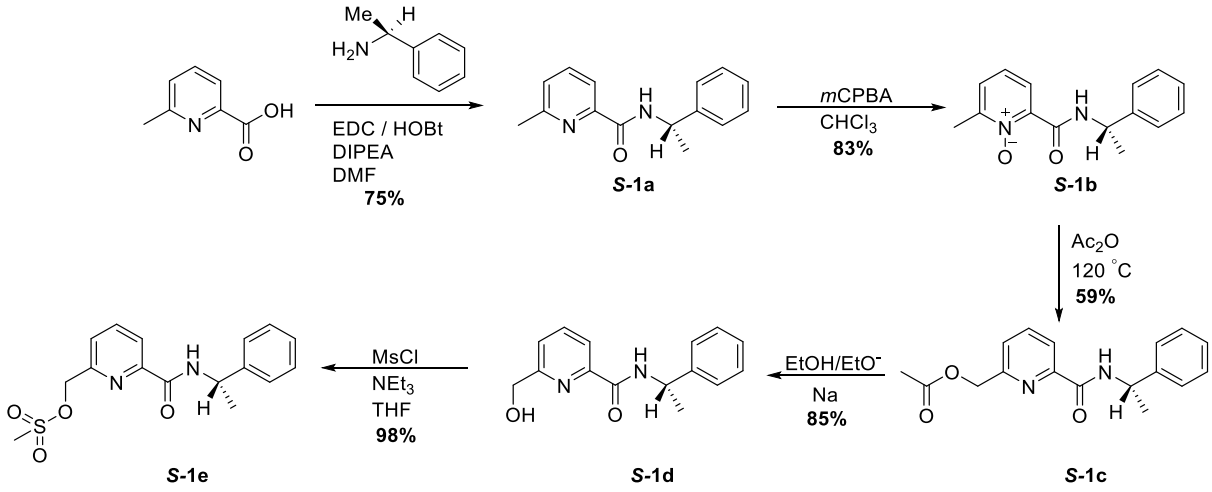

Scheme 9 – Synthesis of the pendant arm, as the mesylate, ***S*-1e**.

The amide coupling reaction of 6-methylpyridine-2-carboxylic acid with *S*-α-methylbenzylamine afforded the desired amide, ***S*-1a**, in good yield. The amide, ***S*-1a**, was treated with *m*CPBA in chloroform to give the N-oxide, ***S*-1b**, in 83% yield. Conversion to the alcohol was initially attempted using trifluoroacetic anhydride at 60 ºC, followed by *in situ* hydrolysis. However, no formation of the trifluoroacetate ester intermediate was observed. Initial thoughts were, that the transformation was inhibited by an energy barrier, associated with intramolecular hydrogen bonding between the amide NH and pyridine N atom. The N-oxide was treated with acetic anhydride as the reaction could then be heated to a higher temperature (120 ºC). Under these reaction conditions, the desired ester intermediate was obtained. This rearrangement reaction was followed by ester solvolysis, catalysed by ethoxide, to furnish the alcohol, ***S*-1d**, in 85% yield. Mesylation of the alcohol under standard conditions gave ***S*-1e**, which was used directly in the next step with no further purification. Alkylation of 9-N_3 was carried out using the crude mesylate in acetonitrile in the presence of K_2CO_3. A mixture of mono-, di- and tri-substituted products was obtained and the ligands were separated by column chromatography on neutral alumina. The di- and tri-substituted ***S*-L^{30}** ligands were isolated in yields of 22% and 55% respectively. The enantiomeric ligand ***R*-L^{30}** was synthesised *via* an identical pathway starting from *R*-α-methylbenzylamine.

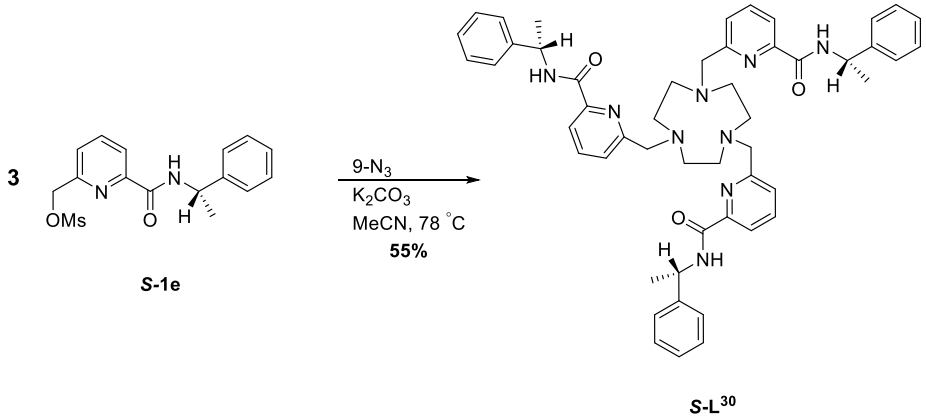

Scheme 10 – Synthesis of ligand ***S*-L^{30}**.

The purified ligand, ***S*-L^{30}**, was reacted with the appropriate lanthanide trifluoromethanesulfonate (triflate) salt at 80 ºC in dry acetonitrile. Trituration with cold ether yielded the lanthanide complexes *S*-[Ln.**L^{30}**]$(CF_3SO_3)_3$ in quantitative yield (Ln = Ce, Pr, Nd, Eu, Gd, Tb, Dy, Ho, Er, Tm, Yb). For comparative analysis, *R*-[Eu.**L^{30}**]$^{3+}$ and *R*-[Tb.**L^{30}**]$^{3+}$ were synthesised using an analogous complexation procedure.

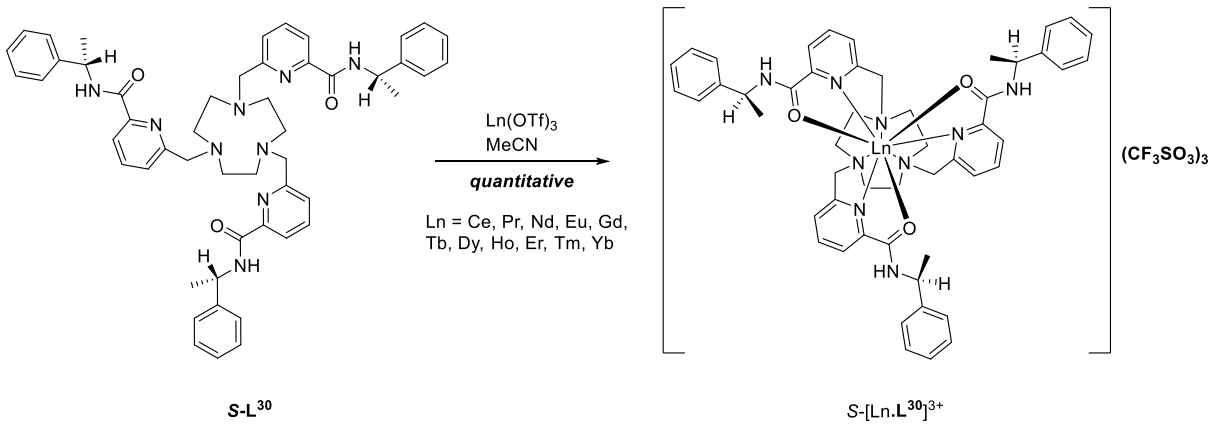

Scheme 11 – Formation of the lanthanide complex *S*-[Ln.**L**^{30}](CF$_3$SO$_3$)$_3$.

2.2.2. Synthesis of the extended chromophore systems, *S*-[Ln.L^{31a-d}]$^{3+}$

The initial design for the synthesis of ligands **L**$^{31a-d}$ was adapted from that of the parent ligand **L**^{30}, employing previously reported methodology of the related tri-pyridylphosphinate ligand.[154] The presence of a halide group in the 4-position on the pyridine ring was required, in order to facilitate the cross coupling step that would be used to furnish the alkyne at a later point.

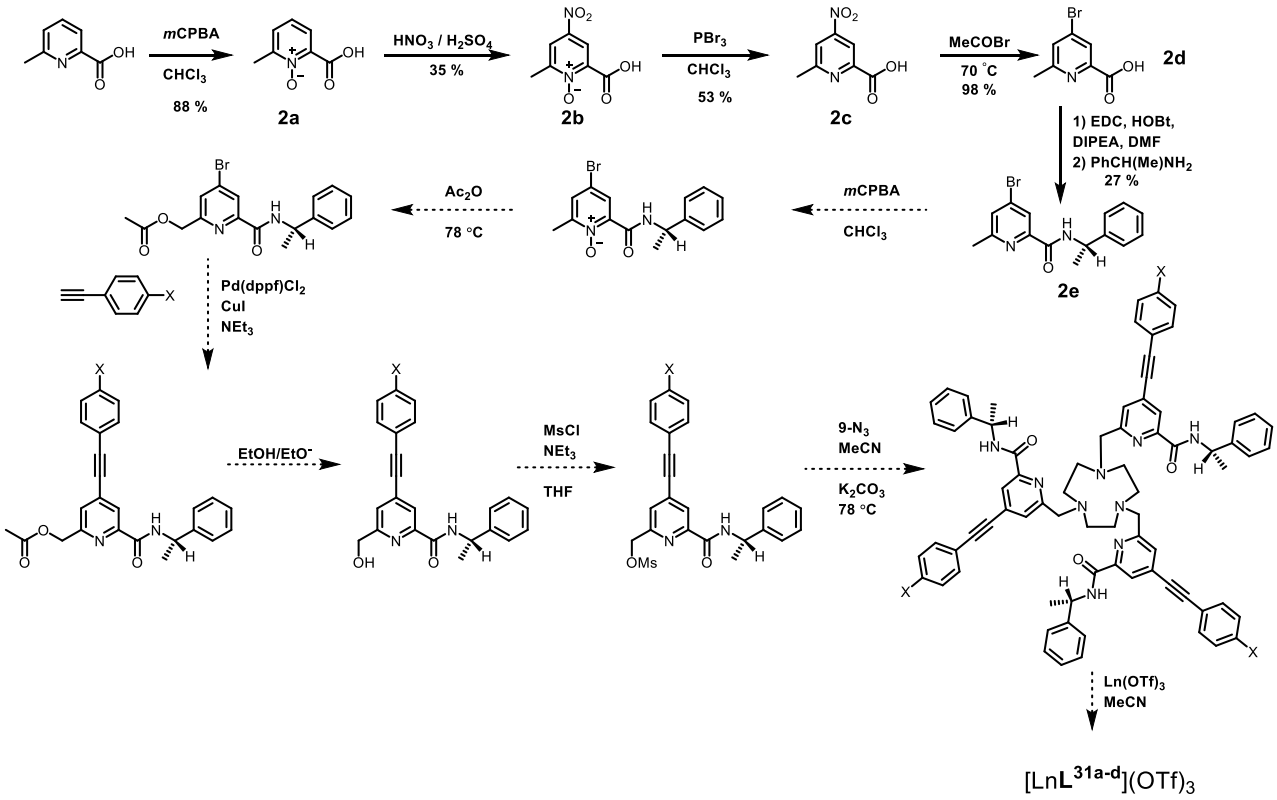

Scheme 12 – Initial synthetic scheme considered for the preparation of $[Ln.\mathbf{L}^{31a\text{-}d}]^{3+}$.

The conversion of 6-methyl-2-carboxylic acid to the N-oxide, **2a**, was achieved using *m*CPBA in chloroform in good yield. Subsequent nitration at the 4-position was attempted using an equimolar mixture of concentrated HNO_3 (70%) and H_2SO_4 (98%) followed by heating to 100 ºC. After 24 h, limited conversion to the desired nitrated product, **2b**, was observed by ESI-MS and ^{1}H NMR spectroscopy. The reaction was retreated with the active species numerous times and left for a total of 96 h at 100 ºC before significant conversion to the product was observed (~60%). Purification by flash column chromatography on silica was carried out using an isocratic gradient system (0.2% acetic acid, 49.8% EtOAc, 50% hexane). However, the product was isolated in a poor yield, 35%, suggesting that significant product was lost during the purification step. Deoxygenation followed by bromo substitution of the nitro group was carried out in good yields using literature methods.[154] The substitution reaction was followed by an amide coupling employing the same coupling agents, EDC and HOBt, that were used in the synthesis of $\mathbf{L}^{30}$. The desired amide, **2e**, was isolated in a very poor yield (27%) along with multiple by-products. The major by-product was isolated and characterised by LC-MS and ^{1}H NMR spectroscopy which revealed substitution of the bromo group in the *para* position by the

amine nucleophile. At this stage, progression along the original synthetic pathway was halted and an alternative, more viable route was created, in an attempt to circumvent the problems that had been encountered.

The synthesis began with the preparation of 6-(hydroxymethyl)-4-iodo picolinic acid, **3a**, using well established literature procedures.[154,155] The *para*-iodo group was incorporated in the hope that it would not be displaced in the amide coupling step, as the carbon atom of the C-X bond is less electrophilic compared to the bromo analogue. Another advantage of incorporating an iodo instead of a bromo group is the enhanced reactivity in the subsequent Sonogashira cross-coupling reaction. The synthesis of the precursor began with the conversion of the *para*-hydroxyl group of chelidamic acid to a chloro group followed by *in situ* formation of the methyl ester. Subsequent transformation of the chloro group to an iodo group was carried out using NaI, followed by reaction with acetyl chloride in acetonitrile. The reaction mixture was sonicated for 45 minutes to yield the desired *p*-iodo-pyridine in excellent yield (86%). Selective reduction of the di-ester was carried out using $NaBH_4$ in CH_2Cl_2:CH_3OH solvent mixture at 0 ºC. The reaction was closely monitored by TLC and instantly quenched with 1 M HCl on disappearance of the starting material, to avoid over reduction of the compound.

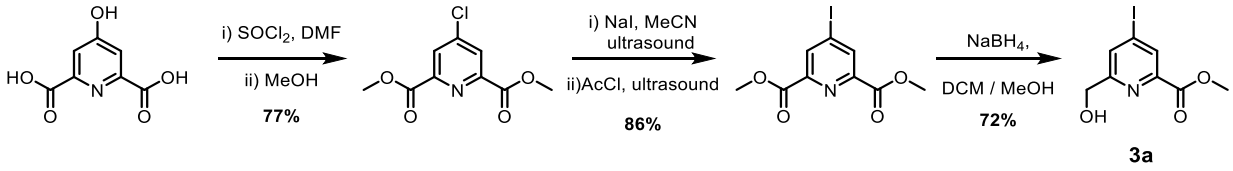

Scheme 13 – Synthesis of the intermediate **3a**.

A five step synthetic route starting from **3a** was then devised, beginning with the preparation of the mono-hydroxymethyl *p*-iodo mono-carboxylic acid *via* base catalysed hydrolysis of the methyl-ester (Scheme 14). Subsequent formation of the amide bond proved slightly troublesome due to a competing oligomerisation reaction between the hydroxyl group of the starting material with the reactive activated ester. Systematic variation of the coupling reagents, solvent, temperature and order of addition was considered. The optimal reaction conditions were found to be; stirring the coupling reagents, base and amine in a solvent mixture of CH_2Cl_2-DMF (1:1) followed by slow, dropwise addition of the carboxylic acid. The amide coupling reaction was promoted over the competing oligomerisation reaction, by having a large initial concentration of amine compared to the carboxylic acid, which gave the amide, ***S*-3c**, in a reasonable yield (58%).

The alkynes, were synthesised by a Sonogashira cross-coupling reaction between the *p*-iodo-pyridyl amide and various *p*-substituted arylalkynes, using catalytic Pd(dppf)Cl_2 and CuI in THF. Cu (II) complexes are known to facilitate the oxidative dimerisation of alkynes to form diynes, known as the Glaser or Hay reaction.[158] This competing reaction is catalysed in the presence of oxygen[159] and so special care was given to ensure a completely oxygen free environment by employing Schlenk-line techniques, degassed solvents and an argon atmosphere. Mesylation followed by alkylation of 9-N_3 was carried out under standard conditions to give ligands ***S*-L^{31a-d}**. Complexation with Eu(OTf)$_3$ in acetonitrile at 80 ºC gave the triflate salt of the europium complexes, *S*-[Eu.**L**$^{31a-d}$](CF$_3$SO$_3$)$_3$, following trituration with cold ether. Conversion to the chloride salt was achieved using a strong ion exchange resin in the hope that this would improve the water solubility of the lanthanide complexes.

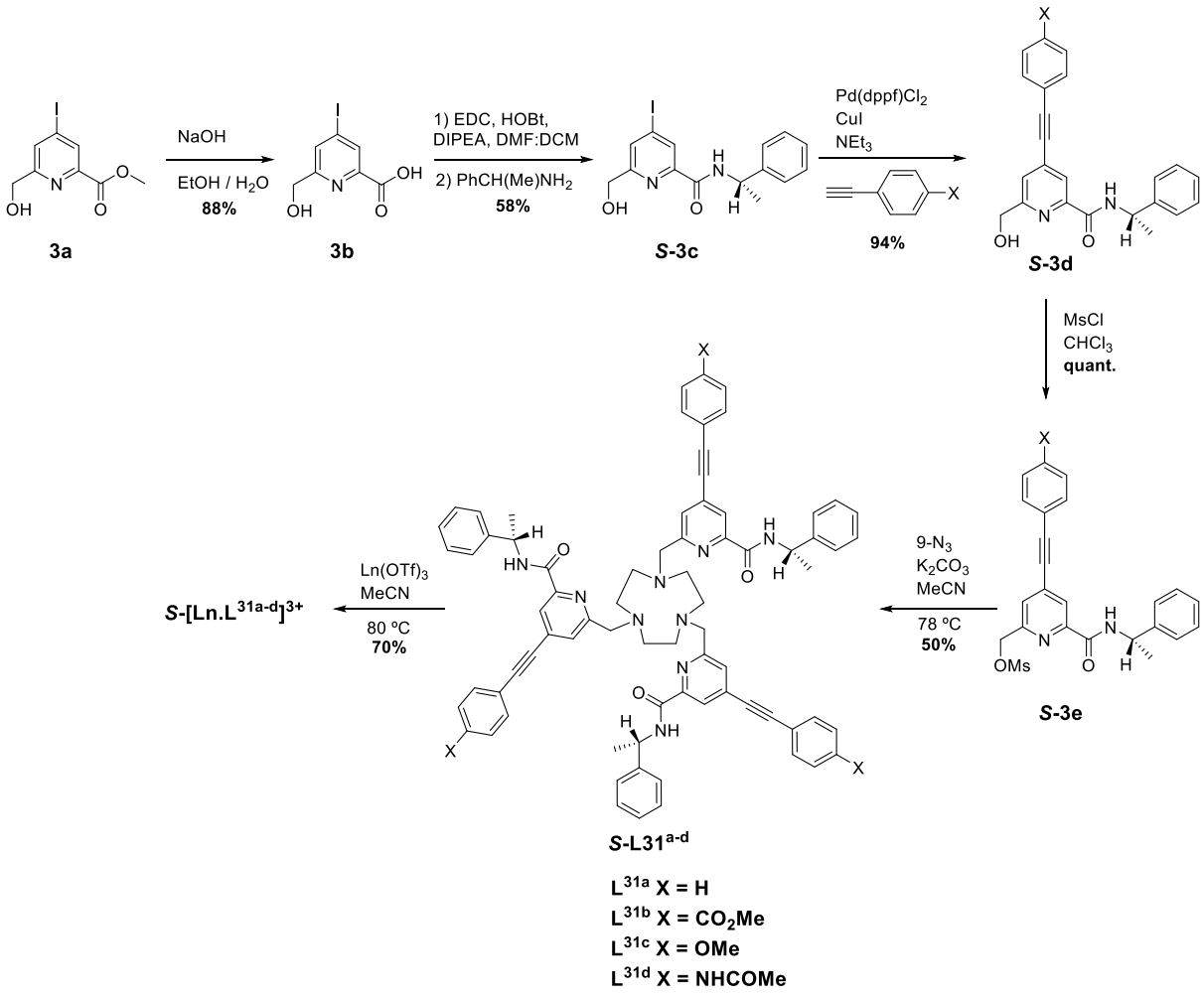

Scheme 14 – Reaction pathway for the synthesis of lanthanide complexes *S*-[Ln.**L**$^{31a-d}$]$^{3+}$.

2.3. Structure elucidation of $[Ln.L^{30}]^{3+}$ and $[Ln.L^{31a-d}]^{3+}$

In order to assess the level of stereocontrol imparted on the system by the chosen enantiopure ligands, a full structural analysis of both sets of complexes based on ligands **L**^{30} and **L**^{31}, was conducted. A variety of techniques were used to identify the isolated complexes and determine the absolute configuration of the major isomer in each case. High resolution mass spectrometry allowed determination of accurate masses that were compared with predicted isotope patterns, confirming the constitution of each complex.

2.3.1. Solution NMR studies and HPLC

The ^{1}H NMR spectra for the series of complexes, $[Ln.\mathbf{L}^{30}]^{3+}$, were assigned using measurements of the longitudinal relaxation rate, R_1 ($R_1 = 1/T_1$) of each resonance at different fields. The longitudinal relaxation time, T_1, was measured using inversion recovery methods of different time intervals. The size of R_1 depends on the distance of the proton nucleus from the paramagnetic centre (r^{-6}) and the field of the spectrometer; values are fastest for the protons that are closest to the lanthanide nucleus. In tandem with analysis of X-ray crystallographic data, an assignment of the ^{1}H NMR spectrum could be made for every complex where line broadening was not too severe. Partial assignment of the ^{1}H NMR spectra of $[Eu.\mathbf{L}^{31a-d}]^{3+}$ were made by comparison with that of $[Eu.\mathbf{L}^{30}]^{3+}$.

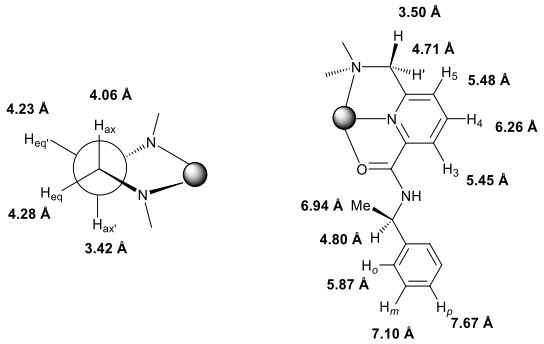

Table 2 – Proton NMR assignments (δ_H/ppm) of the major isomeric species observed for paramagnetically shifted ligand resonances in $[Ln.\mathbf{L}^{30}]^{3+}$ (295 K, CD_3OD)[a], showing the distance to the Eu centre based on X-ray analysis.

Ln	H_{ax}	H'_{eq}	H_{eq}	pyCHN	CH_3	C*H*NH	H^o	H^p	H^m	H'_{eq}	H^5	H^4	H^3	pyCH'N
Tm	-79.8	-30.5	-29.0	-22.0	-7.5	+9.3	10.8	10.7	10.4	11.3	19.2	19.6	23.0	+70.4
Yb	-18.8	-6.7	-4.2	-2.8	-1.1	+6.2	7.6	8.2	8.3	8.9	11.4	11.2	11.6	+22.3
Eu	-6.6	-2.2	-1.5	-0.7	+1.2	+4.0	5.7	6.9	6.7	5.1	7.4	7.3	7.5	+7.6

[a]Data for other Ln complexes are given in Chapter 5 but were not fully assigned due to severe line broadening of certain protons within 4.5 Å of the metal ion.

The ^{1}H NMR spectra of the series of lanthanide complexes, [Ln.**L**^{30}]$^{3+}$, revealed that two C_3 symmetric species were present in each case. The major:minor isomer ratio was measured, where possible, by integration of the corresponding proton peaks in the ^{1}H NMR spectrum. The ratio of these diastereoisomers varied as a function of the Ln (III) ion and fell from 9:1 (Ce) to 4:1 (Yb) across the series. Such a variation is consistent with a trend induced by the lanthanide contraction; as the size of the metal ion decreases, the preferential orientation of the phenyl and methyl groups is reduced resulting in a smaller diastereomeric induction effect. Intriguingly, the diastereoisomer ratio for [Eu.**L**$^{31a\text{-}d}$]$^{3+}$ increased to 15:1. We can tentatively suggest that in these systems, the more polarisable pyridine N may have a shorter bond to the lanthanide ion, enhancing the impact of steric demand of the proximate chiral centre. However, in the absence of X-ray crystal data, the difference in Ln-N_{py} bond length between the parent and extended chromophore complex cannot be identified as the primary reason for enhanced diastereomeric induction. The proton NMR spectrum of *R*-[Eu.**L**^{30}]$^{3+}$ was also recorded and revealed identical shift values and integration ratios to *S*-[Eu.**L**^{30}]$^{3+}$. These observations allowed us to conclude that the major isomer of both *S*-[Eu.**L**^{30}]$^{3+}$ and *R*-[Eu.**L**^{30}]$^{3+}$ are enantiomeric. Analytical HPLC was used to corroborate these results in all cases. The isomers were separated by crystallisation or reverse-phase HPLC.

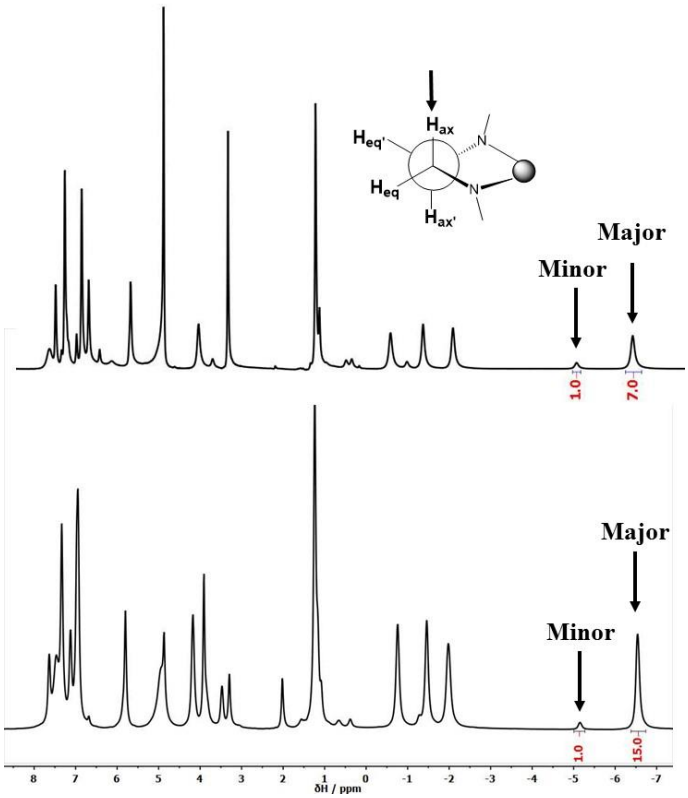

Figure 35 – ^{1}H NMR spectra of *S*-[Eu.**L**^{30}]$^{3+}$ (*top*) and *S*-[Eu.**L**^{31c}]$^{3+}$ (*bottom*) showing isomeric ratios of 7:1 and 15:1 respectively (CD_3OD, 295 K, 400 MHz).

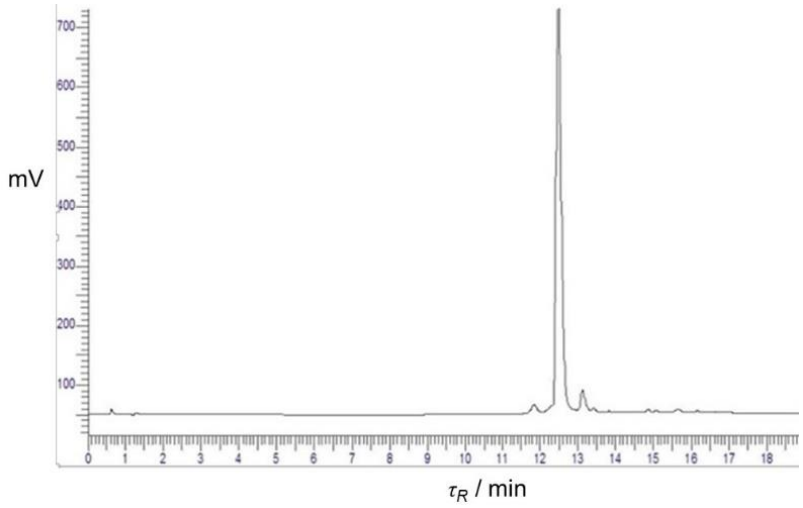

Figure 36 – HPLC trace of [Eu.$\mathbf{L^{31c}}$]$^{3+}$: major isomer t_R = 12.5 min, minor isomer t_R = 13.1 min (10-100 MeOH (0.1% formic acid) in H_2O (0.1% formic acid) over 15 min, detector λ = 350 nm).

Variable temperature ^{1}H NMR spectra were recorded for *S*-[Yb.$\mathbf{L^{30}}$]$^{3+}$ in D_2O at 600 MHz, to determine if isomeric exchange between the major and minor diastereoisomer was occurring on an NMR timescale. The Yb complex was selected for this study as it has the simplest ^{1}H NMR spectrum to interpret out of the series of synthesised lanthanide complexes. The isomer ratio for [Yb.$\mathbf{L^{30}}$]$^{3+}$ was invariant with temperature over the range 298 – 353 K (4:1). No coalescence of the two separate resonances occurred on increasing the temperature, suggesting that the two isomers do not interconvert on the NMR timescale within this temperature range. This result further supports the hypothesis that the complex exists in two non-exchanging diastereomeric forms. It was noted that the chemical shift of a given resonance reduced in size as temperature (T) increased, as a result of the paramagnetic shift dependence on temperature: $\delta_{para} \alpha (kT)^{-2}$.

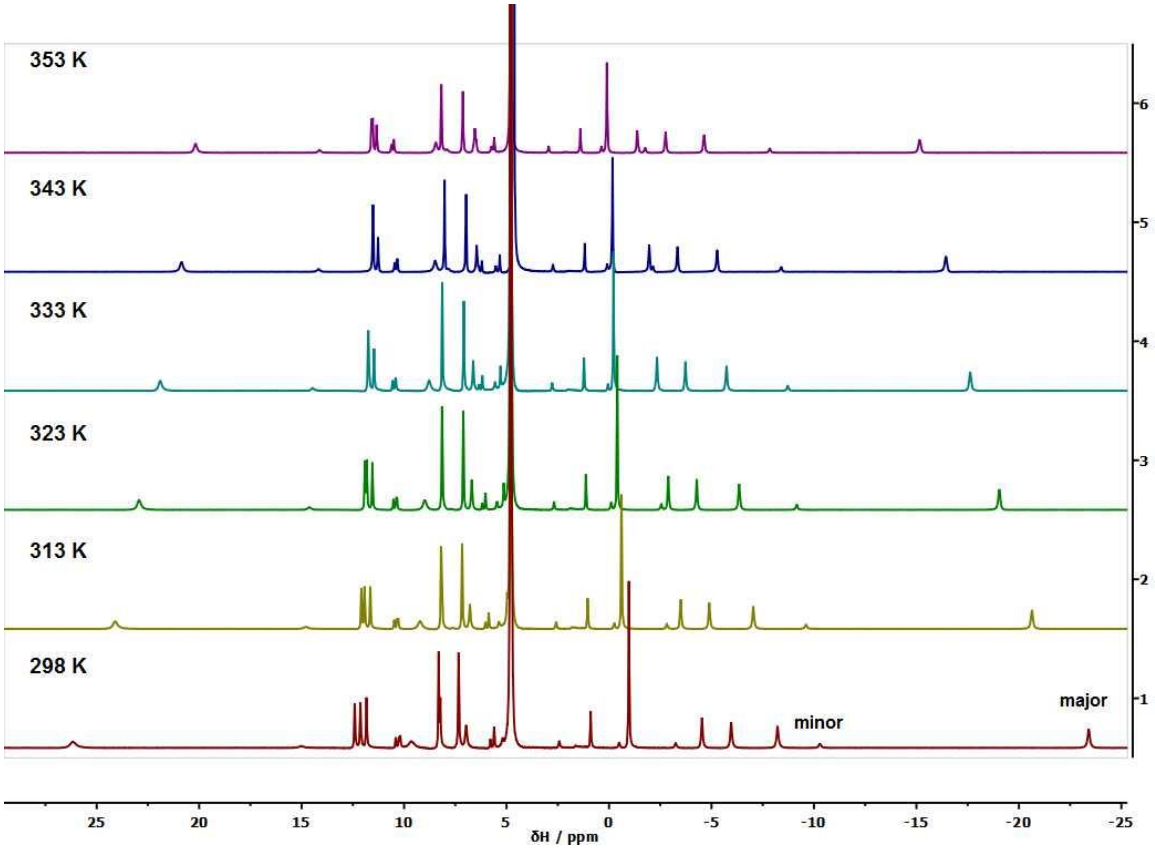

Figure 37 – Variable temperature ^{1}H NMR spectra of *S*-*Δ*-[Yb.**L**^{30}]$^{3+}$ highlighting the major and minor isomer resonance of the most shifted axial ring proton (D_2O, 600 MHz).

2.3.2. X-ray crystallographic analysis

Crystals of [Ln.**L**^{30}]$(CF_3SO_3)_3$ grew readily from aqueous methanol (1:1). The complexes *R*-[Eu.**L**^{30}]$^{3+}$ (CCDC 965910) and *S*-[Eu.**L**^{30}]$^{3+}$ (CCDC 965909) crystallised in the trigonal space group R_3. Crystallographic analysis of *S*-[Yb.**L**^{30}]$^{3+}$ (CCDC 965911) revealed that it was isostructural with the Eu complexes. This result strongly suggests that the series of lanthanide complexes of **L**^{30} would adopt a common structure, at least from Eu to Yb, as has been verified for the related tri-pyridylphosphinate complex.[100] The triflate anions are slightly disordered, and a severely disordered solvent molecule is present in each structure. The lanthanide ion is nonadentate, coordinated by three N atoms of 9-N_3, three pyridyl N atoms and three amide O atoms. The complexes adopted a distorted tricapped trigonal prism structure, with a pseudo C_3 axis passing through the metal atom and the centre of the macrocyclic ring.

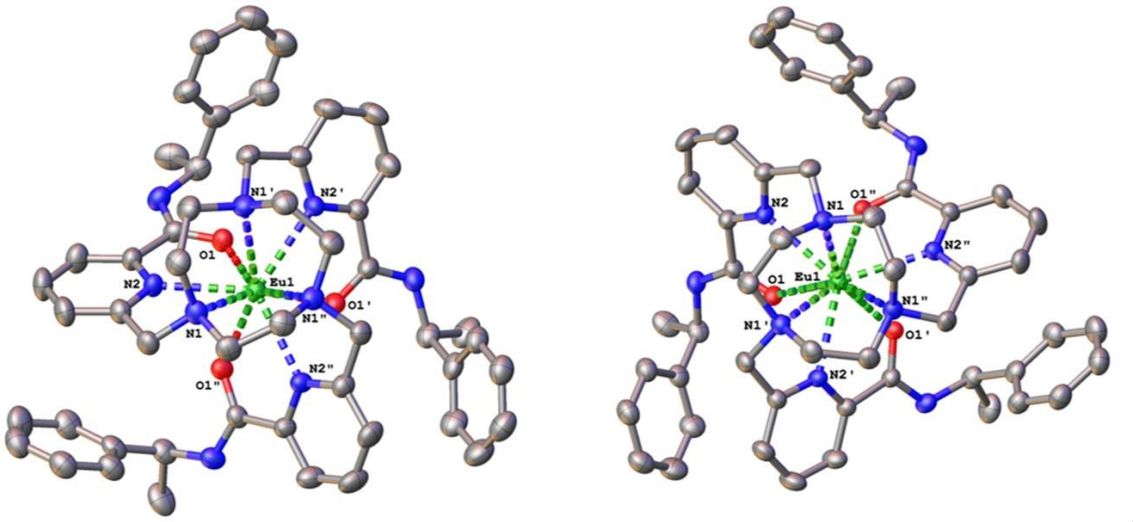

Figure 38 – Views of the structures of the tri-positively charged cations of *S*-*Δ*-(*λλλ*)-[Eu.**L**^{30}] (*left*) and *R*-*Λ*-(*δδδ*)-[Eu.**L**^{30}] (*right*) (120 K). CCDC 965909-965910.

Analysis of the lengths of the lanthanide-donor atom bonds revealed a longer Ln-O bond for [Ln.**L**^{30}]$^{3+}$ compared to the values reported for [Ln.**L**^{32,33}]$^{3+}$,[100,102] as expected with a neutral amide donor (Table 3). The Ln-N_{ring} distance was shorter, indicating that the lanthanide ion is sitting closer to the plane of the 9-N_3 ring for [Ln.**L**^{30}]$^{3+}$.

Table 3 – Selected mean distances (Å) of ligand donor atoms to the lanthanide ion[a] for [Ln.**L**^{30}]$^{3+}$ and [Ln.**L**^{32}].[100,102]

[Ln.**L**^{n}]	Eu	Yb
Ln.**L**^{30}-O	2.40	2.34
Ln.**L**^{32}-O	2.33	2.25
Ln.**L**^{30}-N_{ring}	2.63	2.57
Ln.**L**^{32}-N_{ring}	2.68	2.62

[a] Effective ionic radii (Å) in 9-coordinate systems are 1.12 (Eu) and 1.04 (Yb).[160]

The crystal structures show that the major diastereoisomer of the complex derived from the enantiopure *S* ligand system has a *Δ* configuration ($NCCN_{py}$ = +36.5º) and a *λ* conformation for each 5-ring chelate derived from the 9-N_3 ring (NCCN = -46.9º). The europium complex derived from the enantiopure *R* ligand system is enantiomeric, with *Λ* helicity and a *δ* LnNCCN chelate ring conformation. The same sense of asymmetric induction was observed in tris-lanthanide Eu complexes of 2,6-picolinamides[89] and with related 12-N_4 based tetra-amides.[103]

The ^{1}H NMR spectrum of the isolated crystals confirmed that it was the major diastereoisomer that had crystallised in each case.

2.3.3. Chiroptical spectral behaviour

Before beginning a thorough investigation into the chiroptical properties of the title complexes, it was first necessary to calibrate the CPL spectrometer and ensure accurate and reproducible results were being obtained. With the help of Prof. Gilles Muller (GM) and his group, we were able to record the CPL spectra of [Eu.($\mathbf{L^{1}}$)$_3$]$^{3+}$ and [Eu.$\mathbf{L^{31d}}$]$^{3+}$ on the instrument at Durham University and the GM spectrometer at San José State University and compare the spectra and measured g_{em} values. The CPL spectra of the two europium complexes recorded on both the custom-built spectrometers were identical in form, despite being slightly less resolved when measured using the GM spectrometer. The g_{em} values for [Eu.$\mathbf{L^{31d}}$]$^{3+}$ were in good agreement when calculated from both sets of spectra. The validation of the CPL spectra and g_{em} values recorded on the Durham spectrometer, allows for confident measurement of CPL and the presentation of results within the rest of this study.

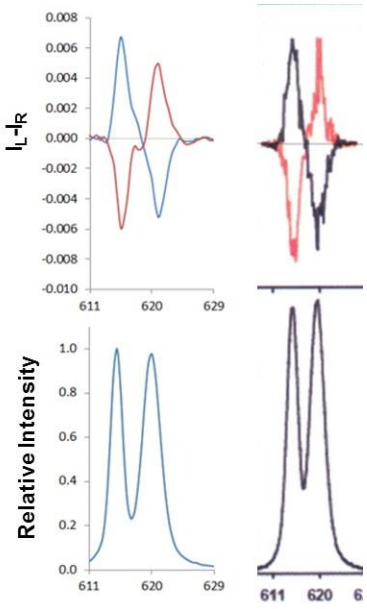

Figure 39 – CPL (*top*) and total emission spectra (*bottom*) of ΔJ = 2 transition of *R*-[Eu.$\mathbf{L^{31d}}$]$^{3+}$ (*red*) and *S*-[Eu.$\mathbf{L^{31d}}$]$^{3+}$ (*blue*) measured on Durham spectrometer (*left*) and GM spectrometer (*right*), (λ_{exc} = 352 nm, D_2O, 295 K).

Table 4 – Measured g_{em} values for *S*-[Eu.$\mathbf{L^{31d}}$]$^{3+}$ (λ_{exc} = 352 nm, D_2O, 295 K).

***S*-[Eu.$\mathbf{L^{31d}}$]$^{3+}$**	Wavelength / nm	g_{em} (Durham)	g_{em} (GM)
	615	+0.013	+0.012
	621	-0.011	-0.012

The CPL spectra of the *Δ* and *Λ* isomers of [Ln.**L**^{30}]$^{3+}$ were examined and showed mirror image behaviour (Ln = Eu, Tb). The sign of each transition depends on the sense of the helical twist of the macrocyclic arms around the metal centre. The emission dissymmetry values, g_{em}, were measured for the europium and terbium complexes of **L**^{30}, with values of up to +0.35 recorded in the *ΔJ* = 4 transition of *S*-*Δ*-(*λλλ*)-[Tb.**L**^{30}]$^{3+}$. There was no significant change to the g_{em} values on the inclusion of the arylalkynyl moiety into the ligand framework, suggesting that the stereochemical environment and degree of conformational rigidity is similar to that of the parent complex.

Table 5 – Emission dissymmetry values, g_{em}, for *S*-*Δ* complexes [Eu.**L**^{30}]$^{3+}$, [Eu.**L**^{31d}]$^{3+}$ and [Tb.**L**^{30}]$^{3+}$.

		***S*Δ-(*λλλ*)-[Eu.L^{30}]$^{3+}$**	
λ / nm	592	653	712
g_{em}	-0.14	-0.19	-0.15
		***S*Δ-(*λλλ*)-[Eu.L^{31d}]$^{3+}$**	
λ / nm	592	653	712
g_{em}	-0.15	-0.15	-0.19
		***S*Δ-(*λλλ*)-[Tb.L^{30}]$^{3+}$**	
λ / nm	539	620	623
g_{em}	+0.11	+0.17	-0.35

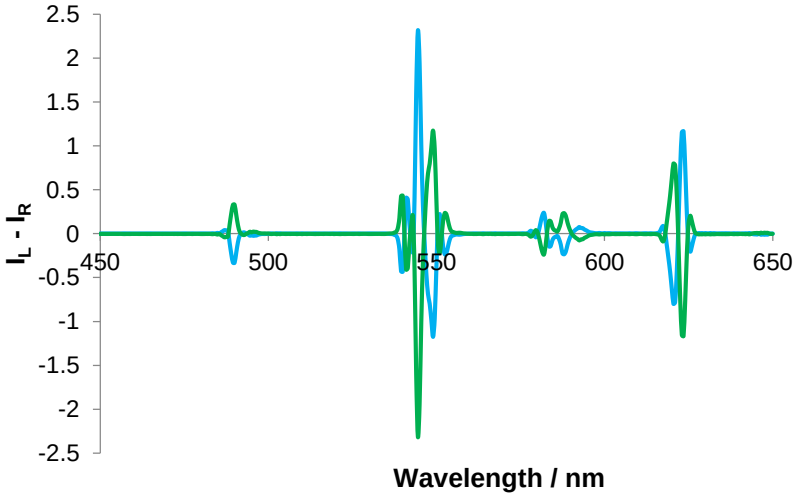

Figure 40 – CPL spectra of *S*-*Δ*-(*λλλ*)-[Tb.**L**^{30}]$^{3+}$ (*green*) and *R*-*Λ*-(*δδδ*)- [Tb.**L**^{30}]$^{3+}$ (*blue*) (λ_{exc} = 280 nm, H_2O, 295 K).

The CPL spectra of [Eu.**L**^{30}]$^{3+}$ and [Eu.**L**^{31d}]$^{3+}$ were also recorded. With these examples, the *ΔJ* = 1 band was not resolved in the total luminescence spectra but was clearly resolved in the CPL spectra, allowing the two Zeeman components of the A_1-E transition to be observed. Analysis

of the energies of these transitions allows an estimate to be made of the second order crystal field term, B_0^2.[161] In the case of [Eu.**L**^{30}]$^{3+,}$ the splitting of the two transitions was found to be 70 cm^{-1}, corresponding to a B_0^2 value of +233 cm^{-1}, compared to +110 cm^{-1} for [Eu.**L**^{32}] and +75 cm^{-1} for [Eu.**L**^{33}].[72]

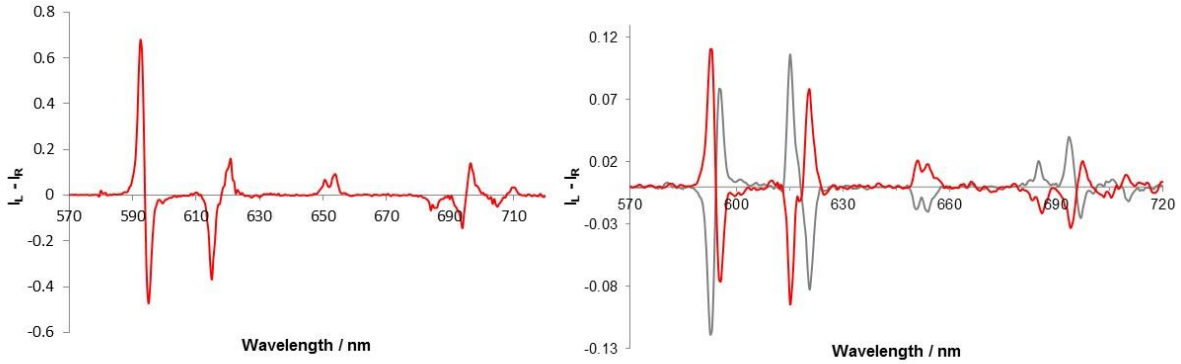

Figure 41 - *left*: CPL spectrum of *R*-*Λ*-(*δδδ*)- [Eu.**L**^{30}]$^{3+}$ (λ_{exc} = 280 nm, pH 5, H_2O, 295 K). *right*: CPL spectra of *S*-*Δ*-(*λλλ*)-[Eu.**L**^{31d}]$^{3+}$ (*grey*) and *R*-*Λ*-(*δδδ*)- [Eu.**L**^{31d}]$^{3+}$ (*red*) (λ_{exc} = 348 nm, pH 5, H_2O, 295 K).

Within a series of complexes based on very similar ligand frameworks, e.g. **L**^{30} and **L**^{31}, accurate determinations of absolute configuration and helicity assignment can be made through comparison of the lanthanide CPL spectra, as can be seen in (Figure 41). Using this data, we were able to confidently assign the absolute configuration of *S*- and *R*-[Eu.**L**$^{31a\text{-}d}$]$^{3+}$ as *Δ*-(*λλλ*) and *Λ*-(*δδδ*) respectively, by comparison of the CPL spectra with that of [Eu.**L**^{30}]$^{3+}$, whose absolute configuration was determined by X-ray crystallography. However, at this stage, it becomes more challenging to find strict correspondence between CPL spectra of complexes derived from different ligand systems. For example, the CPL spectrum of *Δ*-[Eu.**L**^{30}]$^{3+}$ is quite different to that of the structurally similar complexes, *Δ*-[Eu.**L**^{32}] and *Δ*-[Eu.**L**^{33}],[73,102] as well as related C_4-symmetric 12-N_4 tetra-amide systems.[115]

2.4. Comparative analysis of related C_3 symmetrical lanthanide 9-N_3 systems

A detailed comparison of the complexes [Eu.**L**^{30}]$^{3+}$, [Eu.**L**^{32}] and [Eu.**L**^{33}] was undertaken in order to gain a deeper understanding of the effect of changing the nature of the oxygen donor on the ligand field. Systematic comparison of shift and relaxation data allowed conclusions to

be drawn about the main factors that contribute to the size of the ligand field. The work discussed in this section is detailed in the referenced communications.[162,163]

Paramagnetic longitudinal relaxation in these lanthanide complexes arises from rotational and conformational modulation of the electron-nuclear dipolar coupling, when solvent molecules approach the metal centre, as in the equation **2.1**:

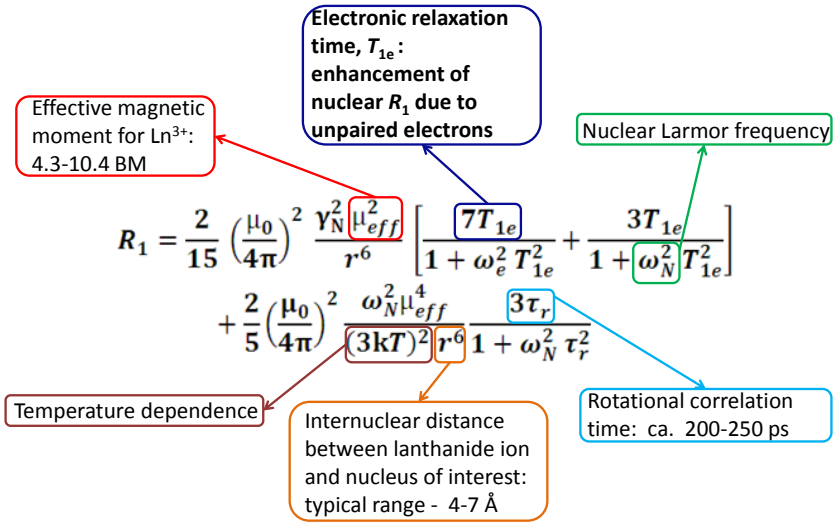

(2.1.)

where μ_0 is vacuum permeability, τ_r is the rotational correlation time assuming isotropic motion, ω_e is the electron Larmor frequency, $(\mu_{eff})^2$ is the square of the effective magnetic moment, T_{1e} is the relaxation time of the electronic spin and r is the electron-nuclear distance. Because R_1 is field-dependent, this allows global minimisation methods to be undertaken, analysing sets of data for several lanthanide complexes in parallel. With the help of Dr. Alexander Funk, the variation of experimental R_1 values with field was used to estimate Ln-proton average distance, r, the rotational correlation time, τ_r, and the electronic relaxation time, T_{1e}. Data obtained in this manner for [Yb.**L**^{30}]$^{3+}$, allowed a comparison to be made with results previously obtained for [Yb.**L**^{32,33}].[100,101] The calculated estimates of Ln-proton average distance corroborated well with the experimental X-ray distances, Table 6.

Table 6 - Tabulated data for calculated and X-ray determined values of *r* for each Yb complex. Values were calculated fitting nuclear relaxation data by Dr. Alexander Funk.

	[Yb.**L**^{30}]$^{3+}$		[Yb.**L**^{32}]		[Yb.**L**^{33}]	
Ln	*r* calc / Å	*r* X-ray / Å	*r* calc / Å	*r* X-ray / Å	*r* calc / Å	*r* X-ray / Å
H_{ax}	4.26	4.06	4.34	4.12	4.01	4.10
H_{ax}'	3.28	3.42	3.47	3.45	n.d.	3.43
H_{eq}	4.46	4.28	4.57	4.35	4.34	4.31
H_{eq}'	4.38	4.23	4.51	4.30	4.33	4.27
pyCHN	4.67	4.31	4.34	4.35	4.42	4.31
pyCH'N	3.43	3.50	3.45	3.50	3.41	3.47
pyH^3	5.47	5.45	5.68	5.53	5.46	5.46
pyH^4	6.23	6.26	6.68	6.36	6.29	6.22
pyH^5	5.51	5.48	5.68	5.59	4.45	5.40

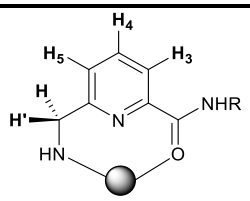

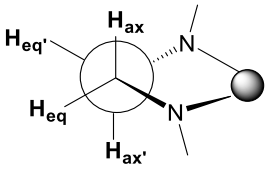

A full analysis of the electronic relaxation time, T_{1e}, and magnetic susceptibility, μ_{eff}, of each complex in the series (for lanthanide complexes amenable to ^{1}H NMR study) was then undertaken using the values of *r* derived from X-ray analysis, and globally minimising the data sets simultaneously (Table 7). Such an approach has been demonstrated to be effective at estimating these variables, especially as the rotational correlation time, τ_r, is not expected to vary significantly from one lanthanide complex to another in an isostructural series.[72,164] The values of T_{1e} fell in the range expected for such complexes with rather weak ligand field i.e. less than or close to *kT*. The data showed that the largest values of T_{1e} were calculated for the tri-amide complexes followed by tri-phosphinate and then the tri-carboxylate system. Furthermore, the estimates of the magnetic susceptibility values were also found to be in reasonable agreement with literature values that, in turn, are derived from aqua ion or solid-state metal oxide data. Literature μ_{eff} values for the aqua ions are typically as follows: Tb, 9.8; Dy, 10.3; Ho, 10.4; Er, 9.4; Tm, 7.6 and Yb, 4.3 BM.[165–167]

Table 7 – Calculated values of magnetic susceptibility (μ_{eff}/μ_B) and electronic relaxation times (T_{1e}, ps) for [Ln.**L**^{n}] (n = 30, 31, 32), derived from global fitting of the field dependence of longitudinal relaxation rate (R_1) data.[a,b] (CD_3OD, 295 K)[c]

	[Ln.**L**^{30}]$^{3+}$		[Ln.**L**^{32}]		[Ln.**L**^{33}]	
Ln	μ_{eff}/μ_B	T_{1e}/ps	μ_{eff}/μ_B	T_{1e}/ps	μ_{eff}/μ_B	T_{1e}/ps
Tb	9.59(03)	0.27(03)	9.40(03)	0.21(04)	9.65(02)	0.26(03)
Dy	10.09(03)	0.29(03)	10.21(03)	0.32(03)	10.47(01)	0.28(02)
Ho	10.31(02)	0.21(03)	10.22(01)	0.11(02)	10.44(01)	0.17(02)
Er	8.80(03)	0.22(04)	9.05(02)	0.26(03)	9.23(02)	0.23(03)
Tm	7.77(02)	0.15(03)	7.66(03)	0.09(03)	7.43(01)	0.08(02)
Yb	4.56(04)	0.17(04)	4.36(03)	0.12(06)	4.27(02)	0.09(04)

[a]Values of τ_r estimated simultaneously were: [Ln.**L**^{30}], 196(1) ps; [Ln.**L**^{32}], 205(6) ps; [Ln.**L**^{33}], 132(1) ps. [b]In each case, for every set of resonances considered, the distance r from the proton to the Ln ion was taken from the X-ray crystallographic analysis. [c]Data for [Ln.**L**^{33}] was recorded in D_2O; earlier work has shown T_{1e} values are independent of solvent viscosity.[72]

In 2012, Fries investigated the factors that influence T_{1e} using time correlated functions and proposed that $T_{1e}\ \alpha\ 1/B_0^2$.[168] In 2013, Funk conducted a study on a series of isostructural lanthanide complexes taking into account higher order terms (B_0^4, B_0^6) that had previously been neglected, and found that instead, there was a direct proportionality between B_0^2 and T_{1e}.[72]

The calculated values of T_{1e} were in accordance with the B_0^2 values calculated from the energies of the relative transitions in the ΔJ = 1 manifold, as discussed on page 60. The highest B_0^2 value was obtained for [Ln.**L**^{30}]$^{3+}$ (+233 cm^{-1}) followed by [Ln.**L**^{32}] (+110 cm^{-1}) and finally [Ln.**L**^{33}] (+75 cm^{-1}). As this parameter also determines the magnitude of the dipolar shift in NMR spectroscopy (equation **2.2.**),[169] this trend was reflected in the relative shifts of the ligand protons, best illustrated in the ^{1}H chemical shift data for the Yb complexes of **L**^{30,32,33} (Table 8). Thus, the most shifted ring proton (H_{ax}) resonates at -18.8, -13.8 and -4.8 for [Yb.**L**^{30}]$^{3+}$, [Yb.**L**^{32}] and [Yb.**L**^{33}] respectively. The total spectral width for each complex is 30, 24 and 14 ppm in that sequence.

$$\delta_{para} = \frac{-2C_J\beta^2}{(kT)^2}\left[\frac{3cos^2\theta - 1}{r^3}\right]B_0^2 \qquad \textbf{(2.2.)}$$

Therefore, these calculations support the hypothesis of Funk et al., which states that there is direct proportionality between the electronic relaxation time and the second order crystal field splitting parameter in highly symmetric complexes i.e. $T_{1e}\ \alpha\ B_0^2$. These examples also highlight

the fact that the sign of B_0^2 in these C_3 symmetric complexes is positive and opposite to that of the multitudinous C_4 $12N_4$ analogues, explaining the different sense of the NMR shifts observed.[163]

Table 8 – Assignment of furthest shifted proton resonances in the ^{1}H NMR spectra of Yb complexes, highlighting the paramagnetic spectral width correlation with B_0^2 (CD_3OD, 295 K, 400 MHz).

^{1}H resonance	[Yb.**L**^{30}]$^{3+}$ (*major isomer*)	[Yb.**L**^{32}]	[Yb.**L**^{33}]
H_{ax}	-18.8	-13.7	-4.8
pyCH'N	22.3	20.7	11.1
Spectral Width / ppm	**30.2**	**24.4**	**13.6**
B_0^2 / cm^{-1}	**+232**	**+110**	**+75**

The rigidity of the complex, the symmetry surrounding the lanthanide ion and the polarisability of the axial donor are all possible factors that determine the lanthanide electronic relaxation in solution.[70,72,163] The value of T_{1e} and hence B_0^2 should be greatest for complexes where the axial donor ligand is the most highly polarisable. This trend is again observed in the case of the three complexes studied, as highest T_{1e} and B_0^2 values were observed for [Ln.**L**^{30}]$^{3+}$ containing a highly polarisable amide oxygen atom, followed by the less polarisable phosphinate and carboxylate oxygen donors.

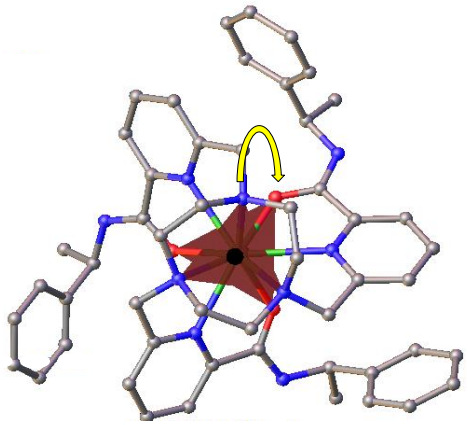

Figure 42 – X-ray crystal structure of *R*-*Λ*-(*δδδ*)-[Eu.**L**^{30}]$^{3+}$ showing the twist angle associated with the trigonal prism distortion.

An investigation into the effect of local symmetry of the complexes on T_{1e} was initiated. The complexes each adopted a distorted tricapped trigonal prism structure. The distortion angle is defined by the twist of the mean plane of 9-N_3 with reference to the three bound oxygen atoms of the amide, phosphinate or carboxylate groups (Figure 42). However, no significant

differences in twist angle (22 ± 2°) were found for the europium or ytterbium complexes of **L**^{30} compared to the corresponding values of [Ln.**L**^{32}] and [Ln.**L**^{33}]. This result suggests, that within this set of complexes, the polyhedral distortion is not an influential factor in the determination of the size of the ligand field.

2.5. Photophysical studies

2.5.1. Characterisation of parent complex [Eu.L^{30}](CF$_3$SO$_3$)$_3$

Photophysical studies such as the measurement of total luminescence and determination of quantum yield, excited state lifetime data and hence number of metal bound waters, *q*, can be very useful in the characterisation of a lanthanide complex. Therefore, a thorough investigation of the photophysical properties of *S*-[Ln.**L**^{30}]$^{3+}$ was undertaken (the *S*-*Δ* isomer was studied unless stated otherwise).

2.5.1.1. Absorption and emission spectral properties

The series of lanthanide complexes of **L**^{30} possess an absorption band at 280 nm attributed to the π-π* transition in the pyridyl chromophore. The emission spectra for the Eu, Tb and Dy complexes were recorded, and revealed spectral profiles that were characteristic for the metal in question. The europium emission spectral profile strongly resembled that of the related 9-N$_3$ pyridylphosphinate complex [Eu.**L**^{32}] under the same conditions.[100] However, the $\Delta J = 2/\Delta J = 1$ ratio is 25% greater for [Eu.**L**^{30}]$^{3+}$ (5:1) compared to the phosphinate complex [Eu.**L**^{32}] (4:1), which can be tentatively attributed to the greater polarisability of the amide oxygen atoms.

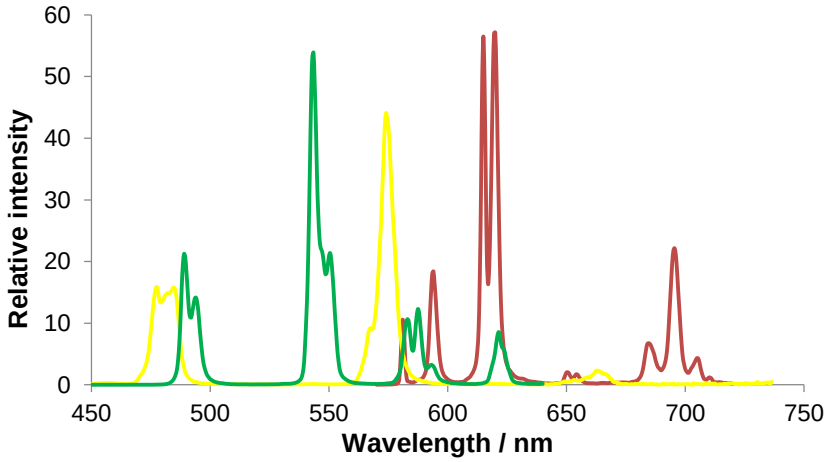

Figure 43 – Total emission spectra of *S*-*Δ*-[Eu.**L**^{30}]$^{3+}$ (*red*), *S*-*Δ*-[Tb.**L**^{30}]$^{3+}$ (*green*) and *S*-*Δ*-[Dy.**L**^{30}]$^{3+}$ (*yellow*) (λ_{exc} = 280 nm, H$_2$O, 295 K).

2.5.1.2. Excited state emission lifetimes and estimation of complex hydration state, *q*

In order to determine the hydration state of the complexes, the excited state lifetimes of the europium and terbium complexes were measured in H_2O and D_2O. There is much less efficient energy transfer from a lanthanide ion to overtones of X-D oscillators compared to X-H oscillators, due to less effective energy matching as a result of the much lower X-D stretching frequencies.[170] This effect means that for a given complex, the diminution of luminescence intensity will occur more slowly in D_2O than H_2O, and allows the number of metal bound water molecules, *q*, to be estimated according to equations **2.3** and **2.4**.[117,170]

$$q\big(Eu(III)\big) = A[\left(\frac{1}{\tau_{H2O}} - \frac{1}{\tau_{D2O}}\right) - 0.25 - 0.075x] \qquad \textbf{(2.3.)}$$

$$q\big(Tb(III)\big) = A[\left(\frac{1}{\tau_{H2O}} - \frac{1}{\tau_{D2O}}\right) - 0.06] \qquad \textbf{(2.4.)}$$

Here, *A* is the proportionality constant and reflects the sensitivity to quenching of the particular lanthanide ion by metal bound water molecules ($A_{(Eu3+)}$ = 1.2 ms, $A_{(Tb3+)}$ = 5 ms). The above equations also take into account the effect of second sphere water molecules and proximate N-H oscillators of amide donors, *x*. A *q* value of approximately zero was calculated for both [Eu.**L**^{30}]$^{3+}$ and [Tb.**L**^{30}]$^{3+}$, indicating that there are no inner sphere water molecules present in the complexes, as expected for these 9 coordinate lanthanide complexes.

Table 9 – Lifetime measurements and derived *q* values of [Eu.**L**^{30}]$^{3+}$ and [Tb.**L**^{30}]$^{3+}$ in H_2O and D_2O (pH 7.4).

	$\tau_{(H2O)}$ / ms	$\tau_{(D2O)}$ / ms	*q*
S-Δ-[Eu.**L**^{30}]$^{3+}$	0.98	1.42	-0.19
S-Δ-[Tb.**L**^{30}]$^{3+}$	1.87	2.12	0.02

2.5.2. Absorption and emission properties of [Eu.L^{31a-d}]Cl$_3$

After an extensive investigation into the structural and photophysical properties of complexes [Ln.**L**^{30}]$^{3+}$, work then turned to the preparation of the related complexes [Eu.**L**$^{31a-d}$]$^{3+}$, where an extended arylalkynyl chromophore was appended to the ligand framework. Substitution of the aromatic group of the chromophore allowed for fine-tuning of the absorption and emission

properties, such as the excitation wavelength, λ_{exc}, molar extinction coefficient, ε, and quantum yield, ϕ_{em}, as well as physical properties such as hydrophilicity, log*P*. The photophysical properties were studied and the results revealed the best suited europium complexes for application in biological studies and *in cellulo*.

2.5.2.1. Absorption and emission spectral properties

The inclusion of an extended arylalkynyl chromophore in the complex system was shown to cause a bathochromic shift of the absorption band of up to 75 nm (for [Eu.$\mathbf{L^{31c}}$]$^{3+}$ and [Eu.$\mathbf{L^{31d}}$]$^{3+}$) compared to the parent complex, [Eu.$\mathbf{L^{30}}$]$^{3+}$. This property is highly desirable if the probes are to be employed *in cellulo*, as a lower energy excitation source can be used and the co-excitation of common biomolecules will be avoided. This absorption band was very intense (ε values in MeOH ranged from 63 000 to 69 000 M^{-1} cm^{-1} to about 55 000 M^{-1} cm^{-1} in H_2O), in accordance with earlier work on the related phosphinate[154] and carboxylate[171] donors, and is consistent with significant ICT (internal charge transfer) character in the excited state.

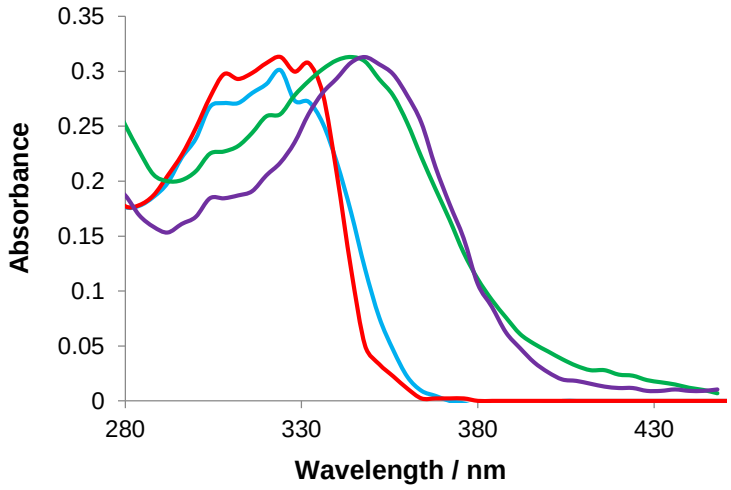

Figure 44 – UV- absorption spectra of [Eu.$\mathbf{L^{31a}}$]$^{3+}$ (*blue*), [Eu.$\mathbf{L^{31b}}$]$^{3+}$(*red*), [Eu.$\mathbf{L^{31c}}$]$^{3+}$ (*purple*), [Eu.$\mathbf{L^{31d}}$]$^{3+}$ (*green*) (H_2O, 295 K).

The position of the absorption band was particularly sensitive to solvent polarity, and there was a hypsochromic shift of the absorbance maxima observed in solvents of lower polarity (Table 10). Such behaviour is consistent with the lowering of energy of the relaxed ICT excited state in more polar protic solvents.[172,173]

Table 10 – Solvatochromism data observed with [Eu.$\mathbf{L^{31a-d}}$]$^{3+}$ (295 K).

Solvent	λ_{max}/nm				
	E_T^{30}normalised	[Eu.$\mathbf{L^{31a}}$]$^{3+}$	[Eu.$\mathbf{L^{31b}}$]$^{3+}$	[Eu.$\mathbf{L^{31c}}$]$^{3+}$	[Eu.$\mathbf{L^{31d}}$]$^{3+}$
H_2O	1.00	332	328	356	352
MeOH	0.76	332	328	355	352
EtOH	0.65	331	327	355	349
^{i}PrOH	0.55	320	324	336	344
DMF	0.40	308	316	332	336

[a] E_T^{30} values are based on Reichardt's normalised solvent polarity scale.[174]

The europium emission spectra for all of the complexes were very similar and almost identical to the behaviour of [Eu.$\mathbf{L^{32,33}}$] and their extended chromophore analogues, consistent with time-averaged C_3 symmetry. The spectra of the tri-amide, [Eu.$\mathbf{L^{31c}}$]$^{3+}$, and related tri-carboxylate, [Eu.$\mathbf{L^{35}}$] (Figure 46),[171] complexes were compared to C_3 symmetrical europium complexes with ida (iminodiacetate) and dpa (2,6-pyridinedicarboxylate) ligands. The complexes of $\mathbf{L^{31}}$ (D) and $\mathbf{L^{35}}$ (C) showed particularly strong resemblance to [Eu.$(dpa)_3$]$^{3-}$(B), with a ratio of intensities of $\Delta J = 2/\Delta J = 1$ of around 4 or 5 in each case (Figure 45).

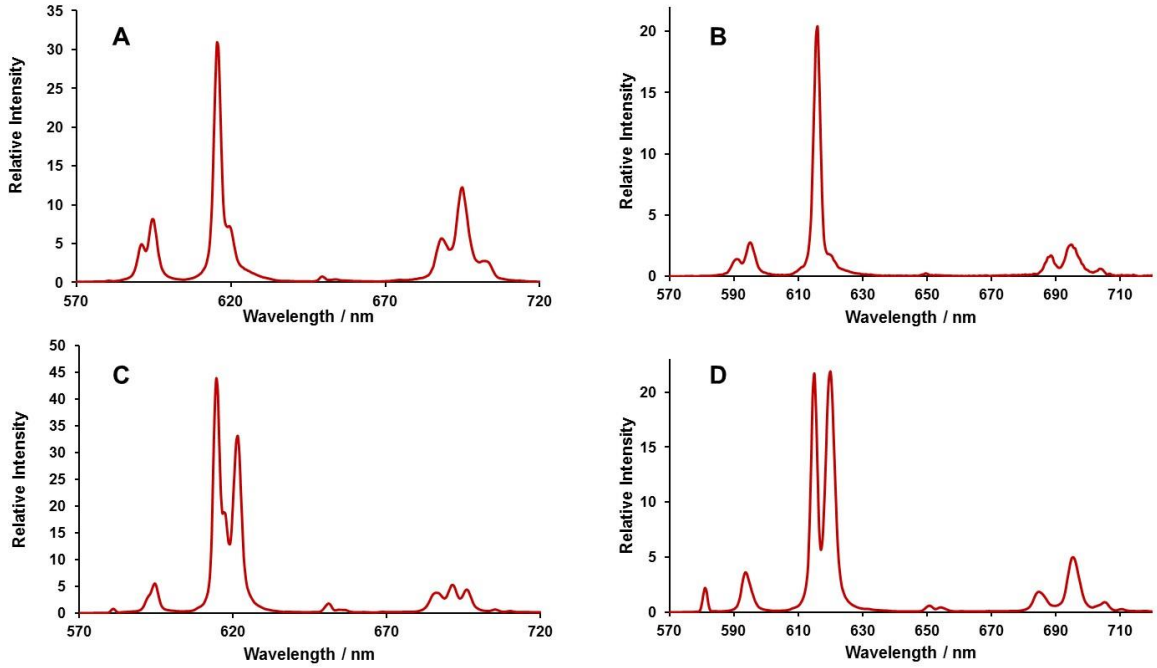

Figure 45 – Comparison of total emission spectra for C_3-symmetric Eu(III) complexes: (A) [Eu.$(ida)_3$]$^{3-}$ (λ_{exc} = 395 nm, H_2O, pH 8.5); (B) [Eu.$(dpa)_3$]$^{3-}$ (λ_{exc} = 395 nm, H_2O, pH 8.5); (C) [Eu·$\mathbf{L^{35}}$] (λ_{exc} = 352 nm, H_2O, pH 7.4); (D) [Eu·$\mathbf{L^{31c}}$](λ_{exc} = 352 nm, H_2O, pH 6).

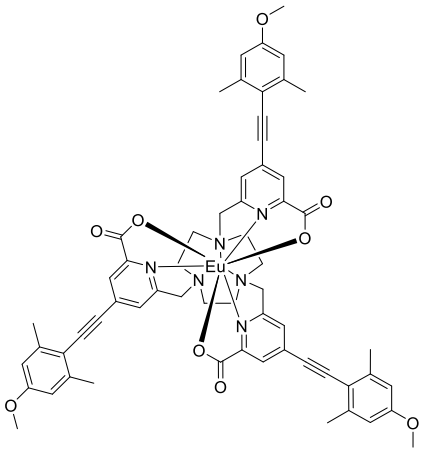

[Eu.L^{35}]

Figure 46 - Structure of the tri-carboxylate Eu (III) complex, [Eu.**L^{35}**].[171]

Quantum yield calculations were carried out by comparison to a known standard [Eu.**L^{36}**], where the quantum yield had been accurately determined using a Labsphere Optical Spectralon integrated sphere.[149] The arylalkynyl chromophore acts as an efficient sensitiser of europium emission, and quantum yields in methanol were between 4 and 8%, for each complex of the four ligands **L^{31a-d}** (Table 11). These quantum yield values were significantly lower than those obtained for the related tri-phosphinate (ϕ_{em} = up to 54% in methanol)[154] and tri-carboxylate complexes (ϕ_{em} = up to 55% in methanol).[171] The luminescence lifetimes for [Eu.**L^{31c}**]$^{3+}$ and [Eu.**L^{31d}**]$^{3+}$ (X = OMe and NHOAc) were also shorter than expected; 0.49 and 0.46 ms respectively, compared to 0.81 and 0.80 ms for [Eu.**L^{31a}**]$^{3+}$ and [Eu.**L^{31b}**]$^{3+}$ in water.

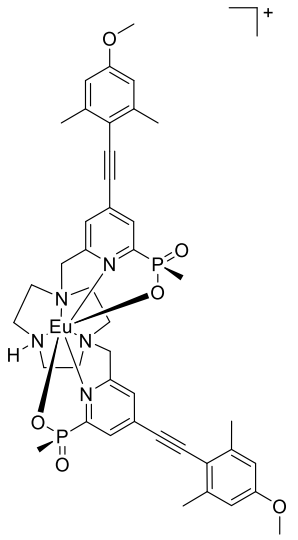

[Eu.L^{36}]$^{+}$

Figure 47 – Structure of europium complex [Eu.**L^{36}**]$^{+}$.

Table 11 – Photophysical data for the complexes *S*-[Eu.**L**$^{31a-d}$]Cl_3 (295 K).

Complex	λ_{max}	ε(MeOH)/M^{-1} cm^{-1}	τ(MeOH)/ms	τ(H_2O)/ms	ϕ_{em}(MeOH)	ϕ_{em}(H_2O)
[Eu.**L**^{31a}]$^{3+}$	332	69 000	0.67	0.80	0.08	0.35
[Eu.**L**^{31b}]$^{3+}$	328	63 000	0.65	0.81	0.03	0.37
[Eu.**L**^{31c}]$^{3+}$	355	65 000	0.45	0.49	0.04	0.02
[Eu.**L**^{31d}]$^{3+}$	352	65 000	0.54	0.46	0.03	0.02

The lower quantum yields and emission lifetimes for [Eu.**L**^{31c}]$^{3+}$ and [Eu.**L**^{31d}]$^{3+}$ suggested that the intramolecular energy transfer step from the relaxed ICT state may be partially reversible, and therefore thermally activated. To investigate this hypothesis further, a variable temperature emission study of [Eu.**L**^{31c}]$^{3+}$ in a glass of EPA (ether-isopentane-methanol 5:5:2) was carried out over a temperature range of 298 to 80 K (Figure 48). As the temperature was lowered, the emission intensity increased by a factor of five over the range 295 to 235 K, consistent with the suppression of thermally activated back energy transfer from the excited Eu (III) $^5D_0$ state to the ICT excited state.

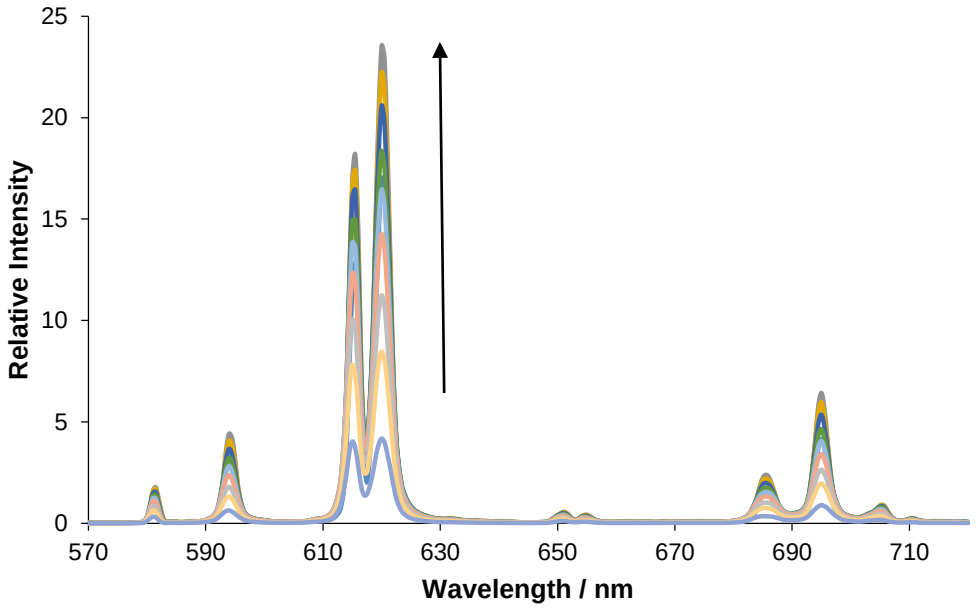

Figure 48 – Variation of the Eu (III) emission spectrum of [Eu.**L**^{31c}]$^{3+}$ with decreasing temperature from 298 to 80 K (λ_{exc} = 356 nm, ether:isopentane:ethanol 5:5:2).

Further evidence for the presence of an ICT centred excited state was gathered by investigating the phosphorescence spectrum of [Gd.$\mathbf{L}^{\mathbf{31d}}$]$Cl_3$, recorded at 85 K in a glass of EPA (5:5:2). A very broad structureless band at low temperature was observed, centred at 450 nm (530 nm shoulder). This observation was consistent with the intermediacy of an excited state with predominant ICT character, rather than a triplet excited state, where you would expect to observe a sharp well-defined band possessing vibrational fine structure.

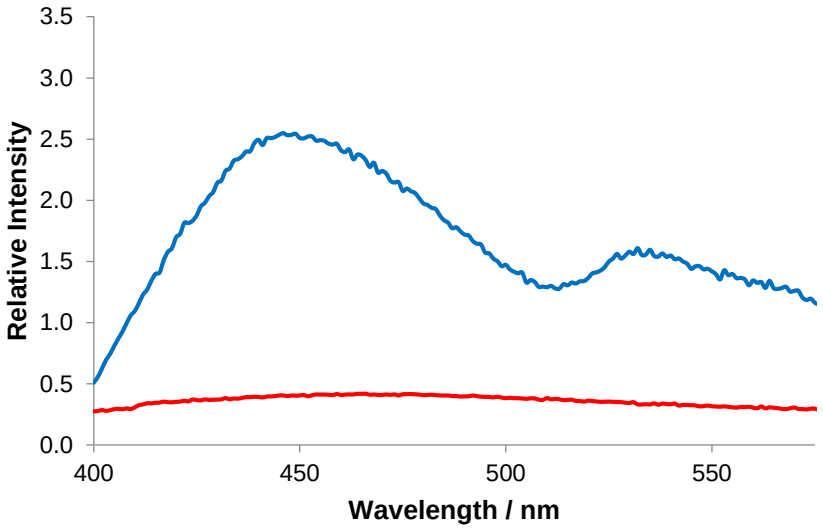

Figure 49 – Phosphorescence spectra of *S*-[Gd.$\mathbf{L}^{\mathbf{31d}}$]$Cl_3$ at 298 K (red) and 85 K (blue) showing a broad emission band centred at 450 nm with a shoulder at 530 nm (ether:isopentane:ethanol 5:5:2).

In water at pH 6.5, the emission quantum yields of [Eu.$\mathbf{L}^{\mathbf{31a}}$]$^{3+}$ and [Eu.$\mathbf{L}^{\mathbf{31b}}$]$^{3+}$ (X = H and CO_2Me) were 35 and 37% respectively. These are among the highest values reported for sensitised emission of any europium complex in aqueous solution, and compare to 39% for the closely related tri-phosphinate system.[154] As the quantum yields were higher for the two complexes containing weak donor and electron withdrawing groups ($\mathbf{L}^{\mathbf{31a,31b}}$), we can hypothesise that in an aqueous environment, the ICT state of these complexes lies at a higher energy and consequently, a contribution from the classical triplet mediated sensitisation process may occur.[171,175] Such behaviour is in contrast to the complexes containing strongly donating moieties ($\mathbf{L}^{\mathbf{31c,31d}}$), where sensitisation is most definitely occurring *via* an ICT excited state (Figure 50), as demonstrated in the preceding discussion.

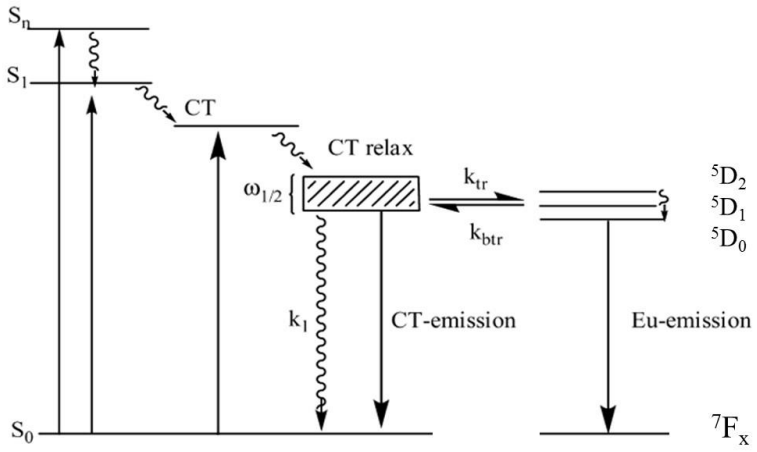

Figure 50 – Simplified Jablonski diagram illustrating sensitised Eu (III) emission *via* a solvent relaxed internal charge transfer state.[173]

The emission intensities of [Eu.$\mathbf{L}^{\mathbf{31a}}$]$^{3+}$ and [Eu.$\mathbf{L}^{\mathbf{31b}}$]$^{3+}$, in the presence of a thousand-fold excess of EDTA at pH 6.5, were monitored as a function of time over a period of seven days; after an initial 15% reduction, no significant change in intensity was observed in each case, consistent with the high kinetic stability of these systems with respect to dissociative ligand exchange.

The water solubility of the complexes was assessed by calculation of the partition coefficient, log*P*. Of the four complexes studied, the chloride salts of [Eu.$\mathbf{L}^{\mathbf{31c}}$]$^{3+}$ and [Eu.$\mathbf{L}^{\mathbf{31d}}$]$^{3+}$ were the least soluble in water by empirical observational analysis. A log*P* value for the most water soluble complex, [Eu.$\mathbf{L}^{\mathbf{31b}}$]$Cl_3$ (X = CO_2Me), was calculated by preparation of three equimolar solutions in methanol. The solvent was removed under reduced pressure and the resulting solid was dissolved in three 0.9 mL H_2O-octanol mixtures (2:1, 1:1 and 1:2 v/v) and stirred for 24 h at r.t. (approx. 2 µM complex in each mixture). After equilibration, an emission spectrum for each layer was recorded in MeOH (50 µL solution in 1 mL MeOH). For each mixture, the log*P* value was calculated according to equation **2.5**.

$$logP = log\left(\frac{\int_{605\ nm}^{635\ nm} I(oct)}{\int_{605\ nm}^{635\ nm} I(H_2O)}\right) \qquad \textbf{(2.5.)}$$

A partition coefficient of +0.9 was calculated for [Eu.**L**^{31b}]Cl_3. The small positive number indicated that the complex is more soluble in organic solvents, and only partially soluble in water.

2.5.2.2. pH dependent emission behaviour and calculation of pK_a of *S*-[Eu.L^{31c}]Cl_3

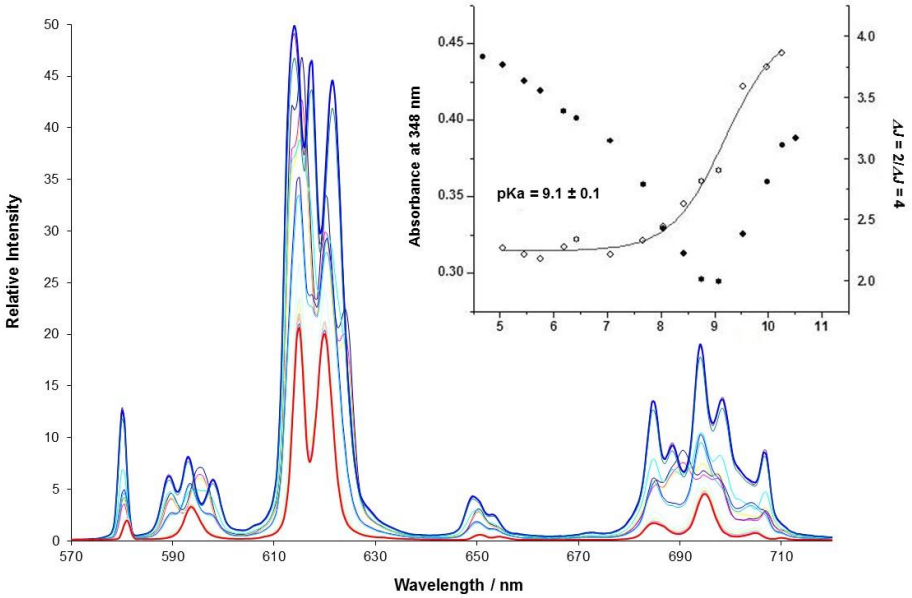

Figure 51 – Variation of the Eu (III) emission spectrum as a function of pH for *S*-[Eu.**L**^{31c}]Cl_3, pH 4.08 – *red*, pH 10.52- *blue* (^{i}PrOH-H_2O 80:20 v/v, 5 µM complex, 298 K, λ_{exc} = 348 nm). Inset shows absorbance changes at 348 nm with pH (*filled circles*), and variation of ΔJ =2/ ΔJ = 4 relative emission intensity ratio with pH (*open circles*) (pK_a 9.1 ± 0.1).

The absorption and emission spectral behaviour of the complexes [Eu.**L**^{31c}]$^{3+}$ and [Eu.**L**^{31d}]$^{3+}$, absorbing at longer wavelength in protic solvents, was also sensitive to the apparent pH. The pH response of *S*-[Eu.**L**^{31c}]$^{3+}$ was explored and a pK_a value in the ground and excited state was calculated. The complex was dissolved in an 80:20 v/v ^{i}PrOH-water mixture, as this allowed for observation of the most significant changes in emission spectral form and ensured full solubility of the complex in solution throughout the titration. The apparent pH was varied using conc. NaOH (aq.) and HCl (aq.) solutions to ensure negligible change to the overall volume, and thus concentration of the complex. The pH was measured before and after each data point was recorded. As the apparent pH was varied, both the absorbance at 348 nm and the europium emission spectral form changed. The spectral changes observed were completely reversible. The emission spectral changes were particularly striking and led to the appearance of a number of additional transitions, consistent with a lowering of the symmetry around the Eu ion, and a change in the Eu coordination environment (Figure 51). Of particular note was the change in

the ΔJ = 1 transition around 595 nm, which evolved from a broad single manifold into three distinct transitions. For a Eu complex, three transitions are symmetry-allowed in systems lacking a C_n symmetry axis. The absorption spectral changes were characterised by a shift to the blue at higher pH, moving the primary absorption band from 355 to 328 nm (Figure 52). The excited state lifetime decreased upon lowering the apparent pH from 0.73 ms at pH 10.52 to 0.54 ms at pH 4.08.

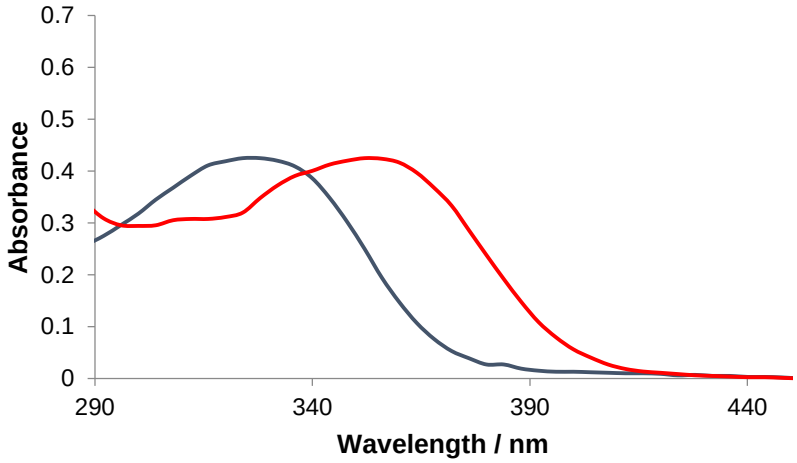

Figure 52 – UV-absorption spectra of *S*-[Eu.$\mathbf{L^{31c}}$]Cl_3 in ^{i}PrOH-H_2O (80:20 v/v) at an apparent pH of 10.3 (*blue*) and 4.4 (*red*).

Values of the apparent pK_a for the ground and excited state were derived by iterative fitting of the observed spectral changes to a two-state equilibrium, and were estimated to be 9.1 in each case. Taken together, this behaviour is consistent with a deprotonation of one amide NH proton, reversibly generating an amide enolate in which the anionic oxygen atom is coordinated to the europium centre (Figure 53). Indeed, in several examples of 12-N_4 lanthanide tetra-amide complexes, similar pK_a values (range 7.9 – 11.1) have been associated with amide deprotonation in aqueous media.[176–178]

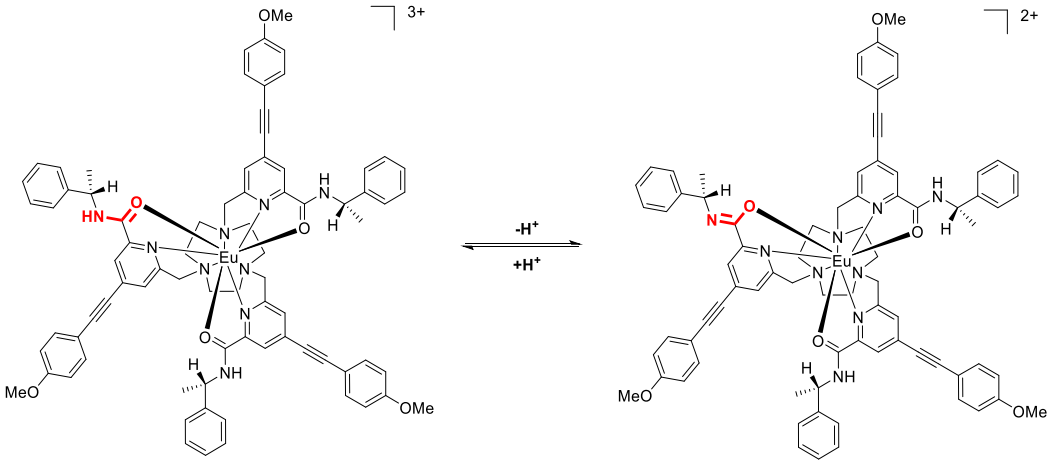

Figure 53 – Possible amide deprotonation mechanism of *S*-[Eu.**L**^{31c}]Cl_3 leading to the observed changes in absorption and emission spectral form (apparent pK_a 9.10).

2.6. Conclusions

A novel enantiopure ligand system, **L**^{30}, based on an amide substituted 9-N_3 macrocycle derived from either *R*-(+) or *S*-(-)-α-methylbenzyl amine was synthesised. The series of chiral lanthanide complexes based on this model system, [Ln.**L**^{30}]$(CF_3SO_3)_3$, were prepared and fully characterised using crystallographic, NMR, HPLC and CPL methods. The remote chiral centre of the amide was shown to induce the formation of one major diastereoisomer upon complexation with the lanthanide metal. The proportion of the major isomer in solution was 9:1 for Ce and Pr, 7 or 6:1 from Nd to Tm falling to 4:1 for Yb. The level of remote stereocontrol in complexation is inferior to that created by C-substitution directly on the macrocyclic ring, where it has been shown that incorporation of one methyl substituent onto the ring led to preferential formation of one enantiomeric complex (>96%).[73] The stereogenic centre of the remote amide determines the helicity of the metal complex in this new range of nonadentate Ln (III) complexes based on triazacyclononane. The major species of the parent complex, [Eu.**L**^{30}]$^{3+}$, was determined by X-ray crystallography, and was found to exist as *S*-*Δ*-(*λλλ*) and *R*-*Λ*-(*δδδ*). The major species of *S*-[Yb.**L**^{30}]$^{3+}$ was identified as *Δ*-(*λλλ*) using similar methods, providing strong evidence that the complexes are isostructural across the series.

A ^{1}H NMR spectroscopic comparative study of [Ln.**L**^{30}]$^{3+}$ and the closely related tri-phosphinate and tri-carboxylate complexes, [Ln.**L**^{32}] and [Ln.**L**^{33}], was conducted. A systematic comparison of shift and relaxation data allowed for a full analysis of the electronic relaxation time, T_{1e}, of the lanthanide complexes to be assessed. The study supported previous

investigations regarding the proportionality of the pseudocontact shift with the ligand field parameter, B_0^2, for an axially symmetric isostructural series of lanthanide complexes.[72] The values of B_0^2 were determined using emission and CPL data, and compared to the measured values of T_{1e}. The results showed that there is direct proportionality between the electronic relaxation time and the second order crystal field splitting parameter, which in turn can be correlated to the total spectral width of the ^{1}H NMR spectrum of the complex. The highest values of T_{1e} and B_0^2 were calculated for the tri-amide complex and were attributed to the increased polarisability of the oxygen donor compared to the tri-phosphinate and tri-carboxylate complexes.

The parent system was further developed to include *para*-substituted arylalkynyl chromophores which allowed fine-tuning of the photophysical properties of this new class of complexes. The diastereomeric induction of four analogous europium complexes, [Eu.**L**$^{\mathbf{31a-c}}$]Cl_3, was improved and the complexes were found to exist as one major isomer in solution in a ratio of 15:1. The maximum excitation wavelength was red-shifted up to 75 nm for [Eu.**L**$^{\mathbf{31c}}$]$^{3+}$ in aqueous solution, compared to a value of λ_{exc} = 280 nm for the parent system, [Eu.**L**$^{\mathbf{30}}$]$^{3+}$. Each complex absorbs light strongly *via* an ICT transition in the range 320 to 356 nm (ε = 55 000 M^{-1} cm^{-1} in H_2O) that is strongly solvatochromic. However, in the case of the two complexes that absorb at the longer wavelengths ([Eu.**L**$^{\mathbf{31c,d}}$]$^{3+}$), the quantum yield and excited state lifetime values are low ([Eu.**L**$^{\mathbf{31c}}$]$^{3+}$: ϕ_{em} = 2%, τ = 0.49 ms, H_2O). Variable temperature emission spectroscopy revealed a thermally activated back energy transfer process was occurring, quenching the excited state of these particular complexes. On the contrary, two examples absorbing light at around 332 nm, albeit with a broad transition that extends to 355 nm, possess overall emission quantum yields at Eu of 35 and 37% in aerated water. These values are amongst the highest recorded for sensitised europium emission in aqueous solution. All four complexes display strong CPL activity with well-defined spectral form and high g_{em} values (*S*-[Eu.**L**$^{\mathbf{31c}}$]$^{3+}$ g_{em}(592 nm) = -0.15), consistent with a conformationally rigid chiral system.

Taking into account all the physical and photophysical properties, it is clear that a compromise must be made between maximum excitation wavelength, and the luminescent lifetime and brightness of the complex. This investigation has shown that a high level of stereocontrol can be imparted on a complex using this enantiopure ligand system, resulting in the synthesis of bright chiral europium complexes that exhibit strong CPL. Such behaviour augurs well for the use of analogues of these systems as the basis of CPL probes, in which the sign and intensity

of selected CPL transitions can be monitored following addition of a chiral analyte. The following chapter investigates the use of dynamically racemic complexes as CPL probes, based on analogues of the ligand systems **L**$^{\mathbf{31a-d}}$.

CHAPTER THREE

INDUCED CPL FROM DYNAMICALLY RACEMIC EU (III) COMPLEXES

3.1. Introduction

The emissive lanthanide excited state can be perturbed in a variety of different ways, including changes in the local solvent structure and static and dynamic charge transfer quenching processes.[179] In particular, changes in the ligand field can arise from reversible binding of an analyte to the metal or the ligand.[5,151] The latter modulation is of particular use in signalling the presence of a chiral species in solution.

For Eu (III), perturbation of the ligand field can have a dramatic effect on the emission profile, most notably in the intensity of the hypersensitive $\Delta J = 2$ transition. Several practical examples exploiting this effect have been demonstrated, including assays of citrate,[180] lactate[181] and bicarbonate[119,182] in biofluids. In each case, the interaction with the lanthanide complex is signalled by modulation of the total emission spectrum. However, such analyses are not normally sensitive to chiral aspects that arise from specific stereochemical interactions.

Chiroptical methods, such as CPL, must be employed to address such issues. The observation of induced CPL has been demonstrated for lanthanide complexes based on dpa and dpa-derived ligands, in the presence of a number of chiral additives, as discussed in Chapter 1, Section 1.5.1. However, in these examples, the observed effects are attributed to an outer sphere association mechanism as opposed to direct binding to the metal centre. A recent example of the reversible binding of acute phase proteins, α_1-AGP and α_1-AAT, to a lanthanide complex has been reported, in which induced CPL was used to signal the detection.[146]

A racemic mixture of Ln (III) complexes in an achiral environment exhibits no CPL. However, the addition of a chiral agent can give rise to strong induced CPL, following stereoselective interactions between the two species. The relative intensity of the induced signal will be a function of the energy difference between the two diastereoisomeric adducts, the selectivity and affinity of binding, and the conformational rigidity of the complex on the emission timescale.

The intrinsic brightness of the complex, $B(\lambda) = \varepsilon(\lambda)\phi_{em}(\lambda)$, is also an important practical aspect, as the acquisition of the total emission (I_L+I_R) and CPL (I_L-I_R) should be as rapid as possible, with maximum signal to noise. Recent work has introduced a new series of very bright Eu (III) complexes based on a 9-N_3 core ligand structure, with various substituted pyridyl-aryl-alkynyl groups acting as the sensitising chromophore. The

substituted pyridyl pendant arms include pyridyl-phosphinates,[60,154,183] pyridyl-carboxylates[171] and finally the series of pyridyl-amides[162] that were presented in Chapter 2. Coordinatively unsaturated heptadentate complexes have also been reported that can bind to anions reversibly in aqueous media.[149]

Determining the enantiomeric purity of chiral therapeutic agents is of great importance in the pharmaceutical industry. Traditional methods of assessing the enantiomeric composition of a sample include NMR spectroscopy, HPLC and GC. CPL exists as a complementary tool that can aid in the chiral analysis of a sample, allowing for discrimination between enantiomeric compounds. Several studies using $[Ln.(dpa)_3]^{3-}$ have shown the possibility of using lanthanide complexes in the determination of the enantiomeric excess of a sample in conjunction with CPL spectroscopy.[50] A more recent example has reported a linear variation of the enantiomeric composition of a sample with g_{em} values for dynamically racemic Eu^{3+} and Tb^{3+} complexes.[15]

This chapter describes the preparation of four dynamically racemic heptadentate Eu (III) complexes detailed in the referenced publication.[184] The complexes differ in nature by the overall charge of the system; the bis-phosphinate and bis-carboxylate europium complexes are monocationic, whereas the bis-amide complex is tri-positively charged. The steric demand around the metal centre led to further distinction between the complexes, where the phosphinate ligand creates a more sterically hindered environment compared to the analogous carboxylate ligand system. The aryl-alkynyl chromophore of each complex was altered leading to variation in the maximum excitation wavelength, λ_{exc}, and emission quantum yield, ϕ_{em}. The work presented will compare and contrast the behaviour of these complexes in order to trace the key ligand structural features that allow them to act as effective chirality probes for CPL. The rate of racemisation of $[Ln.(dpa)_3]^{3-}$ and related complex $[Eu.(\mathbf{L^1})_3]^{3+}$ will be investigated using EXSY (EXchange SpectroscopY) and saturation transfer NMR experiments and compared to the observed findings regarding the rate of exchange in the title complexes, $[Eu.\mathbf{L^{37\text{-}40}}]$. The nature of the binding interaction between the complexes and a number of enantiopure α-hydroxy acids will be investigated, in order to deepen our understanding of their mode of binding, the mechanism of induced CPL and allow us to draw informative structure-spectral correlations. The application of these complexes in the determination of enantiomeric purity of a sample with unknown composition will also be demonstrated.

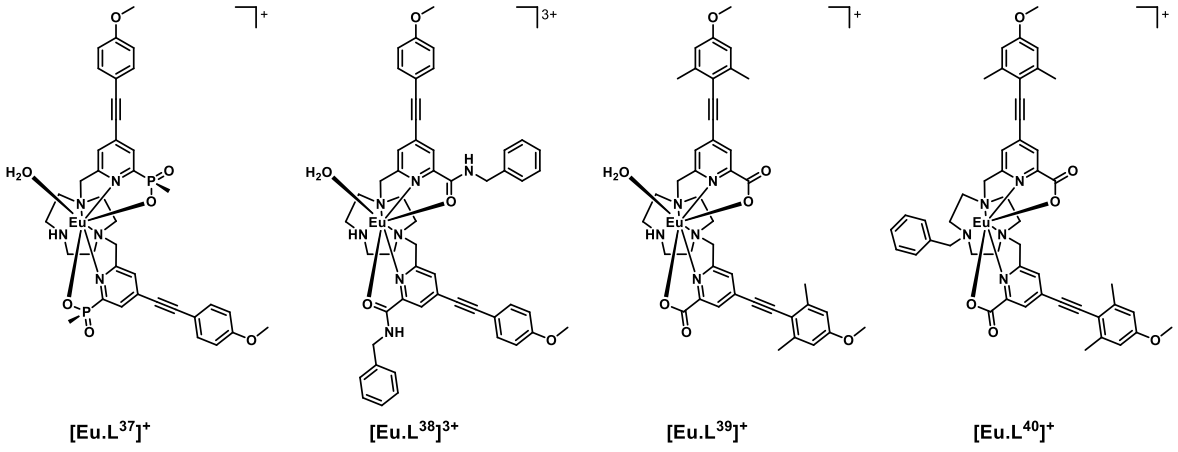

Figure 54 – Structures of Eu (III) complexes of $\mathbf{L^{37\text{-}40}}$.

3.2. Synthetic aspects

The preparation of the di-phosphinate complex, [Eu.$\mathbf{L^{37}}$]$^{+}$, was reported first by McMahon in preliminary work.[15,149]

3.2.1. Synthesis of a bis-pyridylamide-9-N_3 europium complex, [Eu.L^{38}]$^{3+}$

The synthesis of the pendant arm was based on the pathway outlined in Scheme 14, Chapter 2, beginning with intermediate **3a**. Base hydrolysis followed by amide coupling, using achiral benzylamine as opposed to chiral α-methylbenzylamine, afforded the benzylamide, **4b**. A Sonogashira cross-coupling reaction with 4-methoxy-phenylalkyne employing a Pd(II)/Cu(II) catalyst system, gave the alcohol, **4c**, which was converted to the mesylate under standard conditions (Scheme 15).

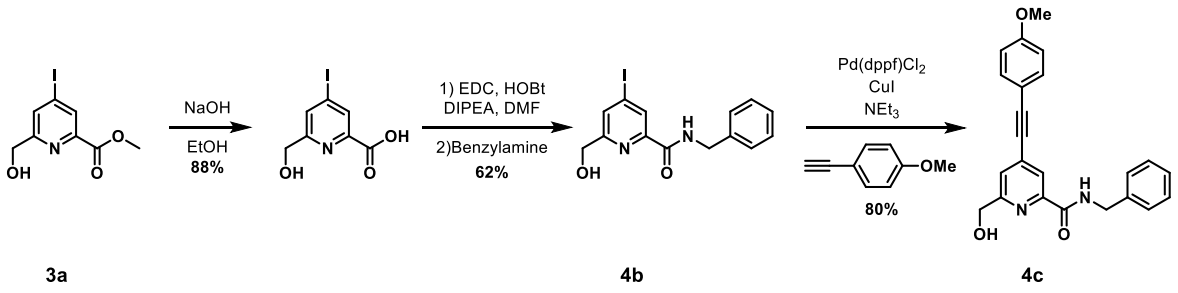

Scheme 15 – Synthesis of the achiral pendant arm of $\mathbf{L^{38}}$.

In order to synthesise the di-substituted ligand $\mathbf{L^{38}}$, it was first necessary to prepare *tert*-butyl-1,4,7-triazacyclononane-1-carboxylate (mono-BOC 9-N_3).[149] This was achieved

using an orthogonal protection strategy. Two sites on the 9-N_3 macrocycle were alkylated with a bulky carbobenzyloxy (Cbz)-protecting group. The free secondary amine was then reacted with *N-tert*butoxycarbonylsuccinimide to furnish a BOC protecting group at the third site. The Cbz-protecting groups were removed by hydrogenation over a palladium hydroxide/C catalyst at 4 atmospheres generating the desired mono-protected macrocycle in good yield (Scheme 16).

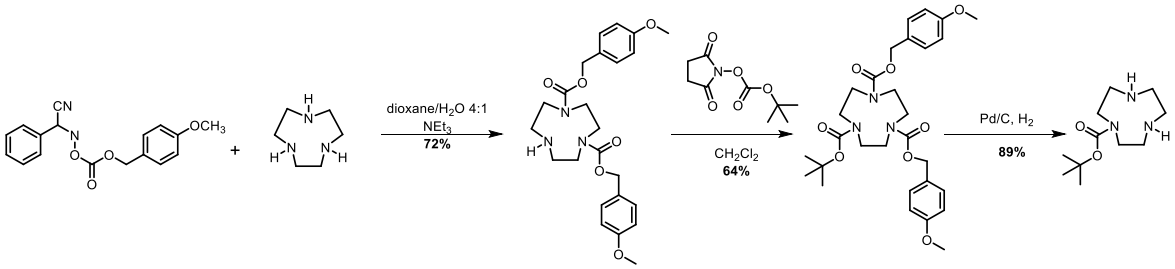

Scheme 16 – Mono-protection strategy for 1,4,7-triazacyclononane.[149]

Alkylation of mono-BOC 9-N_3 with two equivalents of the mesylate, **4d**, gave the carbamate, **4e**, from which the Eu (III) complex was prepared, following deprotection with TFA and reaction with europium triflate in methanol.

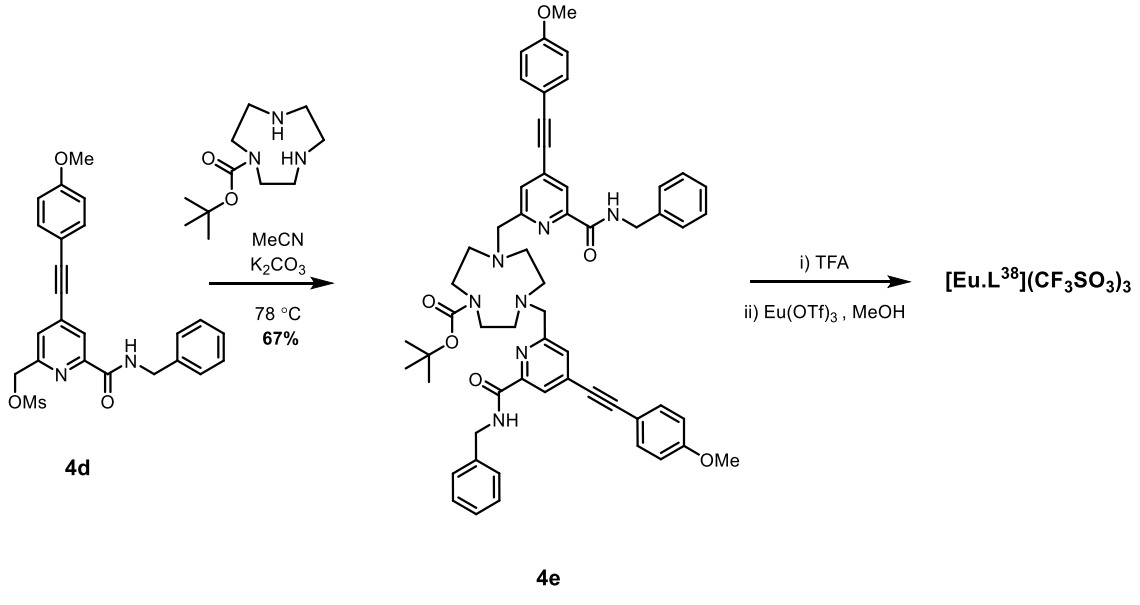

Scheme 17 – Synthesis of [Eu.**L**^{38}](CF$_3$SO$_3$)$_3$.

In the BOC-deprotection step, approximately 40% of the alkyne was converted to the hydrated product, catalysed by the presence of strong acid. The two products were

inseparable by column chromatography, and so reverse phase HPLC was employed to separate the desired ligand from the hydrated by-product. After successful purification by preparative HPLC (H_2O 0.1% formic acid / MeOH 0.1% formic acid), the ligand was passed down an ion exchange column, to ensure complete removal of formate. The complexation reaction progressed very slowly, and the observation after 48 h of a broad fluorescence band below 550 nm in the emission spectrum, signalled the presence of free ligand. Efforts to push the reaction to completion (time, temperature, excess Eu (III)) resulted in no significant improvement on the extent of the reaction. The instability of the complex meant that HPLC in the presence of formic acid resulted in full decomplexation, and no alternative solvent system for purification could be found. The tri-positive nature of the complex also prohibited purification using column chromatography. The studies outlined in the following sections were carried out on a mixed ligand-complex mixture of **L**[38] (~1:5).

3.2.2. Synthesis of bis-pyridylcarboxylate-9N_3 europium complexes, [Eu.L[39,40]]$^+$

3.2.2.1. Synthesis of the chromophore

Based on previous studies of the related tri-carboxylate europium complexes,[171] the incorporation of an electron rich aromatic group in the chromophore framework, results in a significant bathochromic shift of the excitation wavelength. For example, the addition of two *ortho*-methyl substituents to a *para*-methoxy arylalkyne complex moves the excitation wavelength from λ_{exc} = 339 nm to λ_{exc} = 351 nm. With this in mind, a *para*-methoxy di-*ortho*-methyl arylalkyne was selected as a suitable chromophore.

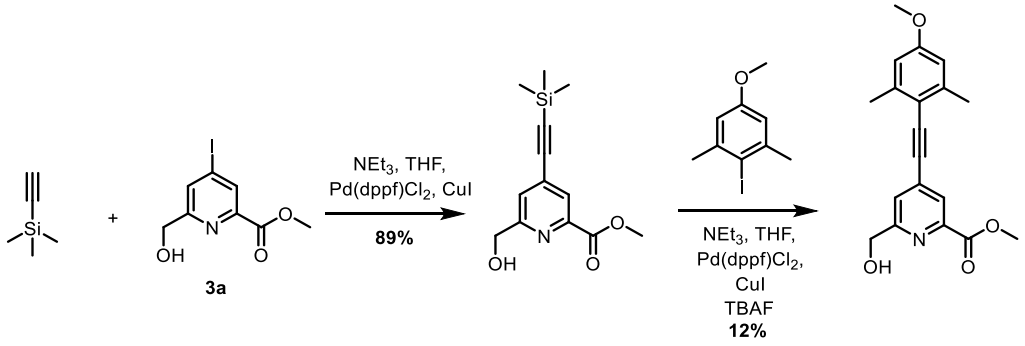

Scheme 18 – Initial synthetic pathway for the synthesis of the pendant arm.[171]

The initial synthetic pathway for the synthesis of the pendant arm was designed beginning with the aryl-iodide, **3a** (Scheme 18). Cross-coupling of **3a** with ethynyltrimethysilane

was carried out in excellent yield using Pd(dppf)Cl_2 and CuI. Attempts were then made at *in situ* deprotection of the silyl protecting group using tetra-*n*-butylammonium fluoride (TBAF) followed by a second cross coupling with the desired aromatic halide. However, a very low yield (12%) of the product was obtained and the crude mixture proved very difficult to purify in the presence of the excess TBAF. Triethylammonium trihydrofluoride was employed as a milder alternative for the silyl deprotection step. However, significant formation of a by-product was observed, which MS studies revealed to be the dimer of the starting material. This observation suggested that the free pyridyl-alkyne was unstable and highly reactive towards dimerisation under these conditions.

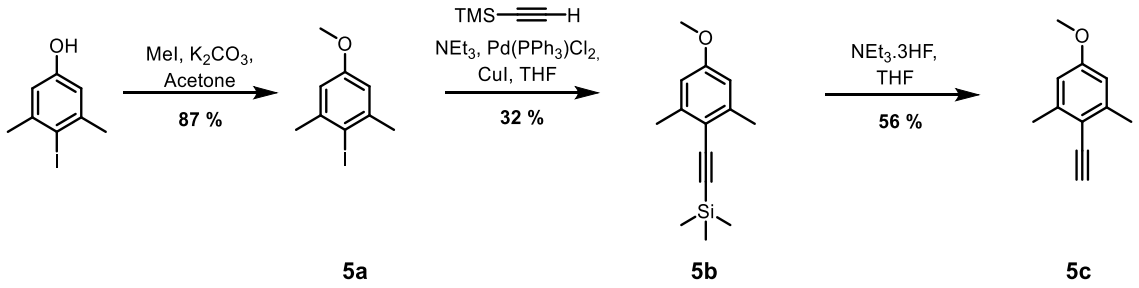

5a **5b** **5c**

Scheme 19 – Reaction scheme for the synthesis of the aryl-alkynyl chromophore, **5c**.

An alternative strategy was then designed, which focussed on the synthesis of the alkyne, **5c** (Scheme 19). Sonogashira coupling of the electron rich aromatic-halide, **5a**, to ethynyltrimethylsilane proved slightly tricky. The presence of two *ortho*-methyl groups provided significant steric hindrance and the nature of the electron rich aryl-group inhibited the oxidative addition step with the palladium catalyst. Taking into account these two factors, the selection of the most appropriate palladium catalyst was considered. [1,1-Bis(triphenylphosphine)]palladium (II) dichloride was selected, as the catalyst contains less sterically bulky groups compared with the previously employed Pd(dppf)Cl_2 catalyst. The presence of strongly electron donating phosphine ligands may also allow improvement in the rate of the oxidative addition step. Employing an aromatic iodide as the starting material, as opposed to the bromide, also improved the reactivity in the oxidative addition step, due to the weaker C-X bond. With these reaction modifications, successful formation of the protected alkyne was achieved. A subsequent deprotection step gave the desired arylalkyne chromophore, **5c**.

3.2.2.2. Synthesis of complexes [Eu.L^{39}]Cl and [Eu.L^{40}]Cl

Cross-coupling of **5c** with **3a** under standard conditions, gave the alcohol, **5d**, in modest yield, which underwent a subsequent mesylation reaction. Controlled di-alkylation of 9-N_3 was carried out in order to avoid exposure of the electron rich alkyne to the strongly acidic conditions present in the mono-BOC strategy (Scheme 17), as it is sensitive to acid-catalysed hydration. The formation of the di-alkylated ligand was attained using controlled reaction conditions. The number of equivalents of the pendant arm was kept below two (1.9 equiv.), a large solvent volume was used, the reaction temperature was maintained at a lower value of 60 ºC and the reaction was monitored every 10 minutes by LC-MS. After 1 h the reaction was terminated, following observation of significant formation of the desired di-alkylated ligand (some mono- and tri-alkylated product were also observed by LC-MS). Column chromatography on silica gel allowed separation of the alkylated species and isolation of the di-alkylated ligand, **L^{39}**, in modest yield (35%). A simple alkylation reaction between the free secondary amine of ligand **L^{39}** and benzyl bromide, afforded **L^{40}**, after purification by column chromatography.

Base hydrolysis (pH 12) of the methyl ester groups was followed by addition of the europium salt, $EuCl_3.6H_2O$, at pH 6.5. The reaction was left to stir for 24 h and complete complexation was confirmed by ESI-MS (no column) and emission spectroscopy, to give the complexes [Eu.**L^{39}**]Cl and [Eu.**L^{40}**]Cl.

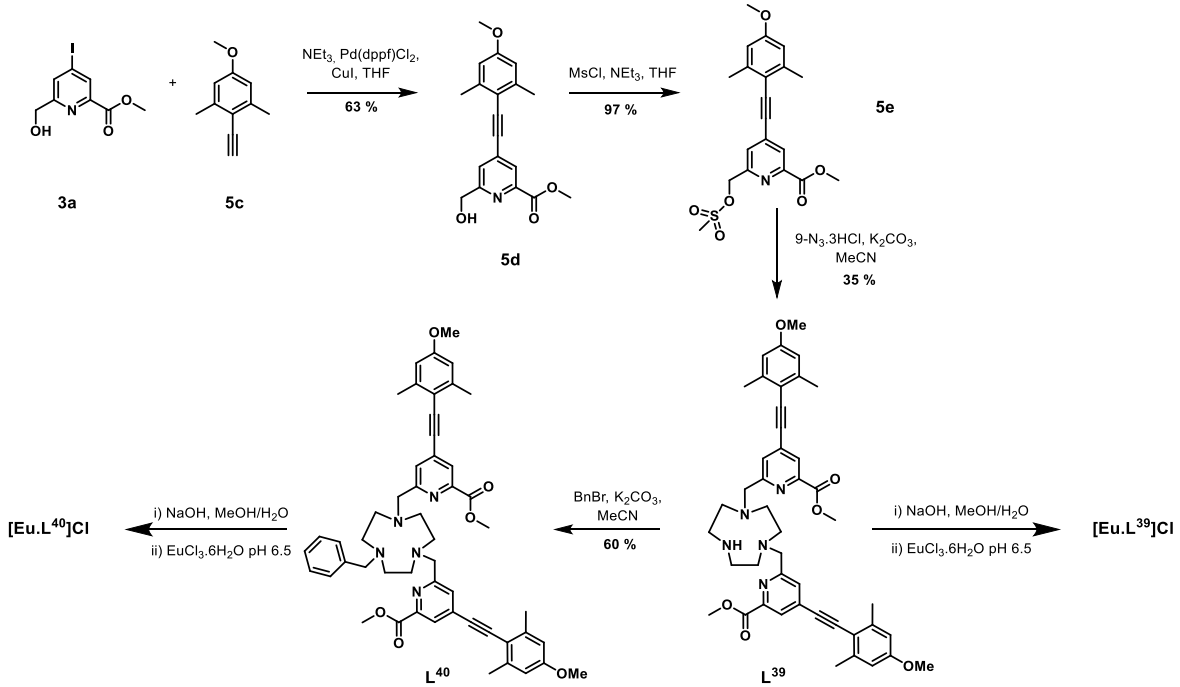

Scheme 20 – Synthesis of ligands **L^{39}** and **L^{40}** and their europium (III) complexes.

3.3. Photophysical behaviour

Photophysical data of the four europium (III) complexes in MeOH are summarised in Table 12, and highlight the difference in the key parameters between the complexes. The data for [Eu.**L**^{37}]$^{+}$ are taken from reference 149.

Table 12 - Photophysical properties of the Eu (III) complexes of **L**$^{37\text{-}40}$ (295 K, MeOH; selected emission decay rate constant data are given in H_2O and D_2O)[a,b]

	[Eu.**L**^{37}]$^{+}$	[Eu.**L**^{38}]$^{3+}$	[Eu.**L**^{39}]$^{+}$	[Eu.**L**^{40}]$^{+}$
λ/nm	332	348	352	348
ε/mM^{-1} cm^{-1}	38.6	40.0	35.0	36.0
ϕ	0.19	0.02	0.20	0.18
k/ms^{-1}	2.94	2.17	2.56	1.20
$k(H_2O)$/ms^{-1}	2.97	3.85	3.70	2.00
$k(D_2O)$/ms^{-1}	2.04	2.33	2.63	1.89
q	0.8	1.3	1.0	0

[a] errors on k values are ±10%, errors on quantum yields are ±20%. [b] q values in water were determined as defined in equation **2.3**, page 67, at pH 6.[117]

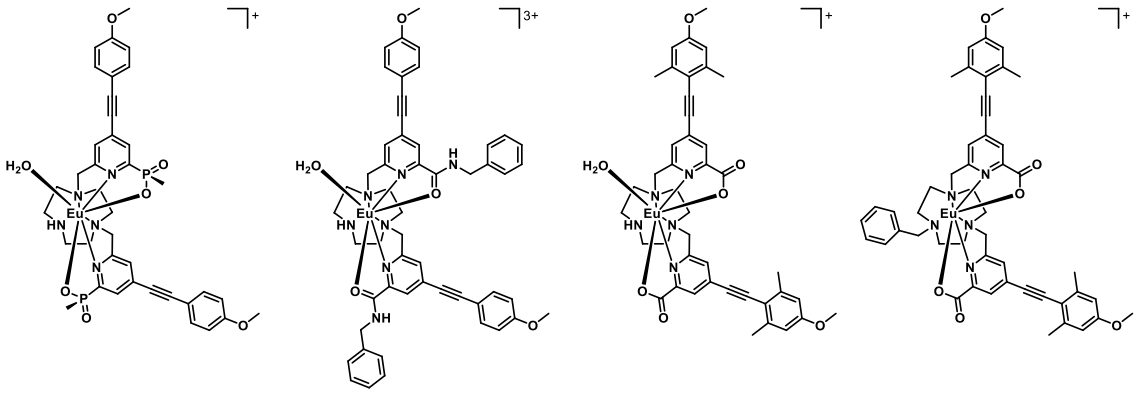

The high absorbance of each complex in the range of 332 to 352 nm is as a result of the strongly absorbing ICT excited state. Evidence for the presence of an ICT band was provided for the related tris-amide complexes in Chapter 2. A similar solvatochromism study was conducted for [Eu.**L**^{38}]$^{3+}$, in which a hypsochromic shift of the absorbance band was observed in solvents of lower polarity.

The amide complex, [Eu.**L**^{38}]$^{3+}$, possesses a low overall emission quantum yield, presumably due to less favourable intermolecular energy transfer, as discussed in the previous chapter. The other three complexes have quantum yields in the range 18 to 20%. These are high values, especially for systems with a coordinated amine NH group and a bound water molecule ([Eu.**L**^{37}]$^{+}$ and [Eu.**L**^{39}]$^{+}$).

The presence of a coordinated amine NH oscillator has been shown to effectively quench the Eu (III) excited state, *via* efficient vibrational coupling.[170] Such excited state quenching explains the faster emission decay rate of [Eu.**L**^{39}]$^{+}$ compared to the *N*-benzyl complex [Eu.**L**^{40}]$^{+}$, where the observed rate of emission is nearly twice as slow in methanol (Table 12). Measurements of the radiative rate of decay of europium (III) emission in water and D_2O allowed solvation states to be estimated according to equation **2.3**, page 67.[117,170] The complexes of **L**$^{37\text{-}39}$ are octadentate with one metal-bound water molecule. Interestingly, the *N*-benzyl complex [Eu.**L**^{40}]$^{+}$, possesses no coordinated water, perhaps owing to the increased steric demand imposed by the *N*-substituent. It represents an unusual example of a seven-coordinate Eu (III) complex in aqueous solution.

3.3.1. pH dependent emission behaviour

A strong pH influence on the emission spectral output and the luminescence lifetime of the bis-amide, [Eu.**L**^{38}]$^{3+}$, and bis-carboxylate, [Eu.**L**^{39}]$^{+}$, complexes was observed. No such behaviour was displayed for the bis-phosphinate, [Eu.**L**^{37}]$^{+}$ nor the *N*-benzyl complex [Eu.**L**^{40}]$^{+}$. For example, a *q* value of 1.0 was calculated for [Eu.**L**^{39}]$^{+}$ at pH 5.5, as expected for an unsaturated europium (III) complex. However, upon increasing the pH to 7.6, the lifetime of the complex in water increased from 0.27 ms to 0.37 ms, from which, a *q* value of zero was estimated. Similar behaviour was observed in the total emission spectral changes (Figure 55). On increasing the pH from 5 to 7, a four-fold increase in emission intensity was observed.

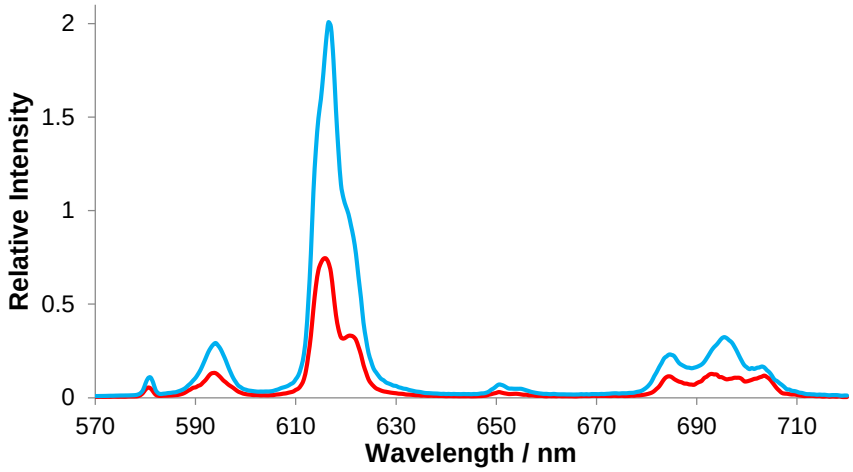

Figure 55 – Emission spectra of [Eu.**L**^{39}]$^{+}$ at pH 5.35 (*red*) and pH 7.56 (*blue*) (λ_{exc} = 352 nm, H_2O, 295 K).

Bicarbonate anions may be present in solutions of higher pH *via* the transformation of dissolved carbon dioxide, according to the equilibria defined by equations **3.1** and **3.2**.

$$CO_2 + H_2O \rightleftharpoons H_2CO_3 \qquad \textbf{(3.1.)}$$

$$H_2CO_3 \rightleftharpoons H^+ + HCO_3^- \qquad \textbf{(3.2.)}$$

The bidentate binding of bicarbonate to a lanthanide centre is a well-known phenomenon.[5,116] The pH dependent emission response suggests that at high pH, a bicarbonate anion may be bound to the Eu^{3+} centre leading to a displacement of the metal bound water molecule, resulting in an increase in total emission intensity and a *q* value of zero. The very low concentration of bicarbonate present in aqueous solution at pH 7.6 suggests that [Eu.**L**^{39}]$^{+}$ has an extremely high binding affinity for bicarbonate.

A pH emission titration in water was carried out in order to further clarify the putative bicarbonate response of [Eu.**L**^{39}]$^{+}$. The pH of the solution was adjusted using solutions of conc. HCl (aq.) and degassed NaOH (aq.). After each measurement was recorded, the pH was lowered to 5, bubbled with argon and readjusted to the desired pH, before the measurement was recorded again. The total emission intensity was plotted against pH, generating a curve which showed a large exponential increase in intensity, which is most likely attributed to the increasing concentration of bicarbonate present in solutions of higher pH.

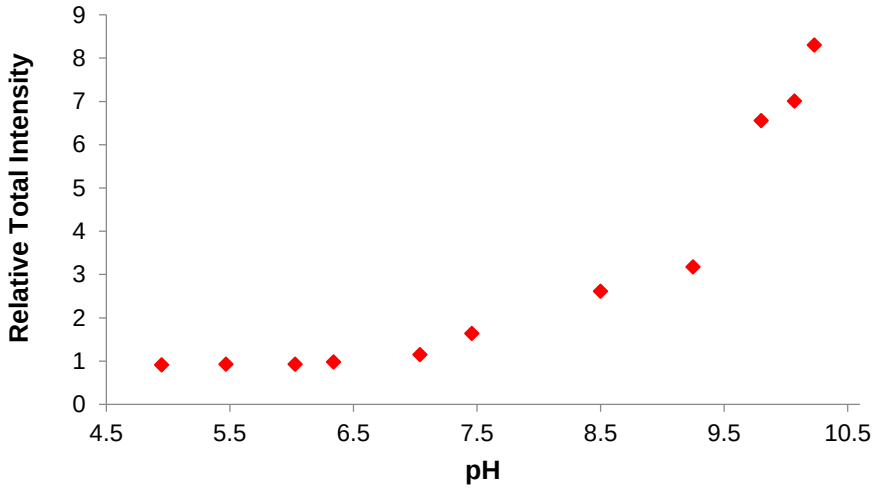

Figure 56 – Plot of the total emission intensity versus pH for [Eu.**L**^{39}]$^{+}$.

The apparent high binding affinity alludes to the possibility that an alternative binding mechanism may be occurring. A tentative suggestion was that the mechanism proceeds *via* the deprotonation of the metal-bound water molecule, resulting in a hydroxide ion bound to the metal centre. It is possible that the metal-bound hydroxide is able to promote the bicarbonate binding mechanism leading to the particularly high affinity. To prevent interference of bicarbonate anions in further studies, emission data was recorded with degassed solutions at pH < 6.

3.4. Binding affinity with chiral anions

The anion binding capabilities of the title complexes, [Eu.**L**$^{37\text{-}40}$], were assessed. Three chiral α-hydroxy acids with sterically different R-groups were selected (Figure 57), with the expectation that their emission and CPL spectra would provide information surrounding the binding mode and chirality in the resulting complexes.

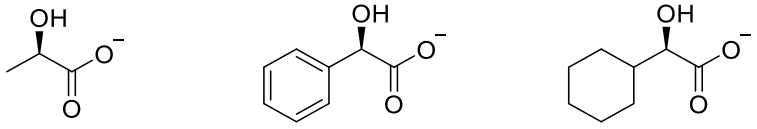

***R*-lactate**
pK_a: 3.86

***R*-mandelate**
pK_a: 3.41

***R*-cyclohexylhydroxyacetate**
pK_a: 3.86

Figure 57 – Structures of the selected enantiopure α-hydroxyacids and their pK_a values (H_2O, I = 0.1, 298 K).

Incremental addition of freshly prepared stock solutions of a given chiral anion, to each europium complex in turn, was monitored by emission spectroscopy until the limiting spectrum was obtained. The pH of the solution was recorded after the addition of each aliquot of anion, and readjusted if necessary, using conc. HCl (aq.) and degassed NaOH (aq.). The change in the relative intensity and form of the Eu (III) emission spectrum was examined. The relative intensity of the $\Delta J = 2$ and $\Delta J = 1$ emission bands was plotted as a function of anion concentration, and the variation was fitted to a 1:1 binding model by iterative non-linear least-squares fitting, to give an estimate of the association constant. The limited water solubility of the mono-cationic Eu (III) complexes meant that these systems were examined in 50% aqueous methanol. The magnitude of the binding constants measured in water and aqueous methanol (1:1, v/v) were very similar, Table 13, suggesting the presence of localised solvent environments, as opposed to an equal dispersion of solvent molecules throughout the sample.[185] Overall, the observed emission intensity increased as anion was added; changes in spectral form were most significant with [Eu.**L**^{37}],[149] and were less marked with [Eu.**L**$^{38\text{-}40}$] (Figure 58). No significant differences were observed in measured binding constants with enantiomeric carboxylates.

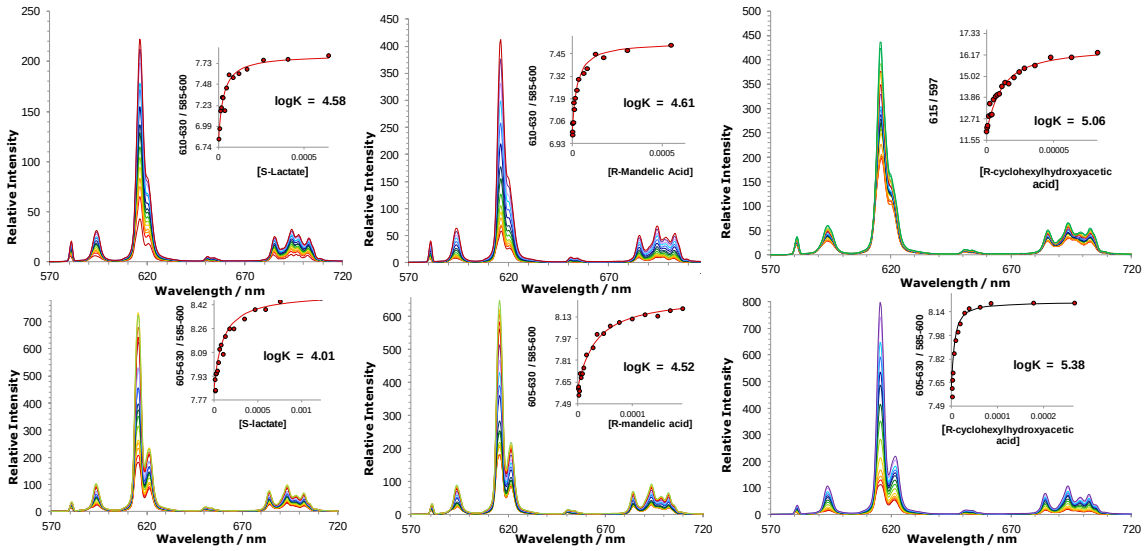

Figure 58 – Variation of the europium (III) emission profile as a function of added anion; (*upper*) [Eu.**L**^{38}]$^{3+}$ (5 μM, λ_{exc} = 348 nm, H_2O, pH 5.5), (*left to right*) lactate, mandelate and cyclohexylhydroxyacetate; (*lower*) [Eu.**L**^{39}]$^{+}$ (5 μM, λ_{exc} = 352 nm, 50% MeOH in H_2O, pH 5.5) plus added anions. Insets show fits to experimental data, following iterative least-squares fitting to a 1:1 binding model.

The nature of the bound adduct was confirmed by direct observation of the sodium salt of the 1:1 adduct in the electrospray mass spectrum (Figure 59).

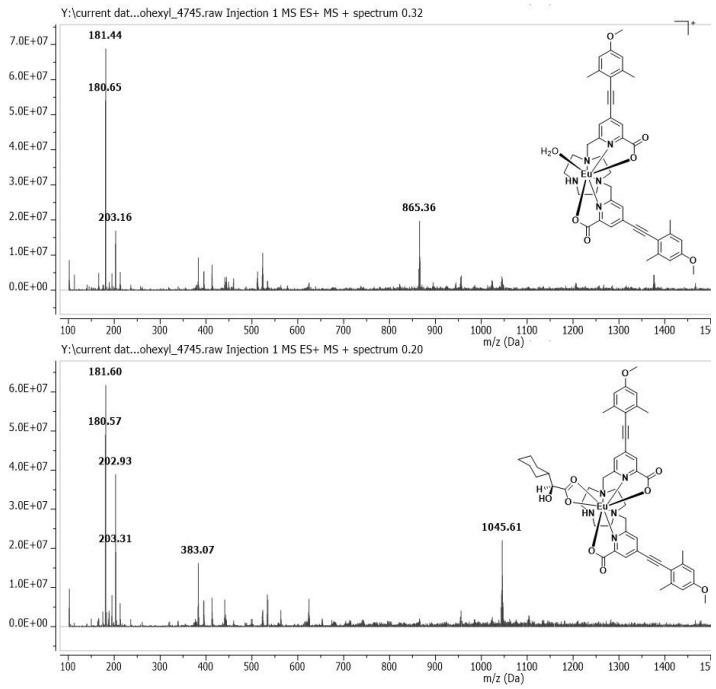

Figure 59 – LRMS data for [Eu.**L**^{39}]$^{+}$ *m/z* 865.4 (*top*) and [Eu.**L**^{39}+*S*-cyclohexylhydroxyacetate+Na]$^{+}$ *m/z* 1045 (*bottom*) (ESI no column, MeOH, positive ion mode).

A number of important trends were identified from the calculated binding affinities, Table 13. Binding constants were largest for all four complexes with cyclohexylhydroxyacetate, consistent with the major role of anion desolvation in the overall free energy change. Cyclohexylhydroxyacetate contains a relatively bulky aliphatic cyclohexyl group and so it is more intuitively hydrophobic (cyclohexyl > Ph > Me). Comparing the behaviour of [Eu.**L**^{39}]$^{+}$ and its *N*-benzyl analogue [Eu.**L**^{40}]$^{+}$, affinity constants were smaller for the latter $q = 0$ complex. The difference in behaviour may be accounted for by the favourable free energy term associated with displacement of the weakly Eu-bound coordinated water molecule and its return to the bulk, where it enjoys full hydrogen bonding to other water molecules. As the estimated hydration state of [Eu.**L**^{40}]$^{+}$ is zero, the favourable free energy term associated with the displacement of the metal-bound water is not present. A final point worth noting is the trend in lactate binding affinity between the four complexes. Strongest binding was observed to the most positively charged bis-amide complex [Eu.**L**^{38}]$^{3+}$, which can be explained by a simple electrostatic argument. The bis-phosphinate complex [Eu.**L**^{37}]$^{+}$ bound anions most weakly, compared to the bis-carboxylate complex [Eu.**L**^{39}]$^{+}$, possibly as a result of the increased steric bulk around the metal centre, as revealed by the X-ray crystal structures of the related tri-substituted complexes.[100,154,155] The weaker affinity for anions of [Eu.**L**^{37}]$^{+}$ may also account for the observation that there was no significant bicarbonate response at higher pH, as was the

case with the bis-amide and bis-carboxylate complexes. Much weaker binding was observed for carboxylate anions lacking a coordinating α-substituent, such as 2-phenylpropionic acid, with a log*K* value estimated to be less than 1.5 for the complexes of **L**$^{37\text{-}40}$. The addition of Me-*S*-lactate resulted in no change in the emission spectrum for each of the complexes, indicating that the carboxylate group is involved in the binding mechanism. No significant change in the emission spectrum was observed with any of the complexes, following addition of amino acids, such as *S*-serine, *S*-aspartate and *S*-glutamate.

Table 13 – Binding constants, log*K*, for chiral anion complexation (295 K, 50% aq. MeOH).[a]

	R-lactate	*R*-mandelate	*R*-cyclohexylhydroxyacetate
[Eu.**L**^{37}]$^{+}$	2.76(04)[2.41[b]]	-	-
[Eu.**L**^{38}]$^{3+}$	4.57(05)[4.58[b]]	4.61(06)[b]	5.06(05)[b]
[Eu.**L**^{39}]$^{+}$	4.01(04)	4.52(06)	5.38(04)
[Eu.**L**^{40}]$^{+}$	3.15(04)	3.85(04)	4.41(05)

[a] errors associated with the fitting analysis of a given data set are given in parentheses; experimental errors were estimated to be ±0.1 log unit [b] measurement in water at pH 5.5 to eliminate the possibility of interference from bicarbonate

There are two possible chelation modes that α-hydroxy acids can adopt when binding to a lanthanide centre. The acids can bind *via* a 5-ring chelate (**1**) involving the α-hydroxyl group, or a 4-ring chelate (**2**) where the binding occurs *via* the carboxylate group.

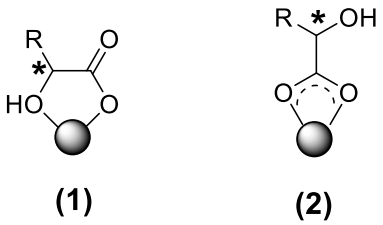

Figure 60 – Possible chelation modes of the chiral α-hydroxy anions at a lanthanide centre. * represents chiral centre.

The mode of anion binding was investigated by examination of the radiative rates of decay of the complexes and their lactate-adducts in water and D_2O (Table 14). A coordinated α-hydroxy-carboxylate in a 5-ring chelate, means that there is one OH oscillator in the Eu (III) inner coordination sphere. Assuming similar Ln-O bond lengths, a quenching effect that is half that of a coordinated water molecule should be observed. X-ray studies of chelated lactate and citrate adducts of lanthanide complexes substantiates this assumption, which show a Ln-O bond distance that is within 0.05 Å of the

corresponding hydrated complexes.[118,170] The rate data obtained (Table 14) revealed that the lactate-bound adducts of [Eu.**L**^{38}]$^{3+}$ and [Eu.**L**^{39}]$^{+}$ show a quenching effect that is half that of the complexes with a metal-bound water (chelation mode **1**). The X-ray crystal structure of the related 12-N_4 tri-amide lanthanide complex bound to lactate, shows that the anion is also coordinated *via* a 5-ring chelate.[118] However, the results imply that in the case of the lactate adduct of [Eu.**L**^{37}]$^{+}$, there is no coordinated OH group, suggesting a dominant carboxylate binding mode (chelation mode **2**). The difference in binding mode could be attributed to the increased steric demand present at the lanthanide centre, for the 9-N_3 phosphinate complexes.

Table 14 – Radiative rate constants for decay of Eu emission in the presence and absence of *R*-lactate (295 K, 10 μM complex, 50 μM lactate).

	[Eu.**L**^{37}]$^{+}$	[Eu.**L**^{37}.lactate]	[Eu.**L**^{38}]$^{3+}$	[Eu.**L**^{38}.lactate]$^{2+}$	[Eu.**L**^{39}]$^{+}$	[Eu.**L**^{39}.lactate]
$k(H_2O)/(ms^{-1})$	2.97	2.33	3.85	2.86	3.70	2.63
$k(D_2O)/(ms^{-1})$	2.00	2.00	2.33	1.89	2.63	2.00
q	0.8	0.08	1.3	0.6	0.9	0.4

3.5. Induced CPL studies

3.5.1. Racemisation rates of [Ln.(dpa)$_3$]$^{3-}$, [Ln.(L^1)$_3$]$^{3+}$ and [Ln.L$^{37-40}$]

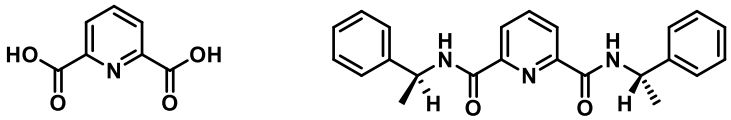

dpa *SS*-**L**^{1}

Figure 61 – Structure of the ligands dpa and *SS*-**L**^{1}.

The majority of studies surrounding the phenomenon of induced CPL are focussed on the interaction of chiral additives with dynamically racemic D_3 lanthanide complexes based on dpa ligands, [Eu.(dpa)$_3$]$^{3-}$ and [Eu.(*SS*-**L**^{1})]$^{3+}$ (Figure 61). Solutions of the two complexes were prepared *in situ* using a 1:5 metal to ligand ratio in deuterated acetonitrile, [Eu.(*SS*-**L**^{1})$_3$]$^{3+}$, and D_2O, [Eu.(dpa)$_3$]$^{3-}$ (6.67 x 10^{-3} M concentration of

ligand). The emission spectra were run and used to characterise the formation of the tris-complex by comparison with literature spectra.[89]

With the help of Dr. Alexander Funk and Dr. Juan Aguilar Malavia, HSQC and EXSY (EXchange SpectroscopY) methods were employed to assign the free ligand and complex resonances in each ^{1}H NMR spectrum of [Eu.(*SS*-**L^1**)$_3$]$^{3+}$ and [Eu.(dpa)$_3$]$^{3-}$.

An approximate value for the rate of exchange of a system can be measured if the rate of exchange is of the same order of magnitude as the longitudinal relaxation time, T_1.[186] The method is based on the selective saturation of one site in an exchange system by irradiation with a second rf field. Transfer of saturated spins from the irradiated site to the exchanging site can be monitored by observation of the signal intensity against a reference signal. The intensity falls to a new steady state level due to transfer of the saturated spins and also its T_1 value (longitudinal relaxation time).

In this experiment, the py-H signal in the complex-bound adduct underwent selective spin saturation, and the intensity of the corresponding py-H signal in the free ligand was monitored against a reference signal. The rate of exchange was calculated according to equation **3.3**, where T_1 is the longitudinal relaxation time of the free py-H without saturation, M_0 is the signal intensity of the free py-H resonance observed in the absence of saturation (*versus* a reference signal), and M is the signal intensity of the same py-H resonance following saturation of the bound py-H resonance (*versus* a reference signal). The exchange rate data allowed for correlations of the structure of each complex to the observed emission and CPL spectra. Most notably, these experiments allow for comparison of rates of exchange with the dynamically racemic 9-N_3 europium complexes [Eu.**L$^{37\text{-}40}$**].

$$k = \frac{1}{T_1}\left(\frac{M_0}{M} - 1\right) \qquad \textbf{(3.3.)}$$

The approximate rate of exchange of [Eu.(dpa)$_3$]$^{3-}$ was 4 s^{-1} which was slightly faster than the exchange rate calculated for [Eu.(*SS*-**L^1**)$_3$]$^{3+}$ where a value of 1 s^{-1} was recorded. The dissociation of the europium (III) complex based on dpa ligands results in the formation of two negatively charged species. The electrostatic repulsion between the two products of dissociation may account for the slightly faster observed rate. These results demonstrate that under the conditions outlined, the rate of dissociation of the two complexes is slow on the emission timescale and the emission and CPL spectra can be

confidently attributed to the most emissive species, which would be the [Ln.$\mathbf{L}_3$] complex. However, it is worth noting that on the addition of a chiral analyte, **L***, the adduct [Ln.$\mathbf{L}_2$.**L***] may be the most emissive species when taking into account the rate data, as opposed to an outer sphere [Ln.$\mathbf{L}_3$]**L*** species.

The dynamically racemic europium complexes discussed in this section, [Eu.$\mathbf{L}^{37\text{-}40}$], exhibit no CPL implying that they exist as a 50:50 mixture of *Δ* and *Λ* isomers on their emission timescales (Figure 62). Multiple attempts at resolution by chiral HPLC were unsuccessful which suggests that there is fast interconversion between the *Δ*/*Λ* isomer on the laboratory timescale. It was not possible to perform a comparative saturation transfer experiment as the ^{1}H NMR spectra of the europium complexes were compromised by considerable line broadening and relatively small dipolar shifts related to the small ligand field. Nevertheless, addition of *R*-lactate to [Eu.$\mathbf{L}^{39}$]$^+$ led to a general sharpening of the observed resonances and the most shifted axial ring proton (assigned by comparison with the ^{1}H NMR spectrum of the related tris-carboxylate complex, [Eu.$\mathbf{L}^{35}$]$^+$)[171] was shown to shift to lower frequency compared to the solvate species. These ^{1}H NMR observations suggest that exchange between the *Δ* and *Λ* isomers is too fast to be observed on the NMR timescale. However, addition of a chiral additive stabilises one particular isomer accompanied by a sharpening and a shift in the proton resonances.

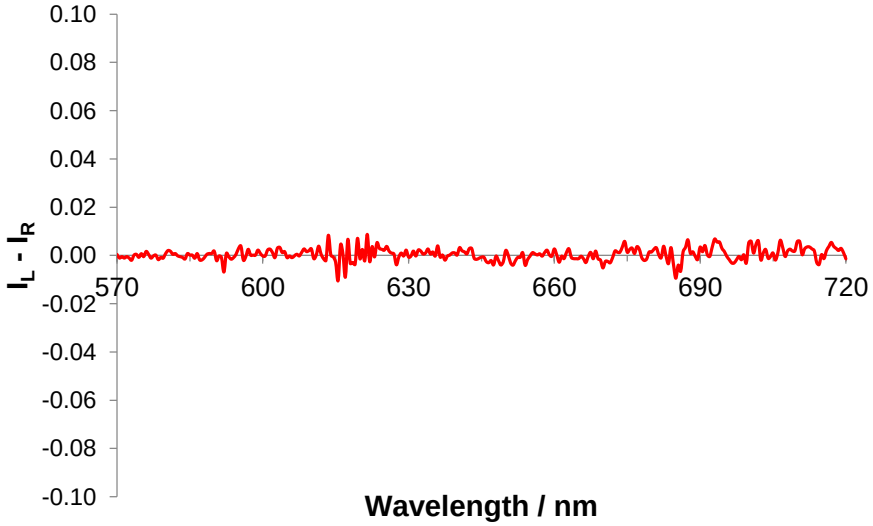

Figure 62 – CPL spectrum of [Eu.$\mathbf{L}^{39}$]$^+$ (λ_{exc} = 352 nm MeOH, 295 K), showing no significant signal.

3.5.2. Induced CPL following binding of enantiopure acids

The addition of enantiopure acids such as lactate, mandelate and cyclohexylhydroxyacetate, to the europium complexes of $\mathbf{L}^{37\text{-}40}$ resulted in distinct

alteration in the total emission spectrum, as discussed in section 3.4, as well as strong induced circularly polarised luminescence (Figure 63). The stability data estimated from total emission changes represents the weighted sum of all stereoisomeric anion adducts, irrespective of their constitution and configuration. As the addition of a given chiral anion induced a CPL response, a binding affinity can also be estimated by monitoring the change in g_{em} with increasing concentration of anion. This estimated binding constant gives information regarding the stability of the major emissive chiral species in solution, i.e. *Δ* over *Λ*. The stability constant for the *R*-mandelate adduct of [Eu.**L**^{39}]$^{+}$ was estimated using this method, and gave a value of log*K* = 5.79 in pure methanol (Figure 64). This value compares to the value of log*K* = 5.44, based on the total emission spectral changes. The slightly higher stability constant estimated from the induced CPL spectral changes suggests that it was associated with the formation of the favoured isomer (*vide infra*: inducing a *Δ* configuration for addition of *R*-mandelate). Similar behaviour was observed for the other systems within this study.

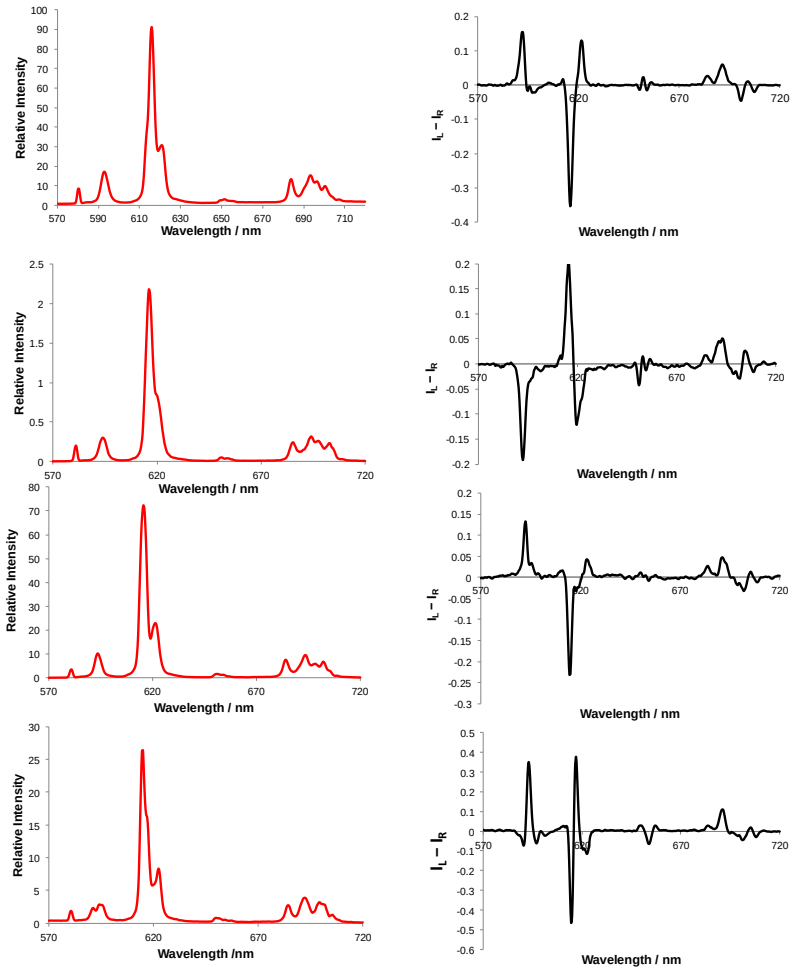

Figure 63 - Emission (*left*) and CPL (*right*) spectra of Eu (III) complexes **L**$^{37\text{-}40}$ (*top to bottom respectively*), following the addition of *R*-cyclohexylhydroxyacetate (1:1 v/v aq. MeOH, 10 μM complex, 50 μM *R*-cyclohexylhydroxyacetate).

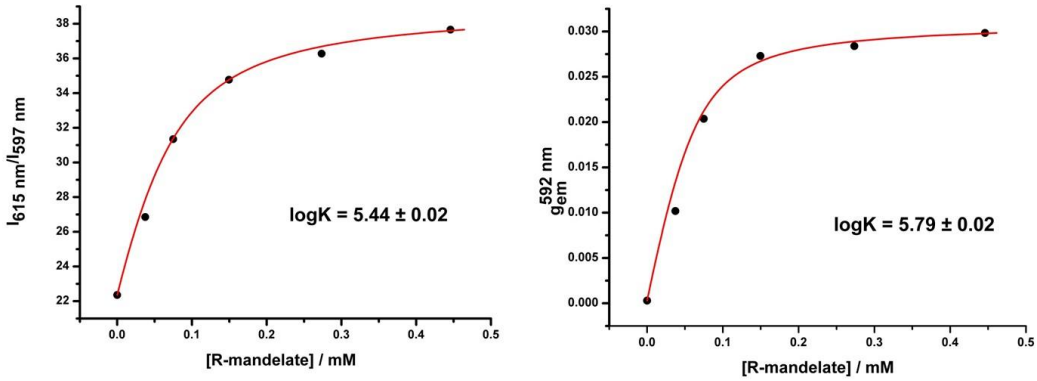

Figure 64 - *Left*: Variation of the ratio of two emission wavelengths *vs*. the concentration of mandelate; *right*: variation of the emission dissymmetry value g_{em} at 592 nm *vs*. concentration of mandelate. Experimental data fit to a 1:1 binding model following iterative least-squares fitting. (λ_{exc} = 352 nm, 6 µM complex, MeOH).

Separate addition of *R* or *S* enantiomers of a given chiral anion gave rise to mirror image induced circularly polarised luminescence spectra (Figure 65). Identical g_{em} values were calculated for a given concentration of *R*- or *S*-anion, indicating that the strength of interaction and thus the induced CPL, is independent of the absolute configuration of the enantiomer.

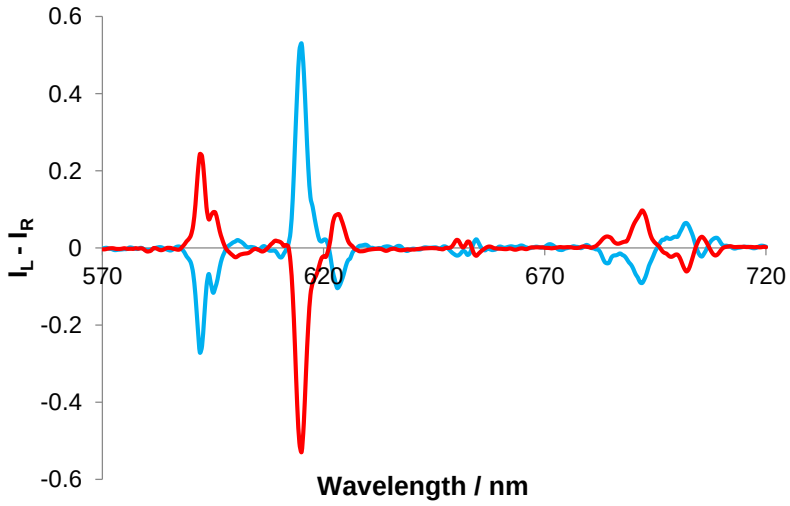

Figure 65 – Induced CPL spectra for [Eu.**L**[39]]$^{+}$ following addition of *R*- (*red*) and *S*-mandelate (*blue*) (λ_{exc} = 352 nm, MeOH, 295 K).

The CPL spectra following addition of enantiopure acids lacking a coordinating α-substituent (e.g. *S*-ibuprofen, *R*-camphanic acid, *R*-phenylsuccinic acid and *R*-

phenylpropionic acid) were particularly weak and less well-defined for the complexes [Eu.**L**$^{38\text{-}40}$], consistent with their much weaker binding affinity (log*K* < 1.5). The CPL signature of the adduct of *R*-phenylpropionic acid and [Eu.**L**^{40}]$^{+}$ (Figure 66), was quite different to that with an α-hydroxy acid such as cyclohexylhydroxyacetic acid, most notably in the ΔJ = 1 and ΔJ = 2 transitions around 590 and 620 nm respectively. The difference in spectral form can be attributed to the 4-ring chelation mode of phenylpropionate, as opposed to the 5-ring chelation mode of the α-hydroxy acids.

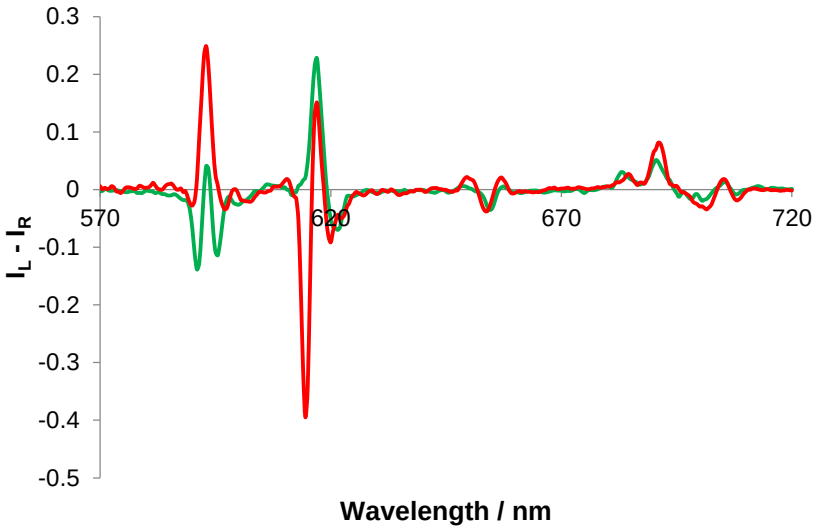

Figure 66 – CPL spectra of [Eu.**L**^{40}]$^{+}$ following addition of *R*-phenylpropionic acid (*green*) and *R*-cyclohexylhydroxyacetic acid (*red*). (λ_{exc} = 348 nm, 2 mM anion, 5 µM complex, MeOH, 295 K).

The induced emission dissymmetry values, g_{em}, were smaller than those measured for the more conformationally rigid, tri-substituted 9-coordinate systems. These values are comparable to values observed in other Eu (III) systems, such as [Eu.(bda)$_2$]$^{-}$ and [Eu.(pda)$_2$]$^{-}$ reported by Iwamura,[150,151] that demonstrate induced CPL on the addition of a small molecule chiral analyte. However a 20,000-fold lower concentration of the target anion is required to induce such a response for the complexes [Eu.**L**$^{37\text{-}40}$] (50 µM). Of the four systems studied, the smallest induced g_{em} values were measured for the bis-phosphinate complex [Eu.**L**^{37}]$^{+}$ (Table 15). Observation of weaker CPL is consistent with the suggestion that in this complex, the added chiral anion binds *via* a 4-ring chelate through the carboxylate moiety, where the stereocentre is situated further from the metal centre compared to the alternative 5-ring binding mode. The *N*-benzyl complex, [Eu.**L**^{40}]$^{+}$, gave rise to the strongest CPL amongst the systems studied, for the simple

carboxylic acids. The spectra were well-defined, with highly resolved transitions and the calculated g_{em} values were highest for 70% of the induced CPL transitions.

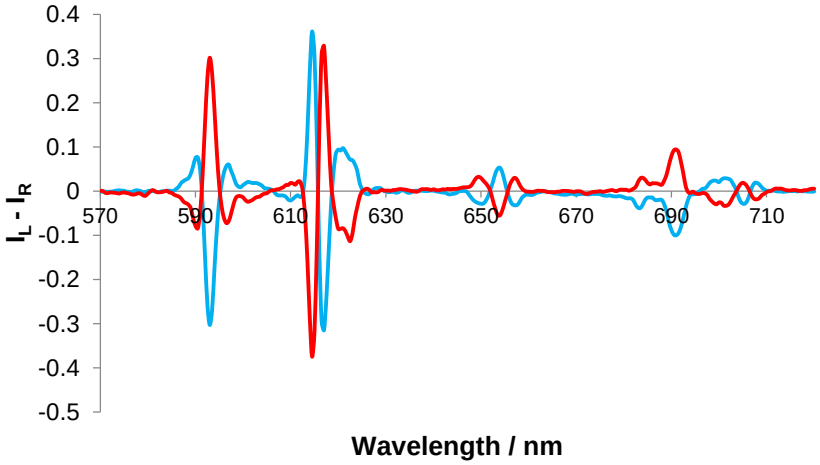

Figure 67 – Mirror image CPL spectra of [Eu.**L**^{40}]$^{+}$ following the addition of *R*- (*red*) and *S*-lactate (*blue*). (λ_{exc} = 348 nm, 10 µM complex, 50 µM lactate, MeOH, 295 K).

Table 15 – Emission dissymmetry values, g_{em}, for Eu (III) complexes in the presence of excess *R*-lactate, mandelate or cyclohexylhydroxyacetate.

R-Lactate	g_{em}	[Eu.**L**^{37}]$^{+}$	[Eu.**L**^{38}]$^{3+}$	[Eu.**L**^{39}]$^{+}$	[Eu.**L**^{40}]$^{+}$
ΔJ = 1	(592 nm)	+0.01	-0.03	+0.02	+0.05
	(683 nm)	+0.005	+0.01	+0.01	+0.01
ΔJ = 4	(692 nm)	+0.02	+0.02	+0.01	+0.02
	(702 nm)	-0.02	-0.01	-0.01	-0.02
	(708 nm)	-0.04	-0.04	-0.03	-0.06
R-Mandelate					
ΔJ = 1	(592 nm)	+0.01	-0.05	+0.04	+0.05
	(683 nm)	+0.01	+0.01	+0.01	+0.01
ΔJ = 4	(692 nm)	+0.02	+0.02	+0.03	+0.03
	(702 nm)	-0.03	-0.01	-0.03	-0.02
	(708 nm)	-0.09	-0.05	-0.06	-0.09
R-Cyclohexylhydroxyacetate					
ΔJ = 1	(592 nm)	+0.02	-0.05	+0.07	+0.06
	(683 nm)	+0.01	+0.01	+0.02	+0.02
ΔJ = 4	(692 nm)	+0.02	+0.03	+0.04	+0.04
	(702 nm)	-0.02	-0.01	-0.07	-0.03
	(708 nm)	-0.09	-0.08	-0.09	-0.11

3.5.3. Spectral correlation with absolute configuration

In Chapter 1, attempts were made to highlight the limited number of structural comparisons that have been linked to CPL spectral form. In Chapter 2, it was noted that it is not obvious to find correlations between helicity of the complex and the form and sign of each CPL active transition in systems based on different ligand frameworks, i.e. 9-N_3 tri-phosphinates *versus* tri-amides *versus* related 12-N_4 complexes. This study has rigorously compared the CPL spectra of a number of related europium (III) complexes, following addition of *R*- and *S*-chiral acids. It can be seen that the *R*-α-hydroxy acids each gave rise to a common induced CPL signature in the $\Delta J = 4$ region, across the whole series of europium complexes involved in this study (Figure 68). This empirical observation could not be extended to analysis of every CPL transition, yet provides a simple CPL fingerprint in this 'hypersensitive' manifold.

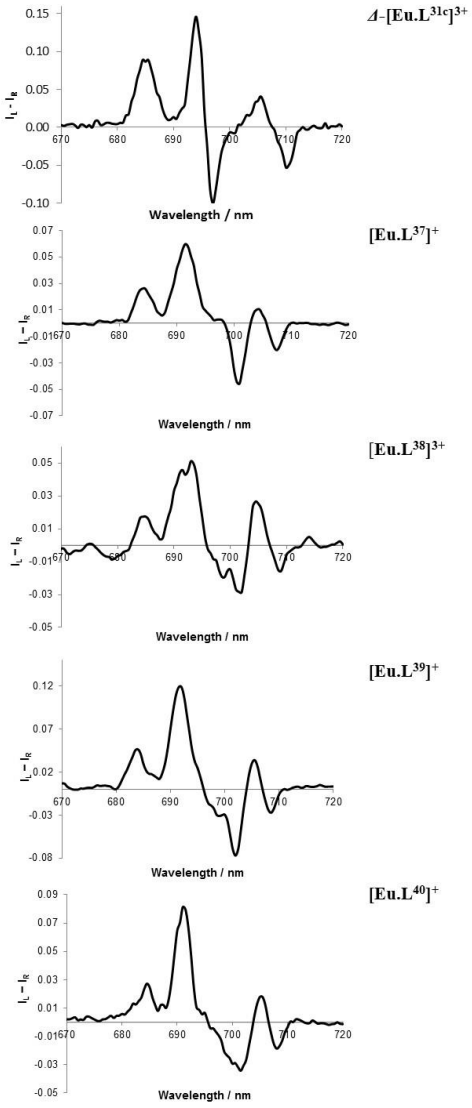

Figure 68 – Partial CPL spectra for Eu^{3+} complexes of $\mathbf{L^{37\text{-}40}}$, compared to *Δ*-[Eu.$\mathbf{L^{31c}}$]$^{3+}$ (*top*), showing the similar $\Delta J = 4$ manifold in the presence of excess *R*-cyclohexylhydroxyacetate (H_2O, 10 μM complex, 295 K).

The induced CPL for these adducts was compared to the spectral behaviour of related C_3-symmetric enantiopure 9-coordinate complexes, whose structure and absolute configuration has been determined by X-ray crystallography (Figure 69).[100,155,162] A tentative correlation was found within a given series, allowing assignment of the *R*-acid adducts to a Δ complex configuration, with a $\lambda\lambda\lambda$ configuration in the three EuNCCN chelates of the 9-membered macrocyclic ring. This surprising empirical observation therefore allows the absolute configuration of the lanthanide complex adduct of a given chiral acid to be distinguished simply by using CPL spectroscopy.

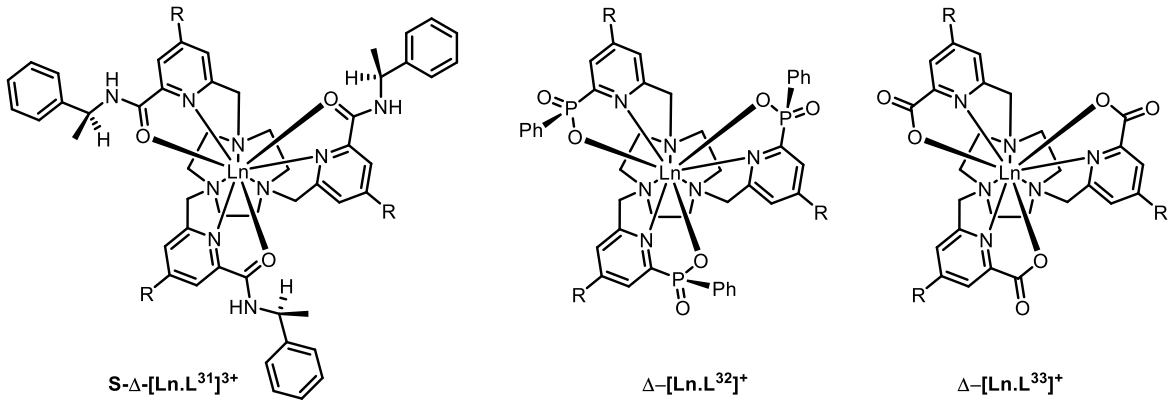

Figure 69 – Structures of the related 9-N_3 C_3-symmetric parent complexes, where the absolute configuration was determined by X-ray crystallography.[100,155,162]

3.5.4. Determination of enantiomeric purity

The development of methods that aid the chiral analysis of a sample and allow for accurate determination of its enantiomeric purity is important. Preliminary work by McMahon investigated the use of [Eu.**L**^{37}]$^+$ in the determination of the enantiomeric purity of samples of lactate.[15] The following study aims to expand on these preliminary findings and develop a quick and accurate method for use in the determination of the enantiomeric purity of samples of chiral anions of unknown composition.

The bis-carboxylate complex [Eu.**L**^{39}]$^+$ was selected for use in this investigation, due to the lower steric demand surrounding the lanthanide centre compared to [Eu.**L**^{37}]$^+$. As discussed previously, this allows an α-hydroxy acid to bind *via* a 5-ring chelate in which the chiral centre is situated closer to the lanthanide core. As a result of the close proximity of the stereocentre, the measured g_{em} values were found to be greater for [Eu.**L**^{39}]$^+$ upon addition of selected chiral acids. The brightness of the probe was comparable to [Eu.**L**^{37}]$^+$

allowing for good signal to noise in the recorded CPL spectra and therefore, an enhanced CPL response.

Scalemic mixtures of predetermined enantiomeric composition of a given chiral acid, in this case mandelic acid, were analysed by the CPL output of [Eu.**L**^{39}]$^{+}$. A linear variation of g_{em} with enantiomeric composition was observed allowing a calibration curve to be generated (Figure 70). After initial calibration, accurate determination of the enantiomeric excess of samples of mandelic acid with unknown composition was demonstrated. Inherently, this technique provides information about sample enantiomeric purity and absolute configuration. It is worth noting that this method can only be employed for chiral anions that bind directly to the metal centre and induce a CPL response.

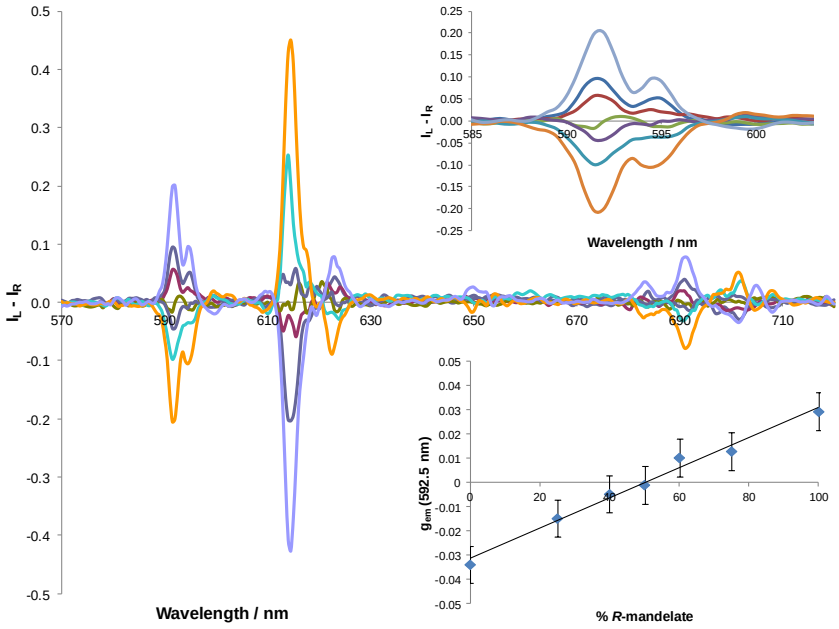

Figure 70 - Changes in the CPL spectrum of [Eu.**L**^{39}]$^{+}$ following addition of mandelate of varying enantiomeric composition (10 μM, λ_{exc} = 352 nm, MeOH). Inset (*top*) shows the ΔJ = 1 manifold; (*bottom*) variation of g_{em} (592.5 nm) with % *R*-mandelate; error bars indicate the standard deviation averaged over 5 runs (R^2 0.98 for shown linear fit).

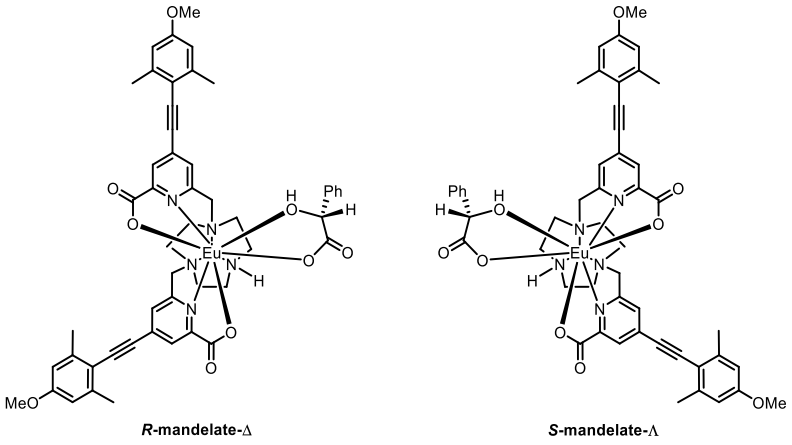

Figure 71 – Structures of the mandelate adducts of [Eu.**L**^{39}]$^{+}$.

3.6. Stereochemical analysis: DFT computational studies

In order to gain further understanding of the structures of the isomeric complexes and their lactate adducts, hybrid-DFT calculations were performed with the help of Dr. Mark Fox. As paramagnetic Eu (III) complexes are very difficult to model computationally, optimised geometries of the analogous diamagnetic yttrium (III) complexes were investigated. Previous studies have shown that the corresponding yttrium (III) complexes act as suitable models for the Eu analogues,[171,187–190] as the Y (III) ionic radius in 8 or 9 coordinate complexes differs from that of a Eu (III) ion by only 0.05 Å. Excellent agreement was observed when comparing an Y (III) model geometry to a reported X-ray geometry of a related europium complex, [Eu.**L**^{30}]$^{3+}$, at B3LYP/3-21G*. The Y-O and Y-N bond lengths were shorter by 0.05 Å on average compared to the corresponding Eu-O and Eu-N bonds, accounted for by the difference in ionic radii of the two lanthanide ions.

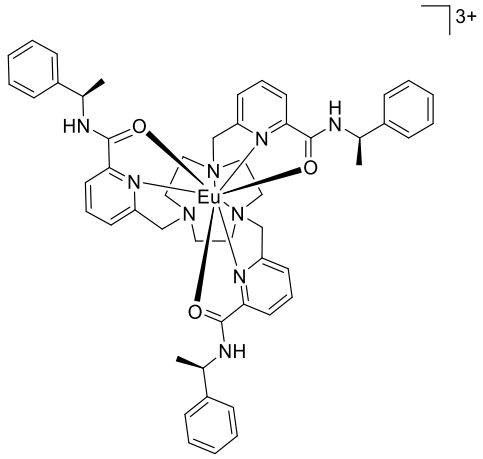

[**Eu.L^{30}**]$^{3+}$

Table 16 - Comparison of experimental and computed bond lengths in angstroms for the europium complex [Eu.**L**^{30}]$^{3+}$ (CSD refcode TITQAQ) and its model yttrium analogue, [Y.**L**^{30}]$^{3+}$, reflecting the difference in ionic radii of Eu (III) and Y(III).

	X-ray [162]		B3LYP/3-21G*	Eu-Y difference
Eu-N	2.628(2)	Y-N	2.567	0.061
Eu-N	2.573(2)	Y-N	2.550	0.023
Eu-O	2.405(2)	Y-O	2.357	0.048

Following the outcome of the emission studies that revealed the complex hydration state using radiative decay rate data (Table 12, page 86), an investigation into the binding of

one water molecule to each of the four complexes was undertaken. The calculated binding energies revealed a trend that was consistent with the observed radiative rate constants for decay of europium (III) emission. The sequence with increasing strength followed the order: $[Y.\mathbf{L^{40}}]^+ < [Y.\mathbf{L^{37}}]^+ < [Y.\mathbf{L^{39}}]^+ < [Y.\mathbf{L^{38}}]^{3+}$ (Table 17).

The relative energies of free and water bound complexes of $[Y.\mathbf{L^{40}}]^+$, did not account for the experimental $q = 0$ hydration state that was estimated, as the steric demand of the benzyl group did not appear to prevent water binding to the metal centre. An alternative explanation may be, that in the solution state, the rotation of the benzyl group restricts secondary stabilising H-bonding interactions with the network of second sphere water molecules, thus resulting in a higher energy for the water-bound europium (III) complex.

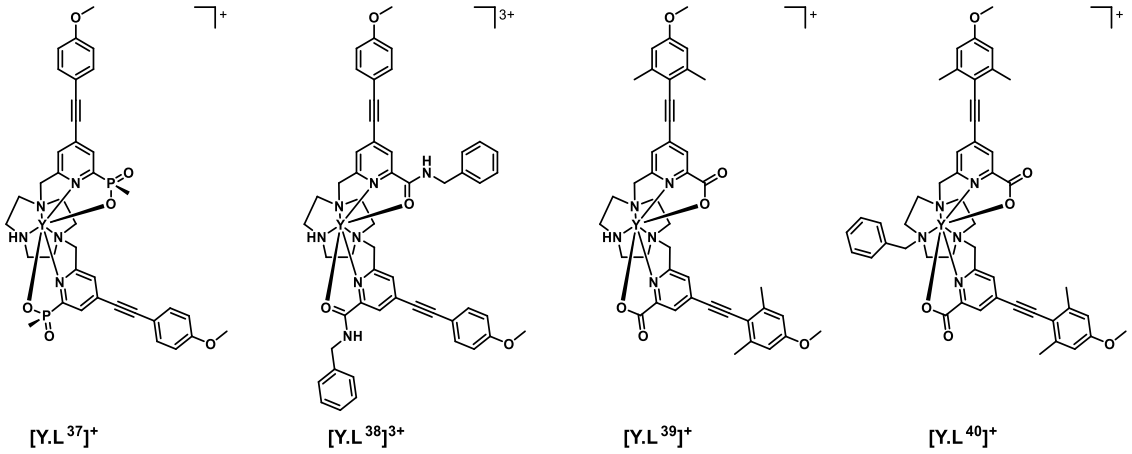

Table 17 - Water binding energies of $[Y.\mathbf{L^{37\text{-}40}}]$ and radiative rates of decay of the corresponding Eu (III) complexes. The trend reveals binding energies of increasing strength in the order $[Y.\mathbf{L^{40}}]^+ < [Y.\mathbf{L^{37}}]^+ < [Y.\mathbf{L^{39}}]^+ < [Y.\mathbf{L^{38}}]^{3+}$.

	Water Binding Energy / kJ mol^{-1}	k (H_2O) / ms^{-1}
$[Y.\mathbf{L^{37}}]^+$	47.5	2.97
$[Y.\mathbf{L^{38}}]^{3+}$	55.6	3.85
$[Y.\mathbf{L^{39}}]^+$	50.8	3.70
$[Y.\mathbf{L^{40}}]^+$	46.4	1.89

A similar approach was taken in order to assess the trend in binding affinities of each of the four europium complexes with *R*-lactate. DFT calculations demonstrated that *R*-lactate binds with increasing strength in the order: $[Y.\mathbf{L^{37}}]^+ < [Y.\mathbf{L^{40}}]^+ < [Y.\mathbf{L^{39}}]^+ < [Y.\mathbf{L^{38}}]^+$. This trend is consistent with the estimated binding affinities that were calculated from total emission spectral changes, where *R*-lactate was shown to bind most strongly to the europium complex with the greatest positive charge (Table 18).

Table 18 – *R*-lactate binding energies of [Y.**L**$^{37\text{-}40}$] in the *Δ* conformation and estimated association constants of [Eu.**L**$^{37\text{-}40}$]. The trend reveals binding energies of increasing strength in the order [Ln.**L**^{37}]$^{+}$ < [Ln.**L**^{40}]$^{+}$ < [Ln.**L**^{39}]$^{+}$ < [Ln.**L**^{38}]$^{+}$.

	R-Lactate Binding Energy / kJ mol^{-1} (calculated)	Log*K* (lactate) (experimental)
[Y.**L**^{37}]$^{+}$	135.1	2.76
[Y.**L**^{38}]$^{3+}$	214.4	4.57
[Y.**L**^{39}]$^{+}$	164.0	4.01
[Y.**L**^{40}]$^{+}$	155.0	3.15

It was interesting to note, that in the calculated geometries of the lactate-bound adduct of [Y.**L**^{37}]$^{+}$, the hydroxyl group of the coordinated lactate does not bind as strongly as in [Y.**L**$^{38\text{-}40}$]. A longer Y-O distance of 2.7 Å was calculated, compared to the corresponding distances of 2.4-2.5 Å for complexes [Y.**L**$^{38\text{-}40}$]. Close inspection of the optimised geometries of the *R*-lactate adducts of [Y.**L**$^{37\text{-}40}$] revealed that the phosphinate groups in [Y.**L**^{37}]$^{+}$ are more sterically bulky than the corresponding carboxylate and amide donors in complexes [Y.**L**$^{38\text{-}40}$], consistent with the X-ray crystal structures of the related 9-coordinate parent structures. The increased steric demand around the metal centre results in less space for lactate binding *via* a 5-ring chelation mode. This interpretation lends support to the hypothesis that lactate coordinates to [Y.**L**^{37}]$^{+}$ *via* the carboxylate group in a 4-ring chelate, in agreement with the experimental radiative decay rate data.

The constitution and relative configuration of the isomeric adducts with a given lanthanide complex are difficult to determine, without X-ray crystallographic data being available. Investigation of the optimised geometries of the four europium (III) complexes using ^{1}H NMR spectroscopy and DFT calculations was undertaken. In principle, four isomeric species can result from the binding of enantiopure lactate to a europium complex. These isomers differ according to the orientation of the α-hydroxy chelate and also in the configuration of the lanthanide complex, *Δ* or *Λ* (Figure 73).

^{1}H NMR analyses in CD_3OD (295 K, 11.7 T) of the solvate and lactate adducts of [Eu.**L**^{39}]$^{+}$ were compromised by considerable line broadening. Nevertheless, addition of *R*-lactate to [Eu.**L**^{39}]$^{+}$ led to a sharpening of the proton resonances and the appearance of four isomeric species for the most shifted ring proton, in the relative ratio 3:1:0.8:0.7 (Figure 72).

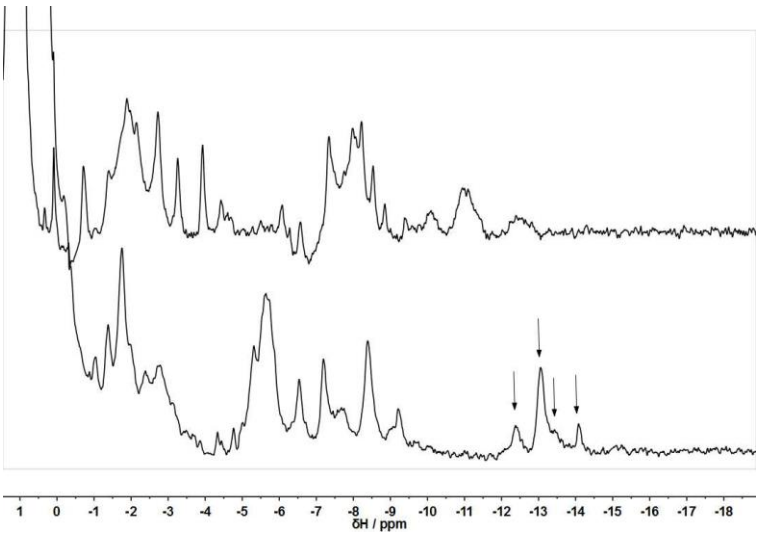

Figure 72 – ^{1}H NMR spectra of [Eu.**L**^{39}(H_2O)]$^{+}$ (*top*) and [Eu.**L**^{39}.*R*-lactate] (*bottom*) showing observation of four isomeric species in the ratio 3:1:0.8:0.7 (CD_3OD, 295 K, 11.7 T).

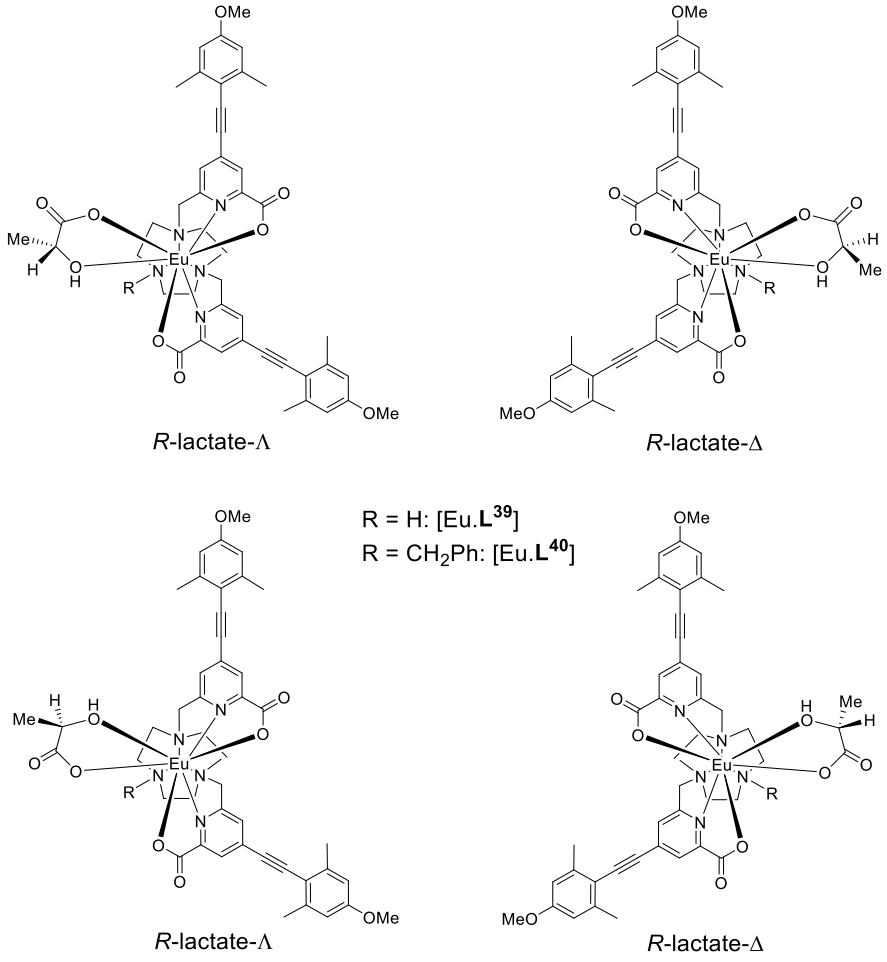

Figure 73 – Structures of the four isomeric species resulting from *R*-lactate chelation to [Eu.**L**^{39}]$^{+}$ and [Eu.**L**^{40}]$^{+}$; the bottom right (*Δ*) isomer was hypothesised to predominate in solution.

In an attempt to rationalise the preferred formation of a particular stereoisomer considering non-bonding steric interactions, calculations were performed to assess the relative energies of the four isomeric adducts, as their Y (III) complexes. For each Y (III) complex, the preferred orientation of the lactate chelate placed the lactate carboxylate in the same plane as the two pyridyl nitrogen atoms of the pendant arms. With this lactate constitution in place, the complex with *Λ* helicity was of higher energy due to unfavourable steric interactions between the lactate Me group and the oxygen lone pair of the ligand carboxylate donor (Figure 74). Therefore, the lowest energy isomer and the predominate isomer in solution was calculated to be *R*-*Δ* (Figure 73, *bottom right*).

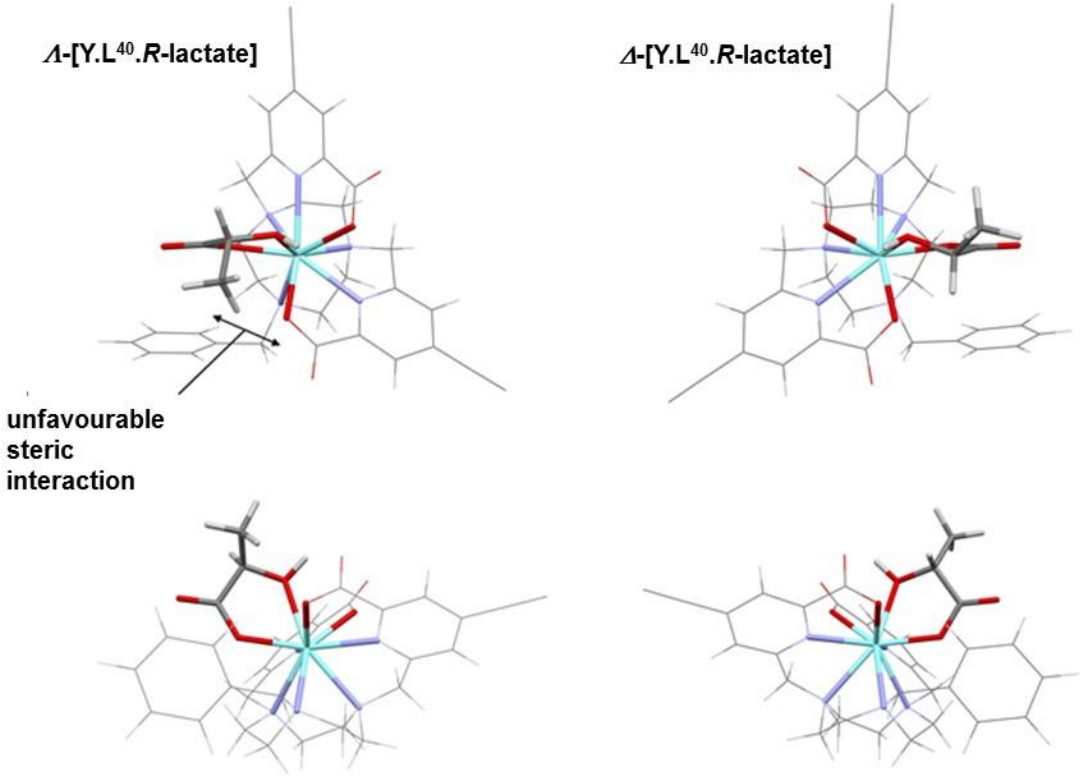

Figure 74 – Optimised geometries of *Λ*-[Y.**L**^{40}.*R*-lactate] and *Δ*-[Y.**L**^{40}.*R*-lactate] showing two views of each complex; the anisyl groups are omitted for clarity. In the *Δ* configuration, the methyl group is shown to point away from the coordinated carboxylate oxygen lone pair resulting in a less unfavourable steric interaction. Thus the *Δ*-isomer is the favoured geometry.

The energy difference between the two lowest energy isomers increases in the order: [Y.**L**^{38}]$^{3+}$ < [Y.**L**^{39}]$^{+}$ < [Y.**L**^{37}]$^{+}$ < [Y.**L**^{40}]$^{+}$ (Table 19). This sequence accords with the observation that the *N*-benzyl complex, [Eu.**L**^{40}]$^{+}$, has the highest g_{em} values for 70% of the induced CPL transitions compared to the other complexes in this study. A tentative assumption is that the *N*-benzyl group may align helically in the same sense as the two

coordinated pyridyl-carboxylate donors, creating a more rigidified local chiral structure around the lanthanide centre.

Table 19 – Relative energies in kJ mol^{-1} of the four isomeric adducts, [Y.**L**.*R*-lactate].

	$\mathbf{L^{37}}$	$\mathbf{L^{38}}$	$\mathbf{L^{39}}$	$\mathbf{L^{40}}$
Δ-Y.**L**-*R*-lactate [a]	0	0	0	0
Λ-Y.**L**-*R*-lactate [a]	2.0	0.7	1.5	2.4
Δ-Y.**L**-*R*-lactate [b]	19.5	25.3	27.0	30.3
Λ-Y.**L**-*R*-lactate [b]	21.6	26.7	31.7	36.1

[a] constitution of lactate chelate with lactate carboxylate in same plane as pyridyl N-atoms. [b] constitution of lactate chelate with lactate OH in same plane as pyridyl N-atoms.

3.7. Conclusions

A series of unsaturated Eu (III) complexes has been developed with attractive photophysical properties and anion binding capabilities. The ability of the complexes [Eu.$\mathbf{L^{37\text{-}40}}$] to form ternary adducts with anions was first assessed by monitoring changes in the emission spectrum on increasing the concentration of added anion. The overall binding affinities were estimated and the strongest binding was observed with the tri-positively charged bis-amide complex [Eu.$\mathbf{L^{38}}$]$^{+}$. This observation was accounted for in terms of a simple electrostatic effect. The overall trend in binding affinities was corroborated by hybrid-DFT calculations of the energies of optimised geometries of the lactate-adducts.

The mode of binding of α-hydroxy acids (lactate, mandelate and cyclohexylhydroxyacetate) with the four europium complexes [Eu.$\mathbf{L^{37\text{-}40}}$] was investigated by examining radiative rates of decay for Eu^{3+} emission in H_2O and D_2O. The results revealed that the α-hydroxy anion was able to bind to the complexes in two different chelation modes. For the complexes [Eu.$\mathbf{L^{38\text{-}40}}$], the anion was bound to the metal centre *via* a 5-ring chelate, with an OH oscillator in the Eu^{3+} inner coordination sphere. In the case of [Eu.$\mathbf{L^{37}}$]$^{+}$, the anion was bound to the lanthanide centre *via* the carboxylate group in a 4-ring chelate. This result was further supported by inspection of the calculated DFT geometries which revealed significant steric hindrance at the lanthanide centre from the more sterically bulky phosphinate groups, compared to the

carboxylate and amide donors. This increase in steric bulk inhibits binding of the acid to the metal centre in a 5-ring chelate.

The utility of such complexes in chiral detection has also been demonstrated and a full investigation of the induced CPL of the complexes on addition of selected chiral anions was undertaken. The CPL experiments established the use of these europium complexes in generating signature or 'fingerprint' induced CPL spectra, depending on the nature of the chiral analyte. The studies provided further information about the stereochemical structure of the resulting complex adduct. A common pattern emerged: an *R* acid configuration favours formation of a *Δ* complex and leads to a strong induced CPL signal. More importantly, empirical analysis of the $\Delta J = 4$ manifold, allowed assignment of absolute configuration. NMR and DFT studies offered some evidence supporting this analysis: a preferred stereoisomer was observed (*R*-*Δ* and *S*-*Λ*), albeit lacking the high stereoselectivity and larger g_{em} associated with the more conformationally rigid tri-substituted 9-coordinate complexes.[154,162,171]

The substitution of the third N position on the macrocyclic ring plays a key role. The *N*-benzyl complex exhibited the strongest, most well-defined induced circularly polarised luminescence, with the highest g_{em} values for 70% of the CPL-active transitions. This chiral amplification may result from the cooperative helical alignment of the *N*-benzyl group in the same sense as the two pyridyl pendant arms, creating a more rigid chiral structure.

The work detailed in this chapter has highlighted the key factors that allow us to select a suitable complex that can be used as a successful chirality probe. The complex must be able to bind to anions with strong affinity. Of the four europium (III) complexes studied, the highest binding affinity was observed for the bis-amide complex [Eu.$\mathbf{L^{38}}$]$^{3+}$. However, the poor quantum yield and complex instability with respect to dissociation limits the use of this complex as a CPL probe. The bis-carboxylate, [Eu.$\mathbf{L^{39}}$]$^{+}$, and bis-phosphinate complexes, [Eu.$\mathbf{L^{37}}$]$^{+}$, are bright with high quantum yields. Of these two complexes, the bis-carboxylate is able to bind to anions most strongly, with enhanced affinity and CPL activity, due to the lack of unfavourable steric interactions imposed on the lanthanide centre by the carboxylate donors. A final iteration of the bis-carboxylate complex, [Eu.$\mathbf{L^{39}}$]$^{+}$, *via* alkylation of the free macrocyclic NH, gave the complex [Eu.$\mathbf{L^{40}}$]$^{+}$, resulting in a chiral amplification effect and enhanced induced CPL.

This work provides a starting point for developing enhanced selectivity in the association of the chiral analyte. For example, based on the *N*-benzyl system, introduction of charged and directed hydrogen bonding or chelating moieties, e.g. NH_2Me^+ or a boronic acid group, into the benzyl ring, may allow additional stabilising interactions to occur that can enhance affinity and selectivity. The outcome of such work is reported in Chapter 4.

CHAPTER FOUR

DYNAMICALLY RACEMIC EU (III) COMPLEXES AS CHIRALITY PROBES

4.1. Introduction

In Chapter 3, the mechanism of inducing CPL from dynamically racemic lanthanide complexes was discussed, following the binding of a chiral anion directly to the metal centre. Enhancing the selectivity for a particular anion can be achieved in a number of ways.[5] When considering direct binding of an anion to a metal centre *via* displacement of a bound water molecule, incorporation of a moiety that can provide secondary stabilising interactions, such as directed hydrogen bonding, can significantly enhance affinity for a particular anion. In devising an appropriate synthetic receptor, it is a challenge to develop a system that is sufficiently selective for the chosen anion over other competing species, to serve as an analytical probe.

Sialic acid (Neu-5-Ac) is an important biomolecule belonging to the family of 9-carbon amino sugars (neuraminic acids). Sialic acid is present in serum as a mixture of α- (5-8%) and β-pyranose (92-95%) forms; the absence of the furanose form can be attributed to the acetamide moiety that is present at the C-5 position. Sialic acid can also be found occupying the terminal positions of carbohydrate chains of glycoproteins and glycolipids of biological membranes. It has a biological importance as it is over-expressed on the surface of tumour cells[191,192] and the variation of its concentration in serum can serve as a useful biological marker, indicating the existence of a cancerous state.[193]

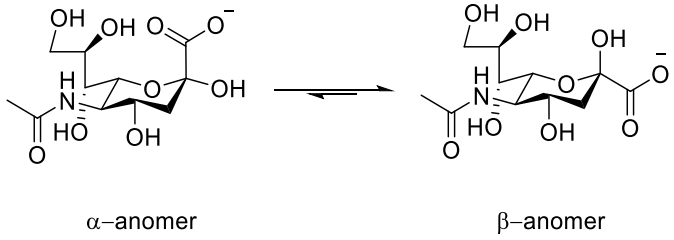

Figure 75 – Structure of sialic acid (Neu-5-Ac) showing the α- and β-pyranose forms, pK_a = 2.6 (H_2O, I = 0.1, 298K).

A number of lanthanide probes have been reported that target sialic acid selectively and signal the detection using MRI[194–196] and emission based techniques.[197,198] Of particular importance is the use of a boronic acid moiety in the selective binding of a diol functionality. The reversible formation of five- and six-membered cyclic boronate esters results from the interaction with 1,2- and 1,3-diols, and has been extensively exploited in the design of various saccharide sensors.[199] The incorporation of a phenylboronic acid (pba) moiety into the ligand framework of a lanthanide complex has also demonstrated

the utility of this moiety in the dynamic covalent binding to the 1,2-diol or the α-hydroxy acid group of sialic acid.[196,197]

Based on the study of four europium (III) complexes incorporating various ligand frameworks, [Eu.**L**$^{37\text{-}40}$], discussed in Chapter 3, a bis-carboxylate complex was selected for application as a chiral probe. The complexes [Eu.**L**^{39}]$^+$ and [Eu.**L**^{40}]$^+$ exhibited high quantum yield values, anion binding capability and gave rise to strong induced CPL following the addition of a chiral analyte. A heptadentate Eu (III) complex based on the bis-carboxylate ligand structure containing a pba moiety, [Eu.**L**^{41}]$^+$, has been designed to target sialic acid selectively. Exploiting the inherent chirality of the molecule, binding at europium was hypothesised to result in a change in the emission spectral form and generate an induced CPL signal. The response of the complex is compared to the bis-carboxylate complex, [Eu.**L**^{39}]$^+$, and the *N*-alkylated derivative, [Eu.**L**^{40}]$^+$, which serve as controls.

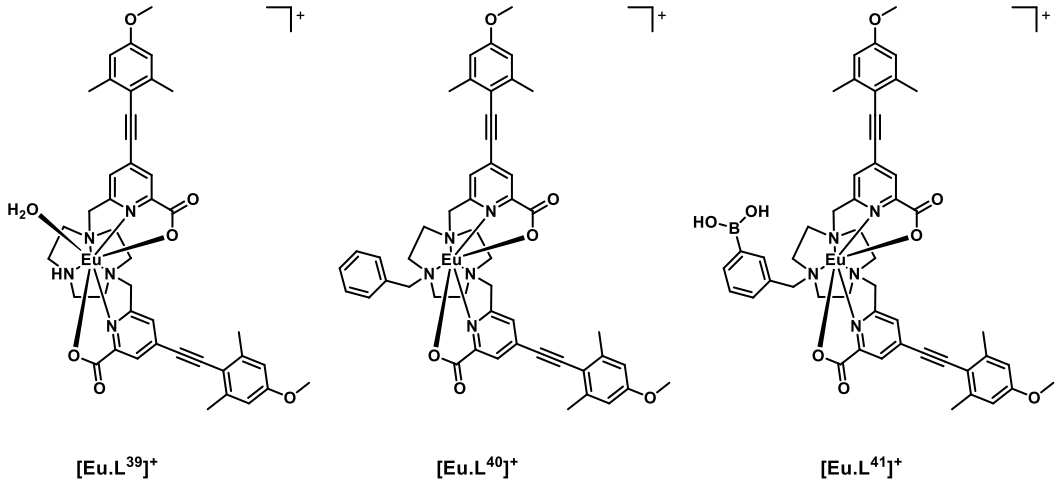

Figure 76 - Structures of Eu (III) complexes of **L**$^{39\text{-}41}$.

Another class of important biologically relevant chiral anions is the family of pentavalent phosphorus anions, including *O*-phosphorylated amino acids and peptides. These *O*-P-amino acids and peptides, are perhaps some of the most important anionic species in nature, and are involved in the control of many cellular processes, such as, differentiation, development and proliferation.[200] The first reports of the sensing of such anions using a chiral lanthanide complex[121] were discussed in detail in Chapter 1, Section 1.4.2.1. These initial studies reported that there was a change in the emission and CPL spectral form following addition of the selected phosphate anion. A higher binding affinity was

estimated for *O*-P-Tyr, compared to *O*-P-Ser and *O*-P-Thr, associated with its lower solvation energy in aqueous media.

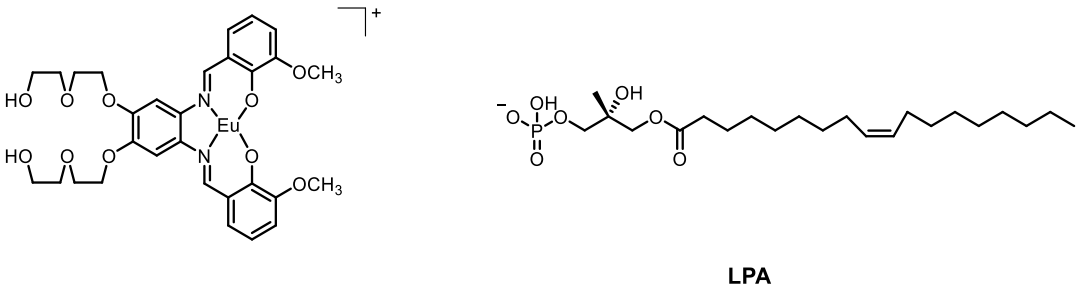

Figure 77 – Structure of Eu (III) salophene complex (*left*) and oleoyl-*L*-α-lysophosphatidic acid (LPA) (*right*).

A related chiral pentavalent phosphorus anion of interest is oleoyl-*L*-α-lysophosphatidic acid (LPA). Perhaps one of the simplest phospholipids, recent studies have demonstrated the presence of increased LPA levels in malignant effusions in patients with cancer, most specifically in ovarian cancer.[201] Therefore, a specific and quantitative method for the detection of LPA in clinical samples is required. Some efforts towards achieving this goal have been reported, based on organic and lanthanide-based fluorogenic sensors.[202–204] LPA is apparently thought to bind selectively in methanolic extracts of human plasma samples by a europium (III) salophene complex, Figure 77, indicated by an increase in the total fluorescence intensity, although it is difficult to understand the chemical basis for this selective binding behaviour.[204]

A europium heptadentate complex has been designed, employing a charged amino group, NH_2Me^+, in order to enhance the binding of important chiral phosphorus anions selectively, including *O*-P-amino acids, *O*-P-peptides and LPA. Accordingly, this complex was synthesised and changes in the emission spectral form and the induced 'fingerprint' CPL response were investigated following chiral anion binding.

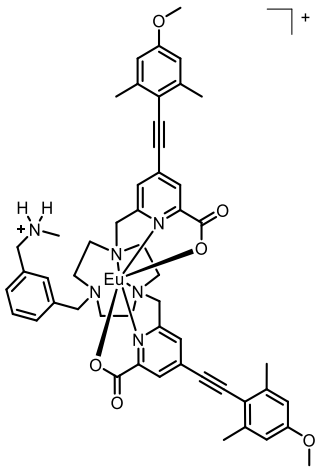

$[Eu.L^{42}]^{2+}$

Figure 78 – Structure of the europium (III) complex of $\mathbf{L^{42}}$ containing a charged amino group.

4.2. Synthetic approaches

4.2.1. Synthesis of $[Eu.L^{41}]^{+}$

A phenylboronic acid moiety was appended to the desired ligand framework, $\mathbf{L^{39}}$, *via* ring *N*-alkylation. Initial protection of the boronic acid group as a cyclic ester was achieved, to facilitate purification at a later stage. Boronic esters are less polar and easier to handle than the acids, due to the loss of the hydrogen bonding capability of the hydroxyl groups. The simple cyclic ester, based on ethylene glycol, was selected as the protecting group. Although sensitive to hydrolysis, the boronic ester was considered to be sufficiently stable to allow purification using column chromatography, under carefully controlled conditions. Subsequent removal of the ester group can be easily achieved using mild base hydrolysis. The use of more stable hindered cyclic esters, such as a pinacol derivative was avoided, as its conversion back to the boronic acid requires more forcing conditions that are not compatible with the presence of other groups in the ligand framework, such as the acid-sensitive alkyne.

Reaction of commercially available 3-(bromomethyl)phenylboronic acid with ethylene glycol in anhydrous pentane over 4 Å molecular sieves, yielded the protected phenylboronate in good yield. Subsequent alkylation with $\mathbf{L^{39}}$ gave the ligand $\mathbf{L^{41}}$, which was purified using flash column chromatography on silica gel. The presence of the boronic ester moiety was confirmed by the observation of a single resonance in the ^{11}B NMR spectrum at 31.3 ppm.

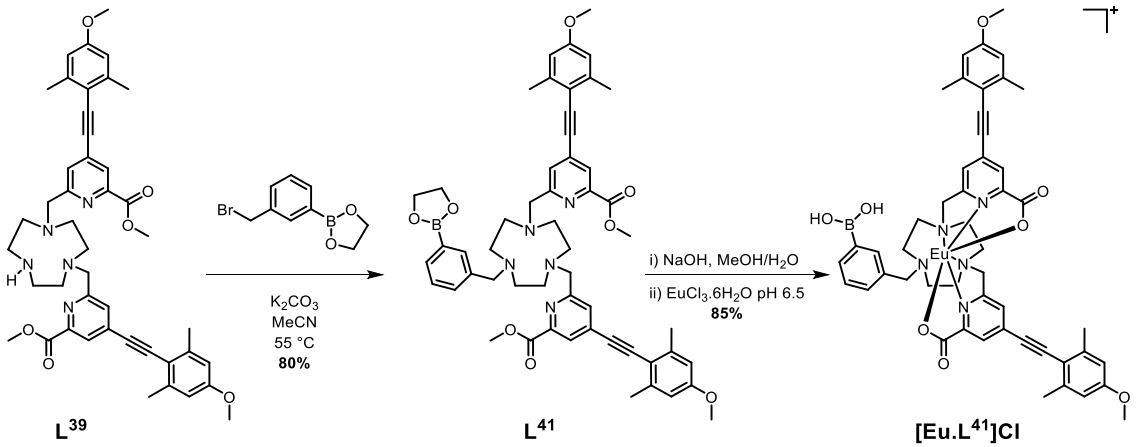

Scheme 21 – Synthesis of the Eu (III) complex of $\mathbf{L^{41}}$ containing a phenylboronic acid moiety.

Base hydrolysis of both the methyl ester and the cyclic boronic ester groups was carried out using NaOH (aq.) in a MeOH-H_2O mixture (1:1, v/v) at pH 12. After confirmation of completion by LC-MS, the pH of the solution was lowered to 6.5 and $EuCl_3.6H_2O$ was added. Successful formation of the complex after 24 h was confirmed by ESI-MS.

4.2.2. Synthesis of $[Eu.L^{42}]^{2+}$ and its precursors

It was necessary first to synthesise an aromatic precursor containing a charged amino group that also contains an electrophilic benzylic substituent at the *meta* position for the alkylation step. An *N*-methylbenzylamine group was selected, as it has an appropriate pK_a value (~9.7), ensuring that it is positively charged at the desired pH (7.4), is not too sterically bulky, and offers scope for stabilising hydrogen-bonding interactions.

The synthetic pathway (Scheme 22) began with the formation of the mono-amide, **6b**, from mono-methyl isophthalate *via* the acid chloride. Reaction of **6a** with oxalyl chloride and catalytic DMF furnished the acid chloride, followed by addition of methylamine to generate the amide, **6b**. Simultaneous reduction of the amide and ester groups using $LiAlH_4$ in THF gave the amino-alcohol **6c**. A high yield was achieved by using the 'Fieser work-up' procedure, which involved careful addition of x H_2O at 0 ºC, followed by x NaOH (15%) and finally 3x H_2O. The granular aluminium salts that formed were easily removed by filtration. Protection of the amine with a formamide group was achieved using 2,2,2-trifluoroethyl formate (TFEF). This protecting group was selected as it can be removed under basic conditions. Therefore, deprotection can occur at the same time as hydrolysis of the methyl ester groups of the ligand. The final step in the synthesis of the

precursor was conversion of the alcohol, **6d**, to the mesylate, **6e**, under standard conditions.

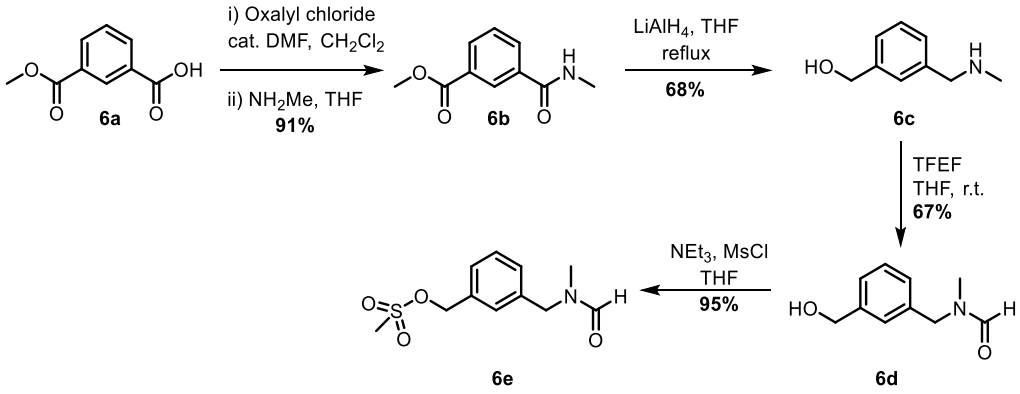

Scheme 22 – Synthetic pathway for the synthesis of the mesylate **6e**.

Alkylation of **L**[39] with the mesylate **6e,** gave the ligand pre-**L**[42], after purification by flash column chromatography. Deprotection of the formamide protecting group and the methyl ester groups was attempted using NaOH in a MeOH-H_2O mixture (1:1, v/v). The reaction was monitored by LC-MS, which showed that incomplete deprotection of the amine was observed after 48 h. The two products (protected and deprotected) were separated by reverse-phase HPLC (10-100% MeOH (0.1% formic acid) in H_2O (0.1% formic acid) over 15 minutes). The ligand was passed down an ion exchange resin to remove the presence of any formate salts. The ligand, **L**[42], was dissolved in MeOH-H_2O (1:1, v/v) at pH 6.5 and $EuCl_3.6H_2O$ was added to give the complex [Eu.**L**[42]]Cl_2.

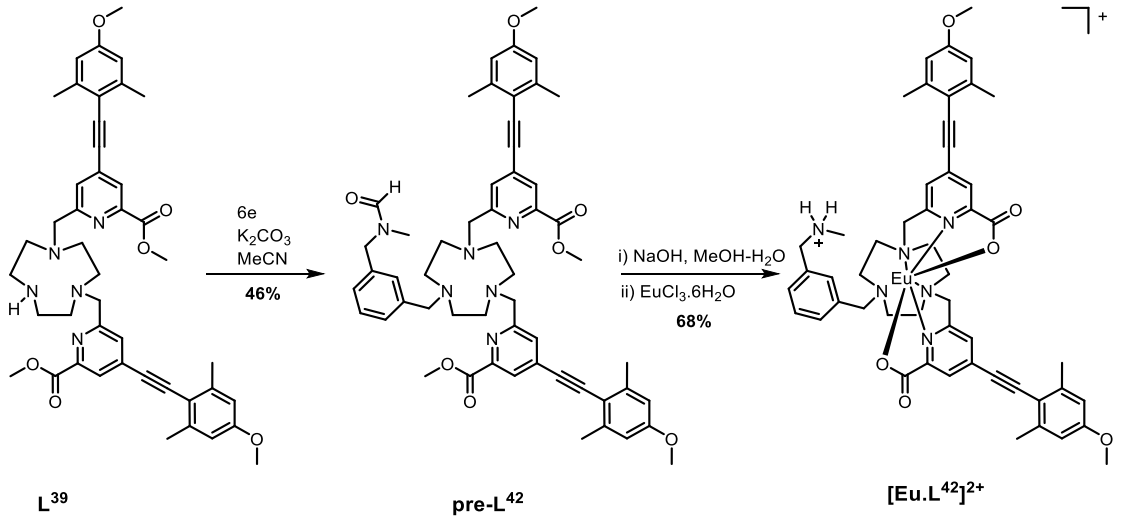

Scheme 23 – Synthesis of $[Eu.\mathbf{L}^{42}]^{2+}$ *via* an alkylation strategy.

4.3. A chiral probe for sialic acid

The photophysical properties of the boronic acid derivative $[Eu.\mathbf{L}^{41}]^{+}$ were assessed in comparison to those determined for the *N*-benzyl complex $[Eu.\mathbf{L}^{40}]^{+}$. The capability of the complex to bind anions was tested using lactate in a model study, and the induced CPL was correlated to the configuration of the complex using the methods described in Chapter 3. The binding affinity of sialic acid was estimated and the emission spectral changes and induced CPL signature were compared to $[Eu.\mathbf{L}^{39}]^{+}$ and $[Eu.\mathbf{L}^{40}]^{+}$. Investigation into the mode of binding of sialic acid was attempted, by comparison of the spectral response with that observed following addition of the methyl-ester derivative of Neu-5-Ac.

4.3.1. Photophysical properties of $[Eu.L^{41}]^{+}$

The key photophysical parameters for $[Eu.\mathbf{L}^{41}]^{+}$ were determined and compared to those of the related complex, $[Eu.\mathbf{L}^{40}]^{+}$ (Table 20). The hydration state in water of the title complex, $[Eu.\mathbf{L}^{41}]^{+}$, was estimated to be $q = 0.2$, as defined in equation **2.3**, page 67.[117] The absence of an inner sphere metal-bound water molecule is consistent with the behaviour of the *N*-benzyl complex, $[Eu.\mathbf{L}^{40}]^{+}$. This observation provides supporting evidence that the steric bulk of the *N*-substituent inhibits coordination of a water molecule to the lanthanide centre.

The europium emission quantum yield of the boronic acid complex, [Eu.**L**^{41}]$^{+}$, was measured to be 5%, which is significantly lower than that of the *N*-benzyl complex, [Eu.**L**^{40}]$^{+}$ (Table 20). Secondly, the radiative rate of decay of Eu^{3+} emission in methanol was nearly twice as fast for [Eu.**L**^{41}]$^{+}$ compared to [Eu.**L**^{40}]$^{+}$. Such behaviour suggests that the europium (III) excited state of [Eu.**L**^{41}]$^{+}$ is being quenched, in a manner that is not possible for [Eu.**L**^{40}]$^{+}$.

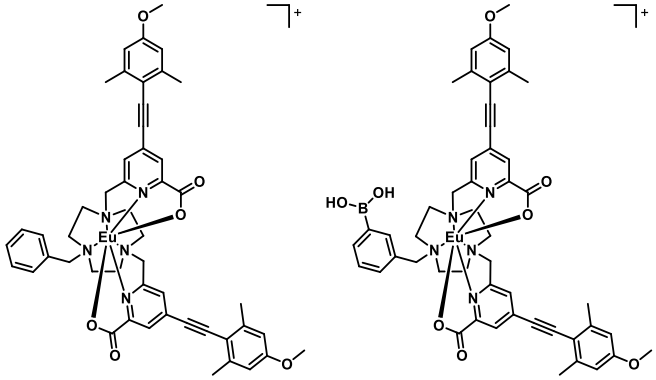

Table 20 – Photophysical properties of the Eu (III) complexes of **L**^{40,41} (295 K, MeOH, selected emission decay rate constants given in H_2O and D_2O). Values of ϕ are (±15%) and the errors on k are (±10%).

	[Eu.**L**^{40}]$^{+}$	[Eu.**L**^{41}]$^{+}$
λ/nm	348	356
ε/mM^{-1} cm^{-1}	36.0	35.0
ϕ	0.18	0.05
k/ms^{-1}	1.20	2.04
$k(H_2O)$/ms^{-1}	2.00	2.63
$k(D_2O)$/ms^{-1}	1.89	2.17
q	0	0.2

It is possible for boronic acid compounds to undergo intermolecular association (e.g. dimer formation, as shown in the X-ray crystal structure of phenylboronic acid)[205] through hydrogen bonding between the boronic acid groups. However, this interaction is typically only observed in the solid state or in non-polar media. A dilution study was carried out in MeOH-H_2O (1:1, v/v) at pH 7.4. The luminescent lifetime of the excited state was monitored as the concentration was successively lowered from 5 μM to 0.63 μM, at which point the sample was too dilute to obtain reliable results. No significant change in the emission lifetime was observed, suggesting that an intermolecular association mechanism does not occur over this concentration range. It is more likely

that the excited state of [Eu.$\mathbf{L^{41}}$]$^+$ may undergo an electron transfer quenching process. Due the acidic nature of phenylboronic acid in aqueous solution, the trivalent neutral form is in equilibrium with the anionic tetrahedral intermediate (pK_a 8.7), Figure 79.[206] The presence of this anionic intermediate, even at low concentration at physiological pH, may be the cause of the observed quenching (electron transfer) of the europium (III) excited state. It is also worth noting that no oxygen/air effect on the luminescent excited state lifetime was observed.

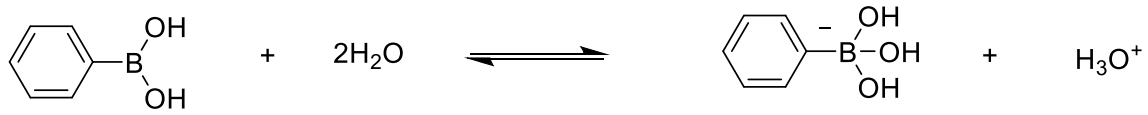

Figure 79 – Ionisation equilibrium of phenylboronic acid in solution.

4.3.2. Preliminary investigations into interactions with anions

As was shown in Chapter 3, the europium emission spectrum is particularly sensitive to the metal coordination environment. The addition of lactate to a series of structurally related Eu (III) complexes ([Eu.$\mathbf{L^{37\text{-}40}}$]) was found to cause significant changes in the total emission spectral response, consistent with anion binding at the metal centre. With this behaviour in mind, the emission spectrum of [Eu.$\mathbf{L^{41}}$]$^+$ was monitored following addition of *S*-lactate (Figure 80). A ten-fold enhancement in the total luminescence intensity was observed, following addition of a 4,000-fold excess of *S*-lactate. The excited state lifetime was also found to increase from 0.49 ms to 0.64 ms. The increase in emission intensity and emission lifetime indicated that anion binding to the metal centre, at least in part, inhibits the quenching mechanism taking place. Lactate can bind to the boronate through the carboxylate and hydroxyl group to form a 5-membered chelate,[207] as well as to the lanthanide centre, consistent with the idea that the electron transfer quenching process that may be occurring in the complex, is not possible when lactate binds.

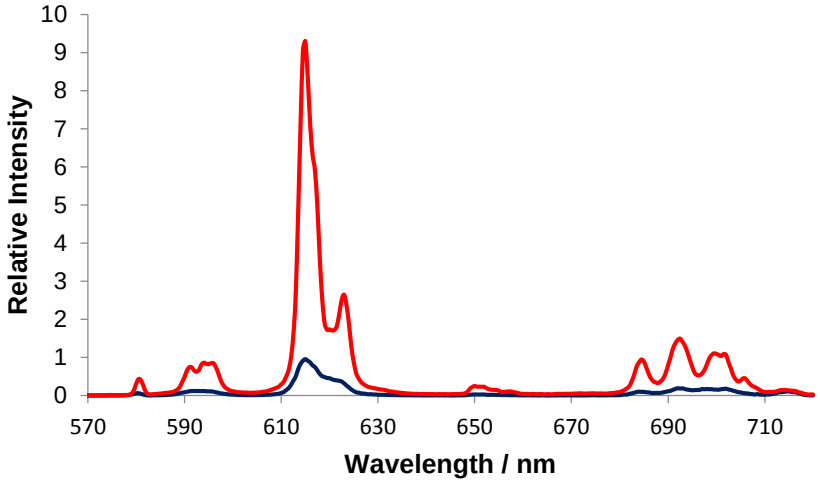

Figure 80 – Total emission spectra of [Eu.**L**^{41}]$^{+}$ (*blue*) and following addition of 2 mM *S*-lactate (*red*) (5 µM complex, λ_{exc} = 356 nm, MeOH, 295 K).

The addition of *R*- and *S*-lactate to the europium complex, [Eu.**L**^{41}]$^{+}$, resulted in the appearance of CPL, identical in nature to that of [Eu.**L**^{40}]$^{+}$, Figure 81. The sign and form of each transition was the same and the measured emission dissymmetry values, g_{em}, were comparable. Empirical analysis of the ΔJ = 4 transition allowed assignment of the absolute configuration of the complex, as discussed in Chapter 3, where addition of *R*-lactate was shown to result in Δ helicity, and *S*-lactate gives Λ helicity.

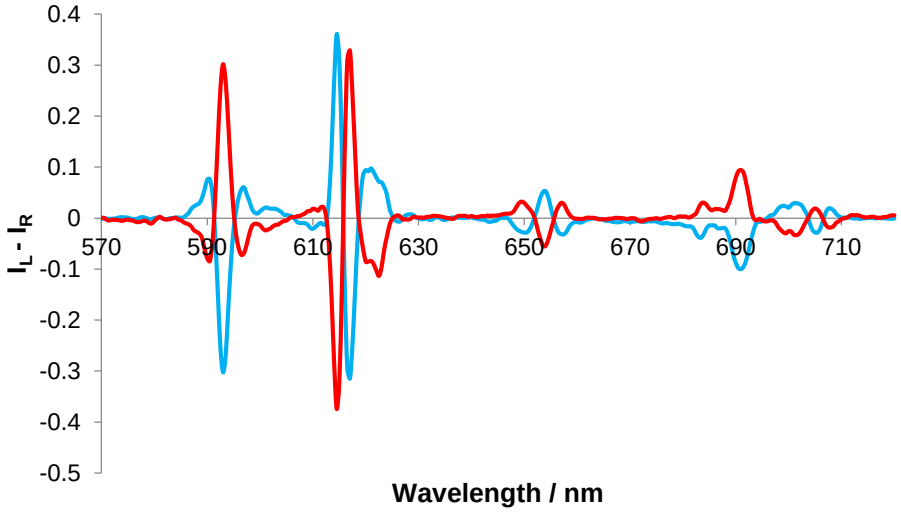

Figure 81 – Induced CPL spectra of [Eu.**L**^{41}]$^{+}$ following the addition of 2 mM *R*- (*red*) and *S*-lactate (*blue*); g_{em}(593 nm) = ± 0.05, g_{em}(654 nm) = ± 0.07 (5 µM complex, λ_{exc} = 356 nm, MeOH, 295 K).

The emission and CPL response of [Eu.**L**^{41}]$^{+}$ on addition of a chiral anion, such as lactate, demonstrates that anion binding at the metal centre can occur in a similar manner to that observed for [Eu.**L**$^{37\text{-}40}$] (Chapter 3).

4.3.3. Investigations into the binding affinity of sialic acid

Sialic acid is an important biomolecule that is considered to be a tumour marker, as it is overexpressed on the surface of tumour cells. Moreover, the level of free sialic acid in serum is altered upon entering a cancerous state. Typical concentrations in healthy adults of free sialic acid in serum lie in the range of 140 – 200 μM.[208]

The interaction of sialic acid with the parent bis-carboxylate europium (III) complex, [Eu.**L**^{39}]$^{+}$ was investigated. An emission titration was carried out in methanol and the spectral changes were monitored as a function of added concentration of sialic acid. A binding affinity in methanol of log*K* = 5.24 was estimated, which demonstrates that there is a significant interaction between the complex and the Neu-5-Ac anion in methanol (Figure 82). No significant interaction was observed in pure water; presumably the solvation energy of the complex and sialic acid are much higher under these conditions.

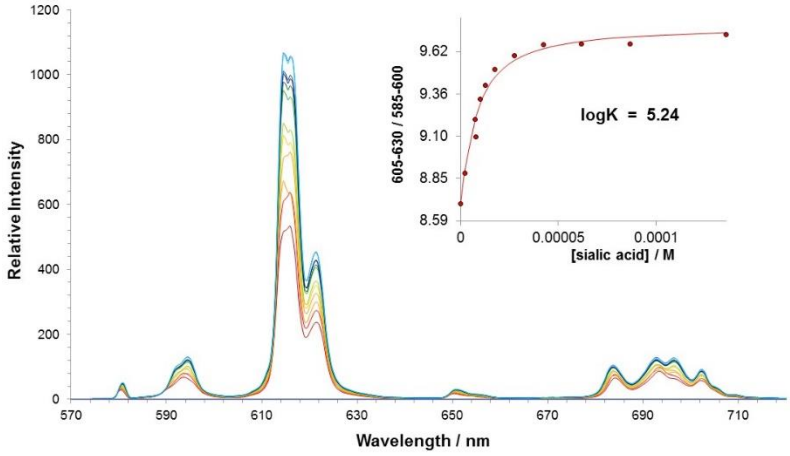

Figure 82 – Variation of the europium (III) emission profile of [Eu.**L**^{39}]$^{+}$ as a function of added sialic acid. (5 μM, λ_{exc} = 352 nm, MeOH). Inset shows the fit to experimental data, following iterative least squares fitting to a 1:1 binding model.

The addition of sialic acid to [Eu.**L**^{39}]$^{+}$ also induced significant CPL. It was interesting to note that the form of the CPL spectrum, particularly in the ΔJ = 1 and ΔJ = 2 manifolds, was remarkably different to that seen following addition of simple carboxylates such as *R*-phenylpropionate, and also in the series of α-hydroxy acids that were discussed in Chapter 3 (Figure 83). The 'signature' CPL response may allow simple differentiation between the detection of sialic acid and other chiral carboxylate anions in a competitive environment. It is worth noting, however, that the ΔJ = 4 region again resembles that of

the *R*-lactate adduct of [Eu.**L**^{39}]$^{+}$ allowing tentative assignment of the complex adduct configuration as *Δ*-[Eu.**L**^{39}.Neu-5-Ac].

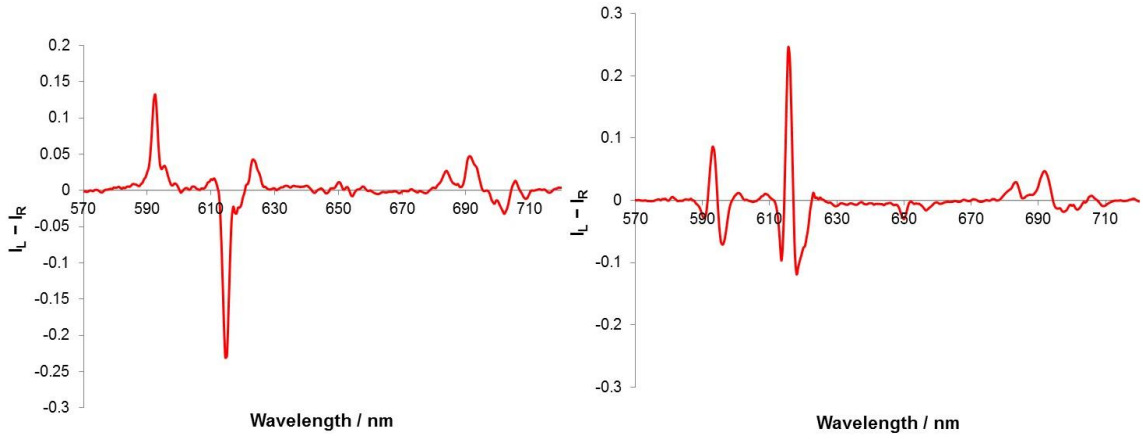

Figure 83 – CPL spectra of [Eu.**L**^{39}]$^{+}$ following addition of *R*-lactate (*left*) and sialic acid (*right*). (5 μM complex, 50 μM anion, λ_{exc} = 352 nm, MeOH).

This proof of concept study demonstrated the capability of lanthanide complexes based on a heptadentate bis-carboxylate ligand, to signal the binding of sialic acid. Further development of this probe saw the incorporation of a phenylboronic acid moiety into the ligand framework, [Eu.**L**^{41}]$^{+}$. Phenylboronic acid is a weak acid (pK_a = 8.72) that is able to bind covalently and reversibly to 1,2-diols,[206] such as the glycerol side-chain of sialic acid, and to α-hydroxy acids.[207] The stability of the esters formed by the tetragonal boronate anion is an order of magnitude greater than for the trigonal boronic acid.[209] Therefore, enhanced affinity is observed under basic conditions. It was hoped that the addition of this secondary stabilising interaction would enhance the affinity of the complex for sialic acid and allow for detection in aqueous solvent systems.

An emission titration of [Eu.**L**^{41}]$^{+}$ and sialic acid in methanol was carried out to allow comparison with [Eu.**L**^{39}]$^{+}$. Plotting the change in *ΔJ* = 2 and *ΔJ* = 1 intensities *versus* concentration of anion generated a curve that did not fit to a 1:1 binding model (Figure 84). The plot revealed that an initial process occurs before 1:1 binding between the anion and the lanthanide ion. It is worth noting that significant changes in the emission spectrum were observed at a 3-fold lower concentration of sialic acid, compared to the response observed for [Eu.**L**^{39}]$^{+}$, suggesting that the addition of a phenylboronic acid moiety increases the affinity of the europium (III) complex for sialic acid. It is also interesting to note that there was no evidence of sialic acid binding to the control *N*-benzyl complex, [Eu.**L**^{40}]$^{+}$, indicating the need for the putative stabilising interaction.

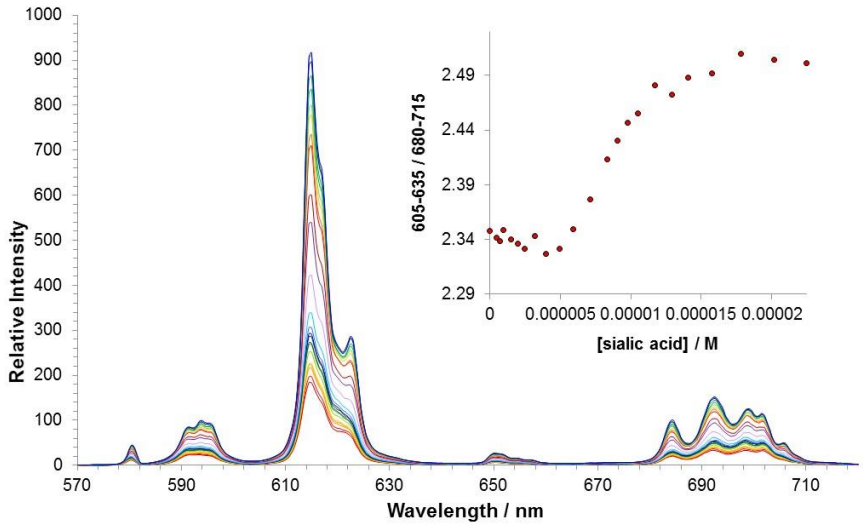

Figure 84 - Variation of the europium (III) emission profile of [Eu.$\mathbf{L}^{41}$]$^+$ as a function of added sialic acid. (5 μM, λ_{exc} = 356 nm, MeOH).

The europium (III) total emission studies have confirmed that there is a binding interaction between the parent complex, [Eu.$\mathbf{L}^{39}$]$^+$, and sialic acid. No binding affinity was observed for the *N*-benzyl complex, [Eu.$\mathbf{L}^{40}$]$^+$, most likely as a result of the increased steric demand around the metal centre. Interestingly, the addition of a boronic acid group to the aromatic ring of the *N*-benzyl complex, [Eu.$\mathbf{L}^{41}$]$^+$, provided an additional stabilising interaction that allowed sialic acid to bind to the europium (III) complex, despite the steric hindrance imposed by the benzyl substituent.

The sign of the induced CPL in the ΔJ = 1 manifold was comparable to that for [Eu.$\mathbf{L}^{39}$]$^+$ following addition of sialic acid. However, very little optical activity was observed in the ΔJ = 3 and ΔJ = 4 transitions. The difference in the CPL spectral form, suggests that a different coordination environment is present in each complex. The emission dissymmetry values, g_{em}, were larger for [Eu.$\mathbf{L}^{41}$.Neu-5-Ac] (g_{em} (593 nm) = +0.03, c.f. +0.015 for [Eu.$\mathbf{L}^{39}$.Neu-5-Ac]), suggesting that enhanced binding affinity and a higher degree of conformational rigidity occurs when sialic acid binds to the metal centre in the boronate complex, [Eu.$\mathbf{L}^{41}$]$^+$. Such behaviour may be due to an additional interaction with the boronic acid group in the adduct.

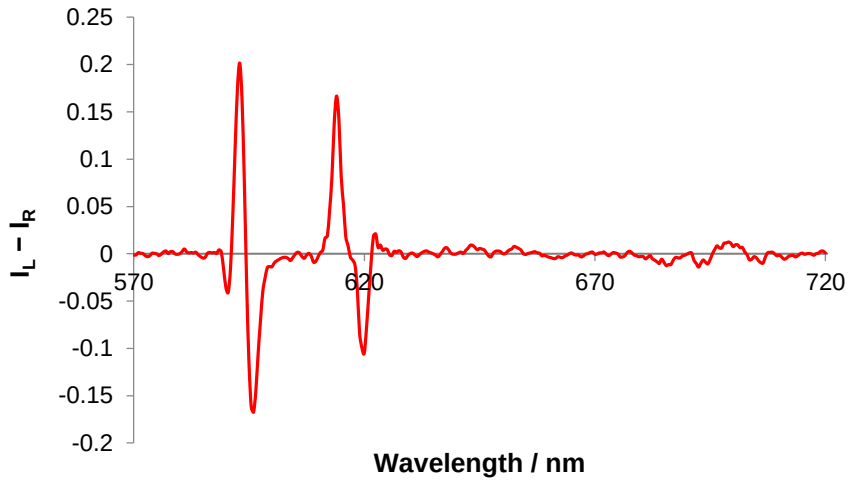

Figure 85 - CPL spectra of [Eu.**L**^{41}]$^+$ following addition of sialic acid (5 µM complex, 50 µM anion, λ_{exc} = 356 nm, MeOH).

No evidence for binding was observed in pure water over the pH range 4-10 for [Eu.**L**^{41}]$^+$. This behaviour could be related to the conformation adopted by sialic acid in different solvents. ^{1}H NMR spectra of sialic acid in MeOD and D_2O were analysed at a pD of 5.5. However, no significant differences were observed between the NMR spectra in each solvent, suggesting a minimal difference in the conformation of sialic acid.

It is still possible that the difference in binding affinity of sialic acid in the two solvent systems is a direct result of the difference in solvation energy. There are five hydroxyl groups present in the molecule, so hydration of the anion in water is likely to be very high and may explain the low affinity it has for the positively charged lanthanide complex in aqueous solution. Systematic variation of the solvent composition and the effect on the emission spectral output was monitored. It was found that significant change in form and intensity was observed when 2 mM sialic acid was added to 1 mL 4:1 MeOH:H_2O sample of [Eu.**L**^{41}]$^+$. However, increasing the water composition any higher, resulted in no evidence for binding of the anion to the metal centre. The poor aqueous solubility of the complex is also a key factor contributing to the decreased affinity for sialic acid in these aqueous systems.

4.3.4. Investigating the mode of binding of sialic acid

The mode of binding of sialic acid to the europium (III) complexes, [Eu.**L**^{39,41}]$^{+}$, was investigated by a comparative study of the induced CPL following addition of sialic acid, its methyl ester derivative and the related molecule *N*-acetyl-*D*-glucosamine (Figure 86).

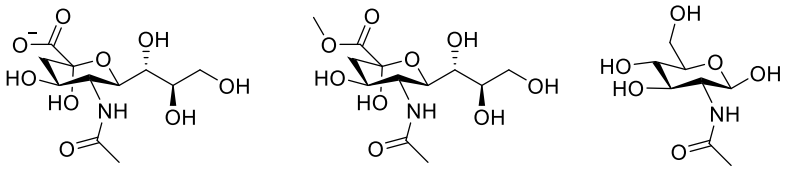

Figure 86 – Structures of sialic acid (*left*), the corresponding methyl ester (*middle*) and N-acetyl-*D*-glucosamine (*right*).

The form and sign of the CPL spectra of [Eu.**L**^{39}]$^{+}$ following addition of sialic acid and its methyl ester derivative was similar, strongly suggesting that the negatively charged carboxylate group of Neu-5-Ac is not involved in the primary binding interaction (Figure 88, **A** *versus* **B**). Methyl ester carbonyl groups are very poor donors to any Ln^{3+} ion, as shown by the addition of methyl-*L*-lactate to the complexes [Eu.**L**$^{37\text{-}41}$], which all showed no evidence of binding to the methyl ester. Therefore, an alternative mechanism for the recognition of sialic acid must be considered, based primarily on binding of the acetamide oxygen within the inner coordination sphere of the lanthanide complex. Such a binding mode was hypothesised recently in the work of Ouchi, who was studying sialic acid binding to a [Ln.(ABNOTA] complex (Figure 87).[198] However, addition of *N*-acetyl-*D*-glucosamine, a monosaccharide containing the same acetamide moiety, resulted in no change to the total emission spectrum and no induced CPL, indicating that other groups in the Neu-5-Ac molecule must also be involved in the binding mechanism.

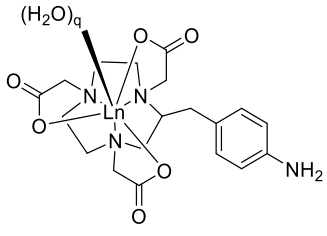

Figure 87 – Structure of Ln^{3+} [Ln.ABNOTA] complex.[198]

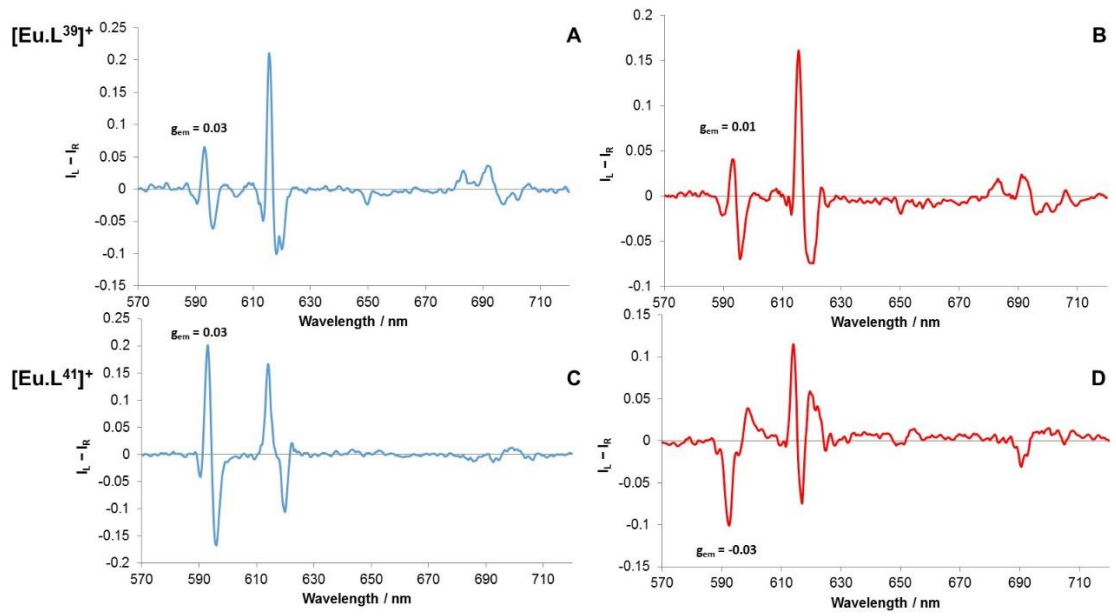

Figure 88 – Induced CPL spectra for [Eu.**L**^{39}]$^{+}$ following the addition of **A**: 2 mM sialic acid; **B**: 2 mM sialic acid methyl ester (MeOH, λ_{exc} = 352 nm, 295 K). Induced CPL spectra for [Eu.**L**^{40}]$^{+}$ following the addition of **C**: 2 mM sialic acid; **D**: 2 mM sialic acid methyl ester (MeOH, λ_{exc} = 356 nm, 295 K). g_{em} values are given for the same ΔJ = 1 transition at 593 nm.

In contrast to the behaviour of [Eu.**L**^{39}]$^{+}$, the induced CPL spectra of [Eu.**L**^{41}]$^{+}$ were significantly different following addition of sialic acid *versus* its methyl ester (Figure 88, **C** *versus* **D**). Subtle differences in the form of the total emission spectra, particularly in the ΔJ = 1 and ΔJ = 4 transition, were also observed. Such behaviour suggests that the carboxylate group may yet be involved in some manner, in the interaction between sialic acid and the europium (III) complex, but not through direct binding to the lanthanide (III) centre.

In related work on a Gd-based MRI contrast agent for sialic acid detection, lanthanide complexes based on diethylenetriamine pentaacetic acid (DTPA) ligands incorporating a phenylboronic acid moiety were also used, **L**^{43} and **L**^{44} (Figure 89).[194] The authors suggested that the interaction between pba and sialic acid occurred either with the glycerine moiety at C-6, or with the carboxylate and hydroxyl group at C-2, to form a five-membered cyclic ester. They did not consider any role for the amide carbonyl group in binding to the Gd^{3+} centre, nor was any direct evidence provided to substantiate their hypothesis.

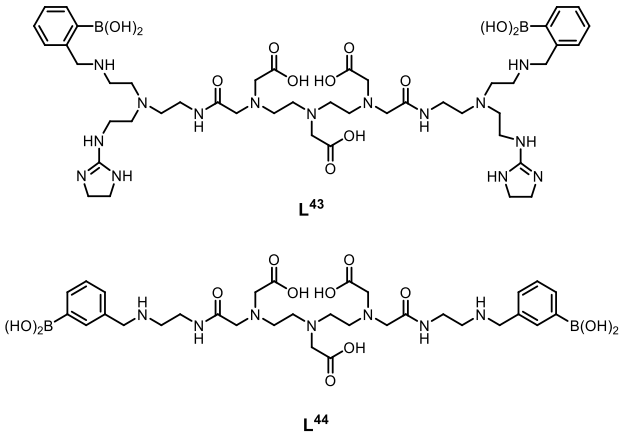

Figure 89 – DTPA-bis amide (DTPA – diethylenetriamine pentaacetic acid) ligands used in Gd-based MRI contrast agents for sialic acid detection.[194]

The study in this thesis has presented the first example of induced CPL for sialic acid recognition. Evidence gathered from the induced CPL response of the pba-europium (III) complex [Eu.**L**^{41}]$^{+}$ following addition of sialic acid, its methyl ester derivative and NAG, allows us to hypothesise that there is a synergistic interaction involved in the binding mechanism of the europium complex and sialic acid. It is likely that this interaction involves the carboxylate group, perhaps in the formation of a cyclic ester with the boronic acid, together with an additional interaction involving metal chelation of the amide carbonyl oxygen and the first hydroxyl group of the glycerol side chain. There is precedence for this hypothesis, derived from the crystal structure data of sialic acid located in the active site of the serum protein complement factor H, in which the potentially favourable orientation for chelation of the amide carbonyl oxygen and the first glycerol hydroxyl group is suggested (Figure 90).[210]

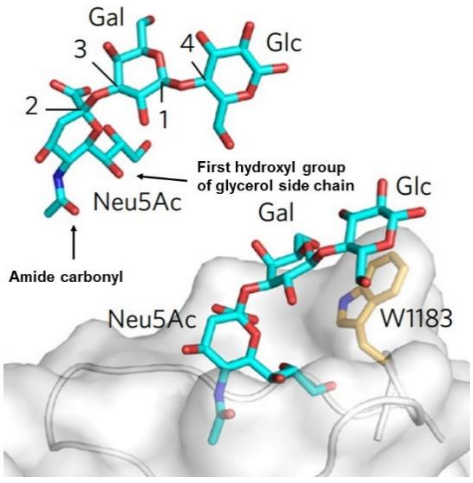

Figure 90 – The sialic acid binding site of the serum protein complement factor H, showing the orientation of the amide carbonyl oxygen and the first glycerol hydroxyl group.[210]

With the methyl ester of sialic acid, the carbonyl group cannot engage in such a secondary interaction with the boronic acid and so the coordination geometry around the metal centre is different. As a result, the induced CPL response is distinctive in form and sign, comparing the two chiral analytes. As the solubility and weak binding affinity prevented studies in an aqueous solvent environment, the pH effect on the mechanism of binding could not be investigated.

Taken together, these results have allowed for the development of a tentative hypothesis for the binding mode of sialic acid in both of these complexes [Eu.**L**^{39}]$^{+}$ and [Eu.**L**^{41}]$^{+}$. However, further evidence is required to gain a more in-depth understanding of how these complexes interact with this important chiral biomolecule. For example, the investigation in the difference in NMR relaxation rate data between the Eu^{3+} and Tb^{3+} complexes with a ^{13}C labelled amide carbonyl group, would help elucidate if this group is bound to the lanthanide centre. Hybrid-DFT calculations of the lowest energy conformers may also provide further evidence regarding the nature of the bound species.

4.4. A chiral probe for *O*-phosphorus oxy-anions

Significant progress has been made over the last ten years in the design of lanthanide-based probes for phosphate oxy-anions.[5] Phosphate is considered to bind to the lanthanide centre in a monodentate manner, through the negatively charged oxygen atom. This hypothesis is based on the analysis of rate data of 12-N_4 systems (which are less sterically demanding than the 9-N_3 systems) where phosphate was confirmed to bind in this way.[115,118] The data is in line with the established tendency of phosphate to act as a monodentate ligand to single metal centres (Na^{+}, Ca^{2+}, Zn^{2+}).[211,212]

This section presents a novel dynamically racemic chirality probe, [Eu.**L**^{42}]$^{2+}$, that can bind to chiral *O*-phosphorus anions, and signal the binding of the analyte *via* the induction of circularly polarised luminescence.

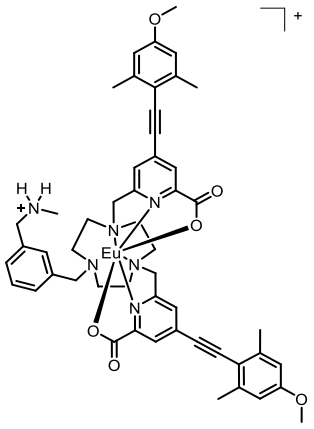

$[Eu.L^{42}]^{2+}$

4.4.1. Photophysical characterisation of $[Eu.L^{42}]^{2+}$

A number of photophysical techniques were used to characterise the complex $[Eu.\mathbf{L}^{42}]^{2+}$ and the data was compared to the control *N*-benzyl complex, $[Eu.\mathbf{L}^{40}]^{+}$. The hydration state of the complex could not be determined using the methodology outlined in Section 2.5.1.2. of Chapter 2, as the complex was not fully soluble in H_2O and the emission intensity was dramatically quenched. Therefore, in order to get an understanding of the number of metal bound water molecules, the rate of radiative decay of europium (III) emission was determined in methanol and d^4-methanol. The derivation of the hydration state, *q*, was estimated using equation **2.3**, page 67. The number of metal-bound solvent molecules was estimated as zero, consistent with the data obtained for the other *N*-alkylated europium (III) complexes presented in this chapter, $[Eu.\mathbf{L}^{40,41}]^{+}$.

The experimentally determined data in methanol for the emission quantum yield, ϕ, the extinction coefficient, ε, and the maximum absorbance wavelength, λ, is given in Table 21. The related experimental data of the control complex, $[Eu.\mathbf{L}^{40}]^{+}$ is given as a reference and no anomalous results were noted.

Table 21 - Photophysical properties of the Eu (III) complexes of $\mathbf{L}^{40,42}$ (295 K, MeOH).

	$[Eu.\mathbf{L}^{40}]^{+}$	$[Eu.\mathbf{L}^{42}]^{2+}$
λ/nm	348	352
ε/mM^{-1} cm^{-1}	36.0	35.0
ϕ	0.18	0.18
k(MeOH)/ms^{-1}	0.83	0.77
k(MeOD)/ms^{-1}	-	1.01

Purification of the complex using HPLC, with formic acid as an additive in the solvent system, can result in the formation of a formate-adduct. Removal of the formate anion was attempted using ion exchange resin. The emission spectral form is comparable to that of [Eu.**L**^{40}]$^{+}$, allowing confident assignment of the complex as the chloride salt, [Eu.**L**^{42}]Cl_2, with no evidence supporting the presence of a formate-adduct (Figure 91).

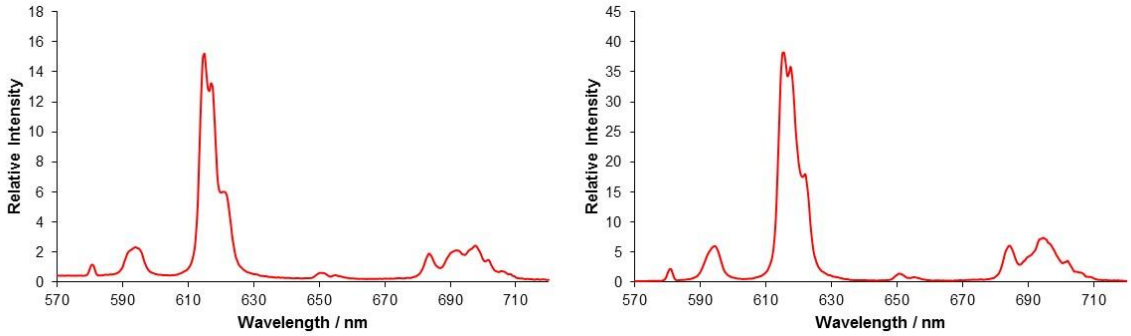

Figure 91 – Total emission spectra of europium (III) *N*-benzyl complex [Eu.**L**^{40}]$^{+}$ (*left*) and europium (III) complex containing a charged amino group [Eu.**L**^{42}]$^{2+}$ (*right*) showing comparable emission spectral form. (MeOH-H_2O 1:1, 'pH' 7.4, 295 K).

4.4.2. Investigation into the anion binding capability of [Eu.L^{42}]$^{2+}$

Previous work has demonstrated the utility of this class of heptadentate europium (III) complexes to bind to a number of different anions. A charged amino group (at physiological pH) was introduced into the ligand structure, in order to enhance the affinity of the complex for anions, *via* electrostatic interactions, and also to provide the opportunity for intermolecular H-bonding interactions.

It was surprising to note, that no well-defined changes in the total emission spectrum were observed on the sequential addition of bicarbonate (HCO_3^-), indicating that the anion is not binding to the lanthanide centre. However, significant changes in the emission spectrum of [Eu.**L**^{42}]$^{2+}$ were observed on the addition of *R*-lactate, Figure 92, characteristic of the changes observed for *N*-alkylated bis-carboxylate europium complexes, following addition of α-hydroxy acids. This behaviour allowed a stability constant, log*K* = 4.37, to be estimated using the methodology outlined in Chapter 3, by plotting the change in the intensity of the $\Delta J = 2$ *versus* $\Delta J = 1$ emission bands against added concentration of anion. The binding affinity for lactate and the di-cation [Eu.**L**^{42}]$^{2+}$, was an order of magnitude greater than for the *N*-benzyl complex [Eu.**L**^{40}]$^{+}$ (log*K* = 3.15), which can be attributed to the enhanced electrostatic attraction arising as a result of the greater positive charge of [Eu.**L**^{42}]$^{2+}$.

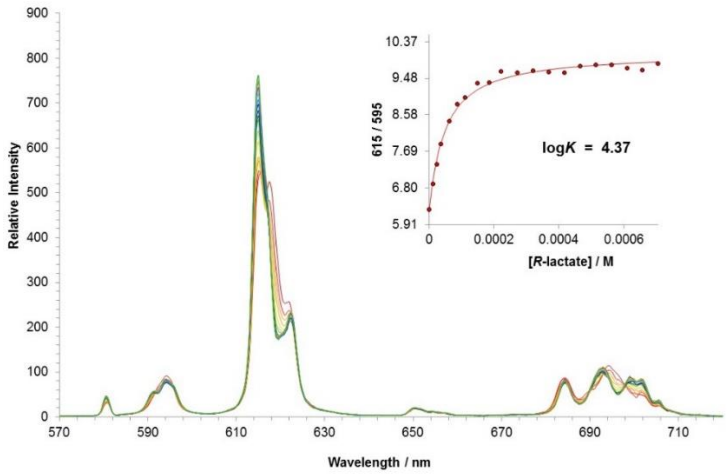

Figure 92 - Variation of the europium (III) emission profile of [Eu.**L**^{42}]$^{2+}$ as a function of added *R*-lactate. (5 µM, λ_{exc} = 352 nm, MeOH-H_2O 1:1, 10 mM HEPES, 'pH' 7.4). Inset shows the fit to experimental data, following iterative least squares fitting to a 1:1 binding model.

Previous work has shown that the addition of inorganic phosphate, HPO_4^{2-}, to the bis-carboxylate complex [Eu.**L**^{39}]$^{+}$, resulted in significant quenching of the europium luminescence and a large increase in ligand fluorescence, indicative of decomplexation. A similar study was carried out for the *N*-benzyl complex [Eu.**L**^{40}]$^{+}$, but no observable change in the emission spectrum was noted on addition of an increasing concentration of phosphate anion. Interestingly, the addition of phosphate to [Eu.**L**^{42}]$^{2+}$ resulted in a significant change in the emission spectrum, and broadening of the ΔJ = 1 manifold. This behaviour allowed an emission titration to be conducted, and an estimated binding affinity of log*K* = 4.20 was calculated (Figure 93).

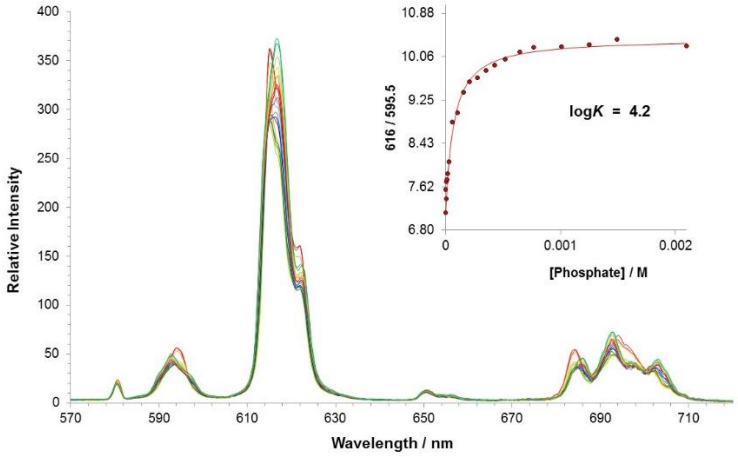

Figure 93 - Variation of the europium (III) emission profile of [Eu.**L**^{42}]$^{2+}$ as a function of added inorganic phosphate HPO_4^{2-}. (5 µM, λ_{exc} = 352 nm, MeOH-H_2O 1:1, 10 mM HEPES, 'pH' 7.4). Inset shows the fit to experimental data, following iterative least squares fitting to a 1:1 binding model.

The presence of the charged amino group on the benzyl ring acts to enhance the affinity of the europium (III) complex for phosphate anions. This may be as a result of the greater electrostatic interaction, and also the H-bonding nature of the amino group, which can direct the binding of the phosphate anion to the lanthanide centre. Hybrid-DFT calculations performed by Dr. Mark Fox on the Y (III) analogue at B3LYP/3-21G*, revealed the hydrogen bonding capability of the aminium ion (Figure 94). The hydrogen atom of the charged amino group is situated directly on the negatively charged oxygen atom of the phosphate anion, demonstrating that directed hydrogen bonding is occurring.

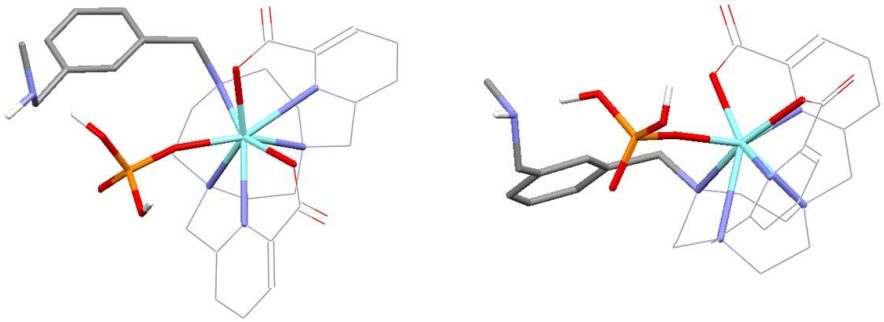

Figure 94 – Top and side views of the optimised geometry of [Y.$\mathbf{L}^{42}$.HPO_4], with the anisyl groups are omitted for clarity. A proton of the charged amino group is directed towards the negatively charged oxygen of the phosphate anion.

With this background in mind, we have begun to explore the utility of [Eu.$\mathbf{L}^{42}$]$^{2+}$ in the detection of a number of important chiral *O*-P-anions, exploiting CPL as the detection technique.

4.4.3. Studies using [Eu.L^{42}]$^{2+}$ and *O*-P-amino acids

The binding of [Eu.$\mathbf{L}^{42}$]$^{2+}$ and three phosphorylated amino acids (*O*-P-Ser, *O*-P-Thr and *O*-P-Tyr) was studied. Analysis of the emission and induced CPL spectra allowed an estimation of the relative binding affinities and the relative configuration of the adduct species.

4.4.3.1. Emission and induced CPL studies of [Eu.L^{42}]$^{2+}$ and *O*-P-amino acids

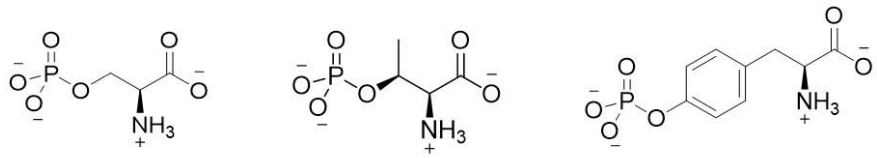

Figure 95 – Chemical structures of *O*-phosphono-amino acids at pH 7.4.

The emission spectral changes of [Eu.**L^{42}**]$^{2+}$ were investigated following the addition of *O*-P-Ser, *O*-P-Thr and *O*-P-Tyr, in a MeOH-H_2O solvent system (1:1, v/v), maintaining the apparent pH at 7.4 using HEPES buffer (10 mM). The form of the total emission spectrum of [Eu.**L^{42}**]$^{2+}$ was comparable to that following addition of inorganic phosphate (Figure 93). The changes were relatively subtle, except in the hypersensitive ΔJ = 4 transitions (Figure 96). Moreover, a broadening from one into three transitions in the ΔJ = 1 manifold was observed. In each case, it was possible to measure an estimated binding constant assuming a 1:1 stoichiometry in the ternary adduct. The stability constant for each *O*-P-amino acid was calculated to be log$K$ = 4.80 ± 0.04, revealing that there is no preference for a particular phosphorylated amino acid. This behaviour is in contrast to previous work based on a 12-N_4 europium (III) complex, where a preference for *O*-P-Tyr was observed in pure water, most likely as a result of the lower hydration energy of tyrosine.[121] However, the study involving [Eu.**L^{42}**]$^{2+}$ was carried out in a 1:1 MeOH-H_2O solvent system, to aid solubility. Selective solvation of the complex by a cluster of methanol molecules is likely to be occurring,[185] and so the effect of the differential anion hydration energy is diminished. It is worth noting that no change in the emission spectrum was observed in the presence of non-phosphorylated amino acids, allowing us to confidently hypothesise that the binding occurs through the phosphate group.

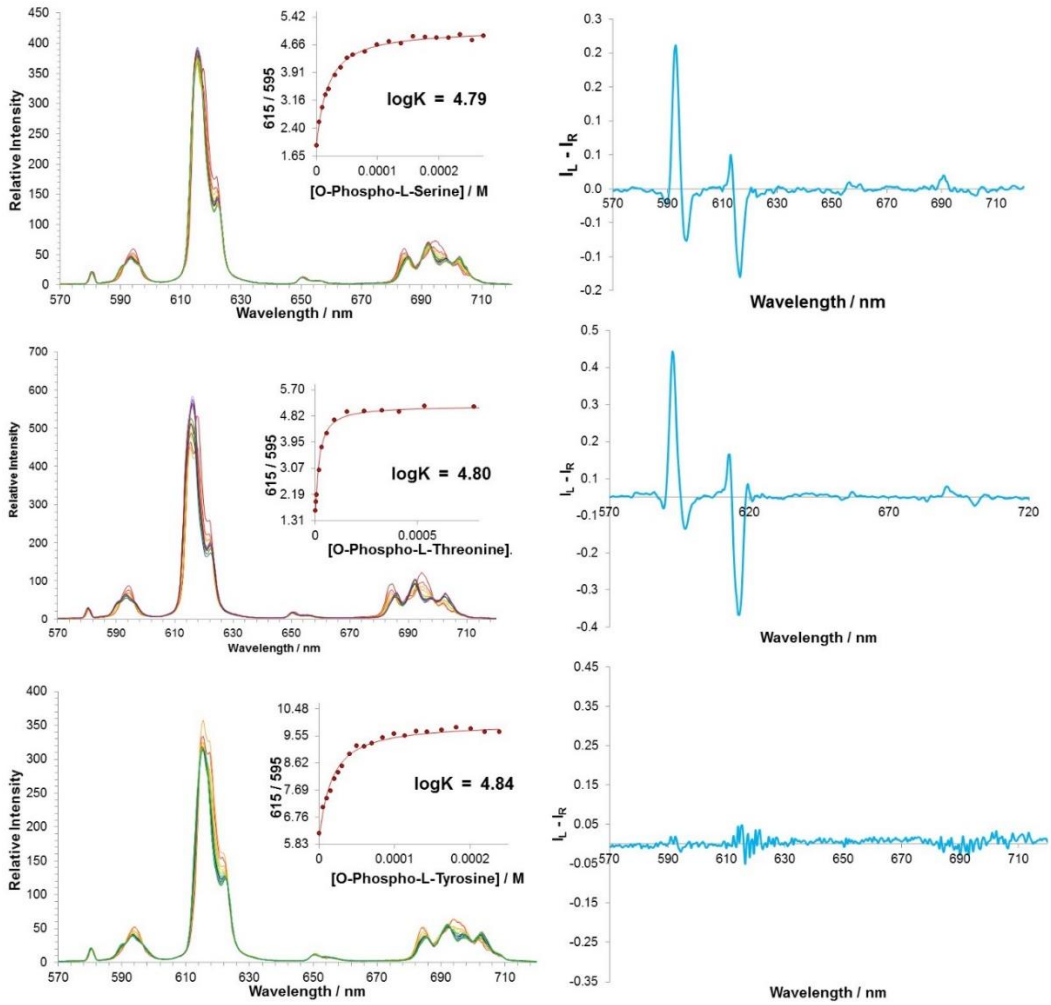

Figure 96 - Variation of the europium (III) emission profile (*left*) and CPL spectra (*right*) of [Eu.**L**^{42}]$^{2+}$ as a function of added anion; (*top*) *O*-phosphono-serine, (*middle*) *O*-phosphono-threonine, (*bottom*) *O*-phosphono-tyrosine (5 μM complex, λ_{exc} = 352 nm, MeOH-H_2O (1:1, v/v, 10 mM HEPES, 'pH' 7.4)). Insets show fits to experimental data, following iterative least-squares fitting to a 1:1 binding model.

The change in emission spectral form was accompanied by the induction of a strong CPL signal, in the case of *O*-P-Ser and *O*-P-Thr (Figure 96). The emission dissymmetry values for the ΔJ = 1 transition were bigger for *O*-P-Thr (g_{em} (592.5 nm) = +0.08 c.f. +0.04 for *O*-P-Ser), perhaps as a result of the additional methyl group providing a slightly higher degree of conformational rigidity at the metal centre. No induced CPL signal could be recorded for the [Eu.**L**^{42}.*O*-P-Tyr] adduct. From the emission studies, it is clear that the phosphorylated amino acid binds to the lanthanide centre in a similar manner to *O*-P-Ser and *O*-P-Thr. Therefore, an alternative explanation must be considered for the lack of induced chiroptical activity. The chiral centre is more remote in the *O*-P-Tyr molecule, and simply explains the lack of CPL activity observed from the resulting europium (III) complex.

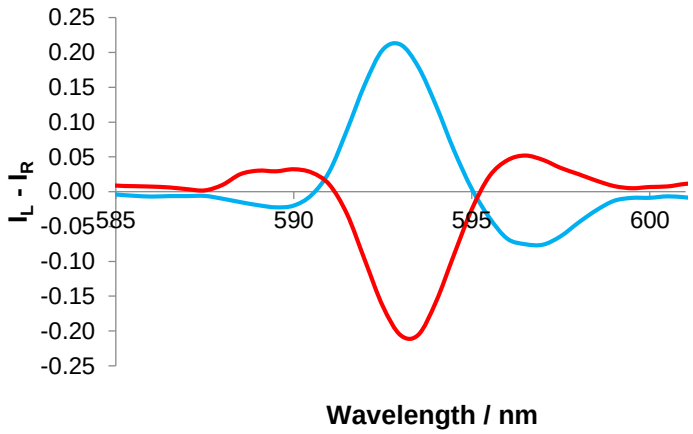

Figure 97 – ΔJ = 1 transition of the CPL spectrum of [Eu.**L**^{42}]$^{2+}$ following the addition of 50 µM *D*- (*red*) and *L*-*O*-P-Ser (*blue*), g_{em} (593 nm) = ±0.04. (5 µM, λ_{exc} = 352 nm, MeOH-H_2O 1:1, 10 mM HEPES, 'pH' 7.4).

Addition of *D*- and *L*-*O*-P-Ser resulted in induced CPL of equal and opposite form, with identical g_{em} values at 593 nm (Figure 97). Comparative analysis with the CPL spectrum of the control *N*-benzyl complex, [Eu.**L**^{40}]$^{+}$, on the addition of *R* and *S*-lactate, allowed a tentative assignment of configuration of the complex adduct, as *Δ*-[Eu.**L**^{42}.*O*-P-*L*-Ser] and *Λ*-[Eu.**L**^{42}.*O*-P-*D*-Ser].

4.4.4. Investigation of [Eu.L^{42}]$^{2+}$ and selected phosphorylated hexapeptides

Following the promising results regarding the binding of *O*-P-amino acids with [Eu.**L**^{42}]$^{2+}$ and the induction of 'signature' CPL, attention then turned to a related series of phosphorylated hexapeptides.

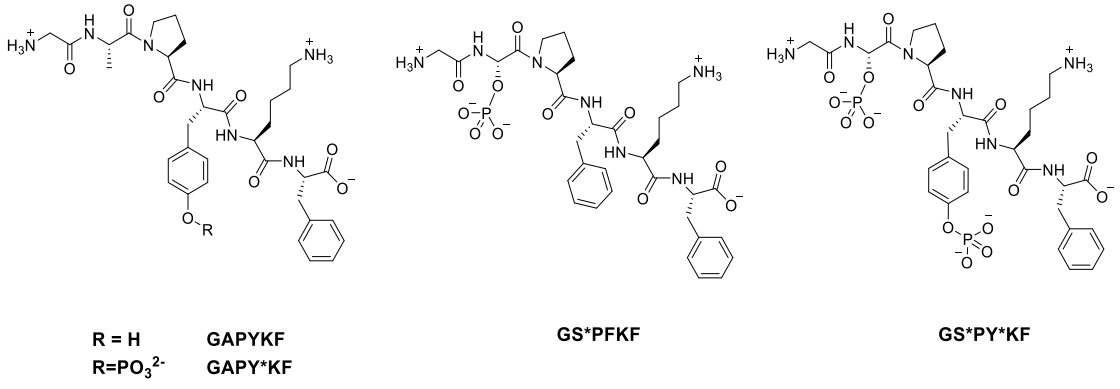

Figure 98 – Structure of the non-phosphorylated hexapeptide Gly-Ala-Pro-Tyr-Lys-Phe (GAPYKF) and the phosphorylated hexapeptides Gly-Ala-Pro-*O*-P-Tyr-Lys-Phe (GAPY*KF), Gly-*O*-P-Ser-Pro-Phe-Lys-Phe (GS*PFKF) and Gly-*O*-P-Ser-Pro-*O*-P-Tyr-Lys-Phe (GS*PY*KF).

4.4.4.1. Structural studies of phosphorylated peptides

Three phosphorylated peptides were selected for this study, varying in the phosphorylated residue (Ser or Tyr) and the number of phosphorylated sites (mono or di), Figure 98. The corresponding non-phosphorylated peptide, GAPYKF, was also studied as a control. In order to try and gain an insight into the solution state structures of the three phosphorylated peptides, electronic circular dichroism (ECD) and 2D ^{1}H NMR methods were employed. The hexapeptides each contain a proline residue, which can induce a turn in the structural backbone of the peptide, particularly if followed by an aromatic residue.[213] Weak ECD activity (around 200-230 nm) was observed for each of the three phosphorylated peptides (Figure 99). The hexapeptides GAPY*KF and GS*PY*KF exhibited ECD spectra that were very similar in form and consistent with the assignment of an open conformation peptide.[214] In the case of GS*PFKF, the ECD spectrum is slightly more well-defined with a positive and negative component at 220 and 200 nm respectively, indicating that perhaps, the mono-phosphorylated hexapeptide has a greater population of a more structured conformer in solution.

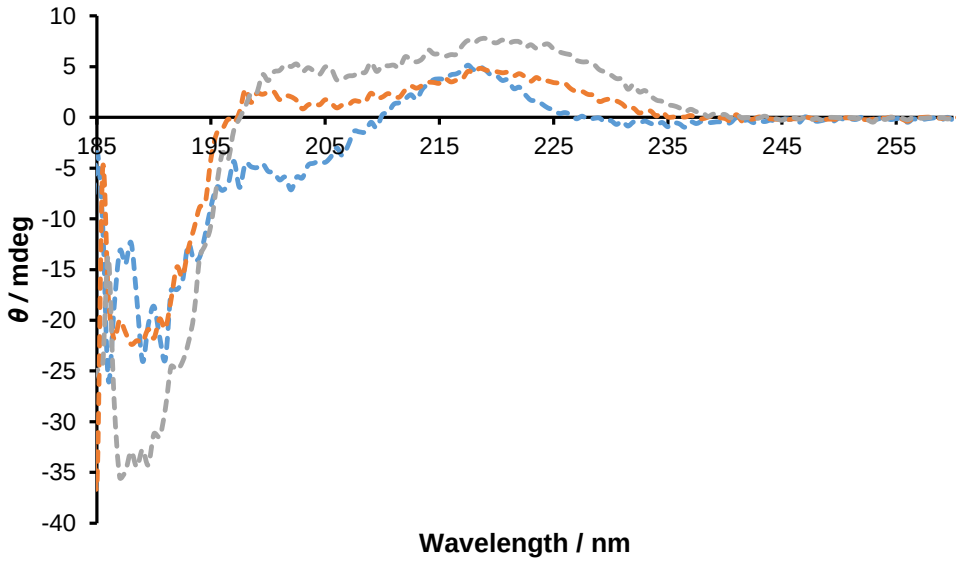

Figure 99 – Electronic circular dichroism spectra for GS*PFKF (*blue*), GS*PY*KF (*orange*) and GAPY*KF (*purple*) (298 K, H_2O, pH 7.4).

Further investigation of the solution state structure of GS*PFKF was analysed using 2D ^{1}H NMR methods with the help of Dr. Juan Aguilar Malavia. Overlaying the ROESY with the TOCSY spectra and the NOESY with the COSY spectra, allowed identification of pure through-space signals, by eliminating discrepancies arising from through-bond

interactions. Assignment of the resonances corresponding to the through-space interactions was achieved using HSQC, HMBC, PSYCHE and COSY methods. The peaks were identified as the aromatic and benzylic protons of a single phenylalanine residue, and are therefore not particularly informative in 3D structure determination. The lack of through-space interaction observed between separate amino acid residues, using the discussed methods, may be as a result of the distance between the two sections of the peptide. If the distance is too great then the interaction will not be observed using NMR methods. The rate at which the peptide conformation is exchanging may also be too fast, and therefore not observable on an NMR timescale.

4.4.4.2. Induced CPL studies

The induced CPL response of [Eu.**L**^{42}]$^{2+}$ was investigated, following addition of a 20-fold excess of each peptide (Figure 100). The addition of the non-phosphorylated control peptide, GAPYKF, resulted in no induced CPL (**D**), providing further evidence that the peptide binds to the europium (III) centre *via* the phosphate group. In the case of the *O*-P-Tyr peptide, GAPY*KF, the CPL spectral form (Figure 100, **A**) resembles that of the *O*-P-amino acids, *O*-P-Ser and *O*-P-Thr (Figure 96). However, it is interesting to recall that the simple *O*-P-Tyr amino acid did not induce a CPL response. In contrast, the *O*-P-Tyr peptide induced significant CPL, with a measured emission dissymmetry value of g_{em} (592.5 nm) = +0.10, which is amongst the highest induced g_{em} values observed from a dynamically racemic europium (III) complex.[15,150,151]

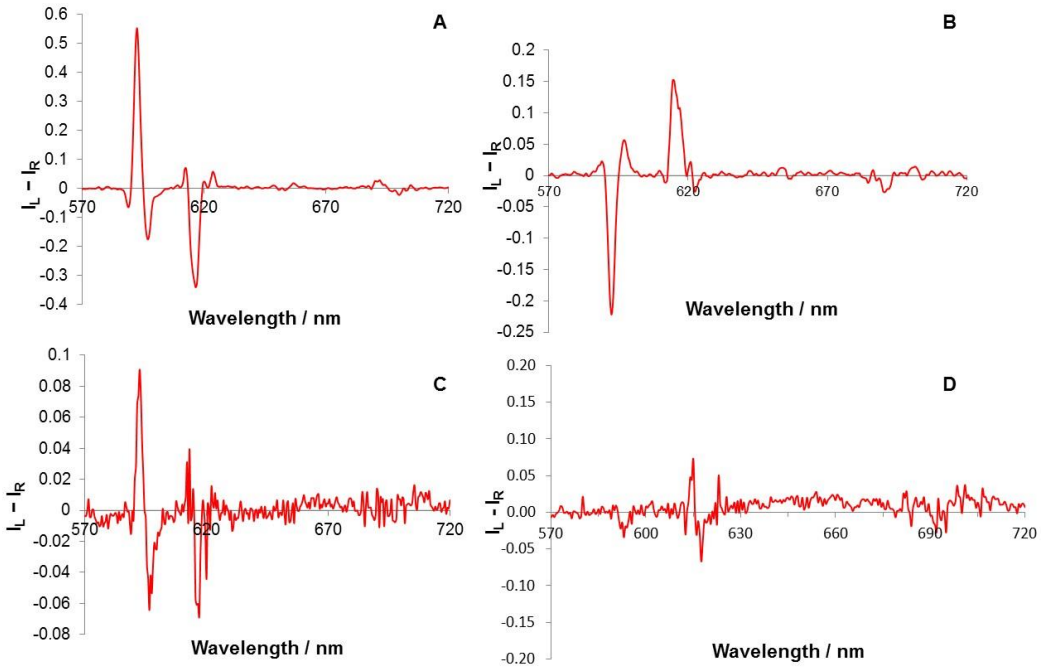

Figure 100 – Induced CPL spectra of [Eu.**L**^{42}]$^{2+}$ following the addition of 200 μM peptide: **A** – GAPY*KF; **B** – GS*PFKF; **C** – GS*PY*KF and **D** – non-phosphorylated GAPYKF. (10 μM , λ_{exc} = 352 nm, MeOH, 295 K).

Another interesting observation, was the induced CPL spectral response of the *O*-P-Ser peptide, GS*PFKF (Figure 100, **B**), which is opposite in sign and form to that of GAPY*KF. The g_{em} value at the same transition, λ = 592.5 nm, was -0.04 and therefore much smaller than the *O*-P-Tyr peptide. Such behaviour, suggests that it may be the chiral structure of the entire peptide, when bound to the lanthanide centre that is responsible for the induced CPL response.

A final point worth noting, is the behaviour of the di-phosphorylated peptide, which contains both a phosphorylated serine and tyrosine residue. The induced CPL is much weaker than for the other two peptides, and appears to be an additive combination of the two separate spectra (Figure 100, **C**). One possible explanation is that the complex has no preferential binding site, as demonstrated by the estimated affinity constants of the *O*-P-amino acids. Therefore, the most emissive species will be a combination of the lanthanide complex bound to the *O*-P-Ser of the peptide or the *O*-P-Tyr. The g_{em} values for the induced CPL were bigger for the *O*-P-Tyr residue, which may explain why the major chiral emissive species for the GS*PY*KF adduct of $[Eu.\mathbf{L^{42}}]^{2+}$, generated an induced CPL spectra that more closely resembled the *O*-P-Tyr hexapeptide.

4.4.4.3. Estimation of the stability constants, log*K*

Investigation of the binding affinities of the three hexapeptides with $[Eu.\mathbf{L^{42}}]^{2+}$ was carried out by monitoring the emission and induced emission dissymmetry values, g_{em}, as a function of peptide concentration.

As can be seen in Figure 101, the emission spectral changes of $[Eu.\mathbf{L^{42}}]^{2+}$ are very subtle, following addition of the phosphorylated peptide, GAPY*KF. It is much easier to monitor the generation of CPL from the system, particularly when the g_{em} values are as large as +0.10. The change in the intensity of the ΔJ = 2 and ΔJ = 1 transitions of the emission spectrum was plotted as a function of added concentration of the peptide, and the data was fitted to a 1:1 binding isotherm, following iterative least-squares fitting. The estimated binding affinity in methanol, log*K* = 5.9, was very large and consistent with the value obtained by plotting the induced g_{em} values against concentration of peptide, log*K* = 6.1. Such behaviour implies that the charged amino complex, $[Eu.\mathbf{L^{42}}]^{2+}$, has a strong binding affinity with GAPY*KF, and that the major chiral species in solution is the most emissive species. Once again, a slightly higher binding affinity was calculated from the CPL data suggesting it is associated with the formation of the favoured isomer (Δ), as was observed for the examples discussed in Section 3.5.2.

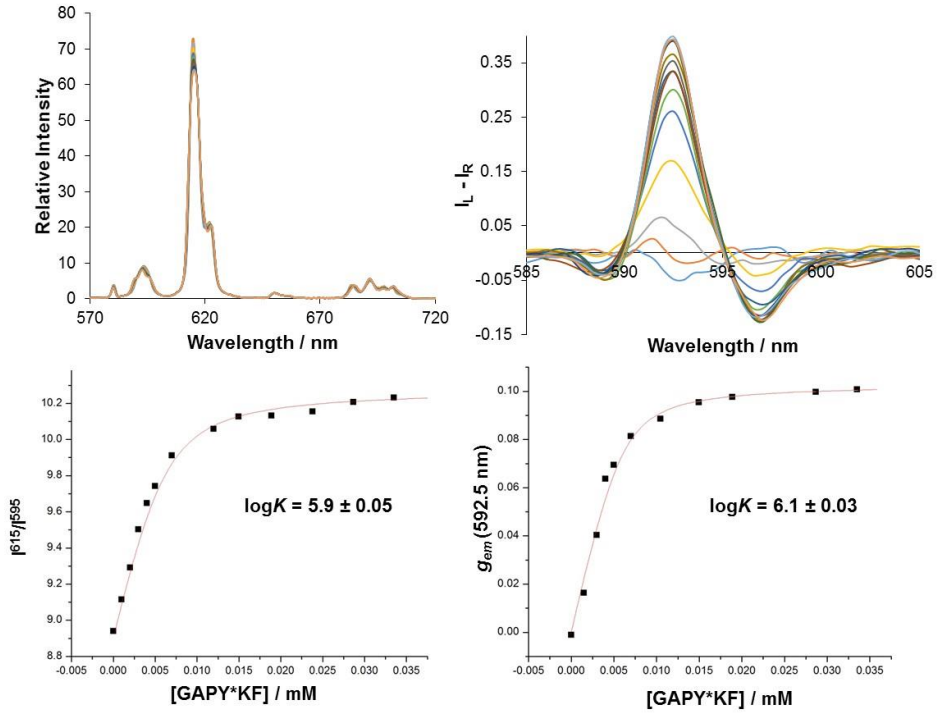

Figure 101 – *left*: variation in Eu (III) emission spectral profile of [Eu.$\mathbf{L^{42}}$]$^{2+}$ as a function of added peptide GAPY*KF (*top*) and fit to experimental data, following iterative least-squares fitting to a 1:1 binding model (*bottom*); *right*: variation in the ΔJ = 1 manifold of the CPL spectrum of [Eu.$\mathbf{L^{42}}$]$^{2+}$ as a function of added peptide GAPY*KF (*top*) and fit to experimental data, following iterative least-squares fitting to a 1:1 binding model (*bottom*). (10 µM complex, λ_{exc} = 352 nm, MeOH, 295 K).

A similar experiment was carried out for the peptide GS*PFKF, however the data did not fit to a 1:1 binding model, and so a stability constant could not be reliably estimated.

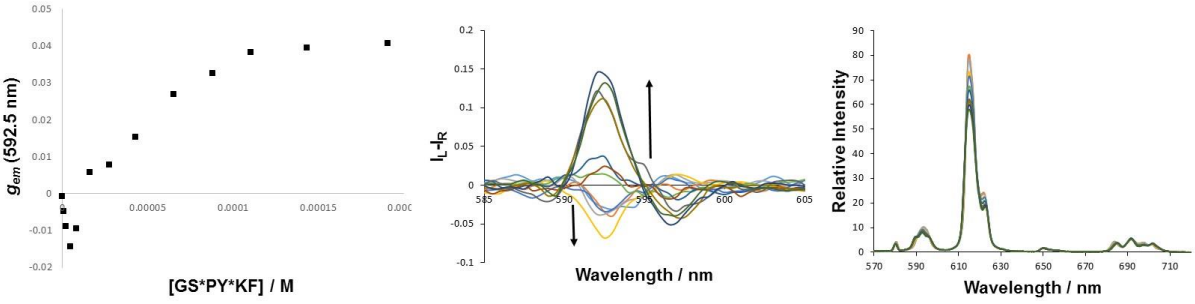

Figure 102 – (*left*) plot of the change in emission dissymmetry value, g_{em}, of [Eu.$\mathbf{L^{42}}$]$^{2+}$ at 592.5 nm *versus* the concentration of the di-phosphorylated peptide GS*PY*KF; (*middle*) change in the ΔJ = 1 transition of the CPL spectrum of [Eu.$\mathbf{L^{42}}$]$^{2+}$; (*right*) variation in the Eu (III) emission spectral profile of [Eu.$\mathbf{L^{42}}$]$^{2+}$ as a function of added peptide GS*PY*KF. (10 µM complex, λ_{exc} = 352 nm, MeOH, 295 K).

In the case of the di-phosphorylated peptide, GS*PY*KF, unusual behaviour was observed following the sequential addition of the peptide to the europium (III) complex. The induced CPL signal at 592.5 nm (ΔJ = 1) initially revealed increasingly negative values until a critical concentration was reached. At this concentration, the sign of the CPL was reversed and increasing positive values were recorded, until a limiting spectral response was achieved (Figure 102). Such behaviour provides further evidence that there is only a very small energy difference between the binding affinities of the two phosphorylated sites (*O*-P-Ser and *O*-P-Tyr). However, at higher concentration of added peptide, the most emissive chiral species that is observed has a positive g_{em} value at 592.5 nm, corresponding to binding at the *O*-P-Tyr residue.

4.4.4.4. Summary of the studies of $[Eu.L^{42}]^{2+}$ and *O*-P-peptides

This study has demonstrated that $[Eu.\mathbf{L}^{42}]^{2+}$ binds to phosphorylated peptides and a CPL response is induced. The investigation has shown that accurate determination of the stability constant can be achieved by monitoring the CPL spectral changes as an alternative to the europium (III) emission spectral change, particularly if the changes in the total emission response are small.

The sign of the g_{em} value in the ΔJ = 1 transition allows differentiation between *O*-P-Ser and *O*-P-Tyr residues. The magnitude of the induced emission dissymmetry value for the *O*-P-Tyr hexapeptide, GAPY*KF, was +0.10 and is amongst the highest values that have been recorded for a dynamically racemic europium (III) system.[15,150,151] The large g_{em} value allows quick and easy detection of this peptide in methanol, when employing CPL as the detection technique. Further work would look to enhance the scope of this complex in the detection and recognition of more complex and structurally diverse series of peptides incorporating phosphorylated tyrosine residues.

4.4.5. Demonstrating the utility of $[Eu.L^{42}]^{2+}$ as a chiral probe for oleoyl-lysophosphatidic acid

Oleoyl-*L*-α-lysophosphatidic acid (LPA) is a phospholipid present at a physiological concentration of <0.1-6.3 μM and at significantly increased levels (≤43 μM) in ovarian cancer cells.[215]

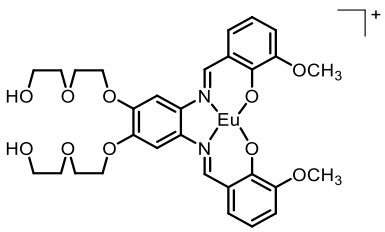

Figure 103 – Chemical structure of the europium (III) salophene complex.[204]

Some progress has been made in the development of lanthanide probes that are able to detect LPA in MeOH by monitoring an increase in the fluorescence intensity of the ligand.[204] In the study of a coordinatively unsaturated europium (III) salophene complex (Figure 103), an apparent selectivity of binding was demonstrated in methanol for a number of competitive analytes such as, proteins (BSA), phospholipids (phosphatidylserine, phosphatidylinositol, phosphatidylethanolamine) and carboxylates (phosphate and citrate). However, the selectivity over bicarbonate and lactate (anions present at the highest physiological concentration) was not discussed. Furthermore, the chemical origin for the particularly high affinity of the europium (III) complex for LPA is not apparent and was not investigated. The study monitored the fluorescence response of the europium (III) complex in methanolic extracts of human serum spiked with LPA. However, no information regarding the composition of the extract was given, making it difficult to determine the exact environment in which LPA was 'selectively' detected. A final point worth noting, is that this particular lanthanide probe relies on ligand-centred emission to detect the biomolecule. Ligand-centred emission is inherently less sensitive than lanthanide-based emission, rendering the structural study of the ternary complex very complex.

4.4.5.1. Binding mode of LPA

LPA has a lower pK_{a2} than phosphatidic acid (PA), the related phospholipid with a simple phosphate head group, illustrated by the calculated values in a phosphatidylcholine bilayer (PA: pK_{a1} 3.2 ± 0.3, pK_{a2} 7.92 ± 0.03; LPA: pK_{a1} 2.9 ± 0.3, pK_{a2} 7.47 ± 0.03).[216] Intramolecular hydrogen bonding is observed between the hydroxyl group on the glycerol backbone of the molecule and the phosphomonoester head group in the crystal structure, and is known to persist at physiological pH (Figure 104).[216,217] Therefore, ionisation of the phosphate hydroxyl group of LPA occurs more easily than for PA (and other

phosphate anions), generating a higher negative charge on the analyte, facilitating proposed binding to a positively charged probe, for example [Eu.**L**^{42}]$^{2+}$.

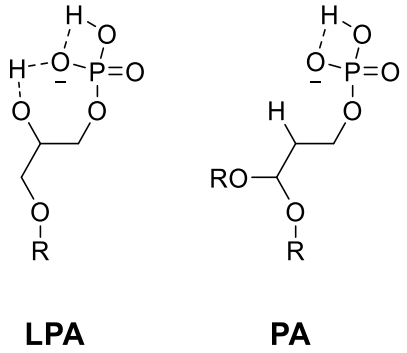

Figure 104 – Intramolecular hydrogen bonding of lysophosphatidic acid (LPA) and phosphatidic acid (PA), R = oleoyl acid chain.[204]

LPA binds to the lanthanide centre *via* the phosphate head group, in the same mode that was discussed for the phosphorylated amino acids and peptides in the preceding sections.

4.4.5.2. Emission and induced CPL studies of [Eu.L^{42}]$^{2+}$ and LPA

Direct binding to the lanthanide centre, as in the case with this probe, enables structural elucidation of the ternary adduct. As LPA is a chiral molecule, detection can be observed by the induction of circularly polarised luminescence.

The emission spectral form changes were particularly apparent in the $\Delta J = 1$ transition, which broadened from a single manifold, into three distinct transitions (Figure 105). This change resembles the emission spectral response of [Eu.**L**^{42}]$^{2+}$ following addition of the other phosphate anions that have been investigated in this study (HPO_4^{2-}, *O*-P-amino acids and *O*-P-peptides). Upon increasing the concentration of LPA, characteristic changes in the total emission spectrum were observed until a limiting spectrum was achieved. Beyond which, the total intensity continued to increase consistently across all transitions, with no further change to the emission spectral form. Such behaviour may be attributed to the long lipophilic chains in the molecule, which may be able to form aggregates, preventing the quenching from solvent molecules and significantly enhancing the europium emission intensity.

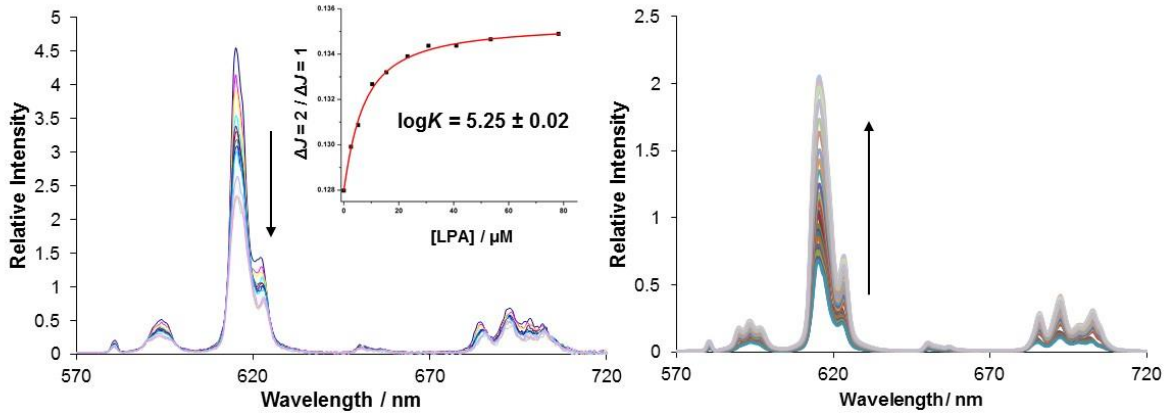

Figure 105 – Variation in the europium (III) emission spectral profile of [Eu.$\mathbf{L}^{42}$]$^{2+}$ as a function of added LPA (*left*). Inset shows the fit to experimental data, following iterative least-squares fitting to a 1:1 binding model, log$K$ = 5.25 ± 0.02. Variation in the emission spectral profile of [Eu.$\mathbf{L}^{42}$]$^{2+}$ following addition of 100-600 μM LPA, showing the large enhancement in total emission intensity (*right*). (5 μM complex, λ_{exc} = 352 nm, MeOH, 295 K).

The limit of detection of LPA is 5 μM and the limiting spectrum is achieved at a concentration of 40 μM, which is in the desired range for LPA detection in ovarian cancer cells. The estimated stability constant in methanol, log$K$ = 5.25, was high, demonstrating that there is indeed a strong binding affinity in the adduct, [Eu.$\mathbf{L}^{42}$.LPA].

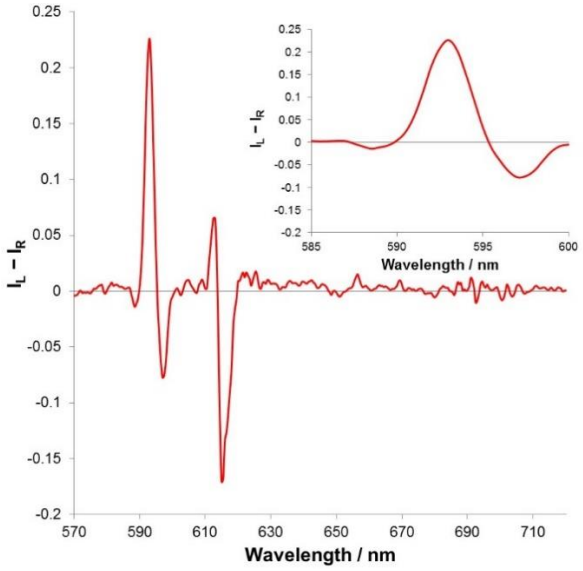

Figure 106 – Induced CPL spectrum of [Eu.$\mathbf{L}^{42}$]$^{2+}$ following addition of 50 μM LPA, inset shows the enlarged ΔJ = 1 transition (585 – 600 nm). (5 μM complex, λ_{exc} = 352 nm, MeOH, 295 K).

The induced CPL response resembled that of *O*-P-Ser, *O*-P-Thr and the related phosphorylated hexapeptides, with not much activity observed in the ΔJ = 3 and ΔJ = 4 region. An emission dissymmetry value, g_{em}, of +0.04 at 593 nm was measured. This

value is lower than that measured for the *O*-P-Tyr phosphorylated peptide, suggesting that there is a lower degree of conformational rigidity, consistent with the structure of LPA, which contains a long, aliphatic carbon chain.

Comparison of the CPL spectrum with the parent *N*-benzyl complex, [Eu.$\mathbf{L}^{40}$]$^{+}$, on addition of a number of chiral analytes, allowed a tentative assignment of the configuration of the complex adduct as *Δ*-[Eu.$\mathbf{L}^{42}$.*L*-LPA]. It is useful to recall that the *O*-P-*L*-amino acids also induced a similar CPL spectral response, resulting in the same *Δ*-assignment of helicity.

Following the promising results of the emission and CPL studies, further work set out to investigate the binding selectivity of the complex and LPA in a competitive environment. The nature of the 'signature' induced CPL response would provide further evidence for the determination of the species that was bound to the europium centre. No evidence of an interaction was observed for other phospholipid species including phosphatidyl-serine, -inositol and –ethanolamine. The addition of HSA (human serum albumin) resulted in no change in the emission spectral form, and significant quenching of the emission intensity was observed at a protein concentration >0.2 mM, with no induced CPL. As discussed in Section 4.4.2. the binding affinities of a number of physiologically relevant anions were estimated, including lactate, bicarbonate and phosphate (Table 22).

Table 22 – Affinity constants, log*K*, for analyte complexation and physiological concentrations of relevant biomolecules. (MeOH-H_2O 1:1, 10 mM HEPES, 295 K). (-) no evidence for a significant binding interaction was observed.

	Concentration in serum / mM	log*K*
HCO_3^-	24-27	-
lactate	0.6-2.3	4.37
HPO_4^{2-}	1.2-1.3	4.20
HSA	0.5-0.75	-
LPA	0-0.05	5.25[a]

[a] affinity constant estimated in 100% MeOH due to solubility of the biomolecule.

It is important to note that the affinity constant for LPA complexation was estimated in 100% MeOH and so is expected to be higher than the value measured in MeOH-H_2O (1:1, v/v), due to the lower solvation energy of the anion. However, with that in mind, analysis of the affinity constants revealed that selective binding of LPA may be possible in a

competitive environment. In aqueous methanolic solution (1:1, v/v. 'pH' 7.4), simulating an extracellular fluid containing HSA (0.4 mM), sodium lactate (2.3 mM), hydrogen phosphate (0.9 mM), citrate (0.13 mM) and sodium bicarbonate (30 mM), the observed emission spectrum of [Eu.$\mathbf{L^{42}}$]$^{2+}$ (5 μM) was the same as that observed for the complex alone. LPA was titrated into the solution in 5 μM aliquots until 100 μM was added. However, neither a change in the emission spectrum nor an induction of CPL was observed.

4.5. Conclusions and future work

The utility of dynamically racemic lanthanide probes in the sensing of important chiral biomolecules, employing CPL spectroscopy as the detection technique, is a research area of growing interest. The sensitivity and selectivity of this type of chirality probe has been demonstrated in a number of examples, as highlighted at the beginning of this chapter and in Chapter 1.

This aim of the work outlined in this section was to develop a new set of heptadentate, dynamically racemic lanthanide complexes, incorporating functionality on the *N*-alkyl substituent that could be used to target and detect a number of chiral biomolecules, such as: sialic acid, *O*-P-amino acids and peptides and LPA. The design of the dynamically racemic europium (III) complexes was based on the results outlined in Chapters 2 and 3 following a detailed and systematic study into the structural and photophysical properties of related systems. The most attractive properties were highlighted and incorporated into the ligand framework in the novel set of europium (III) chirality probes, [Eu.$\mathbf{L^{39\text{-}42}}$].

The detection of sialic acid by the bis-carboxylate complex, [Eu.$\mathbf{L^{39}}$]$^{+}$, and the boronic acid complex [Eu.$\mathbf{L^{41}}$]$^{+}$ was demonstrated *via* the induction of a 'fingerprint' CPL response and changes in the total emission spectrum. This result demonstrates the first example of the use of CPL spectroscopy in conjunction with a lanthanide chirality probe to detect sialic acid. Further work investigated the sign and form of the CPL spectra to elucidate key structural information regarding the ternary adduct, by comparison with the methyl-ester derivative of sialic acid. A proposed binding mechanism was hypothesised, highlighting the nature of the secondary binding interaction provided by the boronic acid moiety.

A europium (III) complex incorporating a charged amino group on the *N*-benzyl substituent, [Eu.$\mathbf{L^{42}}$]$^{2+}$, has been shown to target chiral phosphate anions, as a result of

the enhanced electrostatic interaction and directed hydrogen-bonding. The utility of this probe in the detection of *O*-P-amino acids, *O*-P-peptides and oleoyl-*L*-α-lysophosphatidic acid has been demonstrated. The induced CPL signal differs significantly from the spectrum obtained in the presence of other simple chiral carboxylic acids and α-hydroxy acids. Importantly, the studies have shown that phosphorylated tyrosine residues can be differentiated from phosphorylated serine residues in a set of hexapeptides. Emission dissymmetry values as high as +0.10 were observed for [Eu.$\mathbf{L}^{\mathbf{42}}$]$^{2+}$ and the *O*-P-Tyr peptide (GAPY*KF), allowing easy, accurate and quick measurement of the CPL spectrum for this system.

The detection of LPA using [Eu.$\mathbf{L}^{\mathbf{42}}$]$^{2+}$as a lanthanide probe has also been demonstrated, within the range 5-40 μM. This result is the first example of induced CPL from an LPA adduct. The total emission and circularly polarised luminescence of the probe was monitored as a function of added lysophosphatidic acid. Due to the bright, strongly emissive nature of the lanthanide complex, detection of LPA was readily achieved. Analysis of the europium emission and CPL spectra revealed information about the structure of the ternary adduct, improving upon previous examples of lanthanide LPA probes.[204] The absolute configuration of the [Eu.$\mathbf{L}^{\mathbf{42}}$.*L*-LPA] adduct was tentatively assigned as *Δ*, which is consistent with the helicity assigned for the *O*-P-*L*-amino acids. The selective detection of LPA in simulated extracellular fluid was investigated, however, no evidence for the binding of any anion to the lanthanide centre was observed, most likely due to low solubility of the complex in water.

The results that have been discussed in this chapter are particularly encouraging and show promise in the ability of this class of heptadentate europium (III) complexes to act as effective chirality probes. The complexes are very bright, allowing enhanced signal to noise spectra to be obtained within a short acquisition time (3 scans, 20 min), using a very low (5-10 μM) concentration of the probe. Structural variation of the *N*-alkyl substituent allows the probe design to be tuned to target a specific chiral anion selectively. The complexes are dynamically racemic and fast interconversion between the isomers occurs on the emission timescale. The addition of a chiral analyte preferentially stabilises a particular stereoisomer, revealing an induced 'signature' CPL spectrum that is dependent on the nature of the analyte and the binding mode in the ternary adduct.

With all this in mind, there is a particularly important factor that has not yet been addressed. The poor water solubility of these complexes has limited their use to anion detection in methanol or mixed methanol-water systems. The incorporation of negatively

charged sulfonic acid derivatives into the *para* position of the aryl ring of the chromophore, has been shown to significantly enhance the water solubility of related tri-phosphinate 9-N_3 europium (III) complexes.[183] To improve on the results demonstrated in this chapter, the inclusion of such water-solubilising moieties should allow the investigation of the detection capabilities of the related complexes in a purely aqueous environment (Figure 107).

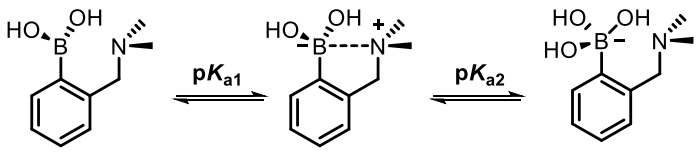

Scheme 24 – The pH dependent equilibria of a phenylboronic acid group containing an aminomethyl group in the *ortho*-position.[194]

It may also be possible to increase the binding affinity, and thus selectivity, of [Eu.**L**^{41}]$^{+}$ for sialic acid through the inclusion of an aminomethyl group in the *ortho*-position of the benzyl substituent (Figure 107). Wulff has shown that conversion of the trigonal boronic acid to the tetrahedral boronate occurs at a lower pH value in the presence of this additional amino group, where the stability of the resulting ester is an order of magnitude greater.[218] The presence of the tetragonal species over a greater pH range can be attributed to the B-N interaction in the phenylboronate and may aid the selective recognition of sialic acid at physiological pH levels (Scheme 24).[219]

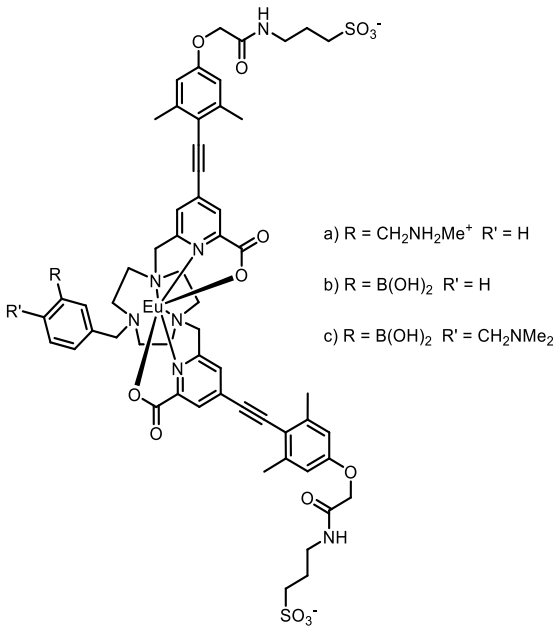

Figure 107 – Structure of next generation europium (III) complexes containing water-solubilising negatively charged sulfonic acid derivatives.

CHAPTER FIVE

EXPERIMENTAL DETAILS

5.1. General experimental

5.1.1. Materials

All reagents were purchased and used as received. Analytical solvents were purchased from Fisher Scientific and were laboratory grade. Anhydrous solvents were freshly distilled over the appropriate drying agent and stored under argon in a septum capped bottle. Water was purified by the 'Purite$_{STILL}$plus' system, with conductivity of ≤ 0.04 μS cm^{-1}. Air sensitive reactions were carried out under an atmosphere of argon using Schlenk-line techniques.

5.1.2. Analytical methods

Thin layer chromatography was carried out on neutral aluminium silica plates (Merck 5554) or neutral aluminium oxide plates (Merck 5550) and visualised under UV irradiation (254/365 nm). Preparative column chromatography was performed using silica gel (Merck Silica Gel 60, 230-400 mesh) or neutral aluminium oxide (Merck 90, 70-320 mesh).

^{1}H, ^{13}C and ^{11}B NMR spectra were recorded on a Varian Mercury-200 (^{1}H 199.975 and ^{13}C 50.289), Varian Mercury-400 (^{1}H 399.945 and ^{13}C 100.566), Bruker Avance-400 (^{1}H 400.052, ^{11}B 128.377 and ^{13}C 100.603), Varian Inova-500 (^{1}H 499.722 and ^{13}C 125.671), Appleby VNMRS-600 (^{1}H 599.832 and ^{13}C 150.828), or Varian VNMRA-700 (^{1}H 699.731 and ^{13}C 175.948) spectrometer. Spectra were recorded in commercially available deuterated solvents. ^{13}C and ^{1}H chemical shift values are quoted in ppm relative to trimethylsilane and all coupling constants are given in Hz. Assignment of the spectra was achieved using COSY, HSQC and HMBC experiments. The operating temperature of the spectrometers (usually 295 K) was measured with the aid of an internal calibration solution of ethylene glycol. The operating temperature of each spectrometer was measured before each set of measurements of relaxation data, using the calibration sample.

Proton NMR longitudinal relaxation data were measured in dilute MeOD solutions at 295 K using the inversion-recovery technique, on spectrometers operating at fields of 4.7, 9.4, 11.7, 14.1 and 16.4 T. The recorded free induction decays were processed using backward linear prediction, optimal exponential weighting, zero-filling, Fourier transform, phasing and baseline correction (by polynomial fitting). The signals were integrated by Lorentzian line fitting.

Relaxation data was fitted with the help of Dr Alexander Funk at Durham University, using a modified algorithm originally provided by Dr Ilya Kuprov at Oxford University. The algorithm uses the Solomon-Morgan-Bloembergen equations to fit the measured relaxation data using the Matlab internal Levenberg-Marquardt minimisation of the non-linear squares error function and the results were analysed iteratively.

Electrospray mass spectra were obtained on a TQD mass spectrometer equipped with an Acquity UPLC, an electrospray ion source and an Acquity photodiode array detector (Waters Ltd, UK). Methanol or acetonitrile were used as the carrier solvent. For LC-MS analyses a 2.1 x 100 mm 1.7 micron Acquity UPLC BEH C18 column was used. LC-MS analyses were performed on a Waters system comprising a 3100 Mass Detector and a 2998 Photodiode array detector.

Accurate masses were recorded on a LCT Premier XE mass spectrometer or a QTOF Premier mass spectrometer both equipped with an Acquity UPLC, a lock-mass electrospray ion source and an Acquity photodiode array detector (Waters Ltd, UK). Methanol or acetonitrile was used as the carrier solvent.

GC-MS data (polar and non-polar mode) was obtained using a Shimadzu QP2010-Ultra instrument operating at 70 eV equipped with an Rxi-5Sil MS column (0.15 µm x 10 m x 0.15 mm) and helium was used as the carrier gas.

Melting points were recorded using Gallenkamp (Sanyo) apparatus and are uncorrected.

Elemental analyses were recorded on an Exeter CE-440 elemental analyser.

5.1.3. HPLC analysis

Reverse-phase preparative HPLC was performed at 295 K using a Shimadzu system consisting of a Degassing Unit (DGU-20A5R), a Prominence Preparative Liquid Chromatograph (LC-20AP), a Prominence UV/Vis Detector (SPD-20A) and a Communications Bus Module (CBM-20A). An XBridge C18 OBD 19 x 100 mm, i.d. 5 µM column was used with a flow rate of 2 mL/min (analytical) or 17 mL/min (prep). The solvent system was H_2O +0.1% formic acid / MeOH +0.1% formic acid (gradient elution, Table 23 -Table 25).

Table 23 – HPLC conditions used for the purification of [Ln.**L**[30, 31a-d]].

Step	Time / min	Flow (analytical/ prep) / mL min^{-1}	H_2O (0.1% FA)	MeOH (0.1% FA)
0	0.0	2.0 / 17.0	90	10
1	3.0	2.0 / 17.0	90	10
2	13.0	2.0 / 17.0	0	100
3	18.0	2.0 / 17.0	0	100
4	19.0	2.0 / 17.0	90	10

Table 24 – HPLC conditions used for the purification of mono-BOC **L**[38].

Step	Time / min	Flow (analytical/ prep) / mL min^{-1}	H_2O (0.1% FA)	MeOH (0.1% FA)
0	0.0	2.0 / 17.0	70	30
1	3.0	2.0 / 17.0	70	30
2	18.0	2.0 / 17.0	0	100
3	21.0	2.0 / 17.0	0	100
4	22.0	2.0 / 17.0	90	10

Table 25 – HPLC conditions used for the purification of pre-**L**[42].

Step	Time / min	Flow (analytical/ prep) / mL min^{-1}	H_2O (0.1% FA)	MeOH (0.1% FA)
0	0.0	2.0 / 17.0	90	10
1	3.0	2.0 / 17.0	90	10
2	18.0	2.0 / 17.0	0	100
3	21.0	2.0 / 17.0	0	100
4	22.0	2.0 / 17.0	90	10

5.1.4. Optical techniques

All samples for optical analyses were contained in quartz cuvettes with a path length of 1 cm and a polished base. Measurements were recorded at 295 K.

UV/Vis absorbance spectra were recorded on an ATI Unicam UV/Vis spectrometer (Model UV2) using Vision version 3.33 software. Samples were measured relative to a reference of pure solvent contained in a matched cell. Emission spectra were recorded on an ISA Joblin-Yvon Spex Fluorolog-3 luminescence spectrometer using DataMax v2.2.10 software.

Lifetime measurements were carried out on a Perkin Elmer LS55 spectrometer using FL Winlab software version 4.00.02. The Ln (III) ion was directly excited *via* the chromophore using a short pulse of light at $\lambda_{exc,}$ followed by monitoring the integrated intensity of the light emitted at a chose wavelength (612-620 nm for Eu), during a fixed gate time, t_g, after a delay time, t_d. Measurements were made for a minimum of 20 delay times, covering more than 3 lifetimes. A gate time of 0.1 ms was used and the excitation and emission slits were set to 10 nm. The observed decay curves were plotted in Microsoft Excel using equation **5.1**.

$$I = A_0 + A_1 e^{-kt} \qquad \textbf{(5.1.)}$$

The excited state lifetime, τ, is the inverse of the radiative decay rate constant, k.

Apparent binding constants were calculated by fitting equation **5.2** to emission or CPL data, using a non-linear least squares fitting algorithm in Microsoft Excel 2010, with the solver add-in.

$$[X] = \frac{\frac{(F-F_0)}{K(F_1-F_0)} + [Eu] * \frac{(F-F_0)}{(F_1-F_0)} - [Eu] * \left(\frac{(F-F_0)}{(F_1-F_0)}\right)^2}{1 - \frac{(F-F_0)}{(F_1-F_0)}}$$

$$Eu + X \leftrightarrow EuX \qquad K = \frac{[EuX]}{[X_f][Eu_f]} \qquad \textbf{(5.2)}$$

[X]: Total concentration of selected analyte in solution

[Eu]: Total concentration of the complex

K: Binding constant

F: Either intensity ratio of selected emission transitions or g_{em} values

F_0: Initial ratio

F_1: Final ratio

[EuX]: The concentration of the analyte-coordination complex

$[X_f]$: The concentration of free analyte

$[Eu_f]$: The concentration of free complex

CPL spectra were recorded on a custom built spectrometer consisting of a laser driven light source (Energetiq EQ-99 LDLS, spectral range 170 to 2100 nm) coupled to an Acton SP2150 monochromator (600 g/nm, 300 nm Blaze) that allows excitation wavelengths to be selected with a 6 nm FWHM band-pass. The collection of the emitted light was facilitated (90 º angle set up, 1 cm path length quartz cuvette) by a Lock-In Amplifier (Hinds Instruments Signaloc 2100) and Photoelastic Modulator (Hinds Series II/FS2AA). The differentiated light was focused onto an Acton SP2150 monochromator (1200 g/nm, 500 nm Blaze) equipped with a high sensitivity cooled Photo Multiplier Tube (Hamamatsu 7155-01 red corrected). The detection of the CPL signal was achieved using the field modulation lock-in technique. The electronic signal from the PMT was fed into the lock-in amplifier (Hinds Instruments Signaloc 2100). The reference signal for the lock-in detection was provided by the PEM control unit. The monochromators, PEM control unit and lock-in amplifier were interfaced with a desktop PC and controlled by Labview code.

A correction factor for the wavelength dependence of the detection system was constructed using a calibrated lamp (Ocean Optics). The measured raw data was subsequently corrected using this correction factor. The validation of the CPL detection systems was achieved using light emitting diodes (LEDs) at various emission wavelengths. The LED was mounted in the sample holder and the light from the LED was fed through a broad band polarising filter and ¼ wave plate (Ocean Optics) to generate circularly polarised light. Prior to all measurements, this technique was used to set the phase of the lock-in amplifier correctly.

Spectra were recorded using a 5 spectral average sequence in the range of 570-720 nm with 0.5 nm spectral intervals and 500 μs integration time. The recorded CPL spectrum

underwent a Savitzky-Golay smoothening protocol using Origin 8.0 Software (Origin Labs) to enhance appearance (all calculations were carried out using raw spectral data).

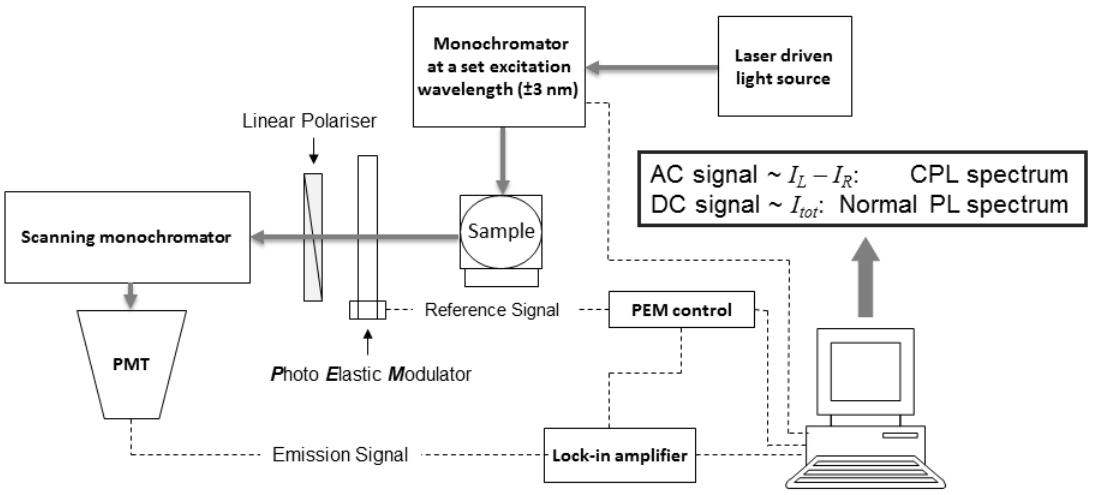

Figure 108 - schematic diagram of Durham CPL instrumentation.

ECD spectra of the *O*-phosphono-peptides studied were measured on a JASCO J-810 CD Spectropolarimeter using Jasco's Spectra Manager^{TM} software. The band width was set to 1.0 nm, response to 2 sec and scan speed to 50 nm/min.

5.1.5. DFT computations

The model geometries [Y.**L**$^{37\text{-}40,42}$] and adducts in this thesis were fully optimised without symmetry constraints using the hybrid-DFT B3LYP functional[i] and 3-21G* basis set[ii] for all atoms with the Gaussian 09 package.[iii] Frequency calculations confirmed the geometries to be true minima. The methyl substituents in the anisyl groups in [Eu.**L**^{39}], [Eu.**L**^{40}] and [Eu.**L**^{42}] complexes were omitted in the model geometries [Y.**L**^{39}], [Y.**L**^{40}] and [Y.**L**^{41}] to reduce computational effort. Geometry optimisations were also carried out using B3LYP and PBE0 functionals,[i,iv] the SVP basis set[v] and the pseudopotentials, SDD and LANL2DZ,[vi] for comparison with B3LYP/3-21G* and reported X-ray geometries (Tables S1-S3). In all computations, the polarised continuum solvent model (PCM)[vii] with the dielectric constant of water was applied. B3LYP/3-21G* is shown to be an appropriate functional/basis set for Y (III) complexes and therefore suitable models for Eu (III) complexes. The paramagnetic Eu (III) complexes are very difficult to model computationally. Figures of the optimised geometries were generated using Mercury software.[viii]

The benzyl group is assumed to be orientated like the pyridyl-methyl groups with respect to the triazacyclononane ligand in each [Y.**L**^{40,42}] complex. For optimised geometries of *R*-lactate coordinated [Y.**L**$^{37\text{-}40}$] complexes, intramolecular hydrogen bonds involving the lactate OH group are assumed to be absent as the lactate OH group is likely to be involved in hydrogen bonding with the surrounding solvent molecules. All binding energies were obtained by differences in total energies between metal bound adducts and the corresponding non-metal bound adducts.

(i) (a) A. D. Becke, *J. Chem. Phys.*, 1993, **98**, 5648-5652; (b) C. Lee, W. Yang and R. G. Parr, *Phys. Rev. B*, 1988, **37**, 785-789.

(ii) (a) J. S. Binkley, J. A. Pople and W. J. Hehre, *J. Am. Chem. Soc.*, 1980, **102**, 939-947; (b) M. S. Gordon, J. S. Binkley, J. A. Pople, W. J. Pietro and W. J. Hehre, *J. Am. Chem. Soc.*, 1982, **104**, 2797-2803; (c) W. J. Pietro, M. M. Francl, W. J. Hehre, D. J. Defrees, J. A. Pople and J. S. Binkley, *J. Am. Chem. Soc.*, 1982, **104**, 5039-5048; (d) K. D. Dobbs and W. J. Hehre, *J. Comp. Chem.*, 1986, **7**, 359-378; (e) K. D. Dobbs and W. J. Hehre, *J. Comp. Chem.*, 1987, **8**, 861-879; (f) K. D. Dobbs and W. J. Hehre, *J. Comp. Chem.*, 1987, **8**, 880-893.

(iii) Gaussian 09, Revision A.02, M. J. Frisch, G. W. Trucks, H. B. Schlegel, G. E. Scuseria, M. A. Robb, J. R. Cheeseman, G. Scalmani, V. Barone, B. Mennucci, G. A. Petersson, H. Nakatsuji, M. Caricato, X. Li, H. P. Hratchian, A. F. Izmaylov, J. Bloino, G. Zheng, J. L. Sonnenberg, M. Hada, M. Ehara, K. Toyota, R. Fukuda, J. Hasegawa, M. Ishida, T. Nakajima, Y. Honda, O. Kitao, H. Nakai, T. Vreven, Jr., J. A. Montgomery, J. E. Peralta, F. Ogliaro, M. Bearpark, J. J. Heyd, E. Brothers, K. N. Kudin, V. N. Staroverov, R. Kobayashi, J. Normand, K. Raghavachari, A. Rendell, J. C. Burant, S. S. Iyengar, J. Tomasi, M. Cossi, N. Rega, J. M. Millam, M. Klene, J. E. Knox, J. B. Cross, V. Bakken, C. Adamo, J. Jaramillo, R. Gomperts, R. E. Stratmann, O. Yazyev, A. J. Austin, R. Cammi, C. Pomelli, J. W. Ochterski, R. L. Martin, K. Morokuma, V. G. Zakrzewski, G. A. Voth, P. Salvador, J. J. Dannenberg, S. Dapprich, A. D. Daniels, O. Farkas, J. B. Foresman, J. V. Ortiz, J. Cioslowski and D. J. Fox, *Gaussian, Inc.*, Wallingford CT, **2009**.

(iv) C. Adamo and V. Barone, *J. Chem. Phys.* 1999, **110**, 6158-6169.

(v) (a) A. Schaefer, H. Horn and R. Ahlrichs, *J. Chem. Phys.*1992, **97**, 2571-2577; (b) A. Schaefer, C. Huber and R. Ahlrichs, *J. Chem. Phys.* 1994, **100**, 5829-5835.

(vi) T. H. Dunning Jr. and P. J. Hay, in *Modern Theoretical Chemistry*, Ed. H. F. Schaefer III, Vol. 3 (Plenum, New York, 1977) 1-28.

(vii) J. Tomasi, B. Mennucci and R. Cammi, *Chem. Rev.* 2005, **105**, 2999-3093.

(viii) C. F. Macrae, I. J. Bruno, J. A. Chisholm, P. R. Edgington, P. McCabe, E. Pidcock, L. Rodriguez-Monge, R. Taylor, J. van de Streek and P. A. Wood, *J. Appl. Cryst.* 2008, **41**, 466–470.

5.2. Synthetic Procedures

5.2.1. $[Ln.L^{30}]^{3+}$ and precursors

(*S*)-6-Methyl-*N*-(1-phenylethyl)picolinamide, *S*-1a

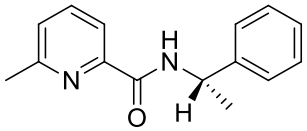

6-Methylpyridine-2-carboxylic acid (1.00 g, 7.29 mmol), HOBt.H_2O (1.48 g, 10.9 mmol), EDC (1.70 g, 10.9 mmol) and DIPEA (3.17 mL, 18.2 mmol) were dissolved in anhydrous DMF (20 mL). (*S*)-(-)-α-Methylbenzyl amine (0.93 mL, 7.29 mmol) was added dropwise to the solution and the mixture was stirred at r.t. for 22 h under an argon atmosphere. Water was added (25 mL) and the mixture extracted with EtOAc (3 x 10 mL). The organic layers were combined and washed successively with water (1 x 10 mL) and brine (1 x 10 mL), dried over $MgSO_4$ and the solvent removed under reduced pressure. The crude mixture was purified by flash column chromatography (silica, gradient elution starting from 30% EtOAc in hexane to 60% EtOAc in hexane) to afford compound ***S*-1a** as a yellow oil (1.32 g, 75%). TLC analysis R_f 0.24 (silica, 30% EtOAc in hexane); ^{1}H NMR (295 K, 400 MHz, $CDCl_3$) δ_H 8.38 (1H, d, ^3J 7.5, CONH), 7.94 (1H, d, ^3J 7.5, py-H^3), 7.64 (1H, t, ^3J 7.5, py-H^4), 7.41 (2H, d, ^3J 7.5, Ph-H^o), 7.35 (2H, t, ^3J 7.5, Ph-H^m), 7.27-7.25 (2H, m, Ph-H^p, py-H^5) 5.26 (1H, dq, ^3J 7, ^3J 7.5 CHCH$_3$), 2.49 (3H, s, py-CH_3), 1.56 (3H, d, ^3J 7, CHCH_3); ^{13}C NMR (295 K, 100 MHz, $CDCl_3$) δ_C 163.4 (CONH), 157.0 (py-C^6), 149.1 (py-C^2), 143.3 (Ph-C^i), 137.4 (py-C^4), 128.5 (Ph-C^m), 127.2 (Ph-C^p), 126.2 (Ph-C^o), 125.8 (py-C^5), 119.3 (py-C^3), 48.6 (CHCH$_3$), 24.1 (py-CH_3), 21.9 (CHCH_3); *m/z* (HRMS$^+$) 241.1334 $[M+H]^+$ ($C_{15}H_{17}ON_2$ requires 241.1335).

(*S*)-6-Methyl-2-((1-phenylethyl)carbamoyl)pyridine 1-oxide, *S*-1b

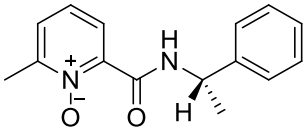

m-CPBA (1.89 g, 10.9 mmol) was added to a stirred solution of amide ***S*-1a** (1.32 g, 5.49 mmol) in anhydrous $CHCl_3$ (16 mL). The resulting solution was stirred at r.t. for 18 h under an argon atmosphere. The solution was washed with $NaHCO_3$ (aq.) (0.5 M, 25 mL)

and extracted with CH_2Cl_2 (3 x 20 mL). The organic layers were combined, dried over $MgSO_4$ and the solvent removed under reduced pressure. The crude mixture was purified by flash column chromatography (silica, gradient elution starting from 40% EtOAc in hexane to 70% EtOAc in hexane) to yield compound ***S*-1b** as a white crystalline solid (1.17 g, 83%). TLC analysis R_f 0.21 (silica, 60% EtOAc in hexane); m.p. 70 -71 °C; ^{1}H NMR (295 K, 400 MHz, $CDCl_3$) δ_H 11.91 (1H, d, ^3J 7.5, CONH), 8.34 (1H, dd, ^3J 8, ^4J 2, py-H^3), 7.40 (2H, m, Ph-H^o), 7.38 (1H, dd, ^3J 8, ^4J 2, py-H^5), 7.34 (3H, m, Ph-H^m, Ph-H^p), 7.25-7.23 (1H, m, py-H^4), 5.31 (1H, dq, ^3J 7, ^3J 7.5 CHCH$_3$), 2.57 (3H, s, py-CH$_3$), 1.62 (3H, d, ^3J 7, CHCH$_3$); ^{13}C NMR (295 K, 100 MHz, $CDCl_3$) δ_C 159.4 (CONH), 150.3 (py-C^6), 143.5 (Ph-C^i) , 141 (py-C^2), 128.9 (Ph-C), 128.1 (py-C^5), 127.4 (py-C^4), 127.1 (py-C^3), 126.5 (Ph-C), 126.4 (Ph-C^o), 49.8 (CHCH$_3$), 22.8 (CHCH$_3$), 18.4 (py-CH$_3$); *m/z* (HRMS$^+$) 257.1280 $[M+H]^+$ ($C_{15}H_{17}N_2O_2$ requires 257.1290).

(*S*)-(2-((1-Phenylethyl)carbamoyl)pyridin-2-yl)methyl acetate, *S*-1c

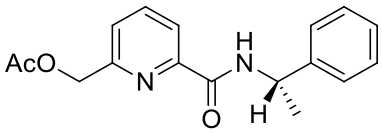

The N-oxide ***S*-1b** (700 mg, 2.73 mmol) was dissolved in acetic anhydride (14 mL) and the solution was heated to 120 °C for 24 h with stirring. The reaction progress was monitored by LCMS and TLC (silica, 50% EtOAc in hexane, R_f (product) 0.38, R_f (reactant) 0.16). The solvent was removed under reduced pressure and the residue purified by column chromatography (silica, gradient elution starting from 20% EtOAc in hexane to 70% EtOAc in hexane) to give ***S*-1c** as dark yellow oil (476 mg, 59%). TLC analysis R_f 0.38 (silica, 50% EtOAc in hexane); ^{1}H NMR (295 K, 400 MHz, $CDCl_3$) δ_H 8.26 (1H, d, ^3J 7.5, CONH), 8.14 (1H, d, ^3J 8, py-H^5), 7.86 (1H, t, ^3J 8, py-H^4), 7.48 (1H, d, ^3J 8, py-H^3), 7.42 – 7.25 (5H, m, Ph-H), 5.36 – 5.28 (1H, dq, ^3J 7, ^3J 7.5, CHCH$_3$), 5.24 (2H, s, py-CH$_2$), 2.16 (3H, s, COCH$_3$), 1.63 (3H, d, ^3J 7, CHCH$_3$); ^{13}C NMR (295 K, 100 MHz, $CDCl_3$) δ_C 170.6 (COCH$_3$), 163.2 (CONH), 154.7 (py-C^6), 149.7 (py-C^2), 143.4 (Ph-C^i), 138.3 (py-C^4), 128.8 (Ph-C^m), 127.5 (Ph-C^p), 126.4 (Ph-C^o), 124.1 (py-C^3), 121.6 (py-C^5), 66.5 (py-CH$_2$), 49.0 (CHCH$_3$), 22.2 (CHCH$_3$), 21.0 (COCH$_3$); *m/z* (HRMS$^+$) 299.1373 $[M+H]^+$ ($C_{17}H_{19}N_2O_3$ requires 299.1396).

(*S*)-6-(Hydroxymethyl)-*N*-(1-phenylethyl)picolinamide, *S*-1d

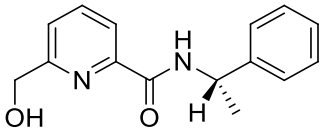

The ester, ***S*-1c**, (350 mg, 1.16 mmol) was dissolved in anhydrous CH_3CH_2OH (12 mL). A small amount of sodium metal (~ 5 mg) was added and the solution stirred at 40 °C under argon for 2 h. The solution was concentrated under reduced pressure and the residue dissolved in CH_2Cl_2 (100 mL). The sodium salts were extracted by washing with water (1 x 25 mL) and the aqueous layer was re-extracted with CH_2Cl_2 (3 x 20 mL). The organic layers were combined, dried over $MgSO_4$, filtered and the solvent removed under reduced pressure. The crude residue was purified by column chromatography (silica, gradient elution starting from 40% EtOAc to 100% EtOAc) to yield compound ***S*-1d** as a white solid (330 mg, 85%). TLC analysis R_f 0.35 (silica, 70% EtOAc in hexane); m.p. 152 – 154 °C; ^{1}H NMR (295 K, 400 MHz, $CDCl_3$) δ_H 8.21 (1H, s, ^3J 7.5, CONH), 8.16 (1H, d, ^3J 7.5, py-H^3), 7.89 (1H, t, ^3J 7.5, py-H^4), 7.49 (1H, d, ^3J 7.5, py-H^5), 7.43-7.25 (5H, m, Ph-H), 5.37 – 5.30 (1H, dq, ^3J 7, ^3J 7.5, CHCH$_3$), 4.83 (2H, s, py-CH$_2$), 2.91 (1H, br s, OH), 1.64 (3H, d, ^3J 7, CHCH$_3$); ^{13}C NMR (295 K, 100 MHz, $CDCl_3$) δ_C 163.1 (CONH), 158.4 (py-C^6), 149.1 (py-C^2), 143.2 (Ph-C^i), 138.7 (py-C^4), 128.9 (Ph-C^m), 127.6 (Ph-C^p), 126.4 (Ph-C^o), 123.5 (py-C^5), 121.7 (py-C^3), 64.6 (py-CH$_2$), 49.1 (CHCH$_3$), 22.1 (CHCH$_3$); *m/z* (HRMS$^+$) 257.1282 $[M+H]^+$ ($C_{15}H_{17}N_2O_2$ requires 257.1290).

(*S*)-(6-((1-Phenylethyl)carbamoyl)pyridine-2-yl)methyl methane sulfonate, *S*-1e

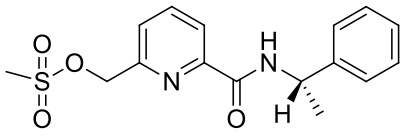

The alcohol, ***S*-1d**, (227 mg, 0.886 mmol) was dissolved in anhydrous THF (5.5 mL) and NEt_3 (0.37 mL, 2.66 mmol) was added. The mixture was stirred at 5 °C, methanesulfonyl chloride (0.12 mL, 1.49 mmol) was added and the reaction stirred at r.t. for 30 minutes and monitored by TLC (silica, 100% ethyl acetate, R_f(product) 0.63, R_f(reactant) 0.53). The solvent was removed under reduced pressure and the residue dissolved in CH_2Cl_2 (25 mL) and washed with water (15 mL). The aqueous layer was re-extracted with CH_2Cl_2 (3 x 10 mL) and the organic layers were combined, dried over $MgSO_4$, filtered and the solvent removed under reduced pressure to leave compound ***S*-1e**, as a bright yellow oil,

which was used directly in the next step without further purification. TLC analysis R_f 0.63 (silica, 100% ethyl acetate); ^{1}H NMR (295 K, 400 MHz, $CDCl_3$) δ_H 8.25 (1H, d, ^3J 8, CONH), 8.19 (1H, d, ^3J 8, py-H^5), 7.91 (1H, t, ^3J 8, py-H^4), 7.59 (1H, d, ^3J 8, py-H^3), 7.42 – 7.26 (5H, m, Ph-H), 6.36 (2H, s, py-CH_2), 5.34 – 5.28 (1H, dq, ^3J 7, ^3J 8, CHCH$_3$), 3.07 (3H, s, SO_2CH_3), 1.63 (3H, d, ^3J 7, CHCH_3); ^{13}C NMR (295 K, 100 MHz, $CDCl_3$) δ_C 162.8 (CONH), 152.5 (py-C^6), 149.9 (py-C^2), 143.3 (Ph-C^i), 138.7 (py-C^4), 128.8 (Ph-C^m), 127.5 (Ph-C^p), 126.4 (Ph-C^o), 124.6 (py-C^3), 122.4 (py-C^5), 70.8 (py-CH_2), 49.0 (CHCH$_3$), 38.3 (OSO_2CH_3), 22.1 (CHCH_3); *m/z* (HRMS)$^+$ 335.1066 $[M+H]^+$ ($C_{16}H_{19}N_2O_4S$ requires 335.1060).

6,6',6''-((1,4,7-Triazonane-1,4,7-triyl)tris(methylene))tris(*N*-((*S*)-1-phenylethyl)picolinamide, *S*-L^{30}

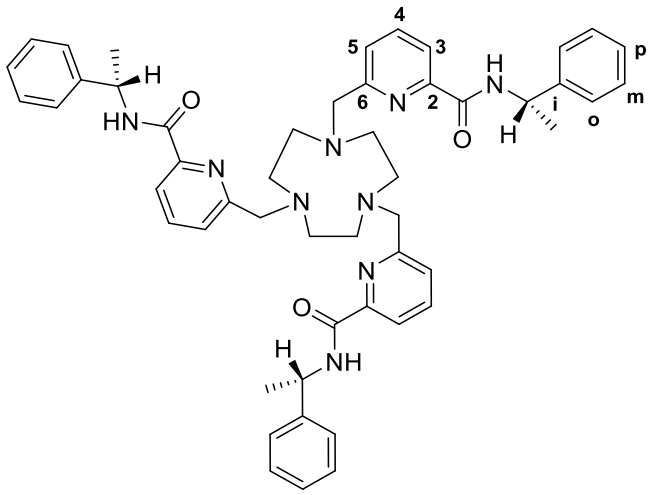

1,4,7-Triazacyclononane (55 mg, 0.427 mmol) and the mesylate, ***S*-1e**, (428 mg, 1.28 mmol) were dissolved in anhydrous CH_3CN (19.5 mL) and K_2CO_3 (59 mg, 0.427 mmol) was added. The mixture was stirred under argon at 78 °C. After 21 h the reaction was cooled and filtered to remove excess potassium salts. The solvent was removed under reduced pressure and the crude material purified by column chromatography (alumina, gradient elution starting from 100% CH_2Cl_2 to 5% CH_3OH in CH_2Cl_2) to give ***S*-L^{30}** as a yellow glassy solid (180 mg, 55%); TLC analysis R_f 0.21 (alumina, 1% CH_3OH in CH_2Cl_2); ^{1}H NMR (295 K, 400 MHz, $CDCl_3$) δ_H 8.53 (3H, d, ^3J 7, CONH), 8.08 (3H, d, ^3J 7.5, py-H^3), 7.77 (3H, t, py-H^4), 7.51 (3H, d, ^3J 7, py-H^5), 7.43 – 7.17 (15H, m, Ph-H), 5.35 (3H, dq, ^3J 7, ^3J 7.5, CHCH$_3$), 3.78 (6H, s, py-CH_2), 2.79 (12H, s, *ring Hs*), 1.62 (9H, d, ^3J 7, CHCH_3); ^{13}C NMR (295 K, 100 MHz, $CDCl_3$) δ_C 163.7 (CONH), 159.3 (py-C^2), 149.5 (py-C^6), 143.6 (Ph-C^i), 137.9 (py-C^4), 128.8 (Ph-C^m), 127.5 (Ph-C^p), 126.6

(Ph-C^{o}), 125.9 (py-C^{5}), 120.9 (py-C^{3}), 64.6 (py-CH$_2$), 56.3 (*ring Cs*), 49.0 (*ring Cs*), 46.0 (CHCH$_3$), 22.05 (CHCH$_3$); *m/z* (HRMS$^+$) 844.4683 $[M+H]^+$ ($C_{51}H_{58}N_9O_3$ requires 844.4663).

_S_-[Eu.L^{30}](CF$_3$SO$_3$)$_3$

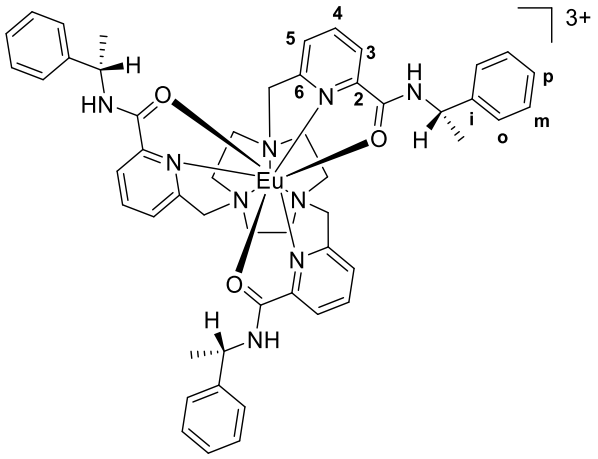

Europium (III) triflate (14 mg, 0.024 mmol) was added to a solution of ligand, ***S*-L^{30}**, (19 mg, 0.024 mmol) in anhydrous acetonitrile (2 mL) and the mixture heated at reflux for 20 h. The solution was concentrated under reduced pressure and cold diethyl ether (2 mL) was added dropwise to the solution. The resulting white solid was filtered and dried under reduced pressure to yield ***S*-[Eu.L^{30}](CF$_3$SO$_3$)$_3$** as a white solid (20 mg, 85%). ^{1}H NMR (295 K, 400 MHz, CD_3OD) δ_H major diastereoisomer: 7.6 (pyCH'N), 7.5 (py-H^3), 7.4 (py-H^5), 7.3 (py-H^4), 6.9 (Ph-H^p), 6.7 (Ph-H^m), 5.7 (Ph-H^o), 5.1 (NCH'$_{ax}$), 4.0 (CHCH$_3$), 1.2 (CHCH$_3$), -0.7 (pyCHN), -1.5 (NCH$_{eq}$), -2.2 (NCH'$_{eq}$), -6.6 (NCH$_{ax}$); *m/z* (HRMS$^+$) 992.3646 $[M-2H]^+$ ($C_{51}H_{55}N_9O_3{}^{151}Eu$ requires 992.3626); $\phi_{em}(H_2O) = 0.07$, $\tau(H_2O) = 0.98$ ms, $\tau(D_2O) = 1.42$ ms, $q = -0.1$; $t_R = 5.63$ min (analytical HPLC, Table 23).

Crystals of the europium complex were grown by slow evaporation of aqueous methanol (1:1 v/v) and examined by X-ray crystallography: $C_{51}H_{57}EuN_9O_3$ x 3 CF_3SO_3, M_r = 1443.22, trigonal (R3); a = 21.6392(5) Å, c = 11.4683(4) Å, V = 4650.6(2) Å^3, Z = 3; μ = 1.205 mm^{-1}, D_{calc} = 1.546 mg.mm^{-3}, T = 120 K; 62 469 reflections were measured ($2.18 \leq 2\Theta \leq 62.06$), 5722 independent reflections (R_{int} = 0.0336), R_1 = 0.0412, ωR_2= 0.1043 ($I \geq 2\sigma(I)$), GOOF = 1.026. Flack parameter -0.0013(11), Hooft parameter 0.004(5), CCDC 965909.

_S_-[Ce.L^{30}](CF$_3$SO$_3$)$_3$

An analogous method to that for **_S_-[Eu.L^{30}]$^{3+}$** using cerium (III) triflate (7 mg, 0.012 mmol) and the ligand **_S_-L^{30}** (10mg, 0.012 mmol) in dry acetonitrile (2 mL) was followed to yield **_S_-[Ce.L^{30}](CF$_3$SO$_3$)$_3$** as a white solid (10 mg, 85%). ^{1}H NMR (295 K, 400 MHz, CD_3OD) δ_H major diastereoisomer: 9.6 (py-H^3), 9.4 (py-H^4), 8.4 (py-H^5), 7.7 (Ph-H), 7.6 (Ph-H), 6.2 (NCH'$_{ax}$), 4.5 (CHCH$_3$), 4.1 (pyCHN), 1.6 (NCH'$_{eq}$), 1.3 (CHCH$_3$), 0.3 (NCH$_{eq}$), -1.0 (NCH$_{ax}$); *m/z* (HRMS$^+$) 981.3506 [M-2H]$^+$ ($C_{51}H_{55}N_9O_3{}^{140}$Ce requires 981.3482).

_S_-[Pr.L^{30}](CF$_3$SO$_3$)$_3$

An analogous method to that for **_S_-[Eu.L^{30}]$^{3+}$** using praseodymium (III) triflate (7 mg, 0.012 mmol) and the ligand **_S_-L^{30}** (10mg, 0.012 mmol) in dry acetonitrile (2 mL) was followed to yield **_S_-[Pr.L^{30}](CF$_3$SO$_3$)$_3$**, as a white solid (10 mg, 85%). ^{1}H NMR (295 K, 400 MHz, CD_3OD) δ_H major diastereoisomer: 11.1 (py-H^3), 10.5 (py-H^4), 10.1 (py-H^5), 9.4 (NCH'$_{ax}$), 8.4 (Ph-H), 8.2 (Ph-H), 8.1 (Ph-H), 6.4 (pyCHN), 4.1 (CHCH$_3$), 1.6 (NCH$_{eq}$), 1.1 (CHCH$_3$), 0.5 (pyCH'N), -1.3 (NCH'$_{eq}$), -5.5 (NCH$_{ax}$); *m/z* (HRMS$^+$) 982.3493 [M-2H]$^+$ ($C_{51}H_{55}N_9O_3{}^{141}$Pr requires 982.3499).

_S_-[Nd.L^{30}](CF$_3$SO$_3$)$_3$

An analogous method to that for **_S_-[Eu.L^{30}]$^{3+}$** using neodymium (III) triflate (7 mg, 0.012 mmol) and the ligand **_S_-L^{30}** (10mg, 0.012 mmol) in dry acetonitrile (2 mL) was followed to yield **[Nd.L^{30}]$^{3+}$**, as a white solid (9 mg, 72%). ^{1}H NMR (295 K, 400 MHz, CD_3OD) δ_H major diastereoisomer: 10.2 (py-H^3), 9.3 (py-H^4), 8.9 (py-H^5), 7.5 (Ph-H), 7.2 (pyCHN), 6.4 (Ph-H), 5.8 (NCH$_{ax}$), 5.3 (CHCH$_3$), 4.1 (NCH'$_{ax}$), 2.7 (NCH$_{eq}$), 2.6 (NCH'$_{eq}$), 1.6 (CHCH$_3$), 0.4 (pyCH'N); *m/z* (HRMS$^+$) 983.3505 [M-2H]$^+$ ($C_{51}H_{55}N_9O_3{}^{142}$Nd requires 983.3530).

_S_-[Tb.L^{30}](CF$_3$SO$_3$)$_3$

An analogous method to that for **_S_-[Eu.L^{30}]$^{3+}$** using terbium (III) triflate (10 mg, 0.017 mmol) and the ligand **_S_-L^{30}** (15 mg, 0.017 mmol) in dry acetonitrile (2 mL) was followed to yield **_S_-[Tb.L^{30}](CF$_3$SO$_3$)$_3$**, as a white solid (16 mg, 92%). ^{1}H NMR (295 K, 400 MHz, CD_3OD) δ_H major diastereoisomer: 57.5 (NCH$_{ax}$), 29.9 (NCH'$_{eq}$), 23.9 (NCH$_{eq}$), 8.6 (CHCH$_3$), 5.8 (CHCH$_3$), 4.5 (Ph-H^m), 2.0 (Ph-H^o), -3.2 (py-H^4), -4.4 (py-H^5), -11.0 (py-H^3), -12.4 (NCH'$_{ax}$), -45.5 (pyCH'N); *m/z* (HRMS$^+$) 1000.369 [M-2H]$^+$ ($C_{51}H_{55}N_9O_3{}^{159}$Tb requires 1000.368); ϕ_{em} (H_2O) = 0.50, τ(H_2O) = 1.87 ms, τ(D_2O) = 2.12 ms.

***S*-[Dy.L^{30}](CF$_3$SO$_3$)$_3$**

An analogous method to that for ***S*-[Eu.L^{30}]$^{3+}$** using dysprosium (III) triflate (11 mg, 0.017 mmol) and the ligand ***S*-L^{30}** (15 mg, 0.017 mmol) in dry acetonitrile (2 mL) was followed to yield ***S*-[Dy.L^{30}](CF$_3$SO$_3$)$_3$**, as a white solid (15 mg, 88%). ^{1}H NMR (295 K, 400 MHz, CD_3OD) δ_H major diastereoisomer, partial assignment: 22.5 (NC$\underline{H}$'$_{ax}$), 18.2, 11.1, 7.0, 6.5 (Ph-$\underline{H}$), 6.2 (Ph-$\underline{H}$), 5.6, 5.0 (py-$\underline{H}^4$), 3.0 (py-$\underline{H}^5$), 1.9 (py-$\underline{H}^3$), -1.5, -3.7 (pyC$\underline{H}$N), -4.8, -14.0, 18.0; *m/z* (HRMS$^+$) 1002.371 [M-2H]$^+$ ($C_{51}H_{55}N_9O_3{}^{161}$Dy requires 1002.370); ϕ_{em} (H_2O) = 0.01, τ(H_2O) = 0.04 ms.

***S*-[Ho.L^{30}](CF$_3$SO$_3$)$_3$**

An analogous method to that for ***S*-[Eu.L^{30}]$^{3+}$** using holmium (III) triflate (8 mg, 0.013 mmol) and the ligand ***S*-L^{30}** (11 mg, 0.013 mmol) in dry acetonitrile (2 mL) was followed to yield ***S*-[Ho.L^{30}](CF$_3$SO$_3$)$_3$**, as a white solid (13 mg, 99%). ^{1}H NMR (295 K, 400 MHz, CD_3OD) δ_H major diastereoisomer, partial assignment: 47.3 (NC$\underline{H}_{ax}$), 23.3 (NC$\underline{H}$'$_{eq}$), 22.6 (NC$\underline{H}_{eq}$), 11.9, 10.2, 9.8, 7.2 (CHC$\underline{H}_3$), 5.8 (C$\underline{H}$CH$_3$), 5.5 (Ph-$\underline{H}^m$), 5.1 (Ph-$\underline{H}^o$), 0.5 (py-$\underline{H}^5$), -0.4 (py-$\underline{H}^4$), -3.7 (NC$\underline{H}$'$_{ax}$), -5.5 (py-$\underline{H}^3$), -32.0 (pyC$\underline{H}$'N); *m/z* (HRMS$^+$) 1006.374 [M-2H]$^+$ ($C_{51}H_{55}N_9O_3{}^{165}$Ho requires 1006.373).

***S*-[Er.L^{30}](CF$_3$SO$_3$)$_3$**

An analogous method to that for ***S*-[Eu.L^{30}]$^{3+}$** using erbium (III) triflate (7 mg, 0.012 mmol) and the ligand ***S*-L^{30}** (10 mg, 0.012 mmol) in dry acetonitrile (2 mL) was followed to yield ***S*-[Er.L^{30}](CF$_3$SO$_3$)$_3$**, as a white solid (12 mg, 99%). ^{1}H NMR (295 K, 400 MHz, CD_3OD) δ_H major diastereoisomer: 12.8, 8.2 (py-$\underline{H}^3$), 8.0 (py-$\underline{H}^5$), 7.9 (py-$\underline{H}^4$), 7.5 (Ph-$\underline{H}^p$), 6.9 (Ph-$\underline{H}^m$), 6.1 (Ph-$\underline{H}^o$), 3.6, 1.9 (C$\underline{H}$CH$_3$), 1.8 (pyC$\underline{H}$N), 0.9 (CHC$\underline{H}_3$), -5.0 (NC$\underline{H}_{eq}$), -5.1 (NC$\underline{H}$'$_{eq}$), -8.8 (NC$\underline{H}_{ax}$); *m/z* (HRMS$^+$) 1009.380 [M-2H]$^+$ ($C_{51}H_{55}N_9O_3{}^{168}$Er requires 1009.377).

***S*-[Tm.L^{30}](CF$_3$SO$_3$)$_3$**

An analogous method to that for ***S*-[Eu.L^{30}]$^{3+}$** using thulium (III) triflate (7 mg, 0.012 mmol) and the ligand *S*-**L^{30}** (10 mg, 0.012 mmol) in dry acetonitrile (2 mL) was followed to yield ***S*-[Tm.L^{30}](CF$_3$SO$_3$)$_3$**, as a white solid (11 mg, 91%). ^{1}H NMR (295 K, 400 MHz, CD_3OD) δ_H major diastereoisomer: 70.4 (pyC$\underline{H}$'N), 23.0 (py-$\underline{H}^3$), 19.6 (py-$\underline{H}^4$), 19.2 (py-$\underline{H}^5$), 11.3 (NC$\underline{H}$'$_{ax}$), 10.8 (Ph-$\underline{H}^o$), 10.7 (Ph-$\underline{H}^p$), 10.4 (Ph-$\underline{H}^m$), 9.3 (C$\underline{H}$CH$_3$), -7.5 (CHC$\underline{H}_3$), -22.0 (pyC$\underline{H}$N), -29.0 (NC$\underline{H}_{eq}$), -30.5 (NC$\underline{H}$'$_{eq}$), -79.8 (NC$\underline{H}_{ax}$); *m/z* (HRMS$^+$) 101.375 [M-2H]$^+$ ($C_{51}H_{55}N_9O_3{}^{169}$Tm requires 1010.376).

_S_-[Yb.L^{30}](CF$_3$SO$_3$)$_3$

An analogous method to that for **_S_-[Eu.L^{30}]$^{3+}$** using ytterbium (III) triflate (10 mg, 0.017 mmol) and the ligand **_S_-L^{30}** (15 mg, 0.017 mmol) in dry acetonitrile (2 mL) was followed to yield **_S_-[Yb.L^{30}](CF$_3$SO$_3$)$_3$**, as a white solid (15 mg, 85%). ^{1}H NMR (295 K, 400 MHz, CD_3OD) δ_H major diastereoisomer: 22.3 (pyCH'N), 11.6 (py-H^3), 11.4 (py-H^5), 11.2 (py-H^4), 8.9 (NCH'$_{ax}$), 8.3 (Ph-H^m), 8.2 (Ph-H^p), 7.6 (Ph-H^o), 6.2 (CHCH$_3$), -1.1 (CHCH$_3$), -2.8 (pyCHN), -4.2 (NCH$_{eq}$), -6.7 (NCH'$_{eq}$), -18.8 (NCH$_{ax}$); *m/z* (HRMS$^+$) 1012.382 [M-2H]$^+$ ($C_{51}H_{55}N_9O_3{}^{171}$Yb requires 1012.379).

Crystals of the ytterbium complex were grown by slow evaporation of aqueous methanol (1:1 *v/v*) and examined by X-ray crystallography: $C_{54}H_{57}F_9N_9O_{12}S_3Yb$, M_r = 1464.30, trigonal (R3); a = 21.836(2) Å, c = 11.1868(17) Å, V = 4619.5(10) Å^3, Z = 3; μ = 1.713 mm^{-1}, D_{calc} = 1.579 mg.mm^{-3}, T = 120 K; 65 596 reflections measured ($2.16 \leq 2\Theta \leq 62.06$), 5472 independent reflections (R_{int} = 0.0398), R_1 = 0.0437, ωR_2= 0.1116 ($I \geq 2\sigma(I)$), GOOF = 1.053, Flack parameter -0.018(11), Hooft parameter 0.003(3). CCDC 965911.

_R_-L^{30} was synthesised in an analogous manner to the **_S_** series starting from *R*-(+)-α-methylbenzyl amine.

_R_-[Eu.L^{30}](CF$_3$SO$_3$)$_3$

An analogous method to that for **_S_-[Eu.L^{30}]$^{3+}$** using europium (III) triflate (14 mg, 0.023 mmol) and the ligand **_R_-L^{30}** (20mg, 0.023 mmol) in dry acetonitrile (2 mL) was followed to yield **_R_-[Eu.L^{30}](CF$_3$SO$_3$)$_3$** as a white solid (22 mg, 96%). ^{1}H NMR (295 K, 400 MHz, CD_3OD) δ_H major diastereoisomer: 7.6 (pyCH'N), 7.5 (py-H^3), 7.4 (py-H^5), 7.3 (py-H^4), 6.9 (Ph-H^p), 6.7 (Ph-H^m), 5.7 (Ph-H^o), 5.1 (NCH'$_{ax}$) 4.0 (CHCH$_3$), 1.2 (CHCH$_3$), -0.7 (pyCHN), -1.5 (NCH$_{eq}$), -2.2 (NCH'$_{eq}$), -6.6 (NCH$_{ax}$); *m/z* (HRMS$^+$) 992.3674 [M-2H]$^+$ ($C_{51}H_{55}N_9O_3{}^{151}$Eu requires 992.3626).

Crystals of the europium complex were grown by slow evaporation of aqueous methanol (1:1 v/v) and examined by X-ray crystallography: $C_{51}H_{57}EuN_9O_3$ x 3 CF_3SO_3, M_r = 1443.22, trigonal (R3); a = 21.6423(8) Å, c = 11.5027 Å, V = 4665.9 Å^3, Z = 3; μ = 1.201 mm^{-1}, D_{calc} = 1.541 mg.mm^{-3}, T = 120 K; 29 561 reflections were measured ($3.76 \leq 2\Theta \leq 62$), 6082 independent reflections (R_{int} = 0.0267), R_1 = 0.0281, ωR_2= 0.0740 ($I \geq 2\sigma(I)$), GOOF = 1.029, Flack parameter -0.012(7), Hooft parameter -0.009(2). CCDC 965910.

***R*-[Tb.L^{30}](CF$_3$SO$_3$)$_3$**

An analogous method to that for ***S*-[Eu.L^{30}]$^{3+}$** using terbium (III) triflate (19 mg, 0.032 mmol) and the ligand ***R*-L^{30}** (27 mg, 0.032 mmol) in dry acetonitrile (2 mL) was followed to yield ***R*-[Tb.L^{30}] (CF$_3$SO$_3$)$_3$** as a white solid (31 mg, 97%). ^{1}H NMR (295 K, 400 MHz, CD_3OD) δ_H major diastereoisomer: 57.5 (NC$\underline{H}_{ax}$), 29.9 (NC$\underline{H}'_{eq}$), 23.9 (NC$\underline{H}_{eq}$), 8.6 (CHC$\underline{H}_3$), 5.8 (C$\underline{H}$CH$_3$), 4.5 (Ph-$\underline{H}^m$), 2.0 (Ph-$\underline{H}^o$), -3.2 (py-$\underline{H}^4$), -4.4 (py-$\underline{H}^5$), -11.0 (py-$\underline{H}^3$), -12.4 (NC$\underline{H}'_{ax}$), -45.5 (pyC$\underline{H}$'N); *m/z* (HRMS$^+$) 1000.368 [M-2H]$^+$ ($C_{51}H_{55}N_9O_3{}^{159}$Tb requires 1000.368).

5.2.2. [Ln.L^{31a-d}]$^{3+}$ and precursors

Dimethyl 4-chloropyridine-2,6-dicarboxylate, CAS: 5371-70-0 [220]

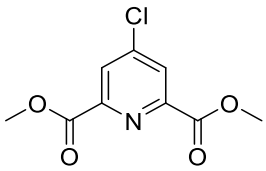

Chelidamic acid (1.00 g, 5.46 mmol) was dissolved in thionyl chloride (5.6 mL) and a few drops of DMF were added. The solution was stirred at 100 °C for 48 h. After complete consumption of the starting material (monitored by LC-MS), the thionyl chloride was removed by vacuum distillation. The residue was dissolved in dry CH_2Cl_2 (3 mL) and cooled to 0 °C. Dry CH_3OH (4 mL) was added dropwise over a period of 10 minutes and the reaction mixture was brought to room temperature. The solvent was removed under reduced pressure and the residue was washed with $NaHCO_3$ (sat. aq.,15 mL) and extracted into CH_2Cl_2 (3 x 40 mL). The organic layers were combined, washed successively with water (1 x 50 mL) and brine (1 x 50 mL), dried over $MgSO_4$, filtered and the solvent removed under reduced pressure to yield the title compound as an orange solid (1.196 g, 95%), which was used directly in the next step with no further purification. TLC analysis R_f 0.60 (silica, 5% CH_3OH in CH_2Cl_2); m.p. 141 – 143 °C (lit. 142 °C)[221]; ^{1}H NMR (295 K, 400 MHz, $CDCl_3$) δ_H 8.29 (2H, s, py-$\underline{H}$), 4.02 (6H, s, $CO_2C\underline{H}_3$); ^{13}C NMR (295 K, 100 MHz, $CDCl_3$) δ_C 164.2 ($\underline{C}O_2CH_3$), 149.5 (py-$\underline{C}$), 146.9 (py-$\underline{C}$), 128.4 (py-$\underline{C}$), 53.6 ($CO_2\underline{C}H_3$); *m/z* (HRMS$^+$) 230.0206 [M+H]$^+$ ($C_9H_9NO_4Cl$ requires 230.0220).

Dimethyl 4-iodopyridine-2,6-dicarboxylate CAS: 112776-84-8 [220]

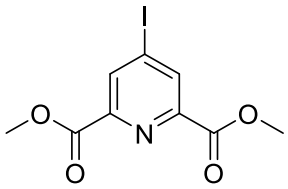

Sodium iodide (3.16 g, 21.1 mmol) was added to a solution of dimethyl 4-chloropyridine-2,6-dicarboxylate (478 mg, 2.11 mmol) in dry acetonitrile (25 mL) and the solution was sonicated (bath sonicator) for 30 min. Acetyl chloride (0.45 mL, 6.33 mmol) was added and the mixture was sonicated for a further 45 min. The solvent was removed under reduced pressure and the residue redissolved in CH_2Cl_2. The solution was washed with sat. Na_2CO_3 (30 mL) and the organic phase separated. The aqueous phase was extracted into CH_2Cl_2 (3 x 25 mL) and all the organic layers were combined, washed successively with $Na_2S_2O_3.5H_2O$ (sat. aq., 25 mL), water (25 mL), dried over $MgSO_4$, filtered, and the solvent removed under reduced pressure. The crude mixture was purified by flash column chromatography (silica, gradient elution starting from 100% CH_2Cl_2 to 1% CH_3OH in CH_2Cl_2) to yield the compound as a white solid (546 mg, 81%). TLC analysis R_f 0.62 (silica, 5% CH_3OH in CH_2Cl_2); m.p. 179-180 °C (lit. 174-175 °C)[222]; ^{1}H NMR (295 K, 400 MHz, $CDCl_3$) δ_H 8.66 (2H, s, py-H), 4.02 (6H, s, CO_2CH_3); ^{13}C NMR (295 K, 100 MHz, $CDCl_3$) δ_C 164.0 (CO_2CH_3), 148.4 (py-C), 137.3 (py-C), 107.1 (py-C), 53.6 (CO_2CH_3) ; *m/z* (HRMS$^+$) 321.9569 $[M+H]^+$ ($C_9H_9NO_4I$ requires 321.9576).

Methyl 6-(hydroxymethyl)-4-iodopicolinate, 3a, CAS: 1247012-08-3 [223]

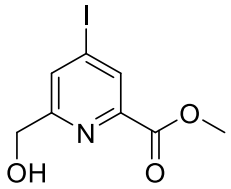

Dimethyl 4-iodopyridine-2,6-dicarboxylate (376 mg, 1.17 mmol) was dissolved in a solution of dry CH_2Cl_2 (3 mL) and dry CH_3OH (2 mL) and cooled to 0 °C. $NaBH_4$ (49 mg, 1.29 mmol) was added to the solution and the reaction was stirred at 0 °C for 1.5 h. The mixture was quenched with the addition of 1 M HCl (2 mL). The volatile components were removed under vacuum and the aqueous solution was extracted into EtOAc (3 x 25 mL). The organic layers were combined, dried over $MgSO_4$, filtered and the solvent removed under vacuum. The crude solid was purified using flash column chromatography

(silica, gradient elution starting from 100% CH_2Cl_2 to 2% CH_3OH in CH_2Cl_2) to give **3a** as a white solid (247 mg, 72%). TLC analysis R_f 0.27 (silica, 5% CH_3OH in CH_2Cl_2); m.p. 140 – 141 °C; ^{1}H NMR (295 K, 400 MHz, $CDCl_3$) δ_H 8.38 (1H, s, py-$\underline{H}^3$), 7.96 (1H, s, py-$\underline{H}^5$), 4.81 (2H, s, $C\underline{H}_2OH$), 3.99 (3H, s, $CO_2C\underline{H}_3$); ^{13}C NMR (295 K, 100 MHz, $CDCl_3$) δ_C 164.5 ($\underline{C}O_2CH_3$), 161.2 ($\underline{C}^6$), 147.4 ($\underline{C}^2$), 133.3 ($\underline{C}^{3/5}$), 133.2 ($\underline{C}^{3/5}$), 106.4 ($\underline{C}^4$), 64.2 ($\underline{C}H_2OH$), 53.3 ($CO_2\underline{C}H_3$); *m/z* (HRMS$^+$) 293.9630 $[M+H]^+$ ($C_8H_9NO_3I$ requires 293.9627); CHN% Found: C, 33.03; H, 2.76; N, 4.80% ($C_8H_8{}^{127}INO_3$ requires C, 32.79; H, 2.75; N, 4.78%).

6-(Hydroxymethyl)-4-iodopicolinic acid, 3b

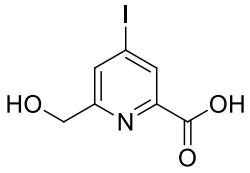

Methyl 6-(hydroxymethyl)-4-iodopicolinate (200 mg, 0.683 mmol) was dissolved in a mixture of ethanol:water (6 mL, 1:1, v/v) and NaOH (2 M, 0.5 mL) was added dropwise. The solution was stirred at room temperature for 1 h. The ethanol was removed under reduced pressure and the aqueous layer was acidified to pH = 4 using a 2 M HCl solution until a white precipitate was formed. The solid was extracted into EtOAc (4 x 50 mL), dried over $MgSO_4$ and concentrated under reduced pressure to yield the compound **3b** as a white solid (168 mg, 88%) which was used directly in the next step without further purification. TLC analysis R_f 0.08 (silica, 15% CH_3OH in CH_2Cl_2); m.p. > 190 °C (dec.); ^{1}H NMR (295 K, 400 MHz, MeOD) δ_H 8.38 (1H, s, py-$\underline{H}^3$), 8.16 (1H, s, py-$\underline{H}^5$), 4.72 (2H, s, py-$C\underline{H}_2$); ^{13}C NMR (295 K, 100 MHz, MeOD) δ_C 166 ($\underline{C}OOH$), 164 ($\underline{C}^6$), 149 ($\underline{C}^2$), 134 ($\underline{C}^5$), 133 ($\underline{C}^3$), 108 ($\underline{C}^4$), 64.7 (py-$\underline{C}H_2$); *m/z* (HRMS$^+$) 279.9478 $[M+H]^+$ ($C_7H_7NO_3{}^{127}I$ requires 279.9471).

(*S*)-6-(Hydroxymethyl)-4-iodo-*N*-(1-phenylethyl)picolinamide, *S*-3c

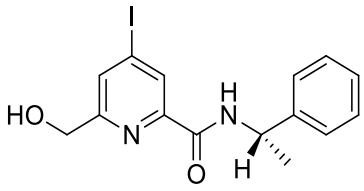

$HOBt.H_2O$ (442 mg, 3.27 mmol), EDC (507 mg, 3.27 mmol), DIPEA (0.76 mL, 4.36 mmol) and (*S*)-(-)-α-methylbenzyl amine (0.30 mL, 2.40 mmol) were dissolved in anhydrous DMF:CH_2Cl_2 (4 mL, 1:1, v/v). The carboxylic acid, **3b**, (608 mg, 2.18 mmol

in 1 mL DMF) was added slowly and dropwise to the solution and the mixture stirred at r.t. for 22 h under an argon atmosphere. The solvent was removed under reduced pressure, water was added to the crude residue and the mixture extracted with EtOAc (4 x 40 mL). The organic layers were combined and washed successively with water (40 mL) and brine (40 mL), dried over $MgSO_4$ and the solvent removed under reduced pressure. The crude mixture was purified by flash column chromatography (silica, gradient elution starting from 20% EtOAc in hexane to 50% EtOAc in hexane) to afford ***S*-3c** as a yellow oil (510 mg, 61%). TLC analysis R_f 0.38 (silica, 50% EtOAc in hexane); ^{1}H NMR (295 K, 400 MHz, $CDCl_3$) δ_H 8.48 (1H, s, py-H^3), 8.08 (1H, d, ^3J 8.5, CONH), 7.92 (1H, s, py-H^5), 7.39 – 7.38 (2H, m, Ph-H^o), 7.36-7.34 (2H, m, Ph- H^m), 7.29-7.27 (1H, m, Ph-H^p), 5.32 (1H, dq, ^3J 8.5, ^3J 7, CHCH$_3$) , 4.76 (2H, s, py-CH$_2$), 1.62 (3H, d, ^3J 7, CHCH$_3$); ^{13}C NMR (295 K, 100 MHz, $CDCl_3$) δ_C 161.9 (CONH), 159.5 (py-C^6), 149.3 (py-C^2), 143.0 (Ph-C^i), 132.6 (py-C^5), 130.9 (py-C^3), 128.9 (Ph-C^m), 127.6 (Ph-C^p), 126.4 (Ph-C^o), 108.0 (py-C^4), 64.3 (py-CH$_2$), 49.1 (CHCH$_3$), 21.9 (CHCH$_3$); *m/z* (HRMS$^+$) 383.0271 $[M+H]^+$ ($C_{15}H_{16}N_2O_2I^{127}$ requires 383.0257).

(4-(Trimethylsilyl)ethynyl)acetanilide, CAS: 81854-47-9

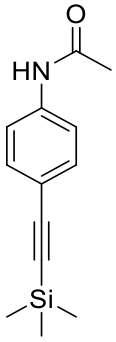

4-((Trimethylsilyl)ethynyl)aniline (200 mg, 1.06 mmol) was dissolved in anhydrous CH_2Cl_2 (3 mL) and acetic anhydride (0.12 mL, 1.27 mmol) was added dropwise. The solution was stirred at room temperature under an argon atmosphere for 2 h. The reaction mixture was washed with Na_2CO_3 solution (sat. aq., 25 mL) and extracted into CH_2Cl_2 (3 x 25 mL). The organic layers were combined, dried over $MgSO_4$, filtered and the solvent removed under reduced pressure to yield the alkyne as a pale brown solid. TLC analysis R_f 0.32 (silica, 50% EtOAc in hexane); m.p. 152 – 153 °C; ^{1}H NMR (295 K, 400 MHz, $CDCl_3$) δ_H 7.47-7.40 (4H, m, Ar-H), 2.17 (3H, s, COCH$_3$), 0.24 (9H, s, Si(CH$_3$)$_3$); ^{13}C NMR (295 K, 100 MHz, $CDCl_3$) δ_C 168.3 (COCH$_3$), 138.2 (Ar-C), 132.9 (Ar-C), 119.3

(Ar-C), 118.9 (Ar-C), 104.9 (alkyne C), 93.8 (alkyne C), 24.9 ($CO\underline{C}H_3$), 0.1 ($Si(\underline{C}H_3)_3$); *m/z* ($HRMS^+$) 232.1148 $[M+H]^+$ ($C_{13}H_{18}NOSi$ requires 232.1158).

_N_-(4-Ethynylphenyl)acetamide, CAS: 35447-83-7

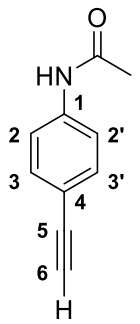

(4-(Trimethylsilyl)ethynyl)acetanilide (213 mg, 0.921 mmol) was dissolved in anhydrous THF (3.5 mL) and triethylammonium trihydrofluoride (1.50 mL, 9.21 mmol) was added. The mixture was stirred at 35 °C under argon for 48 h. The solvent was removed under reduced pressure to give an off-white solid which was purified by column chromatography (silica, gradient elution starting from 100% hexane to 40% EtOAc in hexane) to afford the alkyne as a white solid (104 mg, 71 %). TLC analysis R_f 0.31 (silica, 40% EtOAc in hexane); m.p. 115 – 117 °C; ^{1}H NMR (295 K, 700 MHz, $CDCl_3$) δ_H 7.64 (1H, s, N$\underline{H}$), 7.48 (2H, d, ^3J 8.5, Ar-$\underline{H}^{2,2'}$), 7.43 (2H, d, ^3J 8.5, Ar-$\underline{H}^{3,3'}$), 3.04 (1H, s, $\underline{H}^6$), 2.17 (3H, s, $COC\underline{H}_3$); ^{13}C NMR (295 K, 175 MHz, $CDCl_3$) δ_C 168.7 ($\underline{C}OCH_3$), 138.5 ($\underline{C}^1$), 133.0 ($\underline{C}^{3,3'}$), 119.5 ($\underline{C}^{2,2'}$), 117.8 ($\underline{C}^4$), 83.5 ($\underline{C}^5$), 76.8 ($\underline{C}^6$), 24.8 ($CO\underline{C}H_3$); *m/z* ($HRMS^+$) 160.0751 $[M+H]^+$ ($C_{10}H_{10}NO$ requires 160.0762).

(*S*)-6-(Hydroxymethyl)-N-(1-phenylethyl)-4-(phenylethynyl)picolinamide

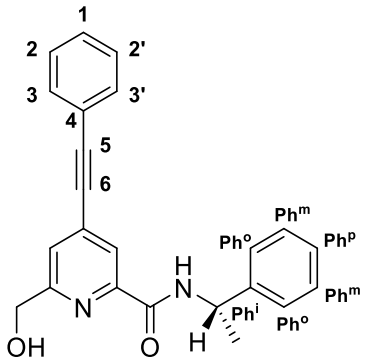

General Sonogashira cross coupling reaction:

The compound ***S*-3c** (100 mg, 0.262 mmol) was dissolved in anhydrous THF (2 mL) and the solution was degassed (freeze-thaw cycle) three times. Phenylacetylene (40 µL, 0.393 mmol) and triethylamine (0.18 mL, 1.31 mmol) were added and the solution was degassed (freeze-thaw cycle) once more. [1,1-Bis(diphenylphosphino)ferrocene]dichloropalladium(II) (19 mg, 26 µmol) and CuI (10 mg, 52 µmol) were added and the resulting brown solution was stirred at 65 °C under argon for 24 h. The solvent was removed under reduced pressure and the resulting brown oil was purified by column chromatography (silica, gradient elution starting from 100% CH_2Cl_2 to 2% CH_3OH in CH_2Cl_2 in 0.2% increments) to give the title compound as a yellow oil (91 mg, 98%). TLC analysis R_f 0.32 (silica, 1% CH_3OH in CH_2Cl_2); ^{1}H NMR (295 K, 400 MHz, $CDCl_3$) δ_H 8.19 (1H, br s, py-H^3), 8.15 (1H, d, ^3J 9, CONH), 7.57 – 7.54 (3H, m, H$^{3,3'}$, py-H^5), 7.42-7.27 (8H, m, H^1, H$^{2,2'}$, Ph-H), 5.35 (1H, dq, ^3J 9, ^3J 7, CHCH$_3$), 4.80 (2H, s, py-CH$_2$), 1.63 (3H, d, ^3J 7 CHCH$_3$); ^{13}C NMR (295 K, 100 MHz, $CDCl_3$) δ_C 162.9 (CONH), 159.1 (py-C^6), 149.2 (py-C^2), 143.1 (Ph-C^i), 134.0 (C^4), 132.1 (Ar-C), 129.6 (Ar-C), 128.8 (Ph-C), 128.6 (Ph-C), 127.5 (py-C^5), 126.4 (Ph-C), 124.9 (py-C^4), 123.4 (py-C^3), 121.9 (C^1), 95.4 (C^5), 86.5 (C^6), 64.7 (py-CH$_2$), 49.0 (CHCH$_3$), 21.9 (CHCH$_3$); *m/z* (HRMS$^+$) 357.1608 $[M+H]^+$ ($C_{23}H_{21}N_2O_2$ requires 357.1603).

(*S*)-Methyl 4-((2-(hydroxymethyl)-6-(1-phenylethylcarbamoyl)pyridin-4-yl)ethynyl)benzoate

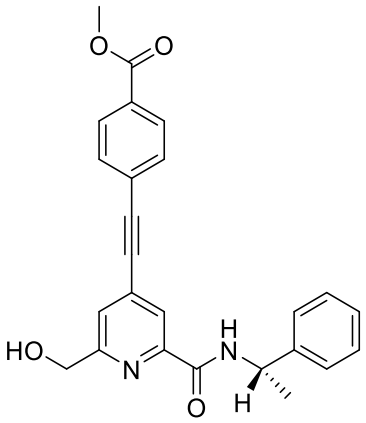

The title compound was obtained as a yellow oil (97 mg, 89%) according to the general cross coupling procedure. TLC analysis R_f 0.19 (silica, 1% CH_3OH in CH_2Cl_2); ^{1}H NMR (295 K, 400 MHz, $CDCl_3$) δ_H 8.21 (1H, br s, py-H^5), 8.13 (1H, d, ^3J 7, CONH), 8.04 (2H, d, ^3J 8, Ar-H$^{2,2'}$), 7.62-7.60 (3H, m, Ar-H$^{3,3'}$, py-H^3), 7.42-7.28 (5H, m, Ph-H), 5.35 (1H, dq, ^3J 7, ^3J 7, CHCH$_3$), 4.82 (2H, s, py-CH$_2$), 3.94 (3H, s, CO$_2$CH$_3$), 2.80 (1H, br s, OH), (1.64, 3H, d, ^3J 7, CHCH$_3$); ^{13}C NMR (295 K, 100 MHz, $CDCl_3$) δ_C 166.4 (CO$_2$Me), 162.8 (CONH), 159.4 (py-C^2), 149.4 (py-C^6), 143.0 (Ph-C^i), 133.4 (C^4), 132.0 (C$^{3,3'}$), 130.7 (C^1), 129.7 (C$^{2,2'}$), 128.8 (Ph-C^m), 127.6 (Ph-C^p), 126.4 (Ph-C^o), 125.0 (py-C^3), 123.4 (py-C^5), 94.1 (C^5), 89.0 (C^6), 64.7 (py-CH$_2$), 52.5, 49.0 (CHCH$_3$), 21.9 (CHCH$_3$); *m/z* (HRMS$^+$) 415.1643 $[M+H]^+$ ($C_{25}H_{23}N_2O_4$ requires 415.1658).

(*S*)-6-(Hydroxylmethyl)-4-((4-methoxyphenyl)-*N*-(1-phenylethyl)picolinamide

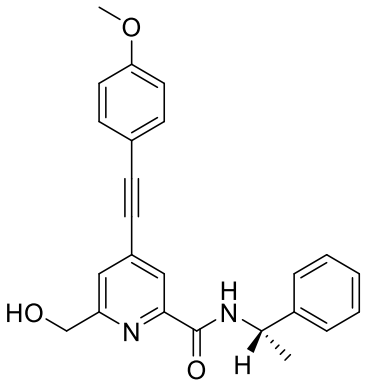

The title compound was obtained as a yellow oil (190 mg, 94%) according to the general cross coupling procedure. TLC analysis R_f 0.18 (silica, 1% CH_3OH in CH_2Cl_2); ^{1}H NMR

(295 K, 400 MHz, $CDCl_3$) δ_H 8.17 (1H, br s, py-H^3), 8.12 (1H, d, ^3J 7.5, CONH), 7.53 (1H, br s, py-H^5), 7.49 (2H, dt, ^4J 2, ^3J 9, H$^{3,3'}$), 7.42-7.35 (4H, m, Ph-H^o, Ph-H^m), 7.29-7.27 (1H, m, Ph-H^p), 6.90 (2H, dt, ^4J 2, ^3J 9, H$^{2,2'}$), 5.36 (1H, dq, ^3J 7.5, ^3J 7, CHCH$_3$), 4.80 (2H, s, py-CH$_2$), 3.84 (3H, s, OCH$_3$), 2.77 (1H, br s, OH), 1.64 (3H, d, ^3J 7, CHCH$_3$); ^{13}C NMR (295 K, 100 MHz, $CDCl_3$) δ_C 162.9 (CONH), 160.7 (C^1), 158.7 (py-C^6), 149.4 (py-C^2), 143.2 (Ph-C^i), 134.5 (C^4), 133.8 (C$^{3,3'}$), 128.9 (Ph-C), 127.6 (Ph-C), 126.4 (Ph-C) 124.7 (py-C^5), 123.4 (py-C^3), 114.4 (C$^{2,2'}$), 114.0 (py-C^4), 96.0 (C^5), 85.6 (C^6), 64.7 (py-CH$_2$), 55.5 (OCH$_3$), 49.0 (CHCH$_3$), 22.0 (CHCH$_3$); *m/z* (HRMS$^+$) 387.1701 $[M+H]^+$ ($C_{24}H_{23}N_2O_3$ requires 387.1709).

(*S*)-4-((4-acetamidophenyl)ethynyl)-6-(hydroxymethyl)-*N*-(1-phenylethyl)picolinamide

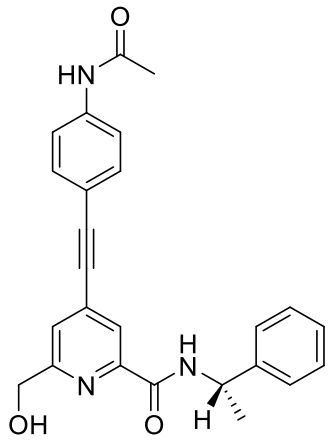

The title compound was obtained as a yellow oil (122 mg, 68%) according to the general cross coupling procedure. TLC analysis R_f 0.49 (silica, 5% CH_3OH in CH_2Cl_2); m.p. >200 °C (dec.); ^{1}H NMR (295 K, 400 MHz, *d*^{6}-DMSO) δ_H 10.19 (1H, s, NHOAc), 9.01 (1H, d, ^3J 8.5, CONH), 7.89 (1H, br s, py-H^3), 7.68-7.67 (3H, m, py-H^5, Ar-H$^{3,3'}$), 7.59-7.57 (2H, m, Ar-H$^{2,2'}$), 7.42-7.33 (4H, m, Ph-H^o, Ph-H^m), 7.24 (1H, t, ^3J 7, Ph-H^p), 5.59 (1H, br t, ^3J 6.5, OH), 5.21 (1H, dq, ^3J 8.5, ^3J 7, CHCH$_3$), 4.68 (2H, d, ^3J 6.3, py-CH$_2$), 2.07 (3H, s, NHCOCH$_3$), 1.54 (3H, d, ^3J 7, CHCH$_3$); ^{13}C NMR (295 K, 100 MHz, *d*^{6}-DMSO) δ_C 168.7 (NHCOCH$_3$), 162.4 (CONH), 161.6 (py-C^6), 149.5 (py-C^2), 144.1 (C^i), 140.7 (C^1), 132.7 (C$^{2,2'}$), 128.3 (Ph-C^m), 126.8 (Ph-C^p), 126.2 (Ph-C^o), 123.9 (py-C^5), 121.3 (py-C^3), 118.8 (C$^{3,3'}$), 114.9 (C^4), 94.7 (C^5), 85.9 (C^6), 63.6 (py-CH$_2$), 48.2 (CHCH$_3$), 24.1 (NHCOCH$_3$), 21.9 (CHCH$_3$); *m/z* (HRMS$^+$) 414.1803 $[M+H]^+$ ($C_{25}H_{24}N_3O_3$ requires 414.1818).

(*S*)-(6-(1-Phenylethylcarbamoyl)-4-(phenylethynyl)pyridin-2-yl)methyl methanesulfonate

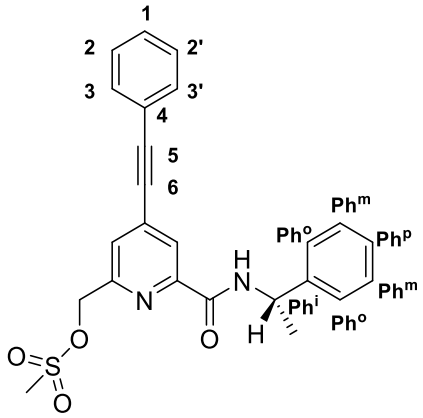

General mesylation procedure:

The alcohol, (*S*)-6-(hydroxymethyl)-*N*-(1-phenylethyl)-4-(phenylethynyl)picolinamide (91 mg, 0.256 mmol) was dissolved in anhydrous THF (2 mL) and NEt_3 (0.12 mL, 0.896 mmol) was added. The mixture was stirred at 5 °C (ice / water bath) and methanesulfonyl chloride (30 µL, 0.383 mmol) was added. The reaction was allowed to warm r.t. and stirred under argon for 30 minutes. The solvent was removed under reduced pressure and the residue dissolved in CH_2Cl_2 (15 mL) and washed with water (15 mL). The aqueous layer was re-extracted with CH_2Cl_2 (3 x 15 mL) and the organic layers were combined, dried over $MgSO_4$, filtered and the solvent removed under reduced pressure to yield the title compound, as a bright yellow oil (111 mg, 99%), which was used directly in the next step without further purification. TLC analysis R_f 0.75 (silica, 100% EtOAc); ^{1}H NMR (295 K, 400 MHz, $CDCl_3$) δ_H 8.25 (1H, d, ^4J 2, py-H^5), 8.22 (1H, d, ^3J 9, CONH), 7.65 (1H, d, ^4J 2, py-H^3), 7.58 – 7.56 (2H, m, Ar-H), 7.43 – 7.27 (8H, m, Ar-H, Ph-H), 5.35 (2H, s, py-CH_2), 5.33 (1H, dq, ^3J 9, ^3J 7, CHCH$_3$), 3.10 (3H, s, SO_2CH_3), 1.64 (3H, d, ^3J 7, CHCH_3); *m/z* (HRMS$^+$) 435.1374 $[M+H]^+$ ($C_{24}H_{23}N_2O_4S$ requires 435.1379).

(*S*)-Methyl 4-((2-((methylsulfonyloxy)methyl)-6-(1-phenylethylcarbamoyl)pyridin-4-yl)ethynyl)benzoate

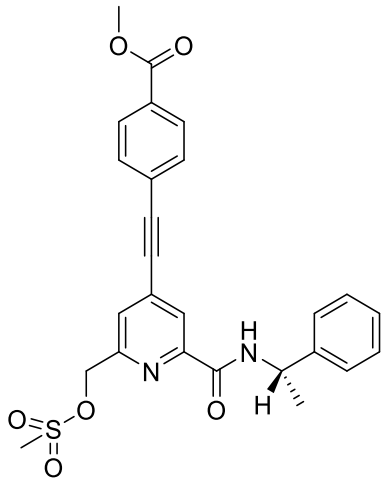

The title compound was obtained as a yellow oil (101 mg, 88%) according to the general mesylation procedure. TLC analysis R_f 0.75 (silica, 100% EtOAc); ^{1}H NMR (295 K, 400 MHz, $CDCl_3$) δ_H 8.27 (1H, br s, py-H^5), 8.21 (1H, d, ^3J 8.5, CONH), 8.06 (2H, d, ^3J 8.5, H$^{2,2'}$), 7.67 (1H, br s, py-H^3), 7.63 (2H, d, ^3J 8.5, H$^{3,3'}$), 7.43-7.35 (4H, m, Ph-H^o, Ph-H^m), 7.28 (1H, t, ^3J 7, Ph-H^p), 5.36 (2H, s, py-CH_2), 5.33 (1H, dq ^3J 8.5, ^3J 7, CHCH$_3$), 3.94 (3H, s, CO_2CH_3), 3.11 (3H, s, SO_2CH_3), 1.64 (3H, d, ^3J 7, CHCH_3); ^{13}C NMR (295 K, 100 MHz, $CDCl_3$) δ_C 166.4 (CO_2CH_3), 162.2 (CONH), 153.0 (py-C^6), 150.2 (py-C^2), 143.1 (Ph-C^i), 134.0 (C^4), 132.1 (C$^{3,3'}$), 130.9 (C^1), 129.8 (C$^{2,2'}$), 128.9 (Ph-C^m), 127.6 (Ph-C^p), 126.4 (Ph-C^o), 125.9 (py-C^3), 124.4 (py-C^5), 94.9 (C^5), 88.5 (C^6), 70.2 (py-CH_2), 52.5 (CO_2CH_3), 49.1 (CHCH$_3$), 38.4 (SO_2CH_3), 22.1 (CHCH$_3$); *m/z* (HRMS$^+$) 493.1421 $[M+H]^+$ ($C_{26}H_{25}N_2O_6S$ requires 493.1433).

(*S*)-(4-((4-Methoxyphenyl)ethynyl-6-((1-phenylethylcarbamoyl)pyridine-2-yl)methyl methane sulfonate

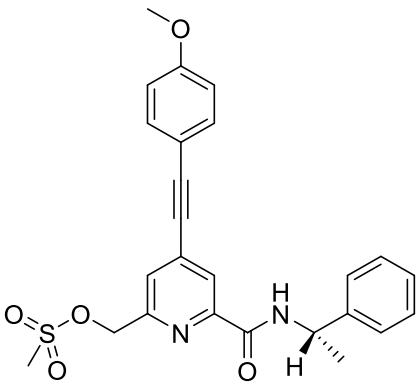

The title compound was obtained as a yellow oil (165 mg, 98%) according to the general mesylation procedure. TLC analysis R_f 0.78 (silica, 100% EtOAc); ^{1}H NMR (295 K, 400 MHz, $CDCl_3$) δ_H 8.23 (1H, br s, py-H^5), 8.12 (1H, br s, CONH), 7.62 (1H, br s, py-H^3), 7.51 (2H, d, ^3J 8.5, H$^{3,3'}$), 7.42-7.28 (5H, m, Ph-H), 6.91 (2H, d, ^3J 8.5, H$^{2,2'}$), 5.34 (2H, s, py-CH_2), 5.32 (1H, t, ^3J 7, CHCH$_3$), 3.85 (3H, s, OCH_3), 3.10 (OSO_2CH_3), 1.64 (3H, d, ^3J 7, CHCH_3); ^{13}C NMR (295 K, 100 MHz, $CDCl_3$) δ_C 162.5 (CONH), 160.8 (C^1), 152.7 (py-C^2), 150.1 (py-C^6), 143.2 (Ph-C^i), 135.0 (C^4), 133.9 (C$^{3,3'}$), 128.9 (Ph-C), 127.6 (Ph-C), 126.4 (Ph-C) 125.7 (py-C^3), 124.2 (py-C^5), 114.4 (C$^{2,2'}$), 96.7 (C^5), 85.4 (C^6), 70.4 (py-CH_2), 55.5 (OCH_3), 49.1 (CHCH$_3$), 38.4 (OSO_2CH_3), 22.1 (CHCH_3).

(*S*)-(4-((4-Acetamidophenyl)ethynyl)-6-(1-phenylethylcarbamoyl)pyridin-2-yl)methyl methanesulfonate,

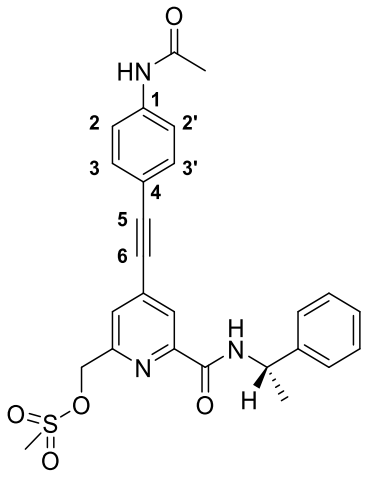

The title compound was obtained as a yellow oil (110 mg, 84%) according to the general mesylation procedure. TLC analysis R_f 0.51 (silica, 100 % EtOAc); ^{1}H NMR (295 K, 400 MHz, d^3-acetonitrile) δ_H 8.50 (1H, s, NHCOCH$_3$), 8.45 (1H, d, ^3J 8.5, CONH), 8.05 (1H, d, ^4J 2, py-H^5), 7.67 (1H, d, ^4J 2, py-H^3), 7.61 (2H, dt, ^3J 9, ^4J 2, Ar-H$^{3,3'}$), 7.52 (2H, dt, ^3J 9, ^4J 2, Ar-H$^{2,2'}$), 7.39-7.21 (5H, m, Ph-H), 5.33 (2H, s, py-CH$_2$), 5.18 (1H, dq, ^3J 8.5, ^3J 7, CHCH$_3$), 3.12 (3H, s, SO_2CH_3), 2.04 (3H, s, NHCOCH_3), 1.53 (3H, d, ^3J 7, CHCH_3); *m/z* (HRMS$^+$) 492.1594 [M+H]$^+$ ($C_{26}H_{26}N_3O_5S$ requires 492.1593).

6,6',6''-(1,4,7-Triazonane-1,4,7-triyl)tris(methylene)tris(N-((*S*)-1-phenylethyl)-4-(phenylethynyl)picolinamide), *S*-L[31a]

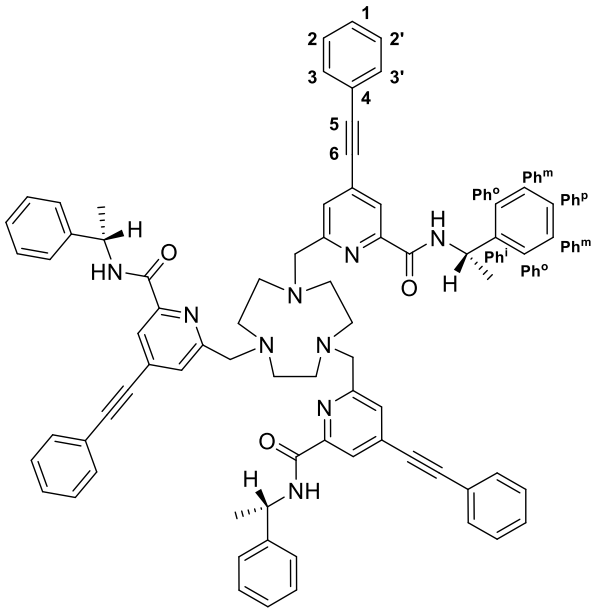

General alkylation procedure:

1,4,7-Triazacyclononane trihydrochloride (20 mg, 0.085 mmol) and the mesylate, (*S*)-(6-(1-phenylethylcarbamoyl)-4-(phenylethynyl)pyridin-2-yl)methyl methanesulfonate, (111 mg, 0.256 mmol) were dissolved in anhydrous CH_3CN (4.5 mL) and K_2CO_3 (71 mg, 0.512 mmol) was added. The mixture was stirred under argon at 78 °C. After 24 h the reaction was cooled and filtered to remove excess potassium salts. The solvent was removed under reduced pressure and the crude material purified by column chromatography (silica, gradient elution starting from 100% CH_2Cl_2 to 10% CH_3OH in CH_2Cl_2) to give ***S*-L[31a]** as a yellow glassy solid (35 mg, 36%). TLC analysis R_f 0.42 (silica, 5% CH_3OH in CH_2Cl_2); ^{1}H NMR (295 K, 600 MHz, $CDCl_3$) δ_H 8.21 (3H, br s, py-H^3), 7.51 (6H, d, ^3J 7, H$^{3,3'}$), 7.42-7.33 (15H, m, py-H^5, H^1, H$^{2,2'}$, Ph-H^o), 7.24 (6H, m, Ph-H^m), 7.16 (3H, t, ^3J 7.2, Ph-H^p), 5.34 (3H, q, ^3J 6.5, CHCH$_3$), 3.87 (6H, s, py-CH$_2$), 2.84 (12H, br s, *ring Hs*), 1.63 (9H, d, ^3J 6.5, CHCH$_3$); ^{13}C NMR (295 K, 150 MHz, $CDCl_3$) δ_C 163.1 (CONH), 159.4 (py-C^6), 149.8 (py-C^2), 143.3 (Ph-C^i), 133.4 (C^4), 132.1 (Ar-C), 129.5 (Ar-C), 128.7 (Ph-C^m), 127.4 (Ph-C^p), 127.1 (py-C^5), 126.4 (Ph-C^o), 122.9 (py-C^3), 122.0 (C^1), 94.8 (C^5), 86.8 (C^6), 64.1 (py-CH$_2$), 56.2 (*ring Cs*), 48.9 (CHCH$_3$), 21.9 (CHCH$_3$); *m/z* (HRMS$^+$) 1144.562 $[M+H]^+$ ($C_{75}H_{70}N_9O_3$ requires 1144.560).

Trimethyl 4,4',4''-(*S*,*S*)-6,6',6''-(1,4,7-triazonane-1,4,7-triyl)tris(methylene)tris(2-((*S*)-1-phenylethylcarbamoyl)pyridine-6,4-diyl)tris(ethyne-2,1-diyl)tribenzoate, *S*-L^{31b}

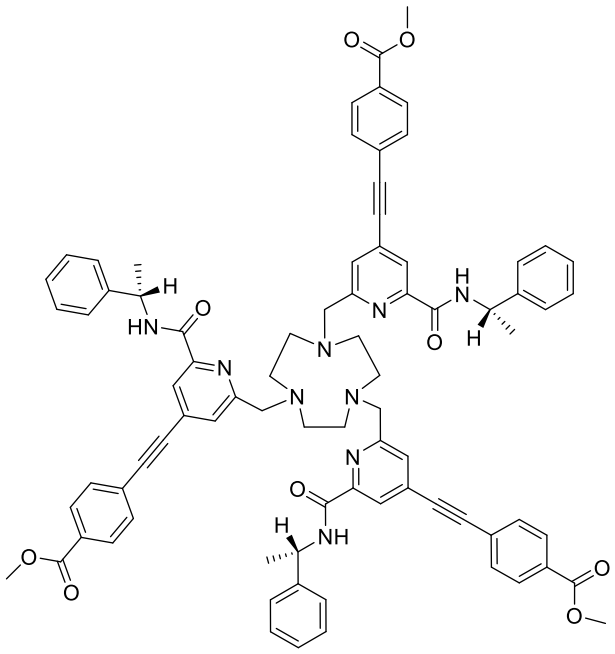

The compound ***S*-L^{31b}** was obtained as a yellow oil (58 mg, 55%) according to the general alkylation procedure. TLC analysis R_f 0.47 (silica, 5% CH_3OH in CH_2Cl_2); ^{1}H NMR (295 K, 700 MHz, $CDCl_3$) δ_H 8.41 (3H, d, ^3J 6, CONH), 8.17 (3H, br s, py-H^3), 8.02 (6H, d, ^3J 8.5, H$^{2,2'}$), 7.64 (3H, br s, py-H^5), 7.56 (6H, d, ^3J 8.5, H$^{3,3'}$), 7.38-7.36 (6H, m, Ph-H^o), 7.2-7.25 (6H, m, Ph-H^m), 7.20 (3H, t, ^3J 7, Ph-H^p), 5.33 (3H, dq, ^3J 6, ^3J 7, CHCH$_3$), 3.93 (9H, s, CO_2CH_3), 3.81 (6H, m, py-CH_2), 2.83 (12H, br s, *ring Hs*), 1.60 (9H, d, ^3J 7, CHCH_3); ^{13}C NMR (295 K, 175 MHz, $CDCl_3$) δ_C 166.4 (CO_2CH_3), 163.0 (CONH), 159.6 (py-C^6), 149.9 (py-C^2), 143.3 (Ph-C^i), 132.9 (C^4), 132.0 (C$^{3,3'}$), 130.7 (C^1), 129.8 (C$^{2,2'}$), 128.7 (Ph-C^m), 127.5 (Ph-C^p), 127.1 (py-C^5), 126.4 (Ph-C^o), 123.0 (py-H^3), 93.7 (C^5), 89.3 (C^6), 64.1 (py-CH_2), 56.1 (*ring Cs*), 52.5 (CO_2CH_3), 48.9 (CHCH$_3$), 21.9 (CHCH_3); *m/z* (HRMS$^+$) 1318.623 $[M+H]^+$ ($C_{78}H_{76}N_9O_6$ requires 1318.627).

6,6',6''-((1,4,7-Triazonane-1,4,7-triyl)tris(methylene))tris(4-((4-methoxyphenyl)ethynyl)-*N*-((*S*)-1-phenylethyl)picolinamide), *S*-L[31c]

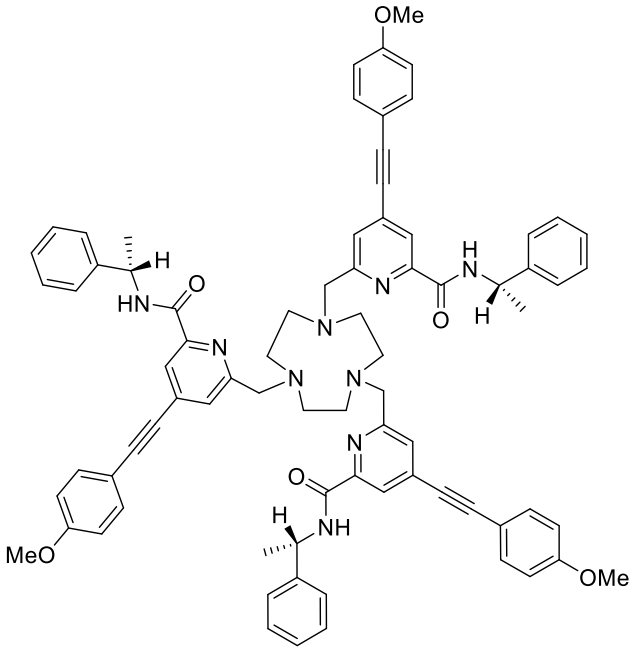

The compound ***S*-L[31c]** was obtained as a yellow oil (42 mg, 28%) according to the general alkylation procedure. TLC analysis R_f 0.68 (silica, 7% CH_3OH in CH_2Cl_2); ^1H NMR (295 K, 600 MHz, $CDCl_3$) δ_H 8.47 (3H, d, ^3J 8.5, CONH), 8.13 (3H, br s, py-H^3), 7.45 (6H, d, ^3J 9, $H^{3,3'}$), 7.38 – 7.18 (18H, m, Ph-H, py-H^5), 6.87 (6H, d, ^3J 9, $H^{2,2'}$), 5.33 (3H, dq, ^3J 8.5, ^3J 6.5 , CHCH$_3$), 3.82 (9H, s, OCH_3), 3.80-3.75 (6H, m, py-CH_2), 2.85-2.79 (12H, m, *ring Hs*), 1.60 (9H, d, ^3J 6.5, CHCH_3); ^{13}C NMR (295 K, 150 MHz, $CDCl_3$) δ_C 163.0 (CONH), 160.4 (C^1), 159.1 (py-C^6), 149.5 (py-C^2), 143.2 (Ph-C^i), 133.6 (C^4), 133.5 ($C^{3,3'}$), 128.5 (Ph-C), 127.2 (Ph-C), 126.7 (Ph-C), 126.2 (py-C^5), 122.6 (py-C^3), 114.2 ($C^{2,2'}$), 113.9 (py-C^4), 95.0 (C^5), 85.7 (C^6), 63.9 (py-CH_2), 56.0 (*ring Cs*), 55.3 (OCH_3), 48.7 (CHCH$_3$), 21.8 (CHCH_3); *m/z* (HRMS$^+$) 1234.592 $[M+H]^+$ ($C_{78}H_{76}N_9O_6$ requires 1234.592).

6,6',6''-(1,4,7-Triazonane-1,4,7-triyl)tris(methylene)tris(4-((4-acetamidophenyl)ethynyl)-N-((*S*)-1-phenylethyl)picolinamide), *S*-L^{31d}

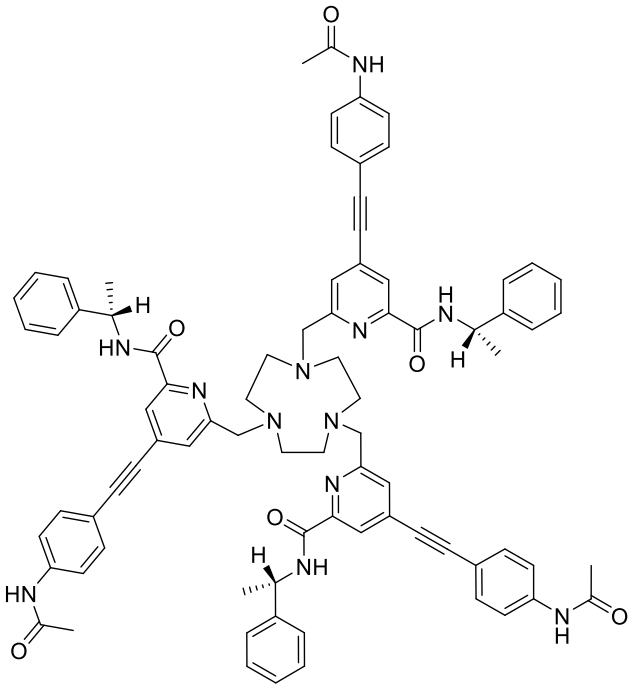

The compound ***S*-L^{31d}** was obtained as a yellow oil (50 mg, 43%) according to the general alkylation procedure. TLC analysis R_f 0.63 (silica, 15% CH_3OH in CH_2Cl_2); ^{1}H NMR (295 K, 600 MHz, CD_3OD) δ_H 7.94 (3H, s, py-H^3), 7.58 (6H, d, ^3J 8.5, H$^{3,3'}$), 7.54 (3H, s, py-H^5), 7.36-7.16 (21H, m, Ph-H, H$^{2,2'}$), 5.20 (1H, s, CHCH$_3$), 4.04 (6H, br s, py-CH$_2$), 3.02 (12H, br s, *ring Hs*), 2.10 (9H, s, NHCOCH$_3$), 1.53 (9H, d, ^3J 6.5, CHCH$_3$); ^{13}C NMR (295 K, 150 MHz, CD_3OD) δ_C 171.6 (NHCOCH$_3$), 164.7 (CONH), 151.4 (py-C^6), 144.4 (Ph-C^i), 141.5 (py-C^2), 135.4 (C^4), 133.8 (C$^{3,3'}$), 129.7 (Ph-C^o), 128.5 (py-C^5), 127.3 (Ph-C^m), 124.2 (py-C^4), 123.0 (py-C^3), 120.6 (C$^{2,2'}$), 117.6 (C^1), 86.6 (C^5), 79.1 (C^6), 64.6 (py-CH$_2$), 50.4 (CHCH$_3$), 24.1 (NHCOCH$_3$), 22.1 (CHCH$_3$); *m/z* (HRMS$^+$) 1315.621 [M+H]$^+$ ($C_{81}H_{76}N_{12}O_6$ requires 1315.624).

R*-L^{31d}** was synthesised in an analogous manner to the ***S series starting from *R*-(+)-α-methylbenzyl amine.

***S*-[Eu.L^{31a}](CF$_3$SO$_3$)$_3$**

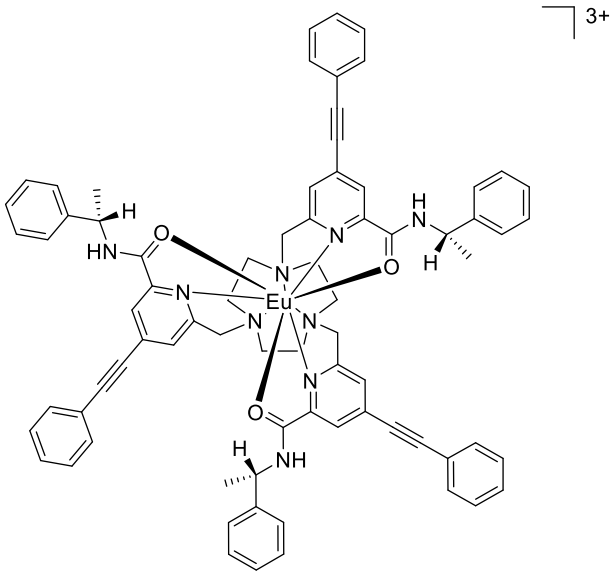

General complexation procedure:

Europium (III) triflate (9 mg, 0.015 mmol) was added to a solution of ligand, ***S*-L^{31a}**, (18 mg, 0.015 mmol) in anhydrous acetonitrile (2 mL) and the mixture heated at reflux for 20 h. The solution was concentrated under reduced pressure and cold diethyl ether (2 mL) was added dropwise to the solution. The resulting solid was isolated and dried under reduced pressure to yield ***S*-[Eu.L^{31a}](CF$_3$SO$_3$)$_3$** as a yellow glassy solid (10 mg, 50%). ^{1}H NMR (295 K, 200 MHz, CD$_3$OD) δ_H major diastereoisomer, partial assignment: 7.7 (pyCH'N), 7.6, 7.4, 7.1, 7.0, 5.9, 4.1, 3.5, 1.2 (CHC$\underline{H}_3$), 0.8, -1.5 (NCH$_{eq}$), -2.1 (NCH'$_{eq}$), -6.5 (NCH$_{ax}$); *m/z* (HRMS)$^+$ 1292.455 [M-2H]$^+$ (C$_{75}$H$_{67}$N$_9$O$_3$^{151}Eu requires 1292.456); ϕ_{em}(MeOH) = 0.08, ε(MeOH) = 69,000 M^{-1} cm^{-1}, τ(MeOH) = 0.80 ms; t$_R$ = 8.4 min (analytical HPLC, Table 23).

***S*-[Eu.L^{31b}](CF$_3$SO$_3$)$_3$**

The complex ***S*-[Eu.L^{31b}](CF$_3$SO$_3$)$_3$** was obtained according to the general complexation procedure, using the ligand ***S*-L^{31b}**, as a white solid (10 mg, 52%). ^{1}H NMR (295 K, 400 MHz, CD$_3$OD) δ_H major diastereoisomer, partial assignment: 8.2, 7.8, 7.4, 7.3, 7.0, 6.1, 5.1, 3.9, 1.2 (CHC$\underline{H}_3$), 0.8, -1.6 (NCH$_{eq}$), -2.5 (NCH'$_{eq}$), -6.7 (NCH$_{ax}$); *m/z* (HRMS$^+$) 734.7366 [M-H]$^{2+}$ (C$_{81}$H$_{72}$N$_9$O$_9$^{151}Eu requires 734.7418); ϕ_{em}(MeOH) = 0.03, ε(MeOH) = 63,000 M^{-1} cm^{-1}, τ(MeOH) = 0.81 ms; t$_R$ = 8.8 min (analytical HPLC, Table 23).

_S_-[Eu.L^{31c}] $(CF_3SO_3)_3$

The complex **_S_-[Eu.L^{31c}]$(CF_3SO_3)_3$** was obtained according to the general complexation procedure, using the ligand **_S_-L**^{2c}, as a white solid (20 mg, 70%). ^{1}H NMR (295 K, 400 MHz, CD_3OD) δ_H major diastereoisomer, partial assignment: 7.6 (pyCH'N), 7.5, 7.3, 7.1, 7.0, 6.7, 5.8, 4.2, 3.9, 3.5, 2.0 , 1.1 (CHC$\underline{H}_3$), -0.8 (pyCHN), -1.5 (NCH_{eq}), -2.0 (NCH'_{eq}), -6.5 (NCH_{ax}); *m/z* (HRMS$^+$) 1382.492 [M-2H]$^+$ ($C_{78}H_{73}N_9O_6{}^{151}$Eu requires 1382.488); ϕ_{em}(MeOH) = 0.04, ε(MeOH) = 65,000 M^{-1} cm^{-1}, τ(MeOH) = 0.49 ms; t_R = 8.4 min (analytical HPLC, Table 23).

_S_-[Eu.L^{31d}]$(CF_3SO_3)_3$

The complex **_S_-[Eu.L^{31d}]$(CF_3SO_3)_3$** was obtained according to the general complexation procedure, using the ligand **_S_-L^{31d}**, as a yellow glassy solid (8 mg, 72%). ^{1}H NMR (295 K, 200 MHz, CD_3OD) δ_H major diastereoisomer, partial assignment: 7.8, 7.6, 7.4, 7.1, 7.0, 6.9, 5.9, 4.1, 2.2, 1.2 (CHC$\underline{H}_3$), 0.7, -1.5 (NCH_{eq}), -2.2 (NCH'_{eq}), -6.6 (NCH_{ax}); *m/z* (HRMS$^+$) 1463.523 [M-2H]$^+$ ($C_{81}H_{76}N_{12}O_6{}^{151}$Eu) requires 1463.520); ϕ_{em}(MeOH) = 0.03, ε(MeOH) = 65,000 M^{-1} cm^{-1}, τ(MeOH) = 0.54 ms; t_R = 8.0 min (analytical HPLC, Table 23).

_R_-[Eu.L^{31d}]$(CF_3SO_3)_3$

The complex **_R_-[Eu.L^{31d}]$(CF_3SO_3)_3$** was obtained according to the general complexation procedure, using the ligand **_R_-L^{31d}**, as a yellow glassy solid (10 mg, 60%). ^{1}H NMR (295 K, 400 MHz, CD_3OD) δ_H major diastereoisomer, partial assignment: 7.8, 7.6, 7.4, 7.1, 7.0, 6.9, 5.9, 4.1, 2.2, 1.2 (CHC$\underline{H}_3$), 0.7, -1.5 (NCH_{eq}), -2.2 (NCH'_{eq}), -6.6 (NCH_{ax}); *m/z* (HRMS$^+$) 1463.523 [M-2H]$^+$ ($C_{81}H_{76}N_{12}O_6{}^{151}$Eu) requires 1463.521); t_R = 8.0 min (analytical HPLC, Table 23).

5.2.3. Achiral bis-amide and bis-carboxylate complexes and precursors

1,4-Bis(4-methoxybenzyloxycarbonyl)-1,4,7-triazacyclononane, CAS: 1417729-26-0

149

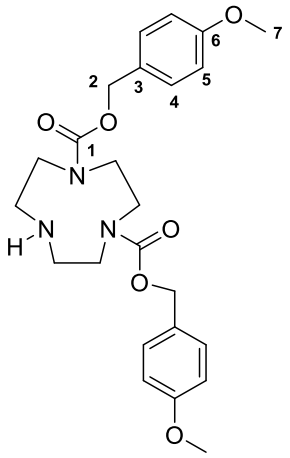

The hydrochloric salt of 1,4,7-triazacyclononane (1.00 g, 4.19 mmol) and 2-(4-methoxybenzyloxycarbonyloxyimino)-2-phenylacetonitrile (2.6 g, 8.38 mmol) were dissolved in a mixed dioxane:water solution (50 mL, 4:1, v/v). The resulting solution was stirred under argon at r.t. for 5 min before the addition of NEt_3 (2.9 mL, 20.53 mmol). The reaction mixture was stirred at r.t. for 24 h until completion was observed by TLC. The solvent was removed under reduced pressure and the residue was dissolved in CH_2Cl_2 (20 mL) and washed with brine (3 x 15 mL). The aqueous layer was re-extracted with CH_2Cl_2 (3 x 15 mL) and the organic layers were combined, dried over $MgSO_4$, filtered and concentrated under reduced pressure. The crude mixture was purified by flash column chromatography (silica, gradient elution starting from 100% CH_2Cl_2 to 10% CH_3OH in CH_2Cl_2) to give the title compound as a yellow oil (1.37 g, 72%). TLC analysis R_f 0.20 (silica, 6% CH_3OH in CH_2Cl_2); ^{1}H NMR (295 K, 400 MHz, $CDCl_3$) δ_H 7.34 – 7.27 (4H, m, $\underline{H}^4$), 6.90 – 6.87 (4H, m, $\underline{H}^5$), 5.11 – 5.05 (4H, m, $\underline{H}^2$), 3.82 (6H, s, $\underline{H}^7$), 3.58 – 3.48 (4H, m, *ring Hs*), 3.29 – 3.24 (4H, m, *ring Hs*), 2.93 – 2.79 (4H, m, *ring Hs*); ^{13}C NMR (295 K, 100 MHz, $CDCl_3$) δ_C 159.6, 156.7, 156.6, 130.0, 128.9, 114.0, 67.1, 55.4, 53.6, 52.8, 52.5, 52.2, 51.2, 50.3, 50.0, 49.2, 48.3, 48.2, 47.8, 47.7 (m, *ring Cs*); *m/z* ($HRMS^+$) 458.2275 $[M+H]^+$ ($C_{24}H_{32}N_3O_6$ requires 458.2291).

1,4-Bis(4-methoxybenzyloxycarbonyl)-7-(tert-butylcarbonate)-1,4,7-triazacyclononane, CAS: 1417729-28-2 [149]

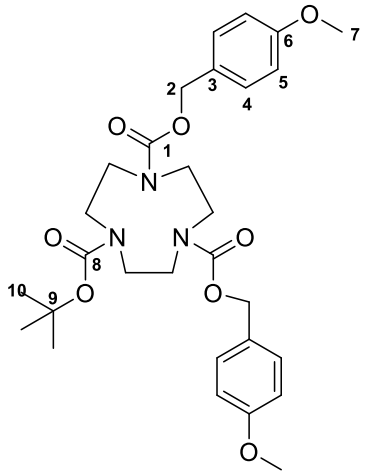

N-(tert-butoxycarbonyl)succinimide (0.935 g, 4.34 mmol) and 1,4-Bis(4-methoxybenzyloxycarbonyl)-1,4,7-triazacyclononane (1.33 g, 2.90 mmol) were dissolved in dry CH_2Cl_2 (40 mL) and the resulting mixture was stirred under argon at r.t. for 24 h. Upon reaction completion, the solution was washed with brine (3 x 25 mL). The aqueous layer was re-extracted with CH_2Cl_2 (3 x 25 mL) and the organic layers were combined, dried over $MgSO_4$, filtered and concentrated under vacuum. The crude material was purified by flash column chromatography (silica, gradient elution starting from 100% CH_2Cl_2 to 1% CH_3OH in CH_2Cl_2) to give the title compound as a colourless oil (1.03 g, 64%). TLC analysis R_f 0.63 (silica, 5% CH_3OH in CH_2Cl_2); ^{1}H NMR (295 K, 400 MHz, $CDCl_3$) δ_H 7.33 – 7.18 (4H, m, $\underline{H}^4$), 6.88 – 6.83 (4H, m, $\underline{H}^5$), 5.08 – 4.92 (4H, m, $\underline{H}^2$), 3.78 - 3.77 (6H, m, $\underline{H}^7$), 3.57 – 3.23 (*ring Hs*), 1.50 – 1.37 (9H, m, $\underline{H}^9$); ^{13}C NMR (295 K, 100 MHz, $CDCl_3$) δ_C 159.6, 156.5, 155.7, 129.9, 128.9, 113.9, 80.1 ($\underline{C}^9$), 67.1, 55.3, 53.8, 50.0, 49.9, 49.5, 49.2, 48.8, 48.7, 30.1, 20.4 ($\underline{C}^7$); *m/z* (HRMS$^+$) 558.2828 $[M+H]^+$ ($C_{29}H_{40}N_3O_8$ requires 228.2856).

Tert-butyl-1,4,7-triazacyclononane-1-carboxylate hydrochloride salt, CAS: 1417729-30-6 [149]

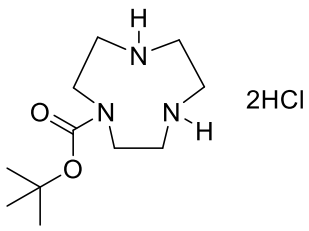

1,4-Bis(4-methoxybenzyloxycarbonyl)-7-(tert-butylcarbonate)-1,4,7-triazacyclononane (1.03 g, 1.85 mmol) was dissolved in 40 mL CH_3OH. Palladium hydroxide on carbon (*ca* 300 mg) was added slowly to the solution. The black mixture was hydrogenated at 4 atm. for 24 h. After reaction completion the mixture was filtered through celite and the solvent was removed under reduced pressure. The crude residue was redissolved in 10 mL CH_3OH and the apparent pH of the solution was lowered to pH 2 using a 1 M HCl solution. The solvent was removed under reduced pressure to give the title compound as a pale yellow solid (500 mg, 89%); ^{1}H NMR (295 K, 600 MHz, D_2O) δ_H 3.62 (4H, br s, *ring Hs*), 3.46 (4H, br s, *ring Hs*), 3.35 (4H, br s, *ring Hs*), 3.21 (9H, s, OCH($C\underline{H}_3$)$_3$); ^{13}C NMR (295 K, 150 Hz, D_2O) δ_C 156.8 ($\underline{C}O_2{}^t$Bu), 183.5 ($\underline{C}(CH_3)_3$), 47.0, 43.1, 42.9 (*ring Cs*), 27.4 (C($\underline{C}H_3$)$_3$); *m/z* (HRMS$^+$) 230.1873 $[M+H]^+$ ($C_{11}H_{24}N_3O_2$ requires 230.1869).

_N_-benzyl-6-(hydroxymethyl)-4-iodopicolinamide, 4b

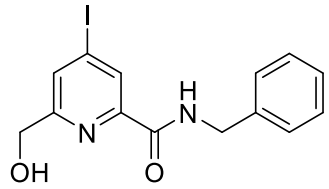

HOBt.H_2O (254 mg, 1.88 mmol), EDC (292 mg, 1.88 mmol), DIPEA (0.44 mL, 2.51 mmol) and benzylamine (0.15 mL, 1.38 mmol) were dissolved in anhydrous DMF (3 mL). The carboxylic acid, **3b**, (350 mg, 1.25 mmol in 1 mL DMF) was added slowly and dropwise to the solution and the mixture stirred at r.t. for 22 h under an argon atmosphere. The solvent was removed under reduced pressure, water was added to the crude residue and the mixture extracted with EtOAc (4 x 20 mL). The organic layers were combined and washed successively with water (1 x 20 mL) and brine (1 x 20 mL), dried over $MgSO_4$ and the solvent removed under reduced pressure. The crude mixture was purified by flash column chromatography (silica, gradient elution starting from 10% EtOAc in hexane to 50% EtOAc in hexane) to afford **4b** as a yellow oil (284 mg, 62%). TLC analysis R_f 0.35 (silica, 50% EtOAc in hexane); ^{1}H NMR (295 K, 400 MHz, $CDCl_3$) δ_H 8.48 (1H, s, py-$\underline{H}^3$), 8.22 (1H, s, CON$\underline{H}$), 7.91 (1H, s, py-$\underline{H}^5$), 7.34 – 7.27 (5H, m, Ph-$\underline{H}$), 4.72 (2H, s, py-$C\underline{H}_2$) , 4.64 (2H, d, ^3J 6, $C\underline{H}_2$Ph); ^{13}C NMR (295 K, 100 MHz, $CDCl_3$) δ_C 162.9 ($\underline{C}$ONH), 159.7 (py-$\underline{C}^6$), 149.2 (py-$\underline{C}^2$), 138.0 (Ph-$\underline{C}^i$), 132.6 (py-$\underline{C}^5$), 130.8 (py-$\underline{C}^3$), 128.9 (Ph-$\underline{C}^m$), 128.0 (Ph-$\underline{C}^p$), 127.8 (Ph-$\underline{C}^o$), 107.9 (py-$\underline{C}^4$), 64.3 (py-$\underline{C}H_2$), 43.7 ($\underline{C}H_2$Ph); *m/z* (HRMS$^+$) 390.9893 $[M+Na]^+$ ($C_{14}H_{13}N_2O_2Na^{127}I$ requires 390.9919).

_N_-benzyl-6-(hydroxymethyl)-4-((4-methoxyphenyl)ethynyl)picolinamide, 6b

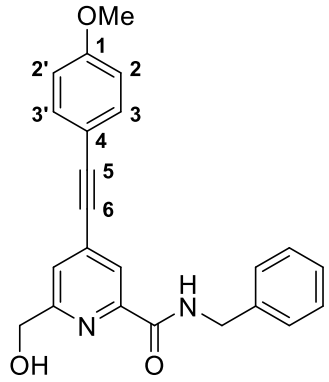

The compound **4b** (263 mg, 0.714 mmol) was dissolved in anhydrous THF (4 mL) and the solution was degassed (freeze-thaw cycle) three times. 4-Ethynyl anisole (140 μL, 1.07 mmol) and triethylamine (0.50 mL, 3.57 mmol) were added and the solution was degassed (freeze-thaw cycle) once more. [1,1-Bis(diphenylphosphino)ferrocene]dichloropalladium(II) (52 mg, 0.07 mmol) and CuI (27 mg, 0.143 mmol) were added and the resulting brown solution was stirred at 65 °C under argon for 24 h. The solvent was removed under reduced pressure and the pale brown solid was purified by column chromatography (silica, gradient elution starting from 100% CH_2Cl_2 to 2% CH_3OH in CH_2Cl_2 in 0.2% increments) to give the compound **4c** as an off white solid (210 mg, 80%). TLC analysis R_f 0.75 (silica, 7% CH_3OH in CH_2Cl_2); m.p. 152 – 153 °C; ^{1}H NMR (295 K, 700 MHz, $CDCl_3$) δ_H 8.23 (1H, br t, ^3J 6, CONH), 8.21 (1H, s, py-H^3), 7.53 (1H, s, py-H^5), 7.50 (2H, dt, ^4J 2, ^3J 8, H$^{3/3'}$), 7.37-7.34 (4H, m, Ph-H^o, Ph-H^m), 7.29 (1H, m, Ph-H^p), 6.91 (2H, dt, ^4J 2, ^3J 8, H$^{2/2'}$), 4.77 (2H, s, py-CH_2), 4.68 (2H, d, ^3J 6, CH_2Ph), 3.85 (3H, s, OCH_3); ^{13}C NMR (295 K, 175 MHz, $CDCl_3$) δ_C 163.7 (CONH), 160.7 (C^1), 158.7 (py-C^6), 149.2 (py-C^2), 138.2 (Ph-C^i), 134.6 (C^4), 133.8 (C$^{3,3'}$), 128.9 (Ph-C), 128.0 (Ph-C), 127.8 (Ph-C), 124.7 (py-C^5), 123.5 (py-C^3), 114.4 (C$^{2,2'}$), 114.0 (py-C^4), 96.1 (C^5), 85.6 (C^6), 64.6 (py-CH_2), 55.5 (OCH_3), 43.7 (CH_2Ph); *m/z* (HRMS$^+$) 373.1561 $[M+H]^+$ ($C_{23}H_{21}N_2O_3$ requires 373.1552).

(6-(Benzylcarbamoyl)-4-((4-methoxyphenyl)ethynyl)pyridin-2-yl)methyl methanesulfonate, 4d

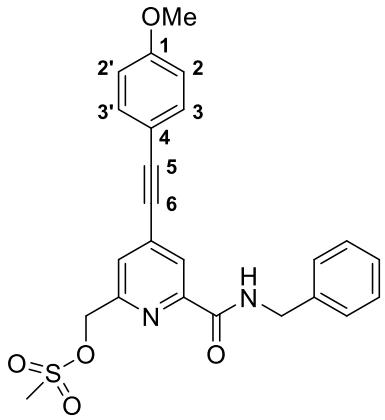

The alcohol **4c** (201 mg, 0.54 mmol) was dissolved in anhydrous THF (4 mL) and NEt_3 (0.26 mL, 1.89 mmol) was added. The mixture was stirred at 5 °C (ice / water bath) and methanesulfonyl chloride (0.06 mL, 0.81 mmol) was added. The reaction was allowed to warm to r.t. and stirred under argon for 30 min. The solvent was removed under reduced pressure and the residue dissolved in CH_2Cl_2 (20 mL) and washed with brine (20 mL). The aqueous layer was re-extracted with CH_2Cl_2 (3 x 20 mL) and the organic layers were combined, dried over $MgSO_4$, filtered and the solvent removed under reduced pressure to yield the compound **4d**, as a bright yellow oil (254 mg), which was used directly in the next step without further purification. TLC analysis R_f 0.72 (silica, 100% EtOAc); ^{1}H NMR (295 K, 700 MHz, $CDCl_3$) δ_H 8.27 (1H, d, ^3J 1.5, py-$\underline{H}^5$), 8.26 (1H, t, ^3J 6, CON$\underline{H}$), 7.63 (1H, d, ^3J 1.5, py-$\underline{H}^3$), 7.51 (2H, dt, ^4J 2.5, ^3J 9, $\underline{H}^{3/3'}$), 7.37 – 7.29 (5H, m, Ph-$\underline{H}$), 6.92 (2H, dt, ^4J 2.5, ^3J 9, $\underline{H}^{2/2'}$), 5.30 (2H, s, py-C$\underline{H}_2$), 4.68 (2H, d, ^3J 6, C$\underline{H}_2$Ph), 3.85 (3H, s, OC$\underline{H}_3$), 3.07 (3H, s, $SO_2C\underline{H}_3$); *m/z* (HRMS$^+$) 451.1320 $[M+H]^+$ ($C_{24}H_{23}N_2O_5S$ requires 451.1328).

Tert-butyl - 4,7-bis((6-(benzylcarbamoyl)-4-((4-methoxyphenyl)ethynyl)pyridin-2-yl)methyl)-1,4,7-triazonane-1-carboxylate, 4e

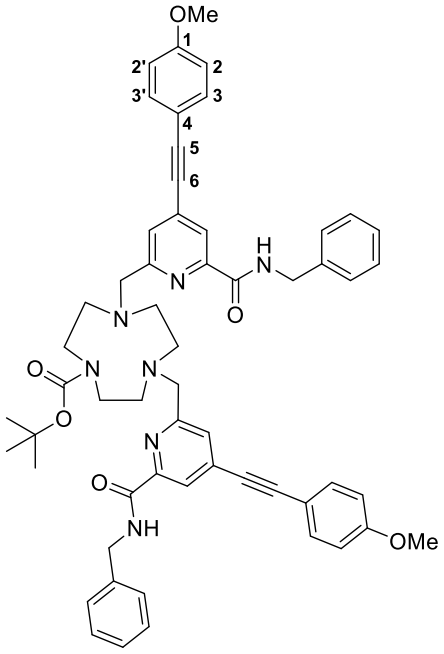

Tert-butyl-1,4,7-triazacyclononane-1-carboxylate dihydrochloride (82 mg, 0.27 mmol) and the mesylate, **4d**, (243 mg, 0.54 mmol) were dissolved in anhydrous CH_3CN (10 mL) and K_2CO_3 (149 mg, 1.08 mmol) was added. The mixture was stirred under argon at 78 °C. After 24 h the reaction was cooled and filtered to remove excess potassium salts. The solvent was removed under reduced pressure and the crude material purified by column chromatography (silica, gradient elution starting from 100% CH_2Cl_2 to 5% CH_3OH in CH_2Cl_2 in 0.2% increments) to give the *tert*-butoxycarbonyl protected ligand, **4e,** as a yellow oil (170 mg, 67%). TLC analysis R_f 0.39 (silica, 5% CH_3OH in CH_2Cl_2); ^{1}H NMR (295 K, 700 MHz, $CDCl_3$) δ_H 8.44 (1H, t, ^3J 6.5, CONH), 8.39 (1H, t, ^3J 6.5, CONH'), 8.17 (1H, s, py-H^5), 8.16 (1H, s, py-H$^{5'}$), 7.64 (1H, s, py-H^3), 7.57 (1H, s, py-H$^{3'}$), 7.48 (4H, d, ^3J 9, H$^{3/3'}$), 7.35-7.24 (10H, m, Ph-H), 6.89 (4H, d, ^3J 9, H$^{2/2'}$), 4.65 (4H, d, ^3J 6.5, CH_2Ph), 3.83 (6H, s, OCH_3), 3.82 (4H, s, py-CH_2), 3.31-3.26 (4H, m, *ring Hs*), 3.05-2.96 (4H, m, *ring Hs*), 2.68-2.62 (4H, m, *ring Hs*), 1.45 (9H, s, O(CH_3)$_3$); ^{13}C NMR (295 K, 175 MHz, $CDCl_3$) δ_C 164.1 (CONH), 164.0 (CONH), 160.6 (C^1), 160.5 (py-C^2), 159.3 (py-C$^{2'}$), 149.5 (py-C^6), 149.3 (py-C$^{6'}$), 138.4 (Ph-C^i), 138.3 (Ph-C^i), 138.4 (C^4), 138.3 (C$^{3/3'}$), 133.8 (Ph-C), 133.7 (Ph-C), 128.8 (Ph-C), 128.7 (Ph-C), 128.0 (py-C^3), 127.9 (py-C$^{3'}$), 122.8 (py-C^5), 122.7 (py-C$^{5'}$), 114.3 (C$^{2/2'}$), 114.1 (py-C^4), 114.0 (py-C$^{4'}$), 95.4 (C^5), 95.1 (C$^{5'}$), 85.9 (C^6), 85.8 (C$^{6'}$), 62.9 (py-CH_2), 56.3 (*ring C*), 55.4 (OCH_3), 54.9 (*ring C*), 54.5 (*ring C*), 53.9 (*ring C*), 50.1 (*ring C*), 49.6 (*ring C*), 43.6 (CH_2Ph), 43.5 (CH_2Ph), 28.7 (O(CH_3)$_3$); *m/z* (HRMS$^+$) 938.4594 $[M+H]^+$ ($C_{57}H_{60}N_7O_6$ requires 938.4605).

6,6'-((1,4,7-triazonane-1,4-diyl)bis(methylene))bis(*N*-benzyl-4-((4-methoxyphenyl)ethynyl)picolinamide), L[38]

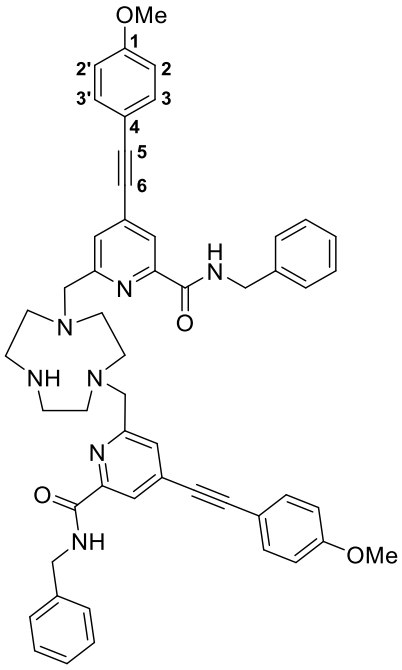

Tert-butoxycarbonyl-protected ligand, **4e**, (60 mg, 0.064 mmol) was dissolved in anhydrous CH_2Cl_2 (3 mL) and trifluoroacetic acid (0.6 mL) was added. The solution was stirred under argon at 23 °C for 30 min. TLC (silica, 10 % CH_3OH in CH_2Cl_2, R_f(product) 0.25, R_f (reactant) 0.61) was used to confirm removal of the tert-butoxycarbonyl group. The solvent was removed under reduced pressure and the residue re-dissolved in CH_2Cl_2 (2 mL). This process was repeated 5 times to ensure removal of excess trifluoroacetic acid. The crude residue was purified by preparative HPLC (Table 24, t_R = 14.6 min) to give **L[38]** as a white solid (41 mg, 72%). TLC analysis R_f 0.25 (silica, 10% CH_3OH in CH_2Cl_2); m.p. 156-158 °C; ^{1}H NMR (295 K, 700 MHz, $CDCl_3$) δ_H 7.92 (2H, s, py-H^3), 7.63 (2H, s, py-H^5), 7.38 (4H, d, ^3J 8.5, H$^{3/3'}$), 7.32-7.21 (10H, m, Ph-H), 6.91 (4H, d, ^3J 8.5, H$^{2/2'}$), 4.59 (4H, s, CH_2Ph), 3.95 (4H, s, py-CH_2), 3.78 (6H, s, OCH_3), 3.06 (4H, m, *ring Hs*), 2.93 (4H, m, *ring Hs*), 2.74 (4H, m, *ring Hs*); ^{13}C NMR (295 K, 175 MHz, $CDCl_3$) δ_C 116.0 (CONH), 162.3 (C^1), 159.9 (py-C^6), 151.1 (py-C^2), 139.7 (Ph-C^i), 135.4 (C^4), 134.6 (C$^{3/3'}$), 129.7 (Ph-C), 128.7 (Ph-C), 128.5 (Ph-C), 128.0 (py-C^5), 123.8 (py-C^3), 115.4 (C$^{2/2'}$), 114.7 (py-C^4), 96.8 (C^5), 86.0 (C^6), 61.5 (py-CH_2), 55.9 (OCH_3), 51.6 (*ring C*), 45.1 (*ring C*), 44.3 (CH_2Ph); *m/z* (HRMS$^+$) 838.4083 $[M+H]^+$ ($C_{52}H_{52}N_7O_4$ requires 838.4081).

[Eu.L^{38}](CF$_3$SO$_3$)$_3$

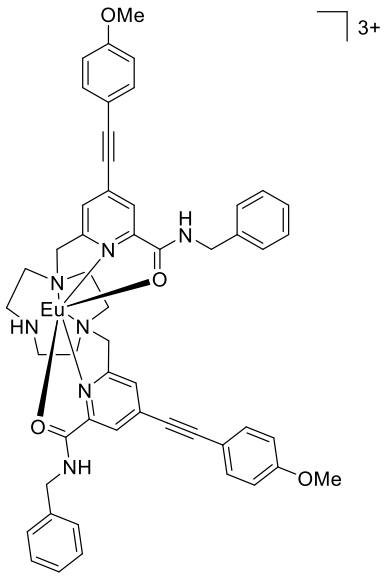

The deprotected ligand, **L^{38}**, was subjected to ion exchange chromatography to remove any formate present (from HPLC purification). The ligand (4 mg, 0.005 mmol) was dissolved in CH_3OH and $[Eu.(CF_3SO_3)]_3$ (3 mg, 0.005 mmol) was added. The solution was stirred at 60 °C for 24 h. The solvent was removed under reduced pressure to give a white solid which was used directly without any further purification. ESI$^+$ (MeCN no column) *m/z* 1285.4 $[M+2(CF_3SO_3)]^+$, 569.9 $[M+(CF_3SO_3)]^{2+}$; λ_{exc} (MeOH) = 348 nm; ϕ_{em} (MeOH) 0.02, ε (MeOH) 40,000 $M^{-1}cm^{-1}$, τ (H_2O) = 0.26 ms, τ (D_2O) = 0.43 ms, q = 1.3.

4-Iodo-3,5-dimethylanisole, 5a, CAS: 90609-47-5

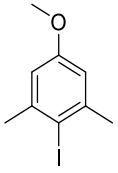

4-Iodo-3,5-dimethylphenol (1.00 g, 4.03 mmol) was dissolved in acetone (10 mL). K_2CO_3 (0.724 g, 5.24 mmol) and iodomethane (0.75 mL, 12.1 mmol) were added and the reaction was heated to reflux and stirred under argon for 24 h. The mixture was filtered to remove the potassium salts and the solvent was removed under reduced pressure. The residue was dissolved in CH_2Cl_2 (50 mL) and washed with water (50 mL). The aqueous layer was extracted into CH_2Cl_2 (3 x 50 mL) and the organic layers were combined, dried over $MgSO_4$, filtered and the solvent removed under reduced pressure. The crude solid was purified by flash column chromatography (silica, 2% CH_2Cl_2 in hexane) to yield **5a** as a

white crystalline solid (1.01 g, 87%). TLC analysis R_f 0.23 (silica, 4% CH_2Cl_2 in hexane); m.p. 36-37 °C (lit. 33-34 °C)[224]; ^{1}H NMR (295 K, 400 MHz, $CDCl_3$) δ_H 6.67 (2H, s, Ar-H), 3.77 (3H, s, OCH_3), 2.45 (6H, s, CH_3); ^{13}C NMR (295 K, 100 MHz, $CDCl_3$) δ_C 159.3 (Ar-C^1), 143.0 (Ar-C), 113.0 (Ar-C), 97.2 (Ar-C), 55.4 (OCH_3), 29.9 (CH_3); *m/z* (HRMS$^+$) 261.9849 ($C_9H_{11}{}^{127}IO$ requires 261.9855). CHN% Found: C, 41.38; H, 4.17; N, 0.09% ($C_9H_{11}{}^{127}IO$ requires C, 41.24; H, 4.23; N, 0.00%).

((4-Methoxy-2,6-dimethylphenyl)ethynyl)trimethylsilane, 5b

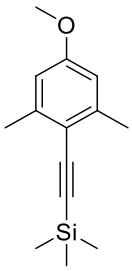

4-Iodo-3,5-dimethylanisole (703 g, 2.68 mmol) was dissolved in anhydrous THF (9 mL) and the solution was degassed (freeze-thaw cycle) three times. Ethynyl trimethylsilane (1.33 mL, 9.39 mmol) and triethylamine (1.87 mL, 13.4 mmol) were added and the solution was degassed (freeze-thaw cycle) once more. [1,1-Bis(triphenylphosphine)] palladium(II) dichloride (188 mg, 0.268 mmol) and CuI (102 mg, 0.536 mmol) were added and the resulting brown solution was stirred at 55 °C under argon for 48 h. The solvent was removed under reduced pressure and the resulting brown oil was purified by column chromatography (silica, gradient elution starting from 100% hexane to 6% CH_2Cl_2 in hexane in 0.2% increments) to give **5b** as a bright yellow oil (410 mg, 66%). TLC analysis R_f 0.19 (silica, 10% CH_2Cl_2 in hexane); ^{1}H NMR (295 K, 400 MHz, $CDCl_3$) δ_H 6.57 (2H, s, Ar-H), 3.77 (3H, s, OCH_3), 2.41 (6H, s, CH_3), 0.25 (9H, s, $Si(CH_3)_3$); ^{13}C NMR (295 K, 100 MHz, $CDCl_3$) δ_C 159.2 (Ar-C^4), 142.6 (Ar-C), 113.1 (Ar-C), 112.5 (Ar-C), 103.1 (alkyne C), 101.0 (alkyne C), 55.3 (OCH_3), 21.4 (CH_3), 0.40 ($Si(CH_3)_3$); *m/z* GC-EI t_R = 4.47 min, 232.1 (M^+), 217.1 (M^+ - CH_3).

2-Ethynyl-5-methoxy-1,3-dimethylbenzene, 5c [225]

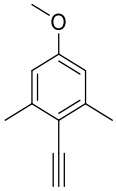

The protected alkyne **5b** (400 mg, 1.72 mmol) was dissolved in dry THF (7 mL) and triethylamine trihydrofluoride (2.80 mL, 17.2 mmol) was added. The solution was stirred at 30 °C under argon for 72 h. The solvent was removed under reduced pressure and the crude residue was purified by flash column chromatography (silica, gradient elution starting from 100% hexane to 2% CH_2Cl_2 in hexane in 0.2% increments) to give the compound, **5c**, as a yellow oil (154 mg, 56%). TLC analysis R_f 0.19 (silica, 10% CH_2Cl_2 in hexane); ^{1}H NMR (295 K, 400 MHz, $CDCl_3$) δ_H 6.60 (2H, s, Ar-H), 3.79 (3H, s, OCH_3), 3.43 (1H, s, alkyne H), 2.44 (6H, s, $2CH_3$); ^{13}C NMR (295 K, 100 MHz, $CDCl_3$) δ_C 159.3 (Ar-C^5), 142.8 (Ar-C), 144.4 (Ar-C), 112.5 (Ar-C), 83.9 (alkyne C), 81.4 (alkyne C), 55.3 (OCH_3), 21.4 ($2CH_3$); *m/z* GC-EI t_R = 3.75 min, 160.1 (M^+), 145.1 (M^+ - CH_3).

Methyl 6-(hydroxymethyl)-4-((4-methoxy-2,6-dimethylphenyl)ethynyl)picolinate, 5d [171]

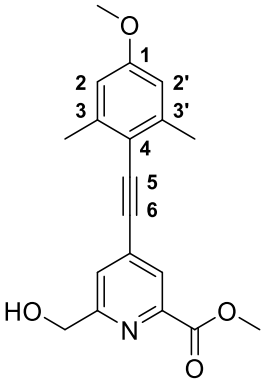

Methyl 6-(hydroxymethyl)-4-iodopicolinate, **3a,** (210 mg, 0.717 mmol) was dissolved in anhydrous THF (5 mL) and the solution was degassed (freeze-pump-thaw cycle) three times. The alkyne, **5c**, (138 mg, 0.860 mmol) and triethylamine (0.50 mL, 3.59 mmol) were added and the solution was degassed (freeze-pump-thaw cycle) once more. [1,1-Bis(diphenylphosphino)ferrocene]dichloropalladium(II) (52 mg, 0.072 mmol) and CuI (27 mg, 0.143 mmol) were added and the resulting brown solution was stirred at 65 °C under argon for 48 h. The solvent was removed under reduced pressure and the resulting

brown oil was purified by column chromatography (silica, gradient elution starting from 100% hexane to 50% EtOAc in hexane in 10% increments) to give the compound **5d** as a white solid (164 mg, 70%). TLC analysis R_f 0.31 (silica, 100% EtOAc); m.p. 177 – 179 °C; ^{1}H NMR (295 K, 700 MHz, $CDCl_3$) δ_H 8.05 (1H, s, py-H^3), 7.58 (1H, s, py-H^5), 6.63 (2H, s, H$^{2,2'}$), 4.86 (2H, s, py-CH_2), 4.01 (3H, s, CO_2CH_3), 3.80 (3H, s, OCH_3), 2.49 (6H, s, CH_3); ^{13}C NMR (295 K, 175 MHz, $CDCl_3$) δ_C 165.5 (CO_2CH_3), 160.6 (C^1), 160.2 (py-C^6), 147.3 (C^4), 143.1 (py-C^2), 134.4 (C$^{3,3'}$), 125.5 (py-C^3), 125.2 (py-C^5), 114.0 (py-C^4), 112.8 (C$^{2,2'}$), 94.0 (C^5), 93.3 (C^6), 64.7 (py-CH_2), 55.3 (OCH_3), 53.1 (CO_2CH_3), 21.5 (CH_3); *m/z* (HRMS$^+$) 326.1378 $[M+H]^+$ ($C_{19}H_{20}NO_4$ requires 326.1392).

Methyl 4-((4-methoxy-2,6-dimethylphenyl)ethynyl)-6-(((methylsulfonyl)oxy)methyl)picolinate, 5e [171]

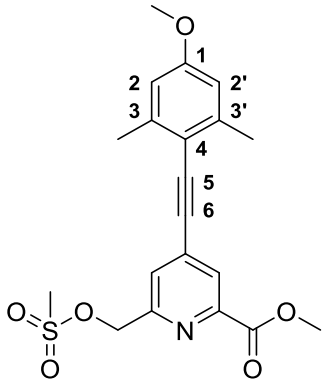

The alcohol **5d** (89 mg, 0.274 mmol) was dissolved in anhydrous THF (3 mL) and NEt_3 (0.13 mL, 0.959 mmol) was added. The mixture was stirred at 5 °C (ice / water bath), methanesulfonyl chloride (30 µL, 0.411 mmol) was added and the reaction was allowed to warm to r.t. and stirred under argon for 30 min. The solvent was removed under reduced pressure and the residue dissolved in EtOAc (15 mL) and washed with water (15 mL). The aqueous layer was re-extracted with EtOAc (3 x 15 mL) and the organic layers were combined, dried over $MgSO_4$, filtered and the solvent removed under reduced pressure to yield the mesylate **5e**, as a bright yellow oil (107 mg, 97%), which was used directly in the next step without further purification. TLC analysis R_f 0.63 (silica, 100% EtOAc); ^{1}H NMR (295 K, 400 MHz, $CDCl_3$) δ_H 8.06 (1H, s, py-H^3), 7.62 (1H, s, py-H^5), 6.58 (2H, s, H$^{2,2'}$), 5.37 (2H, s, py-CH_2OSO_2), 3.97 (3H, s, CO_2CH_3), 3.75 (3H, s, OCH_3), 3.14 (3H, s, SO_2CH_3), 2.44 (6H, s, CH_3); *m/z* (HRMS$^+$) 404.1170 $[M+H]^+$ ($C_{20}H_{22}NO_6S$ requires 404.1168).

Methyl 4-(mesitylethynyl)-6-((4-((4-((4-methoxy-2,6-dimethylphenyl)ethynyl)-6-(methoxycarbonyl)pyridin-2-yl)methyl)-1,4,7-triazonan-1-yl)methyl)picolinate, L[39]

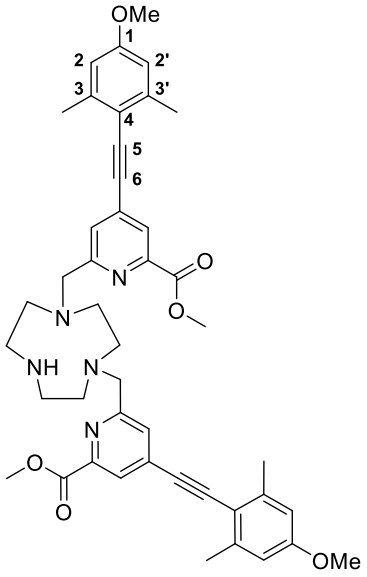

1,4,7-Triazacyclononane trihydrochloride (113 mg, 0.474 mmol) and the mesylate, **5e**, (363 mg, 0.901 mmol) were dissolved in anhydrous CH_3CN (30 mL) and K_2CO_3 (197 mg, 1.42 mmol) was added. The mixture was stirred under argon at 60 °C and carefully monitored by LC-MS. After 1 h significant formation on the bis-alkylated product was observed and the reaction was cooled and filtered to remove excess potassium salts. The solvent was removed under reduced pressure and the crude material purified by column chromatography (silica, gradient elution starting from 100% CH_2Cl_2 to 10% CH_3OH in CH_2Cl_2 in 1 % increments) to give **L[39]** as a yellow glassy solid (183 mg, 52%). TLC analysis R_f 0.18 (silica, 10% CH_3OH in CH_2Cl_2); ^{1}H NMR (295 K, 700 MHz, $CDCl_3$) δ_H 9.48 (1H, br s, ring NH), 7.91 (2H, s, py-H^3), 7.43 (2H, s, py-H^5), 6.59 (4H, s, H$^{2,2'}$), 4.03 (6H, s, CO_2CH_3), 4.02 (4H, s, py-CH_2), 3.74 (6H, s, OCH_3), 3.48 (4H, br s, *ring Hs*), 3.06 (4H, br s, *ring Hs*), 2.81 (4H, s, *ring Hs*), 2.42 (12H, s, CH_3); ^{13}C NMR (295 K, 175 MHz, $CDCl_3$) δ_C 165.2 (CO_2CH_3), 160.2 (C^1), 159.4 (py-C^6), 147.6 (C^4), 134.5 (C$^{3,3'}$), 126.9 (py-C^5), 125.7 (py-C^3), 113.8 (py-C^4), 112.8 (C$^{2,2'}$), 94.2 (C^5), 92.8 (C^6), 60.3 (py-CH_2), 55.3 (OCH_3), 53.9 (*ring Cs*), 53.6 (CO_2CH_3), 50.5 (*ring Cs*), 46.2 (*ring Cs*), 21.4 (CH_3); *m/z* (HRMS$^+$) 744.3765 $[M+H]^+$ ($C_{44}H_{50}N_5O_6$ requires 744.3761).

[Eu.L^{39}]Cl

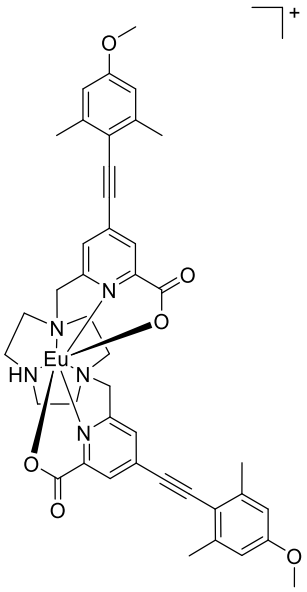

An aqueous solution of sodium hydroxide 0.1 M (0.5 mL) was added to a solution ligand **L^{39}** (10 mg, 13.4 µmol) in methanol (0.5 mL). The mixture was stirred at 65 °C for 4 h. The reaction was monitored by LC-MS. Upon completion, aqueous hydrochloric acid (0.1 M) was added until pH 6.5 was achieved. Europium chloride hexahydrate (5 mg, 15 µmol) was added and the pH was readjusted to 6.5 by addition of aqueous sodium hydroxide (0.1 M). The reaction was stirred at 65 °C for 24 h. The solvent was removed under reduced pressure to give the complex [Eu.**L^{39}**]Cl as a white solid (5 mg, 43%); *m*/*z* (HRMS^{+}) 864.2371 M^{+} ($C_{42}H_{43}N_5O_6{}^{151}Eu$ requires 864.2412); λ_{exc} (MeOH) = 352 nm; ϕ_{em} (MeOH) 0.20, ε (MeOH) 35,000 $M^{-1}cm^{-1}$, τ (H_2O) = 0.27 ms, τ (D_2O) = 0.38 ms, q = 0.9.

Trimethyl 6,6',6''-((1,4,7-triazonane-1,4,7-triyl)tris(methylene))tris(4-((4-methoxy-2,6-dimethylphenyl)ethynyl)picolinate), L^{35} [171]

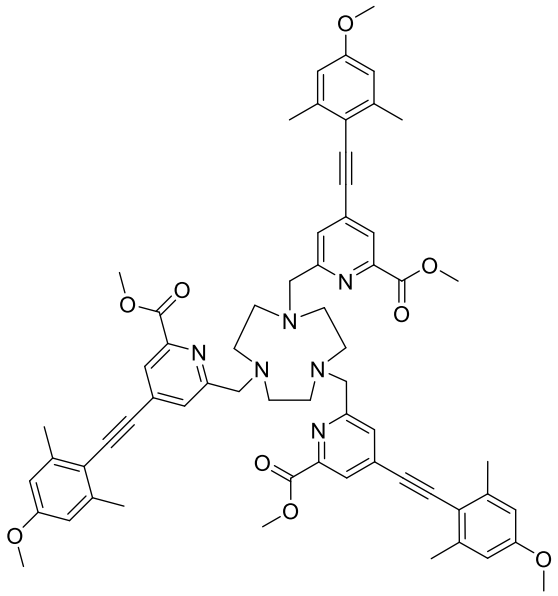

The compound $\mathbf{L^{35}}$ was obtained as a yellow solid (20%) according to the alkylation procedure used for $\mathbf{L^{39}}$. TLC analysis R_f 0.18(silica, 10% CH_3OH in CH_2Cl_2); ^{1}H NMR (295 K, 400 MHz, $CDCl_3$) δ_H 7.96 (3H, s, py-$\underline{H}^3$), 7.68 (3H, s, py-$\underline{H}^5$), 6.61 (6H, s, $\underline{H}^{2,2'}$), 4.39 (6H, s, py-C$\underline{H}_2$), 3.90 (9H, s, $CO_2C\underline{H}_3$), 3.79 (9H, s, $OC\underline{H}_3$), 3.37 (12 H, br s, *ring Hs*), 2.46 (18H, s, C$\underline{H}_3$); ^{13}C NMR (295 K, 100 MHz, $CDCl_3$) δ_C 164.9 ($\underline{C}O_2CH_3$), 160.4 ($\underline{C}^1$), 159.5 (py-$\underline{C}^6$), 147.7 ($\underline{C}^4$), 143.2 (py-$\underline{C}^2$), 134.6 ($\underline{C}^{3,3'}$), 127.7 (py-$\underline{C}^5$), 125.8 (py-$\underline{C}^3$), 113.7 (py-$\underline{C}^4$), 112.8 ($\underline{C}^{2,2'}$), 94.8 ($\underline{C}^5$), 92.9 ($\underline{C}^6$), 60.6 (py-$\underline{C}H_2$), 57.4 (*ring Cs*), 55.3 ($OC\underline{H}_3$), 53.1 ($CO_2C\underline{H}_3$), 21.6 ($\underline{C}H_3$); *m/z* (HRMS$^+$) 1051.499 $[M+H]^+$ ($C_{63}H_{67}N_6O_9$ requires 1051.497).

[Eu.L^{35}] [171]

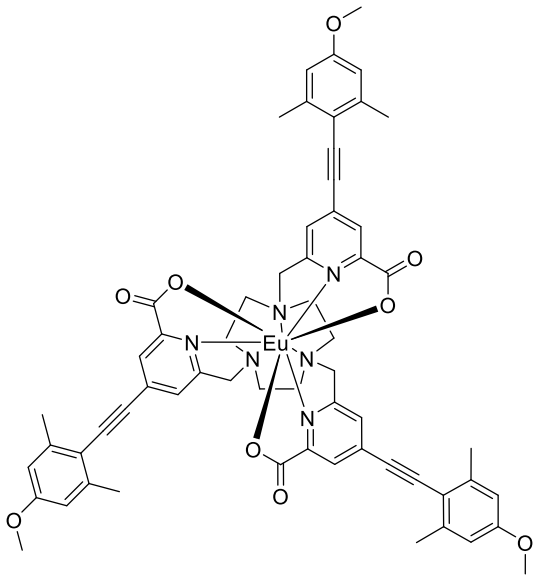

An aqueous solution of sodium hydroxide 0.1 M (0.5 mL) was added to a solution ligand **L^{5}** (11 mg, 10.5 µmol) in methanol (0.5 mL). The mixture was stirred at 65 °C for 4 h. The reaction was monitored by LC-MS. Upon completion, aqueous hydrochloric acid (0.1 M) was added until pH 6.5 was achieved. Europium chloride hexahydrate (4 mg, 11.6 µmol) was added and the pH was readjusted to 6.5 by addition of aqueous sodium hydroxide (0.1 M). The reaction was stirred at 65 °C for 24 h. The solvent was removed under reduced pressure and the resulting solid was purified by flash column chromatography (silica, 100% CH_2Cl_2 to 15% CH_3OH in CH_2Cl_2) to give the complex [Eu.**L^{35}**]Cl as a white solid (8 mg, 66%); *m*/*z* (HRMS$^+$) 1159.349 $[M+H]^+$ ($C_{60}H_{57}N_6O_9{}^{151}Eu$ requires 1159.349); λ_{exc} (MeOH) = 352 nm; ϕ_{em} (MeOH) 0.45, ε (MeOH) 60,000 $M^{-1}cm^{-1}$, τ (MeOH) = 0.90 ms.

Dimethyl 6,6'-((7-benzyl-1,4,7-triazonane-1,4-diyl)bis(methylene))bis(4-((4-methoxy-2,6-dimethylphenyl)ethynyl)picolinate), L[40]

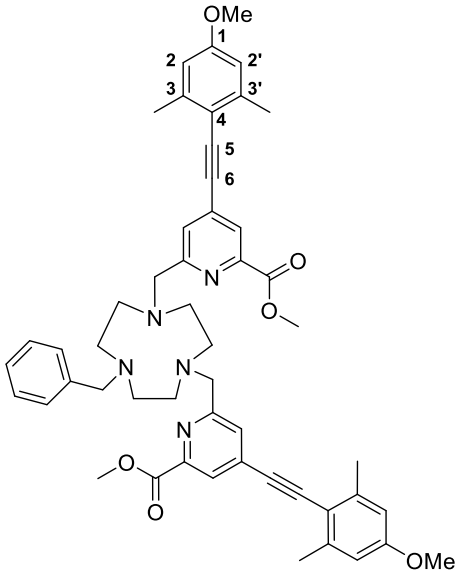

The bis-alkylated ligand, **L[39]** (25 mg, 0.034 mmol) and K_2CO_3 (4 mg, 0.034 mmol) were dissolved in anhydrous CH_3CN (2 mL). Benzyl bromide (6 mg, 0.034 mmol) was added dropwise at room temperature over 15 minutes. The mixture was stirred under argon at 40 °C and monitored by LC-MS. After 3 h the reaction was cooled and filtered to remove excess potassium salts. The solvent was removed under reduced pressure and the crude material purified by column chromatography (alumina, 100% CH_2Cl_2) to give **L[40]** as a yellow glassy solid (17 mg, 60%). TLC analysis R_f 0.52 (alumina, 2% CH_3OH in CH_2Cl_2); ^{1}H NMR (295 K, 700 MHz, MeOD) δ_H 7.95 (2H, s, py-H^3), 7.58 – 7.43 (7H, m, Bn-H, py-H^5),6.64 (4H, s, H$^{2,2'}$), 3.99 (4H, s, py-CH$_2$), 3.92 (6H, s, CO_2CH_3), 3.78 (6H, s, OCH_3), 3.66 (4H, br s, *ring Hs*), 3.06 (4H, br s, *ring Hs*), 2.91 (2H, s, CH_2Ph), 2.42 (12H, s, CH_3) ; ^{13}C NMR (295 K, 175 MHz, $CDCl_3$) δ_C 165.7 (CO_2CH_3), 160.2 (C^1), 147.6 (py-C^6), 143.0 (C^4), 133.9 (C$^{3/3'}$), 129.1 (Bn-C), 128.4 (Bn-C), 127.8 (Bn-C), 126.9 (py-C^5), 125.1 (py-C^3), 114.1 (py-C^4), 112.8 (C$^{2/2'}$), 93.6 (2C, alkyne Cs), 64.7 (py-CH_2), 56.3 (Ph-CH_2), 55.4 (OCH_3), 53.1 (CO_2CH_3), 51.8 (*ring Cs*), 29.8 (*ring Cs*), 21.5 (CH_3); *m/z* (HRMS$^+$) 834.4246 $[M+H]^+$ ($C_{51}H_{56}N_5O_6$ requires 834.4231).

[Eu.L^{40}]Cl

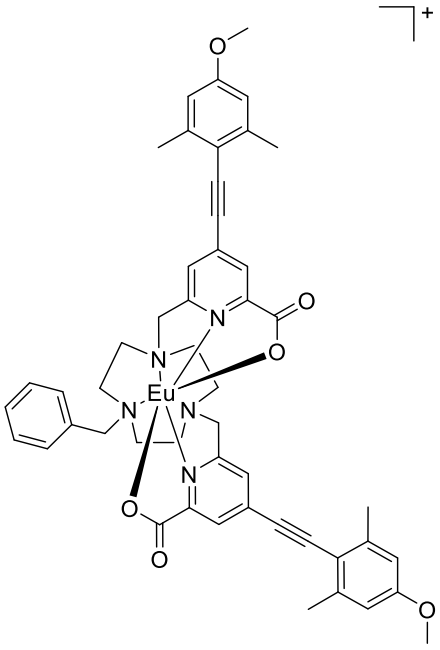

An aqueous solution of sodium hydroxide 0.1 M (0.5 mL) was added to a solution ligand **L^{40}** (11 mg, 13 µmol) in methanol (0.5 mL). The mixture was stirred at 65 °C for 4 h. The reaction was monitored by LC-MS. Upon completion, aqueous hydrochloric acid (0.1 M) was added until pH 6.5 was achieved. Europium chloride hexahydrate (5 mg, 15 µmol) was added and the pH was readjusted to 6.5 by addition of aqueous sodium hydroxide (0.1 M). The reaction was stirred at 65 °C for 24 h. The solvent was removed under reduced pressure and the solid was purified by flash column chromatography (silica, gradient elution starting from 5% CH_3OH to 15% CH_3OH in CH_2Cl_2 in 0.5% increments) to give the complex [Eu.**L^{40}**]Cl as a white solid (10 mg, 80%). *m*/*z* (HRMS$^+$) 954.2896 M^+ ($C_{49}H_{49}N_5O_6{}^{151}Eu$ requires 954.2881); λ_{exc} (MeOH) = 352 nm; ϕ_{em} (MeOH) 0.18, ε (MeOH) 36,000 $M^{-1}cm^{-1}$, τ (H_2O) = 0.53 ms, τ (D_2O) = 0.50 ms, q = 0.

3-(Bromomethyl)phenylethylene boronate CAS: 1225388 -28- 2

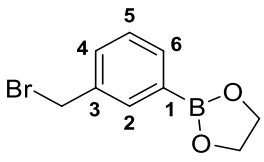

3-(bromomethyl)phenylboronic acid (100 mg, 0.465 mmol) was dissolved in anhydrous pentane (2 mL) over 4 Å molecular sieves. Ethylene glycol (30 µL, 0.465 mmol) was added and the white suspension was allowed to stir at r.t. for 1 h under an atmosphere of

argon. Upon completion, CH_2Cl_2 was added to the reaction mixture and the solution was decanted from the molecular sieves. The solvent was removed under reduced pressure to give 3-(bromomethyl)phenylethylene boronate as a colourless oil which was used with no further purification (80 mg, 72%). TLC analysis R_f 0.28 (silica, 5% CH_3OH in CH_2Cl_2); ^{1}H NMR (295 K, 400 MHz, $CDCl_3$) δ_H 7.85 (1H, s, $\underline{H}^2$), 7.75 (1H, dt, ^3J 7.5, ^4J 1.5, $\underline{H}^6$), 7.51 (1H, dt, ^3J 7.5, ^4J 1.5, $\underline{H}^4$), 7.37 (1H, t, ^3J 7.5, $\underline{H}^5$), 4.50 (s, 2H, C$\underline{H}_2$Br), 4.37 (s, 4H, BO(C$\underline{H}_2$)$_2$O); ^{13}C NMR (295 K, 175 MHz, $CDCl_3$) δ_C 137.4 (Ar-$\underline{C}$), 135.5 (Ar-$\underline{C}$), 134.9 (Ar-$\underline{C}$), 132.2 (Ar-$\underline{C}$), 128.5 (Ar-$\underline{C}$), 66.2 (BO($\underline{C}$H$_2$)$_2$O), 33.5 ($\underline{C}$H$_2$Br); ^{11}B NMR (295 K, 128 MHz, $CDCl_3$) δ_B 31.41; *m/z* GC-EI t_R = 4.68 min, 240.0 (M^+), 161.1 (M^+ - Br).

(3-((4,7-bis((4-((4-methoxy-2,6-dimethylphenyl)ethynyl)-6-(methoxycarbonyl)pyridin-2-yl)methyl)-1,4,7-triazonan-1-yl)methyl)phenyl)boronic acid, L^{41}

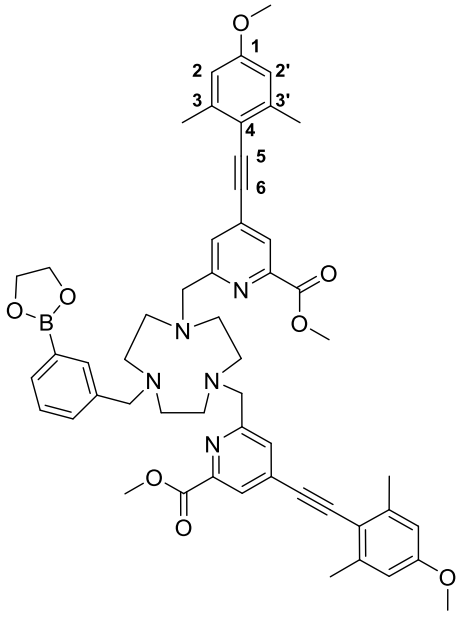

The bis-alkylated ligand, **L^{39}** (15 mg, 0.020 mmol) and K_2CO_3 (3 mg, 0.020 mmol) were dissolved in anhydrous CH_3CN (2 mL) and bubbled with argon (20 minutes). 3-(Bromomethyl)phenylethylene boronate (5 mg, 0.020 mmol) was added and the mixture was stirred under argon at 55 °C and monitored by LC-MS. After 24 h the reaction was cooled and filtered to remove excess potassium salts. The solvent was removed under reduced pressure and the crude material was purified by flash column chromatography (silica, 0 to 5% CH_3OH in CH_2Cl_2) to give **L^{41}** as a glassy solid (20 mg, 85%). ^{1}H NMR (295 K, 600 MHz, $CDCl_3$) δ_H 8.02 (2H, s, py-$\underline{H}^3$), 7.78-7.72 (3H, m, Ph-$\underline{H}$), 7.53 (2H, s,

py-H^{5}), 7.39-7.34 (1H, m, Ph-H), 6.62 (4H, s, H$^{2,2'}$), 4.31 (2H, s, Ph-CH$_2$), 4.02 (4H, s, py-CH$_2$), 3.93 (6H, s, CO$_2$CH$_3$), 3.80 (6H, s, OCH$_3$), 3.53-2.95 (12H, br m, *ring Hs*), 2.46 (12H, s, CH$_3$); ^{13}C NMR (295 K, 150 MHz, CDCl$_3$) δ_C 165.2 (CO$_2$CH$_3$), 160.3 (C^{1}), 157.6 (py-C^{6}), 148.1 (C^{4}), 143.1 (Ph-C), 136.6 (Ph-C), 135.7 (Ph-C), 134.6 (C$^{3/3'}$), 133.86 (Ph-C), 127.8 (py-C^{5}), 126.0 (py-C^{3}), 113.7 (py-C^{4}), 112.8 (C$^{2/2'}$), 94.8 (C^{5}), 92.9 (C^{6}), 66.2 (Ph-CH$_2$), 61.0 (py-CH$_2$), 55.3 (OCH$_3$), 53.6 (*ring Cs*), 53.1 (CO$_2$CH$_3$), 51.8 (*ring Cs*), 46.3 (*ring Cs*), 21.5 (CH$_3$); ^{11}B NMR (295 K, 128 MHz, CDCl$_3$) δ_B 31.3; *m/z* (HRMS$^+$) 877.4350 [M+H]$^+$ ($C_{51}H_{57}{}^{10}BN_5O_8$ requires 877.4337); t_R = 8.8 min (analytical HPLC, Table 23).

[Eu.L^{41}]Cl

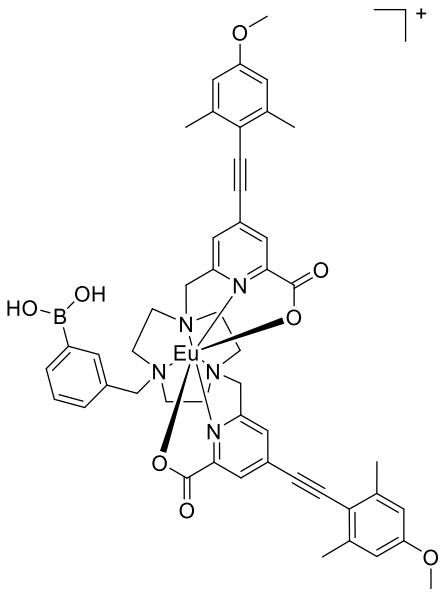

An aqueous solution of sodium hydroxide 0.1 M (0.5 mL) was added to a solution ligand **L^{41}** (5 mg, 6 µmol) in methanol (0.5 mL). The mixture was stirred at 65 °C for 4 h. The reaction was monitored by LC-MS. Upon completion, aqueous hydrochloric acid (0.1 M) was added until pH 6.5 was achieved. Europium chloride hexahydrate (3 mg, 8 µmol) was added and the pH was readjusted to 6.5 by addition of aqueous sodium hydroxide (0.1 M). The reaction was stirred at 65 °C for 24 h. The solvent was removed under reduced pressure to give the complex [Eu.**L^{41}**]Cl as a white solid (7 mg, 80 %). *m*/z ESI (NH_4HCO_3/MeCN) 999.327 [M]$^+$, t_R = 6.2 min; λ_{exc} (MeOH) = 356 nm; ϕ_{em} (MeOH) 0.05, ε (MeOH) 35,000 M^{-1}cm^{-1}, τ (H_2O) = 0.38 ms, τ (D_2O) = 0.48 ms, q = 0.2.

Methyl 3-((methylamino)carbonyl)benzoate, 6b, CAS: 23668-00-0

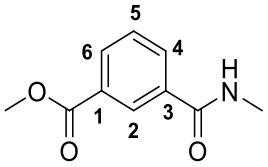

A slurry of mono-methyl isophthalate (250 mg, 1.39 mmol) in anhydrous CH_2Cl_2 (5 mL) at room temperature, was treated with oxalyl chloride (0.23 mL, 2.78 mmol) followed by DMF (1 drop, catalytic). The resultant mixture was stirred under reflux for 90 min. The mixture was cooled to r.t., the solvent removed under reduced pressure and the residue azeotroped with CH_2Cl_2. The residue was dissolved in anhydrous THF (5 mL), cooled to 0 °C and treated with a solution of methylamine (2 M, 1.39 mL, 2.78 mmol) in THF. The mixture was allowed to warm to r.t. overnight. The solvent was removed under reduced pressure and the resultant mixture was partitioned between EtOAc (25 mL) and H_2O (25 mL). The organic layer was washed with $NaHCO_3$ (sat. aq., 20 mL), brine (20 mL), dried over $MgSO_4$, filtered and concentrated under reduced pressure to give **6b** as a white solid (243 mg, 91%). TLC analysis R_f 0.45 (silica, 5% CH_3OH in CH_2Cl_2); m.p. 125–127 °C; ^{1}H NMR (295 K, 400 MHz, $CDCl_3$) δ_H 8.36 (1H, t, ^4J 1.5, $\underline{H}^2$), 8.16 (1H, dt, ^3J 8, ^4J 1.5, $\underline{H}^6$), 8.04 (1H, dt, ^3J 8, ^4J 1.5, $\underline{H}^4$), 7.53 (1H, t, ^3J 8, $\underline{H}^5$), 6.27 (1H, br s, CON$\underline{H}$), 3.94 (3H, s, $CO_2C\underline{H}_3$), 3.04 (3H, d, ^3J 5, CONHC$\underline{H}_3$); ^{13}C NMR (295 K, 100 MHz, $CDCl_3$) δ_C 167.3, 166.5, 135.1 (Ar-$\underline{C}$), 132.4 (Ar-$\underline{C}$), 132.0 (Ar-$\underline{C}$), 130.6 (Ar-$\underline{C}$), 129.1 (Ar-$\underline{C}$), 127.5 (Ar-$\underline{C}$), 52.5 ($CO_2\underline{C}H_3$), 27.1 (CONH$\underline{C}H_3$); *m/z* (HRMS$^+$) 194.0821 $[M+H]^+$ ($C_{10}H_{12}NO_3$ requires 194.0817).

3-((Methylamino)methyl)phenylmethanol, 6c, CAS: 69383-73-9

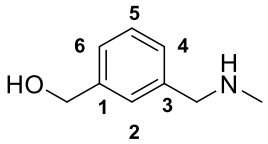

A stirred solution of amide **6b** (243 mg, 1.26 mmol) in anhydrous THF (6 mL) was treated dropwise with a solution of lithium aluminium hydride (2 M, 1.25 mL, 2.52 mmol) in THF. The resultant slurry was stirred under reflux overnight, cooled and treated with water (0.1 mL), 15% NaOH (0.15 mL) and water (0.2 mL). The white solid was removed by filtration and washed multiple times with ethyl acetate. The filtrate was concentrated under reduced pressure and the oily residue was dissolved in EtOAc (50 mL). The organic

layer was washed with brine (50 mL), dried over $MgSO_4$, filtered and concentrated under reduced pressure. The crude oil was purified by flash column chromatography (silica, gradient elution starting from 5% CH_3OH in CH_2Cl_2 to 15% CH_3OH, 1% NH_3 in CH_2Cl_2) to give **6c** as a colourless oil (130 mg, 68%). TLC analysis R_f 0.08 (silica, 15% CH_3OH in CH_2Cl_2); ^{1}H NMR (295 K, 400 MHz, $CDCl_3$) δ_H 7.23-7.08 (4H, m, Ar-H), 4.51 (2H, s, CH_2OH), 3.58 (2H, s, CH_2NHMe), 2.28 (3H, s, $NHCH_3$); ^{13}C NMR (295 K, 100 MHz, $CDCl_3$) δ_C 142.0 (Ar-C), 139.2 (Ar-C), 128.3 (Ar-C), 127.0 (Ar-C), 126.6 (Ar-C), 125.5 (Ar-C), 64.1 (CH_2NH), 55.5 (CH_2OH), 35.4 ($NHCH_3$); *m/z* (HRMS$^+$) 152.1074 $[M+H]^+$ ($C_9H_{14}NO$ requires 152.1075).

N-(3-(hydroxymethyl)benzyl)-*N*-methylformamide, 6d

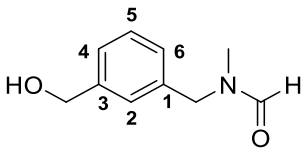

3-((Methylamino)methyl)phenylmethanol, **6c**, (120 mg, 0.795 mmol) was dissolved in anhydrous THF (2 mL) and treated with TFEF (0.39 mL, 3.97 mmol). The resulting mixture was stirred at r.t. for 18 h. The solvent was removed under reduced pressure and the residue dissolved in ethyl acetate. The organic layer was washed with water, $NaHCO_3$ (sat. aq., 25 mL), brine (25 mL), dried over $MgSO_4$, filtered and concentrated under reduced pressure. The crude residue was purified by flash column chromatography (silica, gradient elution starting from 100% CH_2Cl_2 to 5% CH_3OH in CH_2Cl_2 in 0.5% increments) to give **6d** as a colourless oil (96 mg, 67%). TLC analysis R_f 0.28 (silica, 5% CH_3OH in CH_2Cl_2); ^{1}H NMR (295 K, 700 MHz, $CDCl_3$) δ_H mixture of rotamers **a** and **b**: 8.20 (1H, s, NCOH, **a**), 8.08 (1H, s, NCOH', **b**), 7.38-7.06 (4H, m, Ar-H, **a** and **b**), 4.65 (2H, s, CH_2OH, **a** or **b**), 4.63 (2H, s, CH_2OH, **a** or **b**), 4.46 (2H, s, CH_2'NMe, **b**) 4.34 (2H, s, CH_2NMe, **a**), 2.81 (NCH_3'COH, **b**), 2.73 (3H, s, NCH_3COH, **a**), 2.00 (1H, br s, CH_2OH); ^{13}C NMR (295 K, 175 MHz, $CDCl_3$) δ_C 163.0 (NCOH, **a**), 162.8 (NC'OH, **b**), 142.1, 141.9, 136.2, 136.0, 129.0, 128.9, 127.2, 126.7, 126.6, 126.5, 126.3, 125.9, 64.8 (CH_2OH, **a** or **b**), 64.6 (CH_2OH, **a** or **b**), 53.6 (CH_2N, **a**), 47.8 (C'H_2N, **b**), 34.3 (NC'H_3, **b**), 29.6 (NCH_3, **a**); *m/z* (HRMS$^+$) 202.0847 $[M+H]^+$ ($C_{10}H_{13}NO^{23}Na$ requires 202.0844).

3-((*N*-methylformamido)methyl)benzyl methanesulfonate, 6e

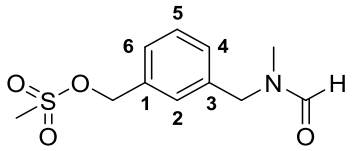

The alcohol **6d** (16 mg, 0.106 mmol) was dissolved in anhydrous THF (1 mL) and NEt_3 (52 µL, 0.371 mmol) was added. The solution was cooled to 0 °C using an ice/water bath. Methanesulfonyl chloride (12 µL, 0.159 mmol) was added and the reaction stirred at 0 °C for 20 min and then warmed to r.t. over 30 minutes. The solvent was removed under reduced pressure and the residue dissolved in CH_2Cl_2 (10 mL) and washed with brine (10 mL). The aqueous layer was re-extracted with CH_2Cl_2 (3 x 10 mL) and the organic layers were combined, dried over $MgSO_4$, filtered and the solvent removed under reduced pressure to yield the mesylate **6e**, as a white solid (26 mg, 95%), which was used directly in the next step without further purification. TLC analysis R_f 0.49 (silica, 100% EtOAc); ^{1}H NMR (295 K, 400 MHz, $CDCl_3$) δ_H mixture of rotamers **a** and **b**: 8.26 (1H, s, NCO<u>H</u>, **a**), 8.14 (H, s, NCO<u>H</u>', **b**) 7.42-7.20 (4H, m, Ar-H, **a** and **b**), 5.20 (2H, s, C<u>H$_2$</u>OS, **a** or **b**), 5.19 (2H, s, C<u>H$_2$</u>'OS, **a** or **b**), 4.50 (2H, s, C<u>H$_2$</u>'NMe, **b**), 4.39 (2H, s, C<u>H$_2$</u>NMe, **a**), 2.96 (3H, s, NC<u>H$_3$</u>'COH, **b**), 2.93 (3H, s, NC<u>H$_3$</u>COH, **a**), 2.84 (6H, s, SO_2C<u>H$_3$</u>); *m/z* (HRMS$^+$) 258.0802 $[M+H]^+$ ($C_{11}H_{16}NO_4S$ requires 258.0800).

Dimethyl 6,6'-((7-(3-((*N*-methylformamido)methyl)benzyl)-1,4,7-triazonane-1,4-diyl)bis(methylene))bis(4-((4-methoxy-2,6-dimethylphenyl)ethynyl)picolinate), Pre-L^{42}

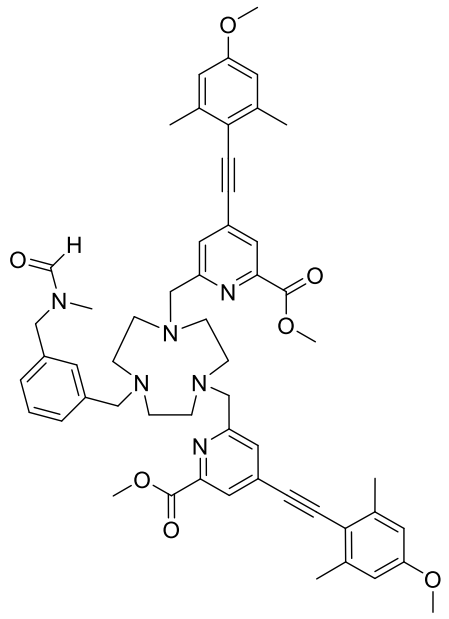

The bis-alkylated ligand, **L^{39}** (23 mg, 0.031 mmol) and K_2CO_3 (5 mg, 0.037 mmol) were dissolved in anhydrous CH_3CN (2.5 mL) and bubbled with argon (20 minutes). The mesylate **6e** (8 mg, 0.031 mmol) was added and the mixture was stirred under argon at 65 °C and monitored by LC-MS. After 24 h the reaction was cooled and filtered to remove excess potassium salts. The solvent was removed under reduced pressure and the crude material was purified by flash column chromatography (silica, gradient elution starting from 100% CH_2Cl_2 to 10% CH_3OH in CH_2Cl_2 in 1% increments) to give **pre-L^{42}** as a glassy solid (13 mg, 46%). TLC analysis R_f 0.32 (silica, 10% CH_3OH in CH_2Cl_2); ^{1}H NMR (295 K, 600 MHz, $CDCl_3$) δ_H 8.25, 8.11 (1H, 2 x s, NCOH, NCOH'), 8.02 (2H, s, py-H^3), 7.62 (2H, s, py-H^5), 7.49–7.14 (4H, m, Ph-H), 6.62 (4H, s, Ar-H$^{2/2'}$), 4.49 (1H, s, NCH$_2$Ph), 4.39 (1H, s, NCH$_2$'Ph), 4.12 (4H, s, py-CH$_2$), 3.93 (6H, s, CO_2CH_3), 3.80 (6H, s, OCH_3), 3.47-2.99 (12H, br m, *rings Hs*), 2.87, 2.74 (3H, 2 x s, NCH_3, NCH_3'), 2.47 (12H, s, Ar-CH_3); ^{13}C NMR (295 K, 150 MHz, $CDCl_3$) δ_C 165.3 (CO_2CH_3), 162.9 (NCOH), 160.4 (Ar-C^1), 157.8 (py-C^6), 148.0 (Ar-C^4), 143.1 (Ar-C$^{3/3'}$), 137.4 (Ph-C), 134.6 (Ph-C), 130.3 (Ph-C), 129.6 (Ph-C), 129.5 (Ph-C), 128.8 (Ph-C), 128.0 (py-C^5), 125.9 (py-C^3), 113.8 (py-C^4), 112.9 (Ar-C$^{2/2'}$), 94.8 (alkyne C^5), 93.0 (alkyne C^6), 61.9 (*ring Cs*), 59.7 (*ring Cs*), 55.4 (OCH_3), 53.6 (CO_2CH_3), 53.1 (py-CH_2), 51.7 (*ring Cs*), 47.7 (NCH$_2$Ph), 34.6, 29.7 (NCH_3), 21.5 (Ar-CH_3); *m/z* (HRMS$^+$) 905.4599 $[M+H]^+$ ($C_{54}H_{61}N_6O_7$ requires 905.4602).

[Eu.L^{42}]Cl$_2$

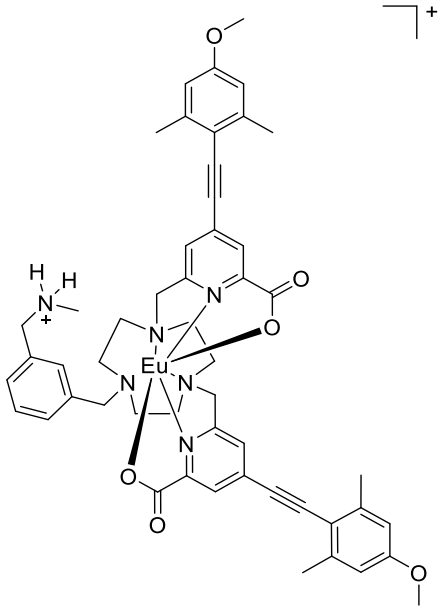

An aqueous solution of sodium hydroxide 0.3 M (0.5 mL) was added to a solution of ligand **pre-L^{42}** (13 mg, 14 µmol) in methanol (0.5 mL). The mixture was stirred at 70 °C for 48 h. The reaction was cooled to r.t. and aqueous hydrochloric acid (0.1 M) was added until pH 7 was achieved. The crude solid was purified by preparative HPLC (Table 25) t_R = 16.5 min. The solid was passed down an ion exchange column to remove the presence of formate. Europium chloride hexahydrate (3 mg, 8 µmol) was added and the pH was readjusted to 6.5 by addition of aqueous sodium hydroxide (0.1 M). The reaction was stirred at 65 °C for 24 h. The solvent was removed under reduced pressure to give the complex [Eu.**L^{42}**]Cl$_2$ as a white solid (5 mg, 68%). *m*/*z* ESI (MeOH no column) 1044 $[M+H]^+$; λ_{exc} (MeOH) = 352 nm; ϕ_{em} (MeOH) = 0.18; ε (MeOH) 36,000 $M^{-1}cm^{-1}$; τ (MeOH) = 0.77 ms.

***N*-Acetyl-α-neuraminic acid methyl ester, CAS: 20298-35-5**

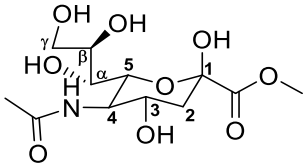

N-Acetylneuraminic acid (50 mg, 0.162 mmol) was dissolved in anhydrous MeOH, dry Dowex® 50Wx4 (H^+) resin (100 mg) was added and the mixture was stirred at r.t. for 6

h under an argon atmosphere. After completion (reaction monitored by LC-MS), the resin was removed by filtration and the solvent was removed under reduced pressure to give *N*-acetyl-α-neuraminic acid methyl ester as a white solid (51 mg, 97%). ^{1}H NMR (295 K, 400 MHz, CD_3OD) δ_H 4.08-3.99 (2H, m, $\underline{H^3}$, $\underline{H^5}$), 3.85-3.79 (2H, m, $\underline{H^4}$, $\underline{H^{\gamma}}$), 3.78 (3H, s, $CO_2C\underline{H_3}$), 3.71 (1H, ddd, $^3J_{H\alpha}$ 9, $^3J_{H\gamma'}$ 5.5, $^3J_{H\gamma}$ 3, $\underline{H^{\beta}}$), 3.62 (1H, dd, $^2J_{H\gamma}$ 11, $^3J_{H\beta}$ 5.5, $\underline{H^{\gamma'}}$), 3.49 (1H, dd, $^3J_{H\beta}$ 9, $^3J_{H5}$ 1.5, $\underline{H^{\alpha}}$), 2.22 (1H, dd, $^2J_{2ax}$ 13, $^3J_{H3}$ 5, $\underline{2H_{eq}}$), 2.02 (3H, s, $NHCOC\underline{H_3}$), 1.90 (1H, dd, $^2J_{2eq}$ 13, $^3J_{H3}$ 11, $\underline{2H_{ax}}$); ^{13}C NMR (295 K, 100 MHz, CD_3OD) δ_C 175.1, 171.8, 96.7, 72.1, 71.6, 70.2, 67.9, 64.8, 54.3, 53.1, 40.7, 22.7; *m/z* ($HRMS^+$) 324.1291 $[M+H]^+$ ($C_{12}H_{22}NO_9$ requires 324.1295).

References

1 S. V. Eliseeva and J.-C. G. Bünzli, *Chem Soc Rev*, 2010, **39**, 189–227.

2 J.-C. G. Bünzli, *Chem. Rev.*, 2010, **110**, 2729–2755.

3 M. C. Heffern, L. M. Matosziuk and T. J. Meade, *Chem. Rev.*, 2014, **114**, 4496–4539.

4 E. G. Moore, A. P. S. Samuel and K. N. Raymond, *Acc. Chem. Res.*, 2009, **42**, 542–552.

5 S. J. Butler and D. Parker, *Chem Soc Rev*, 2013, **42**, 1652–1666.

6 B. N. Samoilov, *J Exp Theor Phys*, 1948, **18**, 1030–1040.

7 J. P. Riehl and F. S. Richardson, *Chem. Rev.*, 1986, **86**, 1–16.

8 F. Zinna and L. Di Bari, *Chirality*, 2015, **27**, 1–13.

9 E. M. Sánchez-Carnerero, A. R. Agarrabeitia, F. Moreno, B. L. Maroto, M. J. Ortiz and S. de la Moya, *Chem. Eur. J.*, 2015, **21**, 13488–13500.

10 F. S. Richardson and J. P. Riehl, *Chem. Rev.*, 1977, **77**, 773–792.

11 J. P. Riehl and G. Muller, in *Comprehensive Chiroptical Spectroscopy: Instrumentation, Methodologies and Theoretical Simulations*, John Wiley and Sons, Hobeken, NJ, USA, 2012, vol. 1, pp. 65–90.

12 C. A. Emeis and L. J. Oosterhoff, *J. Chem. Phys.*, 1971, **54**, 4809–4819.

13 C. K. Luk and F. S. Richardson, *J. Am. Chem. Soc.*, 1974, **96**, 2006–2009.

14 H. P. J. M. Dekkers and L. E. Closs, *J. Am. Chem. Soc.*, 1976, **98**, 2210–2219.

15 R. Carr, R. Puckrin, B. K. McMahon, R. Pal, D. Parker and L.-O. Pålsson, *Methods Appl. Fluoresc.*, 2014, **2**, 024007.

16 I. Steinberg and A. Gafni, *Rev. Sci. Instrum.*, 1972, **43**, 409–413.

17 E. Castiglioni, S. Abbate, F. Lebon and G. Longhi, *Methods Appl. Fluoresc.*, 2014, **2**, 024006.

18 P. H. Schippers, A. van den Buekel and H. P. J. M. Dekkers, *J. Phys. [E]*, 1982, **15**, 945.

19 G. L. Nilmes and J. P. Riehl, *J. Phys. Chem.*, 1983, **87**, 3300–3304.

20 P. H. Schippers and H. P. J. M. Dekkers, *Tetrahedron*, 1982, **38**, 2089 – 2096.

21 R. A. Shatwell and A. J. McCaffery, *J. Phys. [E]*, 1974, **7**, 297.

22 H. G. Brittain and F. S. Richardson, *J. Am. Chem. Soc.*, 1976, **98**, 5858–5863.

23 S. D. Bonsall, M. Houcheime, D. A. Straus and G. Muller, *Chem Commun*, 2007, 3676–3678.

24 C. A. Emeis and L. J. Oosterhoff, *Chem. Phys. Lett.*, 1967, **1**, 129 – 132.

25 M. Grell, M. Oda, K. S. Whitehead, A. Asimakis, D. Neher and D. D. C. Bradley, *Adv. Mater.*, 2001, **13**, 577–580.

26 S. H. Chen, D. Katsis, A. W. Schmid, J. C. Mastrangelo, T. Tsutsui and T. N. Blanton, *Nature*, 1999, **397**, 506–508.

27 I. Sato, R. Yamashima, K. Kadowaki, J. Yamamoto, T. Shibata and K. Soai, *Angew. Chem. Int. Ed.*, 2001, **40**, 1096–1098.

28 N. Steinberg, A. Gafni and I. Z. Steinberg, *J. Am. Chem. Soc.*, 1981, **103**, 1636–1640.

29 P. H. Schippers and H. P. J. M. Dekkers, *J. Am. Chem. Soc.*, 1983, **105**, 145–146.

30 P. H. Schippers, J. P. M. V. der Ploeg and H. P. J. M. Dekkers, *J. Am. Chem. Soc.*, 1983, **105**, 84–89.

31 H. Maeda and Y. Bando, *Pure Appl. Chem.*, 2013, **85**, 1967–1978.

32 A. Gossauer, F. Fehr, F. Nydegger and H. Stöckli-Evans, *J. Am. Chem. Soc.*, 1997, **119**, 1599–1608.

33 E. M. Sánchez-Carnerero, F. Moreno, B. L. Maroto, A. R. Agarrabeitia, M. J. Ortiz, B. G. Vo, G. Muller and S. de la Moya, *J. Am. Chem. Soc.*, 2014, **136**, 3346–3349.

34 M. Gingras, G. Felix and R. Peresutti, *Chem Soc Rev*, 2013, **42**, 1007–1050.

35 K. E. S. Phillips, T. J. Katz, S. Jockusch, A. J. Lovinger and N. J. Turro, *J. Am. Chem. Soc.*, 2001, **123**, 11899–11907.

36 J. E. Field, G. Muller, J. P. Riehl and D. Venkataraman, *J. Am. Chem. Soc.*, 2003, **125**, 11808–11809.

37 T. Thongpanchang, K. Paruch, T. J. Katz, A. L. Rheingold, K.-C. Lam and L. Liable-Sands, *J. Org. Chem.*, 2000, **65**, 1850–1856.

38 K. Nakamura, S. Furumi, M. Takeuchi, T. Shibuya and K. Tanaka, *J. Am. Chem. Soc.*, 2014, **136**, 5555–5558.

39 H. Maeda, Y. Bando, K. Shimomura, I. Yamada, M. Naito, K. Nobusawa, H. Tsumatori and T. Kawai, *J. Am. Chem. Soc.*, 2011, **133**, 9266–9269.

40 Y. Haketa, Y. Bando, K. Takaishi, M. Uchiyama, A. Muranaka, M. Naito, H. Shibaguchi, T. Kawai and H. Maeda, *Angew. Chem. Int. Ed.*, 2012, **51**, 7967–7971.

41 H. Maeda, T. Shirai, Y. Bando, K. Takaishi, M. Uchiyama, A. Muranaka, T. Kawai and M. Naito, *Org. Lett.*, 2013, **15**, 6006–6009.

42 N. Saleh, M. Srebro, T. Reynaldo, N. Vanthuyne, L. Toupet, V. Y. Chang, G. Muller, J. A. G. Williams, C. Roussel, J. Autschbach and J. Crassous, *Chem Commun*, 2015, **51**, 3754–3757.

43 O. Crespo, B. Eguillor, M. A. Esteruelas, I. Fernandez, J. Garcia-Raboso, M. Gomez-Gallego, M. Martin-Ortiz, M. Olivan and M. A. Sierra, *Chem Commun*, 2012, **48**, 5328–5330.

44 L. Norel, M. Rudolph, N. Vanthuyne, J. A. G. Williams, C. Lescop, C. Roussel, J. Autschbach, J. Crassous and R. Réau, *Angew. Chem. Int. Ed.*, 2010, **49**, 99–102.

45 E. Anger, M. Rudolph, L. Norel, S. Zrig, C. Shen, N. Vanthuyne, L. Toupet, J. A. G. Williams, C. Roussel, J. Autschbach, J. Crassous and R. Réau, *Chem. Eur. J.*, 2011, **17**, 14178–14198.

46 C. Shen, E. Anger, M. Srebro, N. Vanthuyne, K. K. Deol, T. D. Jefferson, G. Muller, J. A. G. Williams, L. Toupet, C. Roussel, J. Autschbach, R. Reau and J. Crassous, *Chem Sci*, 2014, **5**, 1915–1927.

47 X.-P. Zhang, V. Y. Chang, J. Liu, X.-L. Yang, W. Huang, Y. Li, C.-H. Li, G. Muller and X.-Z. You, *Inorg. Chem.*, 2015, **54**, 143–152.

48 F. J. Coughlin, M. S. Westrol, K. D. Oyler, N. Byrne, C. Kraml, E. Zysman-Colman, M. S. Lowry and S. Bernhard, *Inorg. Chem.*, 2008, **47**, 2039–2048.

49 R. Carr, N. H. Evans and D. Parker, *Chem Soc Rev*, 2012, **41**, 7673–7686.

50 G. Muller, *Dalton Trans*, 2009, 9692–9707.

51 C. K. Luk and F. S. Richardson, *J. Am. Chem. Soc.*, 1975, **97**, 6666–6675.

52 J. L. Lunkley, D. Shirotani, K. Yamanari, S. Kaizaki and G. Muller, *J. Am. Chem. Soc.*, 2008, **130**, 13814–13815.

53 J.-C. G. Bunzli and C. Piguet, *Chem Soc Rev*, 2005, **34**, 1048–1077.

54 S. I. Weissman, *J. Chem. Phys.*, 1942, **10**, 214–217.

55 D. Parker, *Coord. Chem. Rev.*, 2000, **205**, 109 – 130.

56 M. Kasha, *Discuss Faraday Soc*, 1950, **9**, 14–19.

57 D. L. Dexter, *J. Chem. Phys.*, 1953, **21**, 836–850.

58 T. Forster, *Discuss Faraday Soc*, 1959, **27**, 7–17.

59 A. P. S. Samuel, J. Xu and K. N. Raymond, *Inorg. Chem.*, 2009, **48**, 687–698.

60 M. Delbianco, L. Lamarque and D. Parker, *Org Biomol Chem*, 2014, **12**, 8061–8071.

61 C. M. G. dos Santos, A. J. Harte, S. J. Quinn and T. Gunnlaugsson, *Coord. Chem. Rev.*, 2008, **252**, 2512 – 2527.

62 D. Parker, *Aust. J. Chem.*, 2011, **64**, 239–243.

63 J.-C. G. Bünzli, *Acc. Chem. Res.*, 2006, **39**, 53–61.

64 H. Tsukube and and S. Shinoda, *Chem. Rev.*, 2002, **102**, 2389–2404.

65 F. S. Richardson, *Inorg. Chem.*, 1980, **19**, 2806–2812.

66 R. S. Dickens, J. A. K. Howard, C. L. Maupin, J. M. Moloney, D. Parker, R. D. Peacock, J. P. Riehl and G. Siligardi, *New J Chem*, 1998, **22**, 891–899.

67 D. R. Foster and F. S. Richardson, *Inorg. Chem.*, 1983, **22**, 3996–4002.

68 F. S. Richardson and T. R. Faulkner, *J. Chem. Phys.*, 1982, **76**, 1595–1606.

69 D. H. Metcalf, S. W. Snyder, J. N. Demas and F. S. Richardson, *J. Am. Chem. Soc.*, 1990, **112**, 469–479.

70 R. S. Dickins, D. Parker, J. I. Bruce and D. J. Tozer, *Dalton Trans*, 2003, 1264–1271.

71 J. I. Bruce, D. Parker and D. J. Tozer, *Chem Commun*, 2001, 2250–2251.

72 A. M. Funk, P. H. Fries, P. Harvey, A. M. Kenwright and D. Parker, *J. Phys. Chem. A*, 2013, **117**, 905–917.

73 N. H. Evans, R. Carr, M. Delbianco, R. Pal, D. S. Yufit and D. Parker, *Dalton Trans*, 2013, **42**, 15610–15616.

74 J. I. Bruce, D. Parker, S. Lopinski and R. D. Peacock, *Chirality*, **14**, 562–567.

75 S. D. Pietro and L. D. Bari, *Inorg. Chem.*, 2012, **51**, 12007–12014.

76 O. L. Malta, H. F. Brito, J. F. S. Menezes, F. R. G. e Silva, C. de M. Donegá and S. A. Jr, *Chem. Phys. Lett.*, 1998, **282**, 233 – 238.

77 C. Freund, W. Porzio, U. Giovanella, F. Vignali, M. Pasini, S. Destri, A. Mech, S. D. Pietro, L. D. Bari and P. Mineo, *Inorg. Chem.*, 2011, **50**, 5417–5429.

78 K. Binnemans, *Chem. Rev.*, 2009, **109**, 4283–4374.

79 T. Harada, Y. Hasegawa, Y. Nakano, M. Fujiki, M. Naito, T. Wada, Y. Inoue and T. Kawai, *J. Alloys Compd.*, 2009, **488**, 599 – 602.

80 J. Yuasa, T. Ohno, K. Miyata, H. Tsumatori, Y. Hasegawa and T. Kawai, *J. Am. Chem. Soc.*, 2011, **133**, 9892–9902.

81 T. Harada, Y. Nakano, M. Fujiki, M. Naito, T. Kawai and Y. Hasegawa, *Inorg. Chem.*, 2009, **48**, 11242–11250.

82 T. Harada, H. Tsumatori, K. Nishiyama, J. Yuasa, Y. Hasegawa and T. Kawai, *Inorg. Chem.*, 2012, **51**, 6476–6485.

83 J. Yuasa, H. Ueno and T. Kawai, *Chem. Eur. J.*, 2014, **20**, 8494–8494.

84 C. Piguet, J.-C. G. Bunzli, G. Bernardinelli, C. G. Bochet and P. Froidevaux, *J Chem Soc Dalton Trans*, 1995, 83–97.

85 G. Muller, J.-C. G. Bunzli, J. P. Riehl, D. Suhr, A. von Zelewsky and H. Murner, *Chem Commun*, 2002, 1522–1523.

86 G. Muller, C. L. Maupin, J. P. Riehl, H. Birkedal, C. Piguet and J.-C. G. Bünzli, *Eur. J. Inorg. Chem.*, 2003, **2003**, 4065–4072.

87 G. Muller, B. Schmidt, J. Jiricek, G. Hopfgartner, J. P. Riehl, J.-C. G. Bunzli and C. Piguet, *J Chem Soc Dalton Trans*, 2001, 2655–2662.

88 G. Muller, J. P. Riehl, K. J. Schenk, G. Hopfgartner, C. Piguet and J.-C. G. Bünzli, *Eur. J. Inorg. Chem.*, 2002, **2002**, 3101–3110.

89 K. T. Hua, J. Xu, E. E. Quiroz, S. Lopez, A. J. Ingram, V. A. Johnson, A. R. Tisch, A. de Bettencourt-Dias, D. A. Straus and G. Muller, *Inorg. Chem.*, 2012, **51**, 647–660.

90 O. Kotova, J. A. Kitchen, C. Lincheneau, R. D. Peacock and T. Gunnlaugsson, *Chem. Eur. J.*, 2013, **19**, 16181–16186.

91 J. P. Leonard, P. D. Beer, T. McCabe, J. E. O'Brien, R. D. Peacock, P. E. Kruger and T. Gunnlaugsson, *J. Am. Chem. Soc.*, 2007, **129**, 10986–10987.

92 F. Stomeo, C. Lincheneau, J. P. Leonard, J. E. O'Brien, R. D. Peacock, C. P. McCoy and T. Gunnlaugsson, *J. Am. Chem. Soc.*, 2009, **131**, 9636–9637.

93 L.-L. Yan, C.-H. Tan, G.-L. Zhang, L.-P. Zhou, J.-C. Bünzli and Q.-F. Sun, *J. Am. Chem. Soc.*, 2015, **137**, 8550–8555.

94 G. Bozoklu, C. Gateau, D. Imbert, J. Pécaut, K. Robeyns, Y. Filinchuk, F. Memon, G. Muller and M. Mazzanti, *J. Am. Chem. Soc.*, 2012, **134**, 8372–8375.

95 S. J. Bradberry, A. J. Savyasachi, M. Martinez-Calvo and T. Gunnlaugsson, *Coord. Chem. Rev.*, 2014, **273–274**, 226 – 241.

96 J. F. Desreux, *Inorg. Chem.*, 1980, **19**, 1319–1324.

97 E. J. New, D. Parker and R. D. Peacock, *Dalton Trans*, 2009, 672–679.

98 J. I. Bruce, D. Parker, S. Lopinski and R. D. Peacock, *Chirality*, 2002, **14**, 562–567.

99 G. Tircso, B. C. Webber, B. E. Kucera, V. G. Young and M. Woods, *Inorg. Chem.*, 2011, **50**, 7966–7979.

100 J. W. Walton, R. Carr, N. H. Evans, A. M. Funk, A. M. Kenwright, D. Parker, D. S. Yufit, M. Botta, S. D. Pinto and K.-L. Wong, *Inorg. Chem.*, 2012, **51**, 8042–8056.

101 G. Nocton, A. Nonat, C. Gateau and M. Mazzanti, *Helv. Chim. Acta*, 2009, **92**, 2257–2273.

102 J. W. Walton, L. D. Bari, D. Parker, G. Pescitelli, H. Puschmann and D. S. Yufit, *Chem Commun*, 2011, **47**, 12289–12291.

103 R. S. Dickins, J. A. K. Howard, C. L. Maupin, J. M. Moloney, D. Parker, J. P. Riehl, G. Siligardi and J. A. G. Williams, *Chem. Eur. J.*, 1999, **5**, 1095–1105.

104 M. Woods, S. Aime, M. Botta, J. A. K. Howard, J. M. Moloney, M. Navet, D. Parker, M. Port and O. Rousseaux, *J. Am. Chem. Soc.*, 2000, **122**, 9781–9792.

105 R. S. Ranganathan, R. K. Pillai, N. Raju, H. Fan, H. Nguyen, M. F. Tweedle, J. F. Desreux and V. Jacques, *Inorg. Chem.*, 2002, **41**, 6846–6855.

106 M. Woods, Z. Kovacs, S. Zhang and A. D. Sherry, *Angew. Chem. Int. Ed.*, 2003, **42**, 5889–5892.

107 R. S. Ranganathan, N. Raju, H. Fan, X. Zhang, M. F. Tweedle, J. F. Desreux and V. Jacques, *Inorg. Chem.*, 2002, **41**, 6856–6866.

108 B. C. Webber and M. Woods, *Inorg. Chem.*, 2012, **51**, 8576–8582.

109 S. Petoud, G. Muller, E. G. Moore, J. Xu, J. Sokolnicki, J. P. Riehl, U. N. Le, S. M. Cohen and K. N. Raymond, *J. Am. Chem. Soc.*, 2007, **129**, 77–83.

110 S. Petoud, S. M. Cohen, J.-C. G. Bünzli and K. N. Raymond, *J. Am. Chem. Soc.*, 2003, **125**, 13324–13325.

111 A. P. S. Samuel, J. L. Lunkley, G. Muller and K. N. Raymond, *Eur. J. Inorg. Chem.*, 2010, **2010**, 3343–3347.

112 M. Seitz, E. G. Moore, A. J. Ingram, G. Muller and K. N. Raymond, *J. Am. Chem. Soc.*, 2007, **129**, 15468–15470.

113 M. Seitz, K. Do, A. J. Ingram, E. G. Moore, G. Muller and K. N. Raymond, *Inorg. Chem.*, 2009, **48**, 8469–8479.

114 C. P. Montgomery, B. S. Murray, E. J. New, R. Pal and D. Parker, *Acc. Chem. Res.*, 2009, **42**, 925–937.

115 J. I. Bruce, R. S. Dickins, L. J. Govenlock, T. Gunnlaugsson, S. Lopinski, M. P. Lowe, D. Parker, R. D. Peacock, J. J. B. Perry, S. Aime and M. Botta, *J. Am. Chem. Soc.*, 2000, **122**, 9674–9684.

116 R. S. Dickins, T. Gunnlaugsson, D. Parker and R. D. Peacock, *Chem Commun*, 1998, 1643–1644.

117 R. S. Dickins, D. Parker, A. S. de Sousa and J. A. G. Williams, *Chem Commun*, 1996, 697–698.

118 R. S. Dickins, S. Aime, A. S. Batsanov, A. Beeby, M. Botta, J. I. Bruce, J. A. K. Howard, C. S. Love, D. Parker, R. D. Peacock and H. Puschmann, *J. Am. Chem. Soc.*, 2002, **124**, 12697–12705.

119 D. G. Smith, R. Pal and D. Parker, *Chem. Eur. J.*, 2012, **18**, 11604–11613.

120 D. G. Smith, B. K. McMahon, R. Pal and D. Parker, *Chem Commun*, 2012, **48**, 8520–8522.

121 P. Atkinson, Y. Bretonnière, D. Parker and G. Muller, *Helv. Chim. Acta*, 2005, **88**, 391–405.

122 L. J. Govenlock, C. E. Mathieu, D. Parker, J. A. Gareth Williams, G. Siligardi, C. L. Maupin and J. P. Riehl, *Chem Commun*, 1999, 1699–1700.

123 G. Bobba, S. D. Kean, D. Parker, A. Beeby and G. Baker, *J Chem Soc Perkin Trans 2*, 2001, 1738–1741.

124 G. Bobba, R. S. Dickins, S. D. Kean, C. E. Mathieu, D. Parker, R. D. Peacock, G. Siligardi, M. J. Smith, J. A. Gareth Williams and C. F. G. C. Geraldes, *J Chem Soc Perkin Trans 2*, 2001, 1729–1737.

125 G. Bobba, J. C. Frias and D. Parker, *Chem Commun*, 2002, 890–891.

126 G. Bobba, Y. Bretonniere, J.-C. Frias and D. Parker, *Org Biomol Chem*, 2003, **1**, 1870–1872.

127 C. P. Montgomery, E. J. New, D. Parker and R. D. Peacock, *Chem Commun*, 2008, 4261–4263.

128 D. M. Dias, J. M. C. Teixeira, I. Kuprov, E. J. New, D. Parker and C. F. G. C. Geraldes, *Org Biomol Chem*, 2011, **9**, 5047–5050.

129 J. Yuasa, T. Ohno, H. Tsumatori, R. Shiba, H. Kamikubo, M. Kataoka, Y. Hasegawa and T. Kawai, *Chem Commun*, 2013, **49**, 4604–4606.

130 P. Pfeiffer and K. Quehl, *Berichte Dtsch. Chem. Ges.*, 1931, **64**, 2667–2671.

131 H. G. Brittain, *Inorg. Chem.*, 1981, **20**, 3007–3013.

132 G. Muller and J. P. Riehl, *J. Fluoresc.*, 2005, **15**, 553–558.

133 H. G. Brittain, *J Chem Soc Dalton Trans*, 1984, 1367–1370.

134 E. Huskowska and J. P. Riehl, *Inorg. Chem.*, 1995, **34**, 5615–5621.

135 F. Yan, R. A. Copeland and H. G. Brittain, *Inorg. Chem.*, 1982, **21**, 1180–1185.

136 H. G. Brittain, *J. Coord. Chem.*, 1989, **20**, 331–347.

137 H. G. Brittain, *Coord. Chem. Rev.*, 1983, **48**, 243 – 276.

138 T. N. Parac-Vogt, K. Binnemans and C. Görller-Walrand, *ChemPhysChem*, 2001, **2**, 767–769.

139 A. Moussa, C. Pham, S. Bommireddy and G. Muller, *Chirality*, 2009, **21**, 497–506.

140 D. H. Metcalf, S. W. Snyder, S. Wu, G. L. Hilmes, J. P. Riehl, J. N. Demas and F. S. Richardson, *J. Am. Chem. Soc.*, 1989, **111**, 3082–3083.

141 D. H. Metcalf, S. W. Snyder, J. N. Demas and F. S. Richardson, *J. Am. Chem. Soc.*, 1990, **112**, 5681–5695.

142 T. A. Hopkins, D. H. Metcalf and F. S. Richardson, *Chirality*, 2008, **20**, 511–523.

143 R. B. Rexwinkel, S. C. J. Meskers, H. P. J. M. Dekkers and J. P. Riehl, *J. Phys. Chem.*, 1993, **97**, 13519–13526.

144 S. C. J. Meskers, M. Ubbink, G. W. Canters and H. P. J. M. Dekkers, *J. Phys. Chem.*, 1996, **100**, 17957–17969.

145 S. C. J. Meskers and H. P. J. M. Dekkers, *Spectrochim. Acta Part A*, 1999, **55**, 1857 – 1874.

146 R. Carr, L. Di Bari, S. Lo Piano, D. Parker, R. D. Peacock and J. M. Sanderson, *Dalton Trans*, 2012, **41**, 13154–13158.

147 G.-L. Law, C. Man, D. Parker and J. W. Walton, *Chem Commun*, 2010, **46**, 2391–2393.

148 F. Zsila and Y. Iwao, *Biochim. Biophys. Acta*, 2007, **1770**, 797 – 809.

149 S. J. Butler, B. K. McMahon, R. Pal, D. Parker and J. W. Walton, *Chem. Eur. J.*, 2013, **19**, 9511–9517.

150 M. Iwamura, Y. Kimura, R. Miyamoto and K. Nozaki, *Inorg. Chem.*, 2012, **51**, 4094–4098.

151 K. Okutani, K. Nozaki and M. Iwamura, *Inorg. Chem.*, 2014, **53**, 5527–5537.

152 G. S. Ofelt, *J. Chem. Phys.*, 1962, **37**, 511–520.

153 F. Song, G. Wei, X. Jiang, F. Li, C. Zhu and Y. Cheng, *Chem Commun*, 2013, **49**, 5772–5774.

154 J. W. Walton, A. Bourdolle, S. J. Butler, M. Soulie, M. Delbianco, B. K. McMahon, R. Pal, H. Puschmann, J. M. Zwier, L. Lamarque, O. Maury, C. Andraud and D. Parker, *Chem Commun*, 2013, **49**, 1600–1602.

155 C. Gateau, M. Mazzanti, J. Pecaut, F. A. Dunand and L. Helm, *Dalton Trans*, 2003, 2428–2433.

156 H. Takalo, I. Hemmilä, T. Sutela and M. Latva, *Helv. Chim. Acta*, 1996, **79**, 789–802.

157 D. Parker and R. J. Taylor, *Tetrahedron*, 1987, **43**, 5451 – 5456.

158 A. S. Hay, *J. Org. Chem.*, 1962, **27**, 3320–3321.

159 P. Nguyen, Z. Yuan, L. Agocs, G. Lesley and T. B. Marder, *Inorganica Chim. Acta*, 1994, **220**, 289 – 296.

160 R. D. Shannon, *Acta Crystallogr. Sect. A*, 1976, **32**, 751–767.

161 K. Binnemans and C. Görller-Walrand, *Chem. Phys. Lett.*, 1995, **245**, 75 – 78.

162 E. R. Neil, A. M. Funk, D. S. Yufit and D. Parker, *Dalton Trans*, 2014, **43**, 5490–5504.

163 A. M. Funk, K.-L. N. A. Finney, P. Harvey, A. M. Kenwright, E. R. Neil, N. J. Rogers, P. Kanthi Senanayake and D. Parker, *Chem Sci*, 2015, **6**, 1655–1662.

164 K. H. Chalmers, E. De Luca, N. H. M. Hogg, A. M. Kenwright, I. Kuprov, D. Parker, M. Botta, J. I. Wilson and A. M. Blamire, *Chem. Eur. J.*, 2010, **16**, 134–148.

165 J. Jensen and A. K. Mackintosh, *Rare Earth Magnetism*, Clarendon, Oxford, 1991.

166 B. Chevalier, S. Tencé, G. André, S. F. Matar and E. Gaudin, *J. Phys. Conf. Ser.*, 2010, **200**, 032012.

167 P. Harvey, I. Kuprov and D. Parker, *Eur. J. Inorg. Chem.*, 2012, **2012**, 2015–2022.

168 P. H. Fries and E. Belorizky, *J. Chem. Phys.*, 2012, **136**, 074513.

169 B. Bleaney, *J. Magn. Reson. 1969*, 1972, **8**, 91 – 100.

170 A. Beeby, I. M. Clarkson, R. S. Dickins, S. Faulkner, D. Parker, L. Royle, A. S. de Sousa, J. A. Gareth Williams and M. Woods, *J Chem Soc Perkin Trans 2*, 1999, 493–504.

171 M. Soulié, F. Latzko, E. Bourrier, V. Placide, S. J. Butler, R. Pal, J. W. Walton, P. L. Baldeck, B. Le Guennic, C. Andraud, J. M. Zwier, L. Lamarque, D. Parker and O. Maury, *Chem. Eur. J.*, 2014, **20**, 8636–8646.

172 A. D'Aléo, A. Picot, A. Beeby, J. A. G. Williams, B. L. Guennic, C. Andraud and O. Maury, *Inorg. Chem.*, 2008, **47**, 10258–10268.

173 A. D'Aléo, F. Pointillart, L. Ouahab, C. Andraud and O. Maury, *Coord. Chem. Rev.*, 2012, **256**, 1604 – 1620.

174 C. Reichardt, *Chem. Rev.*, 1994, **94**, 2319–2358.

175 A. Picot, F. Malvolti, B. Le Guennic, P. L. Baldeck, J. A. G. Williams, C. Andraud and O. Maury, *Inorg. Chem.*, 2007, **46**, 2659–2665.

176 D. Parker and J. A. G. Williams, *J Chem Soc Perkin Trans 2*, 1995, 1305–1314.

177 S. Aime, A. Barge, J. I. Bruce, M. Botta, J. A. K. Howard, J. M. Moloney, D. Parker, A. S. de Sousa and M. Woods, *J. Am. Chem. Soc.*, 1999, **121**, 5762–5771.

178 T. Gunnlaugsson, *Chem Commun*, 1998, 511–512.

179 F. Kielar, C. P. Montgomery, E. J. New, D. Parker, R. A. Poole, S. L. Richardson and P. A. Stenson, *Org Biomol Chem*, 2007, **5**, 2975–2982.

180 R. Pal, A. Beeby and D. Parker, *J. Pharm. Biomed. Anal.*, 2011, **56**, 352 – 358.

181 R. Pal, D. Parker and L. C. Costello, *Org Biomol Chem*, 2009, **7**, 1525–1528.

182 D. G. Smith, G. Law, B. S. Murray, R. Pal, D. Parker and K.-L. Wong, *Chem Commun*, 2011, **47**, 7347–7349.

183 M. Delbianco, V. Sadovnikova, E. Bourrier, G. Mathis, L. Lamarque, J. M. Zwier and D. Parker, *Angew. Chem. Int. Ed.*, 2014, **53**, 10718–10722.

184 E. R. Neil, M. A. Fox, R. Pal, L.-O. Palsson, B. A. O'Sullivan and D. Parker, *Dalton Trans*, 2015, **44**, 14937–14951.

185 S. Dixit, J. Crain, W. C. K. Poon, J. L. Finney and A. K. Soper, *Nature*, 2002, **416**, 829–832.

186 J. Sandström, in *Dynamic NMR Spectroscopy*, Academic Press Inc., London, 1982, pp. 53–64.

187 R. S. Dickins, A. S. Batsanov, J. A. K. Howard, D. Parker, H. Puschmann and S. Salamano, *Dalton Trans*, 2004, 70–80.

188 K. Sénéchal-David, A. Hemeryck, N. Tancrez, L. Toupet, J. A. G. Williams, I. Ledoux, J. Zyss, A. Boucekkine, J.-P. Guégan, H. Le Bozec and O. Maury, *J. Am. Chem. Soc.*, 2006, **128**, 12243–12255.

189 F. Pointillart, B. L. Guennic, O. Maury, S. Golhen, O. Cador and L. Ouahab, *Inorg. Chem.*, 2013, **52**, 1398–1408.

190 T. T. da Cunha, J. Jung, M.-E. Boulon, G. Campo, F. Pointillart, C. L. M. Pereira, B. L. Guennic, O. Cador, K. Bernot, F. Pineider, S. Golhen and L. Ouahab, *J. Am. Chem. Soc.*, 2013, **135**, 16332–16335.

191 G. Yogeeswaran, B. S. Stein and H. Sebastian, *Cancer Res.*, 1978, **38**, 1336–1344.

192 J. Roth, C. Zuber, P. Wagner, D. J. Taatjes, C. Weisgerber, P. U. Heitz, C. Goridis and D. Bitter-Suermann, *Proc. Natl. Acad. Sci.*, 1988, **85**, 2999–3003.

193 F. J. Krolikowski, K. Reuter, T. P. Waalkes, S. M. Sieber and R. H. Adamson, *Pharmacology*, 1976, **14**, 47–51.

194 L. Frullano, J. Rohovec, S. Aime, T. Maschmeyer, M. I. Prata, J. J. P. de Lima, C. F. G. C. Geraldes and J. A. Peters, *Chem. Eur. J.*, 2004, **10**, 5205–5217.

195 G. A. Lemieux, K. J. Yarema, C. L. Jacobs and C. R. Bertozzi, *J. Am. Chem. Soc.*, 1999, **121**, 4278–4279.

196 S. Geninatti Crich, D. Alberti, I. Szabo, S. Aime and K. Djanashvili, *Angew. Chem. Int. Ed.*, 2013, **52**, 1161–1164.

197 M. Regueiro-Figueroa, K. Djanashvili, D. Esteban-Gómez, T. Chauvin, É. Tóth, A. de Blas, T. Rodríguez-Blas and C. Platas-Iglesias, *Inorg. Chem.*, 2010, **49**, 4212–4223.

198 K. Ouchi, S. Saito and M. Shibukawa, *Inorg. Chem.*, 2013, **52**, 6239–6241.

199 T. D. James, K. R. A. S. Sandanayake and S. Shinkai, *Angew. Chem. Int. Ed. Engl.*, 1996, **35**, 1910–1922.

200 J. A. Adams, *Chem. Rev.*, 2001, **101**, 2271–2290.

201 R. Sutphen, Y. Xu, G. D. Wilbanks, J. Fiorica, E. C. Grendys, J. P. LaPolla, H. Arango, M. S. Hoffman, M. Martino, K. Wakeley, D. Griffin, R. W. Blanco, A. B. Cantor, Y. Xiao and J. P. Krischer, *Cancer Epidemiol. Biomarkers Prev.*, 2004, **13**, 1185–1191.

202 W. Zhao, W. Liu, W. Zhang, L. Zeng, Z. Fan, J. Wu and P. Wang, *Analyst*, 2012, **137**, 1853–1859.

203 K.-H. Chen, J.-S. Yang, C.-Y. Hwang and J.-M. Fang, *Org. Lett.*, 2008, **10**, 4401–4404.

204 O. Alptürk, O. Rusin, S. O. Fakayode, W. Wang, J. O. Escobedo, I. M. Warner, W. E. Crowe, V. Král, J. M. Pruet and R. M. Strongin, *Proc. Natl. Acad. Sci.*, 2006, **103**, 9756–9760.

205 S. J. Rettig and J. Trotter, *Can. J. Chem.*, 1977, **55**, 3071–3075.

206 J. P. Lorand and J. O. Edwards, *J. Org. Chem.*, 1959, **24**, 769–774.

207 S. Friedman, B. Pace and R. Pizer, *J. Am. Chem. Soc.*, 1974, **96**, 5381–5384.

208 E. Gruszewska, B. Cylwik, A. Panasiuk, M. Szmitkowski, R. Flisiak and L. Chrostek, *BioMed Res. Int.*, 2014, **2014**, 876096.

209 G. Springsteen and B. Wang, *Tetrahedron*, 2002, **58**, 5291–5300.

210 B. S. Blaum, J. P. Hannan, A. P. Herbert, D. Kavanagh, D. Uhrín and T. Stehle, *Nat Chem Biol*, 2015, **11**, 77–82.

211 R. S. Alexander, Z. F. Kanyo, L. E. Chirlian and D. W. Christianson, *J. Am. Chem. Soc.*, 1990, **112**, 933–937.

212 B. Schneider and M. Kabeláč, *J. Am. Chem. Soc.*, 1998, **120**, 161–165.

213 J. Yao, H. J. Dyson and P. E. Wright, *J. Mol. Biol.*, 1994, **243**, 754–766.

214 A. Perczel and G. D. Fasman, *Protein Sci.*, 1992, **1**, 378–395.

215 Y. Xu, Z. Shen, D. W. Wiper, M. Wu, R. E. Morton, P. Elson, A. W. Kennedy, J. Belinson, M. Markman and G. Casey, *J Am Med Assoc*, 1998, **280**, 719–723.

216 E. E. Kooijman, K. M. Carter, E. G. van Laar, V. Chupin, K. N. J. Burger and B. de Kruijff, *Biochemistry (Mosc.)*, 2005, **44**, 17007–17015.

217 I. Pascher and S. Sundell, *Chem. Phys. Lipids*, 1985, **37**, 241–250.

218 G. Wulff, *Pure Appl. Chem.*, 1982, **54**, 2093–2102.

219 S. L. Wiskur, J. J. Lavigne, H. Ait-Haddou, V. Lynch, Y. H. Chiu, J. W. Canary and E. V. Anslyn, *Org. Lett.*, 2001, **3**, 1311–1314.

220 L. C. Gilday, T. Lang, A. Caballero, P. J. Costa, V. Félix and P. D. Beer, *Angew. Chem. Int. Ed.*, 2013, **52**, 4356–4360.

221 Y. Omote, K.-T. Kuo and N. Sugiyama, *Bull Chem Soc Jpn*, 1967, **40**, 1695.

222 G. Chessa, L. Canovese, F. Visentin, C. Santo and R. Seraglia, *Tetrahedron*, 2005, **61**, 1755 – 1763.

223 A. Bourdolle, M. Allali, J.-C. Mulatier, B. L. Guennic, J. M. Zwier, P. L. Baldeck, J.-C. G. Bünzli, C. Andraud, L. Lamarque and O. Maury, *Inorg. Chem.*, 2011, **50**, 4987–4999.

224 R. Brown, F. Eastwood and J. Horvath, *Aust. J. Chem.*, 1995, **48**, 1055–1058.

225 US pat., US2010030810(A1), 2010.

Appendix One – Crystal Data

	Identification code	CCDC
S-*Λ*-(*λλλ*)-[Eu.**L**^{30}]	12srv245	965909
R-*Λ*-(*δδδ*)-[Eu.**L**^{30}]	13srv002	965910
S-*Λ*-(*λλλ*)-[Yb.**L**^{30}]	13srv030	965911

Appendix Two – List of Complexes

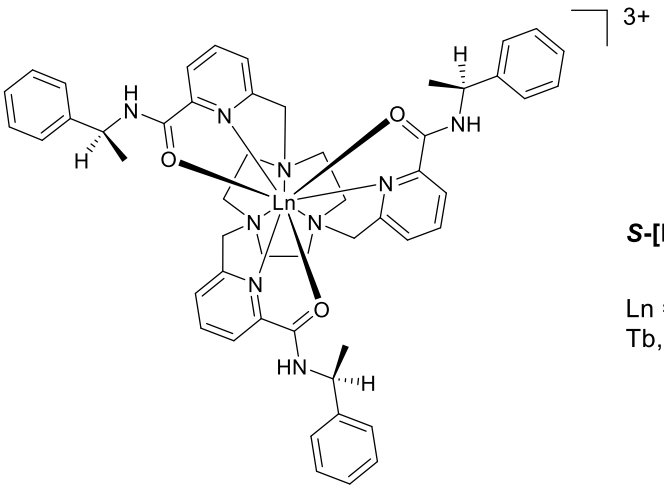

***S*-[Ln.L^{30}](CF$_3$SO$_3$)$_3$**

Ln = Ce, Pr, Nd, Eu, Gd,
Tb, Dy, Ho, Er, Tm, Yb

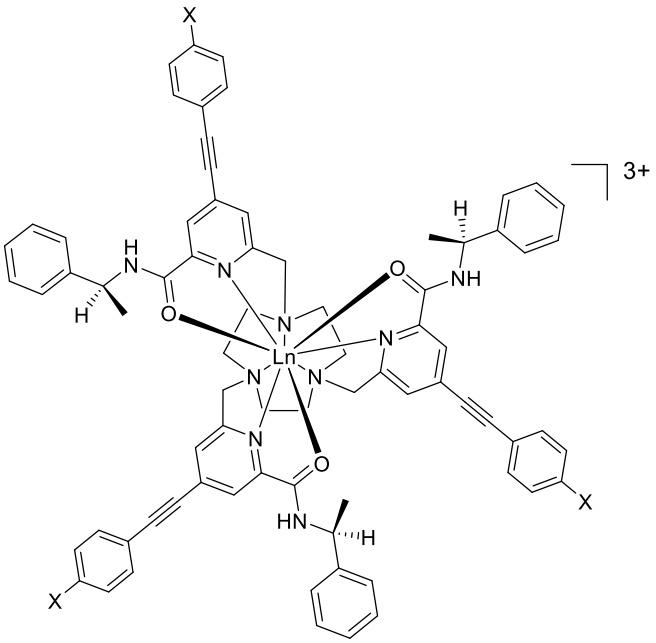

***S*-[LnL^{31a-d}]Cl$_3$**

(*S*)-L^{31a} X = H
L^{31b} X = CO$_2$Me
L^{31c} X = OMe
L^{31d} X = NHCOMe

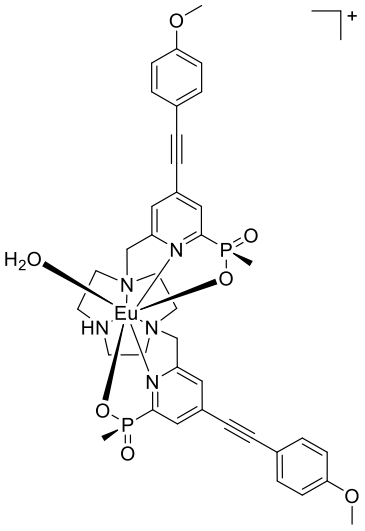

[Eu.L^{37}]$^{+}$

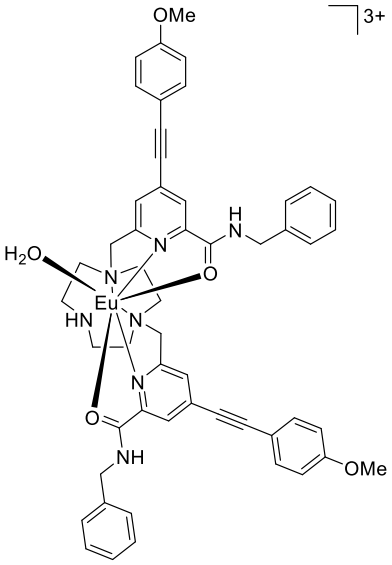

[Eu.L^{38}]$^{3+}$

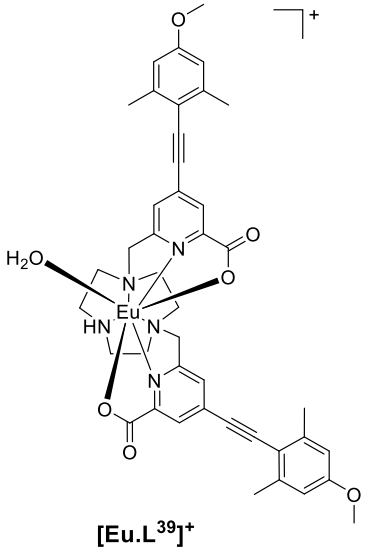

[Eu.L^{39}]$^{+}$

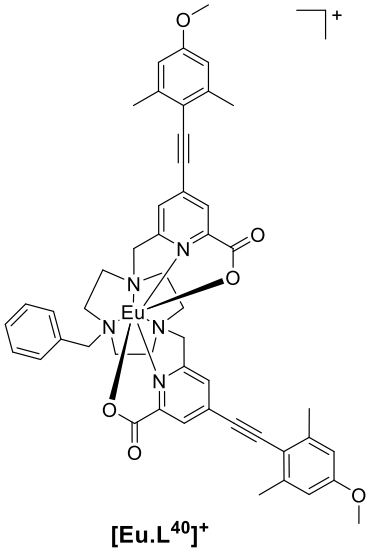

[Eu.L^{40}]$^{+}$

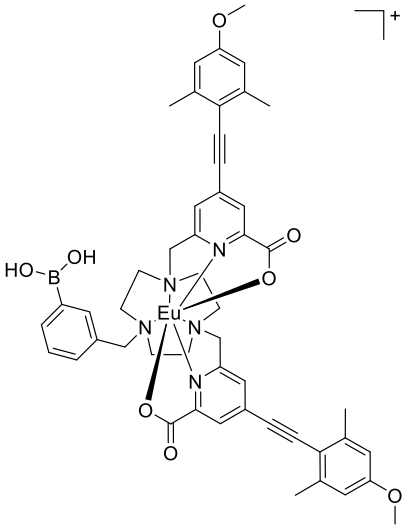

[Eu.L^{41}]$^{+}$

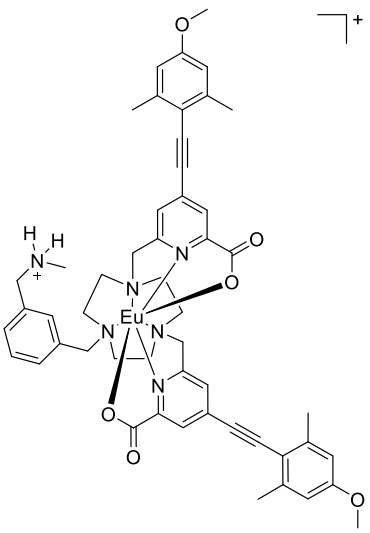

[Eu.L^{42}]$^{+}$